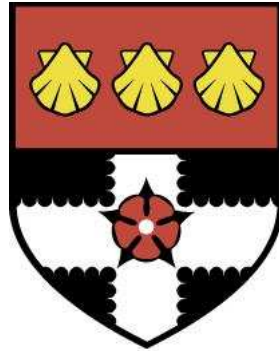


UNIVERSITY OF READING

Department of Meteorology



**Characterising and Understanding
Trends and Variability in African
Rainfall Seasonality**

CAROLINE M. DUNNING

A thesis submitted for the degree of Doctor of Philosophy

May 2018

Declaration

I confirm that this is my own work and the use of all material from other sources has been properly and fully acknowledged.

Caroline M. Dunning

Abstract

Seasonal rainfall over Africa is critical for rain-fed agriculture, domestic water use, energy production and health. Thus, variability and change in precipitation patterns can potentially inflict socio-economic damage, exacerbated by the low adaptive capacity in many countries. This thesis aims to characterise and interpret the seasonality of rainfall over Africa and its changes over time to improve capability for robust, societally relevant projections of future climatic change over Africa.

An objective methodology is developed to quantify the seasonal regime and timing across continental Africa, applicable to both models and observations. Compatibility with known physical drivers of African rainfall, consistency with indigenous methods, and generally strong agreement between satellite-based rainfall datasets confirm that the method realistically captures the seasonal progression of rainfall. Present day seasonality and the role of the El Niño Southern Oscillation are characterised.

Examination of the representation of African rainfall seasonality in the CMIP5 climate models reveals deficiencies in some regions. These include timing biases over the Horn of Africa (long rains 20 days late on average) and an unrealistic seasonal regime over the southern West African coastline, with a failure to capture the agriculturally important Little Dry Season. Further analysis using targeted climate model simulations indicates that the misrepresentation of the biannual regime is related to Atlantic sea surface temperature biases.

Over much of the continent it is found that the CMIP5 models accurately capture the seasonal cycle in rainfall, which adds credence for future projected changes in seasonality. Assessment of future changes in wet season characteristics under RCP4.5 and RCP8.5 scenarios indicates significant projected changes in several regions of Africa. A delay in the wet season over West Africa and the Sahel of over 5-10 days on average and later onset of the wet season over Southern Africa is identified. This is linked with increasing strength of the Saharan Heat Low in late boreal summer and a northward shift in the rain belt over August-December. Average rainfall per rainy day is projected to increase, while the number of rainy days in the wet season declines in regions of stable or declining rainfall (West and Southern Africa) while remaining unchanged in Central Africa where rainfall is projected to increase. Identified changes in seasonal rainfall characteristics over Africa have implications for crop yields, water supplies, and urban flooding, requiring adaptation strategies to reduce potentially detrimental consequences.

Authorship of Papers

The following papers have been included in this thesis. They are included as published/submitted, and have not been modified. The first two papers have been accepted. It is aimed that the third paper will be submitted in Summer 2018, and the final paper is under review at Journal of Climate.

The Supplementary Information for the published papers can be found on the following webpage: <http://www.personal.reading.ac.uk/~vr031288/research/publications.php>. The Supplementary Information for the third and fourth papers can be found in the Appendices.

Below the papers are listed, along with the components carried out by the candidate and the estimated percentage contribution.

Dunning, C.M., E Black, and R.P. Allan (2016) The onset and cessation of seasonal rainfall over Africa. *Journal of Geophysical Research: Atmospheres*, 121 11,405-11,424, doi:10.1002/2016JD025428

Contribution= 80%

C.M.D developed the methodology with the assistance of E.B. and R.P.A. C.M.D. carried out the analysis and led the writing of the paper, with input from E.B. and R.P.A., and valuable contributions from reviewers.

Dunning, C.M., Allan, R.P. and Black, E. (2017) Identification of deficiencies in seasonal rainfall simulated by CMIP5 climate models, *Environmental Research Letters*, 12(11), 114001, doi:10.1088/1748-9326/aa869e

Contribution= 80%

C.M.D designed the study, with the assistance of E.B. and R.P.A., and carried out the analysis. C.M.D. led the writing of the paper, with input from E.B. and R.P.A.

Dunning, C.M., Hirons, L.C., Klingaman, N.P., Allan, R.P., Black, E. and Turner, A.G. (in prep.), The impact of air-sea coupling and ocean mean state biases on the representation of the seasonal cycle of precipitation over southern West Africa in climate models, *Climate Dynamics*

Contribution= 60%

N.P.K and L.C.H designed the model framework, C.M.D and N.P.K designed the study,

with the assistance of E.B., R.P.A., L.C.H. The model simulations were completed by N.P.K and L.C.H, with C.M.D running one simulation (GOML-ATL-N96). C.M.D. carried out the analysis, with input from all co-authors. C.M.D. led the writing of the paper, with input from all co-authors.

Dunning, C.M., E Black, and R.P. Allan (submitted) Later wet seasons with more intense rainfall over Africa under future climate change, *Journal of Climate*

Contribution= 80%

C.M.D designed the study, with the assistance of E.B. and R.P.A., and carried out the analysis. C.M.D. led the writing of the paper, with input from E.B. and R.P.A.

Acknowledgements

Firstly, I would like to thank my supervisors Dr Emily Black and Professor Richard Allan for their guidance, wisdom and support during my PhD. I have really valued our meetings and the knowledge you have shared with me, as well as all the other contributions to this PhD, including all the proof reading over the past few months, much of which seems to have reappeared in my inbox not long after it left! Emily, thank you for always having an open office door, ready for the less positive reviewer comments and other concerns.

Thanks must also go to my monitoring committee members; Professor William Collins and Professor Ros Cornforth, for ensuring that I was on track, and encouraging me to periodically critically analyse my work. Thank you Ros for the collaboration with the Rainwatch project and travel to the Rainwatch workshop in Senegal, and the opportunity to attend COP22 in Marrakech. Both trips demonstrated to me the importance of climate research, and were eye-opening in many ways!

The contributions of the Tropical Weather and TAMSAT research groups to this thesis should not be underestimated; their advice and suggestions have been incredibly helpful. Particular thanks must go to Linda Hirons and Nick Klingaman who gave much assistance with Chapter 4. Nick, thank you so much for enabling me to complete MetUM simulations (using the GOML framework), and your patience when I made mistakes and filled your inbox with questions! Linda, thank you for all your help with the paper writing and figures.

The Department of Meteorology at Reading is a great place to do a PhD, on account of the friendly and supportive atmosphere and the large community of PhD students, who are always ready to provide a distraction when needed, and I'd like to thank all of the PhD students for their friendship. Emma Hopkin and Hannah Bloomfield; thanks for always being ready for a coffee break!

Life doesn't stop for a PhD, and I'd like to thank all my family for helping to care for my grandmother, especially when I was in Africa. Particular thanks must go to my parents for doing their utmost to balance the care responsibility, and providing me with additional resources so that I could both care for her and complete my PhD.

Finally, thanks must go to my fiancé Josh for his love, support, and amazing patience.

Now to him who is able to do immeasurably more than all we ask or imagine, according to his power that is at work within us, to him be glory throughout all generations, for ever and ever! Ephesians 3:20-21

Contents

Declaration	ii
Abstract	iv
Authorship of Papers	vi
Acknowledgements	viii
Table of contents	x
List of Acronyms	xiv
1 Introduction	1
1.1 Motivation	1
1.1.1 Importance of rainfall, its seasonality and interannual variations for society	1
1.1.2 Impacts from climate change	2
1.1.3 Requirement to observe, understand and predict	3
1.2 Background and Challenges	3
1.2.1 Characteristics of African Rainfall Seasonality	3
1.2.2 Thermodynamic and dynamic drivers of water cycle change	6
1.2.3 Deficiencies in climate model simulations over Africa and implications for projections	7
1.2.4 Major challenges	10
1.3 Thesis Aims	11
1.3.1 Develop a method to capture and characterise seasonality in rainfall .	11
1.3.2 Evaluate and identify deficiencies in representation of seasonality over Africa by climate models	14
1.3.3 Elucidate dynamical processes determining seasonality, its variability and climate model representation	15
1.3.4 Interpret projected future changes in seasonal characteristics	16
1.4 Thesis outline	18
2 The onset and cessation of seasonal rainfall over Africa	19
2.1 Introduction	20
2.2 Methodology and Datasets	22
2.2.1 Datasets	22
2.2.2 Extension of the Liebmann Method for all of Africa	24
2.2.3 Regions	28
2.3 Physical Relevance of the Seasonality Metric	30
2.3.1 Movement of the ITCZ/ Tropical Rain Belt	31

2.3.2	Consistency with West Africa Monsoon Dynamics	32
2.3.3	Comparison with other methods for identifying the onset	35
2.4	Evaluation over a range of datasets	35
2.4.1	Annual Rainfall Regime	36
2.4.2	Biannual Rainfall Regime	38
2.4.3	Differences between ERA-I and other datasets over West Africa	41
2.5	Example application; Interpretation of Interannual Variability over East Africa	43
2.6	Discussion and Conclusions	45
3	Identification of deficiencies in seasonal rainfall simulated by CMIP5 climate models	51
3.1	Introduction	52
3.2	Methods and Data	54
3.3	Results	57
3.4	Simulation of the Little Dry Season in Southern Coastal West Africa	62
3.5	Conclusions	65
4	The representation of the seasonal cycle of precipitation over southern West Africa in climate models	69
4.1	Introduction	70
4.2	Model, Methods, Data	73
4.2.1	MetUM Simulations	73
4.2.2	Observations	77
4.2.3	Methods	79
4.3	Performance of MetUM and horizontal resolution	79
4.4	Effect of Air-Sea Interactions and Ocean Mean State	82
4.4.1	Southward Bias in the TRB position in May	87
4.4.2	Overestimation of rainfall during the August LDS	88
4.5	Discussion and Conclusions	91
5	Later wet seasons with more intense rainfall over Africa under future climate change	97
5.1	Introduction	98
5.2	Methods and Data	101
5.2.1	Model output and observational data	101
5.2.2	Methodology for identifying onset and cessation of rainfall seasons	103
5.2.3	Characterisation of dynamical drivers	105
5.3	Changing Rainfall Seasonality and Characteristics	107
5.4	Drivers leading to Later Onset/Cessation of Wet Seasons	115
5.5	Conclusions	122
6	Conclusions	127

6.1	Scientific Advances	127
6.1.1	Development and application of a framework for objectively character- ising seasonal rainfall	127
6.1.2	Investigation of model biases	129
6.1.3	Interpretation of future projections	130
6.2	Limitations	132
6.3	Future Work	135
6.4	Conclusions	138
7	Appendices	141
7.1	Appendix 1: Supplementary Information for ‘The impact of air-sea coupling and ocean mean state biases on the representation of the seasonal cycle of precipitation over southern West Africa in climate models’	141
7.2	Appendix 2: Supplementary Information for ‘Later wet seasons with more intense rainfall over Africa under future climate change’	144
7.2.1	Median Change in Onset/Cessation for RCP 4.5	145
7.2.2	Changes in Seasonal Regime	147
7.2.3	Determining the Position of the Tropical Rain Belt	147
7.2.4	Relationship between Tropical Rain Belt Location and Onset/Cessation in Observations	148
7.2.5	Location of Saharan Heat Low and Angola Low	155
7.2.6	Sahara Heat Low Index and Angola Low Index	157
7.2.7	Sensitivity of SHL/AL index to region used	157
	References	166

List of Acronyms

Acronym	Definition
AEJ	African Easterly Jet
AGCM	Atmosphere-only Global Climate Model
AL	Angola Low
AMIP	Atmospheric Model Intercomparison Project
ARCV2	African Rainfall Climatology version 2
BADC	British Atmospheric Data Centre
CGCM	Coupled Global Climate Model
CHIRPS	Climate Hazards Group InfraRed Precipitation with Stations
CLIMDEX	Datasets for Indices of Climate Extremes
CMIP	Coupled Model Intercomparison Project
CMIP3	Coupled Model Intercomparison Project Phase 3
CMIP5	Coupled Model Intercomparison Project Phase 5
DJF	December, January, February
ENSO	El Niño Southern Oscillation
ERA-I	ERA-Interim
EUMETSAT	European Organization for the Exploitation of Meteorological Satellites
GCM	Global Climate Model
GOML	Global Ocean Mixed Layer
GPCC	Global Precipitation Climatology Centre precipitation dataset
GPCP	Global Precipitation Climatology Project
GPCP 1DD	Global Precipitation Climatology Project 1 Degree Daily
GTS	Global Telecommunication System
IOD	Indian Ocean Dipole
IR	InfraRed
ITCZ	InterTropical Convergence Zone
ITF	InterTropical Front
JAS	July, August, September
JJA	June, July, August
LDS	Little Dry Season
MAE	Mean Absolute Error
MAM	March, April, May

List of Acronyms

Acronym	Definition
MetUM	Met Office Unified Model
P - E	Precipitation - Evaporation
PPC	Pearson Pattern Correlation
RCP	Representative Concentration Pathway
SHL	Saharan Heat Low
SON	September, October, November
SST	Sea Surface Temperature
SWAC	Southern West African Coastline
TAMSAT	Tropical Applications of Meteorology using SATellite data and ground-based observations
TAMSATv3	Tropical Applications of Meteorology using SATellite data and ground-based observations version 3
TARCATv2	TAMSAT African Rainfall Climatology and Timeseries version 2
TEJ	Tropical Easterly Jet
TIR	Thermal Infrared Imagery
TRB	Tropical Rain Belt
TRMM	Tropical Rainfall Measuring Mission
UNDP	United Nations Development Programme

Chapter 1:

Introduction

1.1 Motivation

The aim of this thesis is to improve the capability to produce robust societally relevant projections of future climatic changes over Africa, with particular focus on the seasonal cycle of precipitation over Africa.

1.1.1 Importance of rainfall, its seasonality and interannual variations for society

A large number of Africans are dependent upon the seasonal characteristics of rainfall for crop irrigation and the replenishment of water supplies used for drinking and domestic use (de Wit and Stankiewicz, 2006; Boyard-Micheau et al., 2013; Vizy et al., 2015). Beyond individual livelihoods, rainfall over Africa has implications for energy and health, as a number of vectors that transport diseases such as malaria and dengue fever require standing water during their lifecycle (Tanser et al., 2003). Increasingly, African countries are utilising renewable energy to meet electricity requirements; the seasonal recharge of reservoirs thus has implications for electricity supply from hydropower (Yamba et al., 2011; van Vilet et al., 2016). Recent droughts, including the prolonged drought over the Sahel during the 1980s and the 2011 East African drought, have wide ranging detrimental socio-economic impacts (Lott et al., 2013; Park et al., 2016), with economic losses from the mid-1980s drought totalling several hundred million U.S. dollars (Tarhule and Lamb, 2003).

The socio-economic implications of rainfall extend beyond simply the amount of precipitation that occurs. The timing of the seasonal rainfall, and in particular the onset, affects the planting date of crops and therefore has implications for agronomic management and for crop yield, since a shorter season may mean that crops fail to reach full maturity and yields

are reduced (Kniveton et al., 2009; Boyard-Micheau et al., 2013; Vizy et al., 2015; Guan et al., 2015). Furthermore, longer dry seasons may strain water levels in reservoirs, impacting drinking water supplies and the production of hydroelectric power. Increasingly intense dry seasons are also linked to decreasing net primary productivity (Murray-Tortarolo et al., 2016). The characteristics of rainfall are also important; long dry periods and heavy rainfall events are harmful for certain crops, and may result in increased runoff and soil erosion.

Interannual variations and long term change in rainfall characteristics generate significant impacts. The floods across East Africa during the 1997 short rains season were associated with damage to infrastructure and loss of life, while the drought across Southern Africa during 2015/16 damaged crops, with a regional maize shortfall of 9.3 million tons (OCHA, 2016). Both of these events were associated with the El Niño Southern Oscillation (ENSO). Other modes of variability, including the Indian Ocean Dipole, also act to modulate interannual variability in wet seasons across Africa (Black et al., 2003). Interannual variability associated with large spatial scale modes of climate variability, such as ENSO, has high potential for detrimental consequences, as the geographical extent of events is likely to be greater.

1.1.2 Impacts from climate change

Future changes in precipitation patterns under climate change are likely to have sizeable impacts over Africa, exacerbated by the low adaptive capacity across much of the continent (Boko et al., 2007).

Changes in cloud and precipitation over Africa are strongly linked to the large-scale atmospheric circulation. Hence, changes in tropical circulation (Vecchi and Soden, 2007), changing width of tropical rain belts (Seidel et al., 2008), variations in the seasonal cycle (Feng et al., 2013) and changes in the strength of monsoons (Trenberth, 2011) projected under future climate change (see § 1.2.2) will act to alter African precipitation patterns, including the seasonal cycle of rainfall. Changing patterns of seasonality, leading to longer or shorter wet seasons will impact a range of sectors, including health and energy. Longer dry seasons will have negative implications for net primary productivity (Murray-Tortarolo et al., 2016), hydropower and drinking water supplies, while shorter wet seasons may mean that crops do not reach full maturity and yields are reduced (Guan et al., 2015).

Additionally, amplification of hydrological extremes is anticipated, with more intense and longer droughts resulting from higher temperatures and greater evaporation, and increased atmospheric water vapour fuelling an intensification of extreme rainfall (Trenberth, 2011). More intense rainfall events will affect farmers, as heavy rainfall can damage the flowers of

cash crops (including coffee and cocoa), and degrade soil quality, especially when following a prolonged dry season. Beyond the direct consequences of droughts and floods on food supply and infrastructure, the impacts are often further exacerbated by health problems, especially cholera and malaria (Few et al., 2004; Boko et al., 2007).

1.1.3 Requirement to observe, understand and predict

Given the substantial impact of variability and trends in precipitation, and the low adaptive capacity of many countries in Africa, establishing how current and future changes in atmospheric circulation and precipitation characteristics can impact stakeholders is imperative. Predictive capability is dependent upon the veracity of detailed physics and realism of complex feedbacks depicted by detailed numerical simulations of the global atmosphere, ocean and land surface encapsulated within comprehensive climate models.

Producing robust projections of future climate change requires knowledge of the primary driving factors and a meaningful assessment of model fidelity. Evaluation of models should be tailored to the specific application for which the models will be used. Thus, to examine the drivers of user-relevant rainfall characteristics over Africa, model evaluation should include relevant process-based assessment and examination of the representation of seasonality (Balan Sarojini et al., 2016). In order to conduct such model evaluation, a broad understanding of the observed climate including the physical mechanisms that give rise to the current configuration of seasonal rainfall is necessary. Furthermore, knowledge of the current interannual variability and the associated drivers is key, since internal variability obfuscates attribution of changes to specific climate forcings.

1.2 Background and Challenges

1.2.1 Characteristics of African Rainfall Seasonality

Precipitation over Africa follows a marked seasonal cycle, with one primary wet season per year over West Africa and the Sahel in boreal summer and Southern Africa in austral summer. Some low-latitude areas, including the Horn of Africa, experience two pronounced wet seasons per year, during autumn and spring while remaining equatorial regions experience moist conditions throughout the year.

The traditional perspective of African rainfall seasonality was based upon the seasonal migration of the intertropical convergence zone (ITCZ), a region of low-level convergence, ascent and associated rainfall, which travels north and south following the maximum incoming

solar radiation. While a north-south movement of the main precipitation band is apparent throughout the year, a number of studies argue that the ITCZ paradigm fails to fully explain the seasonality of rainfall over Africa (Riddle and Cook, 2008; Nicholson, 2018). Over West Africa, the region of wind discontinuity and convergence associated with the ITCZ lies over 1000km north of the region of maximum rainfall and ascent (Nicholson, 2013; Parker and Diop-Kane, 2017) and remains north of the equator throughout the calendar year (Nicholson, 2018). Parker and Diop-Kane (2017) also show that during the peak of the West African Monsoon the regions surrounding the inter-tropical discontinuity (ITD), where the moist south-westerly winds meet the dry north-easterly Harmattan wind (Figure 1.1), are associated with low rainfall totals. When considering Southern Africa, Reason et al. (2006) also note that over the Gulf of Guinea the ITCZ stays north of the equator throughout the year.

The role of many other meteorological phenomena on African weather and climate has been examined, including heat lows (e.g. the Saharan Heat Low) and tropical lows (e.g. the Angola Low), low-level and mid-level jets (such as the Turkana Jet and African Easterly Jet), wave disturbances and large scale organised convection (Figure 1.1).

South African climate is dominated by the South Indian Ocean Convergence Zone, a northwest-southeast band of low-level convergence and precipitation, fed by moisture from circulation round the South Indian Ocean High Pressure and circulation round the Angola Low with additional moisture transport from the north-east monsoon (Lazenby et al., 2016). Cloud bands (known as Tropical Temperate Troughs, TTTs) associated with this convergence zone bring much of the seasonal rainfall over subtropical southern Africa (Reason et al., 2006).

Over West Africa and the Sahel, the West African Monsoon dominates the seasonal cycle, with the south-westerly monsoon winds travelling from the cool waters of the Gulf of Guinea towards the Saharan Heat Low, bringing moisture from the Gulf of Guinea onto the continent (Nicholson, 2013). African Easterly Waves, disturbances that develop and propagate westward on the African Easterly Jet, are the dominant synoptic scale weather phenomena over West Africa and promote the initiation and organisation of mesoscale convective systems and squall lines. Precipitation from mesoscale convective systems and squall lines comprises between 75-90% of annual rainfall over the Sahel (Mathon et al., 2002; Skinner and Diffenbaugh, 2013; Parker and Diop-Kane, 2017). The strength and position of the mid-level African Easterly Jet is associated with the Sahara Heat Low (Nicholson, 2013; Parker and Diop-Kane, 2017).

East Africa experiences two wet seasons per year: the long rains in March-May and the short rains in October-December (Camberlin et al., 2009). The atmosphere over East Africa is convectively stable throughout the year, with changes in surface moist static energy

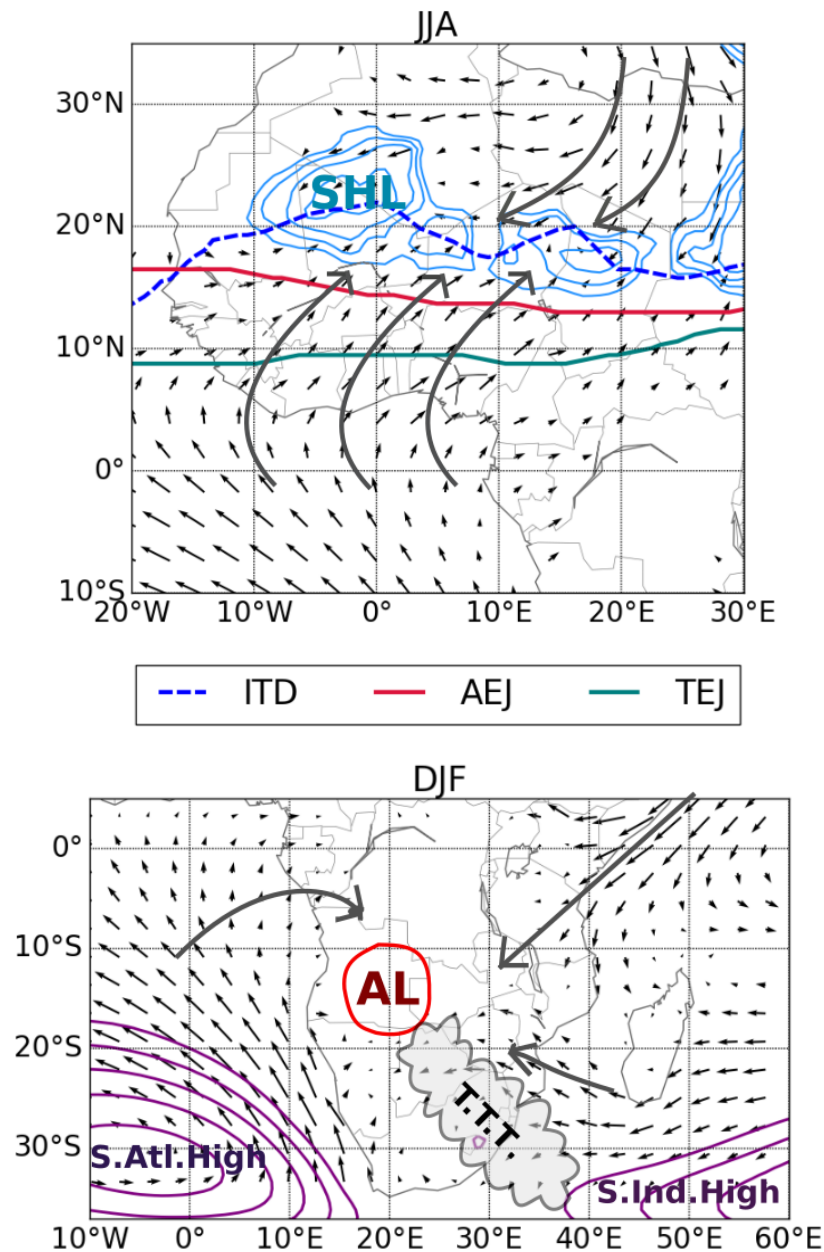


Figure 1.1 Schematics of the atmospheric features influencing boreal summer weather over West Africa (top, JJA) and austral summer weather over Southern Africa (bottom, DJF). Top: Schematic detailing key features of the West African Monsoon; position of the ITD, upper-level air streams (African Easterly Jet (AEJ) and Tropical Easterly Jet (TEJ)), 925hPa winds and the Saharan Heat Low are marked. Grey arrows show the south-westerly monsoon winds to the south, and Harmattan winds to the north. Bottom: Schematic detailing key features of the southern African climate system; positions of the South Atlantic High, South Indian High, and Angola Low are marked. The mean position of Tropical Temperate Troughs (TTTs) is also shown. 800hPa wind are also included. The grey arrows mark the main moisture transport into the region. Produced using ERA-Interim data.

determining the annual cycle (Yang et al., 2015a). The long rains are linked with the formation of the Somali Jet over the western Indian Ocean; in April, the meridional branch of the Somali Jet transports moisture into East Africa, which forms prior to the northern zonal branch of the Somali Jet, that acts to divert moisture eastward away from East Africa from June onwards (Riddle and Cook, 2008). Surface wind patterns during the short rains include north-easterlies across the Horn of Africa, and south-easterlies to the south (Yang et al., 2015a). Unlike the long rains, the short rains are linked with large-scale modes of climate variability, including ENSO and the Indian Ocean Dipole (Black et al., 2003).

Many of the phenomena and teleconnections driving seasonal and inter-annual variability are understudied and poorly represented in climate models (Lazenby et al., 2016; Munday and Washington, 2017; Whittleston et al., 2017; Nicholson, 2018). Accurate forecasting and reliable future projections depend upon good understanding of the meteorological phenomena and physical drivers that affect the seasonal cycle; an area that requires further work (Nicholson, 2018).

1.2.2 Thermodynamic and dynamic drivers of water cycle change

Future changes in climate resulting from elevated greenhouse gas concentrations will impact rainfall seasonality via a number of mechanisms. Increased temperatures will modify the surface energy budget, driving greater evaporation and potentially intensifying drought. However, the direct effect of elevated CO₂ on plant physiology will modify how vegetation uses water and changes in rainfall characteristics are crucial in determining how water is partitioned between runoff and soil moisture (e.g. Mankin et al., 2018). A warmer climate leads to an increase in lower tropospheric water vapour, governed by the Clausius-Clapeyron equation (e.g. Held and Soden, 2006). Elevated atmospheric water vapour will fuel an intensification of extreme rainfall (Trenberth, 2011). These complex drivers are capable of increasing the regional occurrence of both drought and flood events.

Global mean precipitation is primarily constrained by the energy budget (Allen and Ingram, 2002), hence precipitation is expected to increase at a smaller rate than water vapour concentration. However, increased water vapour leads to enhanced moisture transport by the atmospheric circulation from the net evaporative regions to the moist, wet regions that drives an amplification in the pattern of Precipitation - Evaporation (P - E) (Held and Soden, 2006) since moisture transport into an atmospheric column is primarily balanced by the net loss of moisture from the column through P - E. While enhanced moisture export from the net evaporative regions (P - E < 0) will decrease P - E further, implying "drying", this does not

apply over multi-annual scales over land where $P - E$ is positive and balanced by runoff (Greve et al., 2014; Allan, 2014; Byrne and OGorman, 2015). Nevertheless, seasonal and regional manifestation of these driving factors are more complicated and subject to feedbacks (Byrne and OGorman, 2015; Kumar et al., 2015) that may explain enhanced amplitude in rainfall seasonality (Chou et al., 2013) and reduced dry season precipitation over dry land regions (Liu and Allan, 2013).

The larger increase in water vapour compared to precipitation is balanced by a decrease in the convective mass flux and an associated slowing down of atmospheric circulation (Held and Soden, 2006) and weakened monsoons (Trenberth, 2011). Changes to the Hadley Circulation include a widening of the tropical belt (Seidel et al., 2008) and tightening of the region of ascent and associated rain band (Su et al., 2017). In addition to thermodynamic drivers, dynamical changes and variations in atmospheric circulation will have a large influence; Liu and Allan (2013) found that regional precipitation trends are dominated by dynamic processes including spatial changes in atmospheric circulation.

Changes in cloud and precipitation over Africa are strongly linked to the large-scale circulation. Hence, changes in tropical circulation will affect regional African climate. The increasing width of the tropical belt may result in the expansion of the subtropical dry areas, including the Sahara Desert, while a tightening of the tropical rain belt may lead to shorter and more intense wet seasons. As highlighted in § 1.2.1, African climate is dominated by regional drivers, linked to radiative forcing and SST patterns. For example, changes in the radiation budget associated with elevated greenhouse gas have been linked with increases in precipitation over the Sahel (Dong and Sutton, 2015), while changes in Indian Ocean SSTs have been associated with reduced moisture transports over SE Africa and reduced rainfall totals (Funk et al., 2008). Changes in dynamical drivers leading to shifts in atmospheric circulation, in which there is less confidence, may be more important regionally than thermodynamic factors (Shepherd, 2014; Birner et al., 2014). Patterns of interdecadal variability complicate attribution of drivers, and separation of long-term trends from short term variability.

In order to understand and investigate changes and variability in precipitation over Africa thorough understanding of the multiple drivers and complex physical mechanisms is required.

1.2.3 Deficiencies in climate model simulations over Africa and implications for projections

Global climate models are required for generating physically-based future projections of climate in response to a range of plausible scenarios relating to socioeconomic pathways

involving emissions of and radiative forcings by greenhouse gas and aerosol species. However, they are also instrumental for exploring past and present climate variability through elucidating physical mechanisms, investigating the role and impact of teleconnections, examining the response of the climate to different forcings, detection and attribution of past climate change, and advancing understanding of the global climate system.

Global climate models are computer based numerical simulations of the climate system, using the equations for fluid dynamics and energy transfer to represent atmospheric weather patterns and ocean circulation, and parametrisations (approximations) of physical processes operating at scales smaller than the numerical grid (e.g. cloud processes, precipitation and radiation). Coupled climate models consist of component models that represent individual parts of the earth system (including atmosphere, ocean and land surface models), with fluxes (e.g. of heat, momentum and freshwater) exchanged between the components (Williams et al., 2015).

Climate models are not a perfect representation of the climate system; equations are solved using numerical solutions on a discretised grid with processes that occur at smaller scales represented by parametrisations. The simulation of precipitation in climate models relies heavily on parametrised processes and is thus subject to errors and biases over varying regional scales. Much of the seasonal cycle of precipitation in tropical regions is driven by monsoon circulations, which were poorly represented in the previous generation of climate models (CMIP3, Coupled Model Intercomparison Project Phase 3, Flato et al., 2013). Improvements in the representation of monsoon systems have been documented for the recent generation of climate models (CMIP5: Sperber et al., 2013), yet biases in the representation of the monsoon domain and intensity persist. In terms of the West African Monsoon, studies have identified a southward shift of the rainfall, with deficient rainfall over the Sahel (Roehrig et al., 2013), deficiencies in the representation of jet-rainfall coupling (Whittleston et al., 2017), and the Saharan Heat Low (Dixon et al., 2017a,b). Over this region, Roehrig et al. (2013) find little improvement in CMIP5 over CMIP3. Other studies have identified biases in the representation of the seasonal cycle over East Africa (Tierney et al., 2015) and Southern Africa (Munday and Washington, 2017). Figure 1.2, taken from Tierney et al. (2015), shows the incorrect representation of the seasonal cycle over East Africa in coupled CMIP5 models, with a large overestimate in short rains rainfall.

While substantial improvements in climate models have taken place over recent decades, a number of incongruities persist over Africa, where improvements have been more limited in comparison with other regions (James et al., 2017). The first step in climate model devel-

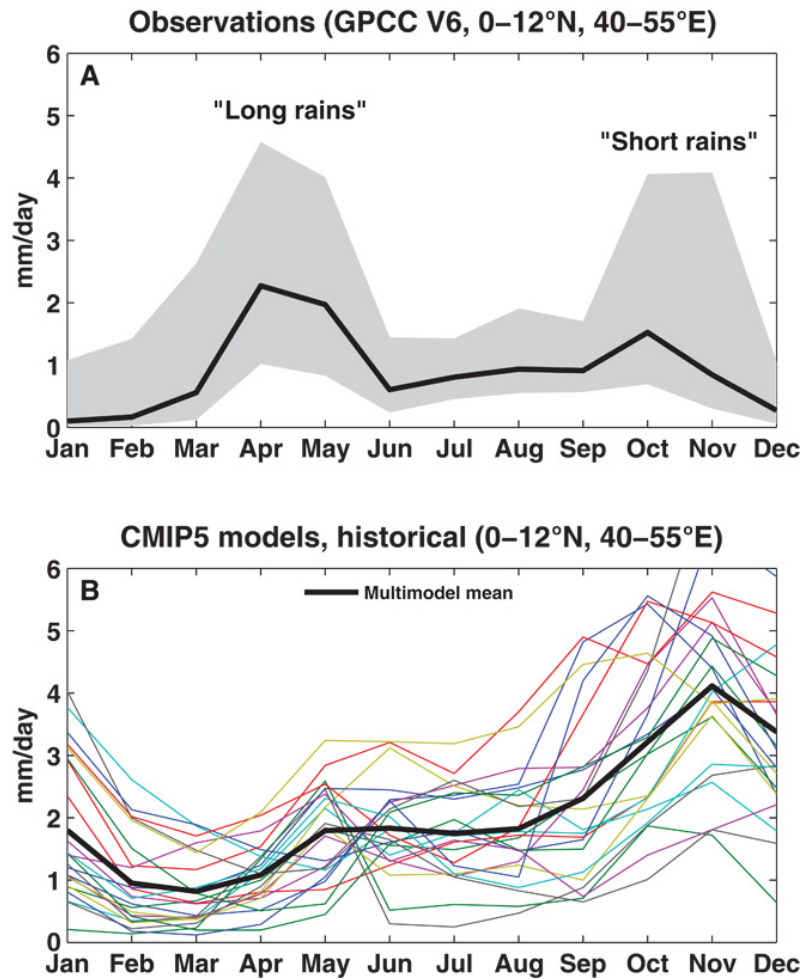


Figure 1.2 Comparison between the observed and the simulated annual cycle in precipitation in the eastern Horn of Africa (average across 0–12°N and 40–55°E). (A) Observed annual cycle in precipitation, GPCC v6 (39). Black line denotes the median values; grey bars denote the 90% confidence interval. (B) Simulated annual cycle in precipitation, from the CMIP5 historical experiments. Black line denotes the multimodel mean; individual coloured lines represent each model. Figure 5 from Tierney et al. (2015).

opment is to produce improved descriptions of physical processes, which are then translated into model components and new parametrisations (Flato et al., 2013).

Model deficiencies, including incorrect simulations of current climate (e.g. Tierney et al., 2015), missing processes and connections (e.g. Whittleston et al., 2017) and incapability to capture multi-decadal oscillations (e.g. Biasutti, 2013) limits the use of climate models for exploring drivers and producing reliable future projections. Moreover, Rowell et al. (2016) shows that model uncertainty in future projections cannot simply be overcome by selecting those models that perform well in representing current climate, quantified using skill metrics. However, Lazenby (2017) found that using a model ranking framework, based on model representation of contemporary climate over Southern Africa, did reduce uncertainty in projections of future precipitation change over Southern Africa. Rowell et al. (2016) and James et al.

(2017) both highlight the need for mechanistic based, region specific model evaluation.

Although progress is required, climate model projections contain much useful information about changes in regional climate variability. Complexities and deficiencies of model representation of key aspects of variability means that careful process-based evaluation is required if climate model output is to be used effectively to support decision making. Using advanced diagnostics and methods, such as those developed by Levy et al. (2013) and Lazenby (2017), that account for model biases, can be useful for exploiting climate model projections to produce robust projections even if models have errors in their basic state.

1.2.4 Major challenges

The previous sections have detailed some of the significant challenges in producing and interpreting robust projections of user-relevant rainfall characteristics over Africa. Not only are there challenges pertaining to model fidelity and the reliability of future projections, but also to understanding societal implications.

The aim of this thesis is to improve the capability to identify and understand projections of user-relevant rainfall characteristics over Africa. As shown in the previous section, this requires not only producing future projections of user-relevant rainfall characteristics but establishing and exploring the underlying physical mechanisms and drivers and carrying out suitable model evaluation. This overarching aim is met by addressing the following objectives:

1. Develop a method to capture and characterise seasonality in rainfall [Chapter 2]
2. Evaluate and identify deficiencies in representation of seasonality over Africa by climate models [Chapter 3]
3. Elucidate dynamical processes determining seasonality, its variability and climate model representation [Chapter 4]
4. Interpret projected future changes in seasonal characteristics [Chapter 5]

These objectives address key challenges for effective exploitation of climate model output. One challenge relates to how 'user-relevant rainfall' is quantified. A primary aim is to develop metrics that not only relate to society (§ 1.1.1) but also can be used for comparing models and observations (§ 1.2.3) and interpreting future projections (§ 1.1.2). The aspect of 'user-relevant rainfall' selected to examine in this thesis is the timing and seasonality of precipitation, which is of significant societal importance (see § 1.1.1 and § 1.3.1).

The need to evaluate models using appropriate techniques, and the challenge of accounting for temporal/spatial biases and ensuring that model analyses are relevant to application (§ 1.2.3) is addressed in the second aim, to evaluate and identify deficiencies in climate model representation of seasonality over Africa.

The importance of understanding the physical processes and drivers is highlighted in § 1.1.3 and § 1.2, and thus the third aim is to elucidate the representation of seasonality in climate models, through analyses of model representation of the dynamical processes governing present-day seasonality and variability. Finally, given the important role that climate change will play over Africa (§ 1.1.2, § 1.2.2) the fourth aim is to interpret predicted changes in seasonal characteristics.

The overarching aim of this thesis is:

‘To improve capability for robust projection of user-relevant rainfall characteristics over Africa’

The following section contains specific background and motivation for each of the thesis aims.

1.3 Thesis Aims

1.3.1 Develop a method to capture and characterise seasonality in rainfall

The first aim concerns the quantification of ‘user-relevant rainfall’. A plethora of such metrics have been proposed, including metrics for quantifying extreme events (for example metrics developed by CLIMDEX (Datasets for Indices of Climate Extremes), e.g. monthly maximum consecutive 5-day precipitation, simple precipitation intensity index, and annual total precipitation in wet days (Caesar et al., 2006; Alexander et al., 2006, 2011; Donat et al., 2013)), metrics for analysing the length of wet and dry spells (maximum length of dry spell, maximum length of wet spell), and metrics for quantifying seasonal characteristics, such as rainfall amount and timing (Rowell et al., 2015a; Cook and Vizzy, 2012). While increasing numbers of studies are exploring extreme events, (Shongwe et al., 2009, 2011; Sillmann et al., 2013; Sylla et al., 2015; Pinto et al., 2016; Pohl et al., 2017) particularly in relation to detection and attribution (Parker et al., 2017), fewer studies are investigating the drivers and changes in timing and characteristics of the wet seasons (see § 5.1). Yet, the timing and seasonality of precipitation across Africa is of high user-relevance, due to its impact on planting date, growing season length, the seasonal recharge of reservoirs and the transmission season of a number of vector borne diseases (see § 1.1.1, § 2.1, § 3.1 and § 5.1). Furthermore,

establishing metrics that quantify the timing and seasonality of rainfall over Africa provides a basis on which other user-relevant metrics can be developed, for example, for quantifying the length of dry spells in the wet season, and number of rainy days in the wet season.

From a scientific perspective, understanding the processes and mechanisms driving the seasonal cycle of rainfall represents a key challenge, as the traditional view of the ITCZ moving north and south has been shown to be insufficient for explaining rainfall seasonality over the equatorial regions (Yang et al., 2015a; Nicholson, 2018). Thus, the aim of this thesis is to develop and utilize metrics that quantify the seasonality of precipitation. In order to relate rainfall seasonality to wider scale mechanisms and drivers, a methodology applicable at the continental scale is required, for regions with one or more rainy season. Previous studies analysing seasonal timing (namely the onset and cessation of the wet season) tend to focus on limited regions (see § 2.1 and § 2.6, see below for two exceptions). These studies use metrics for onset based on fixed rainfall thresholds and follow the format “the onset is the first wet day of N consecutive days receiving at least P millimetres without a dry spell lasting n days and receiving less than p millimetres in the following C days” (Boyard-Micheau et al., 2013). Such metrics cannot be applied at a continental scale, due to the wide variety of rainfall climatologies, and cannot be applied to datasets with different rainfall biases, including climate model output (see § 2.1 and § 2.6). Furthermore, methodologies that account for biases in model mean state enable fairer model evaluation, and in some cases have been shown to reduce the spread in model projections (Levy et al., 2013).

Two studies have explored wet season characteristics at a continental scale. Using a methodology based on comparing precipitation to potential evapotranspiration, Cook and Vizzy (2012) produced future projections of growing season characteristics over Africa, using a single regional climate model run with 6 ensemble members. The model was first validated to ensure it adequately simulated the distribution of growing season days. Comparing mid-twenty-first century with the end of the twentieth century, Cook and Vizzy (2012) found that over the central and eastern Sahel the growing season gets longer, while a shorter growing season is found over Southern Africa and western Sahel (see Chapter 5). Start and end dates were only computed over select regions. An aim is to further their results by analysing projections using an ensemble of CMIP5 models; thus a methodology is required that is applicable across datasets with differing rainfall biases.

Liebmann et al. (2012) used a consistent and objective methodology based on relative precipitation anomalies to document seasonal variations and wet season characteristics across Africa using 3 precipitation datasets for a 12 year period. They found that over much of the

continent more than 80% of the annual precipitation occurs during the wet season. Patterns of onset and cessation were described and composites of rainfall and 200hPa winds produced to identify common dynamical patterns prior to onset. The methodology developed in this thesis to quantitatively capture seasonality is based on Liebmann et al. (2012), as it accounts for biases in the mean state. To conduct a truly continental scale analysis this is extended to account for regions with two wet seasons per year and compared against locally defined agricultural metrics to ensure societal relevance.

Having developed a societally-relevant metric for quantifying seasonality, the aim is to use it for characterising current seasonality and its variability. Specifically, this metric is used to identify regions experiencing one or two wet seasons per year, and to determine onset and cessation dates at the continental scale, to enable better understanding of the seasonal migration of precipitation. Identifying the spatial pattern of onset progression is exploited to highlight important drivers and mechanisms.

Interannual variability, especially that associated with the El Niño Southern Oscillation, has large socio-economic effects due to the large spatial extent of precipitation impact (see § 1.1.1). Furthermore, El Niño has contrasting effects on precipitation over East Africa compared with Southern Africa, with the impacts also varying across ENSO events (Black et al., 2003; Emerton et al., 2017). Quantifying and investigating the differing impacts of ENSO events across East and Southern Africa is a challenge as the wet seasons occur at different times across the region. Specifically, moving toward an El Niño peak, precipitation is higher over East Africa during October-December (Indeje et al., 2000), then coincident with the El Niño peak at the end of the calendar year, dry conditions are found over Southern Africa during December-March (Dieppois et al., 2015). Following the El Niño peak, the relation between the March-May rains over East Africa and ENSO is weaker and only apparent over restricted regions (Indeje et al., 2000; Liebmann et al., 2014). Using the methodology developed in this thesis, which quantifies the seasonal regime at each point individually, this thesis investigates the impact of El Niño events on wet season characteristics across Africa, especially East Africa and Southern Africa. Using this methodology removes some of the 'noise' resulting from the conflation of season length and timing, giving a clearer signal. A particular aim is to spatially map the impact of El Niño events on seasonal timing and rainfall amount across Africa, and explore differing responses for individual El Niño events. This aim is addressed in Chapter 2.

1.3.2 Evaluate and identify deficiencies in representation of seasonality over Africa by climate models

Climate models are not only used for producing projections of future climate under elevated greenhouse gas concentrations, they are also used to explore and investigate physical processes and mechanisms. As noted in § 1.2.3, global climate models are not perfect representations of the climate system; some processes are excluded and others are parametrised, involving a number of simplifying assumptions. Such simplifications and resultant misrepresentation and errors can lead to models being unsuitable for the intended use. Model evaluation should be used to establish the adequacy of a climate model, which is strongly dependent upon the intended use, and therefore model evaluation should be specific to the purpose the model is intended for (Baumberger et al., 2017). Thus in order to use climate models to look at changing rainfall seasonality and the associated drivers, informative model evaluation requires the assessment of the representation of rainfall seasonality and associated physical processes in climate models.

At the present time, the majority of studies that analyse the representation of rainfall over Africa in coupled climate models either focus solely on fixed meteorological seasons (Brands et al., 2013; Kumar et al., 2014; Lee and Wang, 2014; Maidment et al., 2015; Mehran et al., 2014), or average the results over large spatial areas, smoothing out the variability (see § 3.1, e.g. Dike et al., 2015). Those studies that do analyse the seasonal cycle tend to focus on limited regions (§ 3.1, Liu et al., 2002; Tierney et al., 2015; Yang et al., 2015b; Dedekind et al., 2016). Very few studies have conducted assessments establishing how well onset and cessation are represented in the models, and those completed were performed over specific regions (see § 3.1). Hence, the third aim of this thesis is to evaluate and identify deficiencies in representation of seasonality over Africa by climate models.

One challenge regarding model evaluation concerns accounting for spatial/temporal biases in the mean state. A climate model may simulate a feature correctly but slightly shifted in space or time. Not taking into account such biases means that small temporal or spatial shifts in the representation of certain features can be interpreted as spurious or missing features (Allen and Ingram, 2002), and may degrade agreement in model projections (Levy et al., 2013). A number of approaches have been utilised to overcome this, for example, Allan (2012) characterised regimes based on the distribution of temperature and vertical motion, independent of location, while Levy et al. (2013) used brain morphing techniques to help account for geographical biases in the mean state.

Building on these studies that use dedicated approaches to overcome mean state biases,

here the aim is to account for temporal biases in this evaluation of rainfall seasonality. The method of Liebmann et al. (2012) (see § 1.3.1), on which this method is based, identifies the wet season with no timing assumptions imposed. Thus, by using this metric to evaluate rainfall seasonality, wet season timing and drivers can be compared across models where the wet seasons do not coincide exactly.

Under aim 2, the methodology developed under aim 1, which accounts for biases in the mean state, is exploited to conduct climate model evaluation assessing whether the CMIP5 models accurately represent rainfall seasonality over Africa, and therefore may be useful for exploring future changes and drivers of rainfall seasonality over Africa. This aim is addressed in Chapter 3.

1.3.3 Elucidate dynamical processes determining seasonality, its variability and climate model representation

As has been highlighted in previous sections, establishing robust future projections (§ 1.1.2, § 1.2.2), effectively analysing models (§ 1.2.3) and improving knowledge of the current pattern of seasonality (§ 1.1.3) all require good understanding of the meteorological phenomena and physical drivers that affect the seasonal cycle, an area that requires further investigation (Flato et al., 2013; James et al., 2017; Nicholson, 2018). Furthermore, having ascertained the deficiencies in the representation of precipitation seasonality over Africa in climate models (see § 1.3.2), determining which processes are well represented and which are not correctly captured is essential for further model development. Thus the third aim concerns identifying dynamical processes that drive the seasonality, and exploring their representation in climate models.

In particular, focus is on the representation of the precipitation seasonality over the southern West African coastline, a densely populated region with high dependence on seasonal rainfall. The mis-representation of monsoon systems, including the West African Monsoon, is a notable limitation of the current generation of global climate models (Cook and Vizy, 2006; Roehrig et al., 2013; Flato et al., 2013; Monerie et al., 2017; Steinig et al., 2018). Warm biases across the tropical Atlantic are a factor ubiquitous across many coupled climate models (Eichhorn and Bader, 2017), which combined with the sensitivity of the West African monsoon to SSTs (Vizy and Cook, 2001; Cook and Vizy, 2006) is thought to have an adverse effect on model representation of the monsoon. A number of studies have proposed links between the seasonal cycle of precipitation over the southern West African coastline and Gulf of Guinea SST (see § 3.4, 4.1), though few studies have examined the dynamical drivers of

the seasonality in this region. Hence the aim is to investigate the dynamical drivers of the seasonal cycle over the southern West African coastline, and the representation in climate models.

1.3.4 Interpret projected future changes in seasonal characteristics

Africa is vulnerable to the effects of climate change; future changes in precipitation have high potential for detrimental socio-economic impacts, particularly decreases in rainfall amount, or trends of increasingly sporadic rainfall (see § 1.1.2, § 1.2.2).

It is important to understand how onset and cessation, and other wet season characteristics will alter, in order to develop suitable adaptation strategies, which can act to mitigate much of the socio-economic impact if suitably designed. Previous analysis of future changes in African rainfall tend to focus on annual or seasonal means, neglecting the impact of the seasonal cycle (see § 5.1). Studies that do analyse future changes in the seasonality tend to consider regional averages, masking much of the spatial variability (see § 5.1). For example, in the most recent Intergovernmental Panel on Climate Change (IPCC) report projections for onset, retreat and duration of the main wet season were produced for a 'North African' and 'South African' region (Christensen et al., 2013), see Figure 1.3 below. This masks much of the spatial variability, and does not account for those regions that experience two wet seasons per year.

In addition to establishing trends in seasonality, identifying the processes that lead to the changes is key for advancing scientific understanding and furthering model development. Agreement with recent trends and drivers can also add credence to projected trends; thus the aim is to analyse observed trends over the recent period. This aim is addressed in Chapter 5.

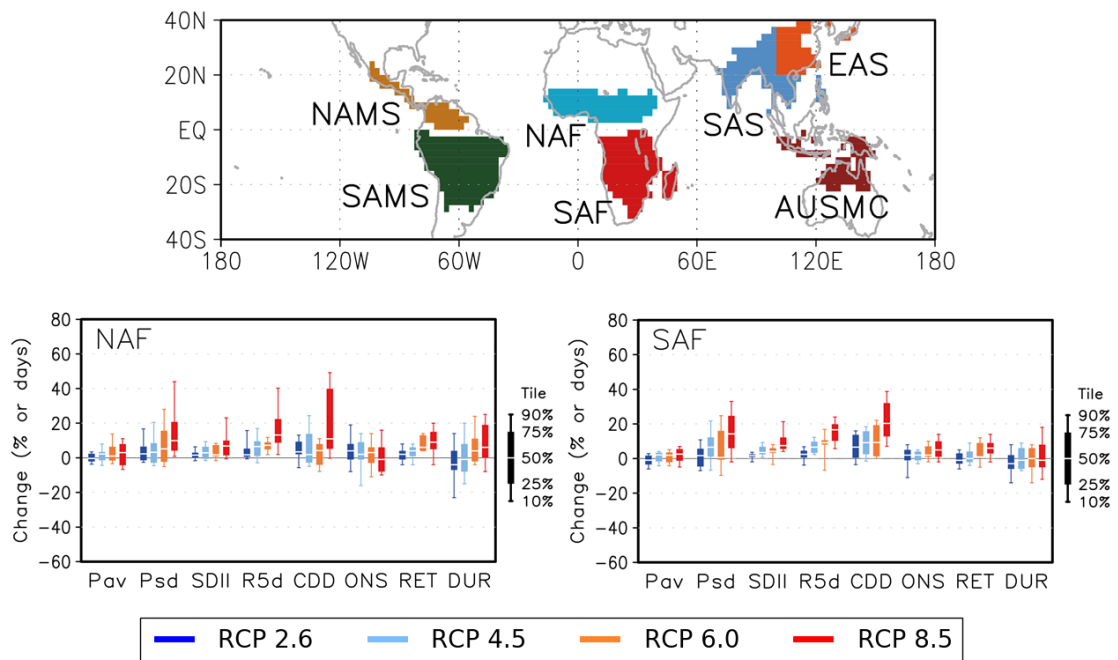


Figure 1.3 Changes in precipitation indices over the regional land monsoon domains (see map) of North Africa (left) and South Africa (right) based on CMIP5 multi-models. Projected changes for the future (2080-2099) relative to the present-day average in averaged precipitation (Pav), standard deviation of interannual variability in seasonal average precipitation (Psd), simple precipitation daily intensity index (SDII), seasonal maximum 5-day precipitation total (R5d), seasonal maximum consecutive dry days (CDD), monsoon onset date (ONS), retreat date (RET), and duration (DUR), under the RCP2.6 (18 models), RCP4.5 (24 models), RCP6.0 (14 models) and RCP8.5 scenarios (26 models). Units are % in Pav, Psd, SDII, R5d, and CDD; days in ONS, RET, and DUR. Box-whisker plots show the 10th, 25th, 50th, 75th and 90th percentiles. All of the indices are calculated for the summer season (May to September in the Northern Hemisphere; November to March in the Southern Hemisphere). The indices of Pav, Psd, SDII, R5d and CDD are calculated for each model's original grid, and then averaged over the monsoon domains determined by each model at the present day. The indices of ONS, RET and DUR are calculated based on the criteria proposed by Wang and LinHo (2002) using regionally averaged climatological cycles of precipitation. Figure 14.1 from Christensen et al. (2013).

1.4 Thesis outline

The remainder of this thesis is structured as follows:

Chapter 2 develops the methodology used to identify onset and cessation dates for regions with both one and two wet seasons per year across Africa. The onset and cessation dates are compared with known physical drivers and indigenous onset methods to establish if the methodology is accurately capturing the seasonal progression of rainfall over Africa. This is used to characterise current seasonality and to explore interannual variability in seasonality over the Horn of Africa and the relation with the El Niño Southern Oscillation and further utilised in Chapters 3 and 5.

In chapter 3, the representation of the seasonal cycle of precipitation over Africa in climate model simulations, produced as part of the CMIP5 process, is evaluated. Atmosphere-only and coupled climate model simulations are analysed separately and compared with observations. Discrepancies are identified in the coupled simulations, in particular over the Horn of Africa and the southern West African Coastline.

Chapter 4 concerns dynamical processes determining African precipitation seasonality. The focus is on the representation of the seasonal cycle of rainfall over the southern West African Coastline in the Met Office Unified Model and explores factors that may influence this and the wider continent. In addition to atmosphere-only and coupled simulations, the Global Ocean Mixed Layer configuration is utilised, to isolate the impact of including air-sea coupling and the role of the mean ocean state. Specific mechanisms related to the Little Dry Season are explored.

In chapter 5 the onset and cessation methodology presented in chapter 2 is used to analyse future changes in seasonal characteristics across Africa. In addition to onset and cessation, future projections of metrics of rainfall intensity are also considered and compared against recent trends. Changes are associated with physical mechanisms, including the seasonal progression of the tropical rain belt and the Saharan Heat Low.

Chapter 6 explores the wider implications of the main conclusions from chapters 2- 5. The major advances are presented, along with proposed directions for future work.

Chapter 2:

The onset and cessation of seasonal rainfall over Africa

In order to address the overall aim to improve capability for robust projection of user-relevant rainfall characteristics over Africa the first challenge concerns the quantification of 'user-relevant rainfall'. As explained in §1.3.1 the facet of 'user-relevant rainfall' investigated here is the seasonality of rainfall, advancing the work of previous studies such as Liebmann et al. (2012) and Cook and Vizzy (2012).

In this chapter the method is presented, and tested using observational datasets. Thus this chapter addresses the first aim to 'Develop a method to capture and characterise seasonality in rainfall'. This methodology will also be used to evaluate the representation of seasonality over Africa by climate models (aim 2, §3) and produce future projections (aim 4, §5), thus it is important that the method is applicable across datasets with contrasting rainfall biases, which is addressed in this chapter.

This chapter also includes characterisation of observed seasonality, an important requirement prior to the evaluation of climate model representation in §3. One application of the methodology is given, namely an investigation of the role of the El Niño Southern Oscillation on precipitation seasonality, which adds a new aspect to the existing literature on the impact of ENSO on African rainfall (Indeje et al., 2000; Black et al., 2003).

This chapter has been published in *Journal of Geophysical Research: Atmospheres* (Dunning et al., 2016) and the Supplementary Information can be found at <https://agupubs.onlinelibrary.wiley.com/doi/full/10.1002/2016JD025428>.

The onset and cessation of seasonal rainfall over Africa

Caroline M. Dunning, Emily C.L. Black, Richard P. Allan

Key Points:

1. Diagnosed patterns in onset/cessation of African rainy seasons, produced using an adapted method, are compatible with physical drivers
2. Consistent onset/cessation characteristics in satellite-based rainfall data, ERA-I deficient for biannual regime
3. Rainy season cessation over the Horn of Africa is 7 days later in El Niño years, 5 days earlier in La Niña

Abstract

Variation in the seasonal cycle of African rainfall is of key importance for agriculture. Here, an objective method of determining the timing of onset and cessation is, for the first time, extended to the whole of Africa. The method is applied to five observational datasets and the ERA-Interim reanalysis. Compatibility with known physical drivers of African rainfall, consistency with indigenous methods, and generally strong agreement between satellite-based rainfall datasets confirm the method is capturing the correct seasonal progression of African rainfall. The biannual rainfall regime is correctly identified over the coastal region of Ghana and the Ivory Coast. However, the ERA-Interim reanalysis exhibits timing biases over areas with two rainy seasons, and both ERA-Interim and the ARCV2 observational dataset exhibit some inconsistent deviations over West Africa. The method can be used to analyze both seasonal - interannual variability and long-term change. Over East Africa, we find that failure of the rains and subsequent humanitarian disaster is associated with shorter as well as weaker rainy seasons, e.g. on average the long rains were 11 days shorter in 2011. Cessation of the short rains over this region is 7 days later in El Niño and 5 days earlier in La Niña years with only a small change in onset date. The methodology described in this paper is applicable to multiple datasets and to large regions, including those that experience multiple rainy seasons. As such, it provides a means for investigating variability and change in the seasonal cycle over the whole of Africa.

2.1 Introduction

Much has been postulated on past changes in African rainfall, including changes in the timing of the seasonal cycle and shifts in the beginning and end of the wet seasons. Anecdotal

evidence from farmers in the region of West Africa south of the Sahel suggests a forward shift in the onset of the rainy season (Van de Giesen et al., 2010). However, evidence of this type is not always indicative of meteorological changes (e.g. Rao et al., 2011), and other studies of this region found no significant trend (Sanogo et al., 2015). Future changes in tropical circulation patterns may alter the seasonality, and lead to increasing uncertainty in the timing of rainy seasons (Feng et al., 2013). For example, the northward extension of rainfall and increase in August rainfall in the Sahel (Dong and Sutton, 2015; Sanogo et al., 2015) may be related to the reduction in August rainfall south of the Sahel (Sanogo et al., 2015) and changes in the onset and duration of the 'little dry season' that occurs along the West African coast during the summer months (Okoloye et al., 2014).

In order to assess whether the seasonality is indeed undergoing large scale shifts and to attribute potential drivers, a generally applicable method of identifying the onset and cessation of the wet season is required. Many previous studies examining the nature of the onset and cessation of rainfall have been conducted, but for the most part, these have focused on the national to regional scale (Liebmann et al., 2012). Relating changes and variability in seasonality to wider scale drivers and physical mechanisms demands a method for determining onset that is applicable across the entirety of continental Africa that experiences a wet season, including those regions with two seasons per year. The method must robustly capture the seasonal cycle across Africa in an automated manner across multiple datasets in order to be applicable to the evaluation and interpretation of climate model simulations.

We present a new method for determining onset and cessation in regions, such as the Horn of Africa that experience two wet seasons per year (Lyon and DeWitt, 2012). This, combined with the onset method of Liebmann and Marengo (2001) and Liebmann et al. (2012), allows onset and cessation dates to be objectively derived for the whole of Africa. The recent publication of daily precipitation datasets for Africa for periods longer than 30 years allows for analysis of variability, which was not possible in the study of Liebmann et al. (2012) due to the short records. This is especially relevant in the context of recently described discrepancies between observed African rainfall datasets, including rainfall underestimation over West Africa (Maidment et al., 2015, 2014; Tarnavsky et al., 2014), and the effect of observational coverage on perceived long-term change in tropical rainfall (Balan Sarojini et al., 2012). Understanding variability and change is essential for interpreting recent changes in African rainfall (Lyon and DeWitt, 2012; Lott et al., 2013). Assessing whether datasets which exhibit different rainfall biases are consistent in seasonality offers greater understanding of different precipitation datasets, and their relative strengths (Awange et al., 2016). The

relative paucity of gauge based data over Africa often results in the use of reanalysis rainfall data (Fitzpatrick et al., 2015; Mounkaila et al., 2015; Shongwe et al., 2015; Yang et al., 2015b), which is compared here alongside satellite-based precipitation estimates.

The remainder of the paper is structured as follows; in section 2 the method and its implementation are described. Section 3 compares the seasons identified firstly to those expected from the published literature on the dynamical drivers of African rainfall and secondly to agriculturally defined seasons. Section 4 demonstrates the applicability of this definition of seasonality to six datasets. Section 5 gives an example of how this method can be used to explore variability. Section 6 contains the discussion and conclusions.

2.2 Methodology and Datasets

2.2.1 Datasets

For this study we require multiple precipitation datasets, at daily resolution, for the entirety of continental Africa. In order to assess whether the method is applicable across datasets with varying rainfall amounts and intensity we have chosen datasets to encompass a range of methodologies of rainfall estimation. Only those that are available for a sufficient period to analyze variability (at least 15 years) were considered. Due to the limited availability of daily rain gauge data (see <http://www.ecmwf.int/en/forecasts/charts/monitoring/dcover>), five gridded combined satellite/gauge-based estimates and one reanalysis product are used. The datasets and main characteristics are summarised in Table 2.1.

African Rainfall Climatology version 2 (ARCV2) is a daily precipitation estimation dataset produced by the National Oceanic and Atmospheric Administration Climate Prediction Centre

Data	Inputs	Spatial Resolution	Period Used	Reference
TARCATv2	TIR	0.0375°	1984-2014	Maidment et al. (2014)
ARCV2	IR, gauges	0.1°	1983-2013	Novella and Thiaw (2013)
GPCP	TIR, PMW, gauges	1°	1997-2014	Huffman et al. (2001)
TRMM 3B42	TIR, VIS, PMW, radar, gauges	0.25°	1998-2014	Huffman et al. (2007)
CHIRPS	CHPClim, TIR, TRMM 3B42, CFSv2, gauges	0.05°	1981-2014	Funk et al. (2015)
ERA-Interim	ECMWF Forecast System	0.75°	1983-2014	Dee et al. (2011)

Table 2.1 Description of some of the characteristics of the datasets of African precipitation used in this study. TIR = Thermal InfraRed Imagery, IR = InfraRed Imagery, PMW = passive microwave, VIS = visible, CHPClim = monthly precipitation climatology, CFSv2 = atmospheric model rainfall fields from the NOAA Climate Forecast System version 2.

(NOAA/NCEP/CPC) for use in famine early warning systems (Novella and Thiaw, 2013). ARCV2 uses infrared data, from the 3-hourly geostationary EUMETSAT (European Organization for the Exploitation of Meteorological Satellites) satellite, and gauge observations from the Global Telecommunication System (GTS). In addition to thermal infrared (TIR) and rain gauge data, the Global Precipitation Climatology Project (GPCP) dataset also uses passive microwave (Huffman et al., 2001). This dataset, however, is available at lower resolution (1° compared to 0.1°), and is only available from 1997 at daily resolution, whereas ARCV2 extends back to 1983. Similarly, the Tropical Rainfall Measuring Mission (TRMM) Multisatellite Precipitation Analysis (TMPA) is also only available from 1998. Here we have used the 3B42 research derived daily product, formed of three-hourly combined microwave-infrared (IR) estimates (with gauge adjustment) and monthly combined microwave-IR-gauge estimates of precipitation (Huffman et al., 2007).

The Climate Hazards Group InfraRed Precipitation with Stations (CHIRPS) dataset also uses TIR imagery and gauge data, in addition to a monthly precipitation climatology, CHPClim, and atmospheric model rainfall fields from the NOAA Climate Forecast System, version 2 (CFSv2) (Funk et al., 2015). Despite CHIRPS being available at higher resolution (0.05° compared with 0.25°), CHIRPS also includes TRMM 3B42, therefore we expect to find similarities between these datasets after 1998, when TRMM becomes available, whereas CHIRPS extends back to 1983. CHIRPS is the only dataset used which includes a monthly climatology.

In common with previous datasets, the TAMSAT (Tropical Applications of Meteorology using SATellite data and ground-based observations) African Rainfall Climatology and Time series (TARCATv2) dataset uses TIR to give precipitation estimates, however, unlike the previous datasets, gauge observations are used only for the spatially varying time invariant calibration, whereas the other datasets, such as ARCV2, merge in contemporaneous gauge data (Maidment et al., 2014; Tarnavsky et al., 2014).

ERA-Interim (ERA-I) reanalysis simulated precipitation was also used. ERA-I is a reanalysis of the global atmosphere produced using the European Centre for Medium Range Weather Forecasts' (ECMWF) Integrated Forecast System combined with data assimilation (Dee et al., 2011). Here, 12-hourly total precipitation on a 0.75° grid was used.

For this analysis, all the datasets have been interpolated onto the GPCP 1DD grid, and have a spatial resolution of 1° . All the observational datasets are at daily resolution, and ERA-I was converted from 12-hourly to daily resolution.

2.2.2 Extension of the Liebmann Method for all of Africa

In this study, the method used by Liebmann et al. (2012) to produce a precipitation climatology for the entire African continent was employed to identify the onset and cessation. This method has been used over Kenya and Tanzania for observational datasets (Boyard-Micheau et al., 2013; Camberlin et al., 2009) and to assess regional climate models over West Africa (Diaconescu et al., 2015). The method is described below in sections 2.2.2.1-2.2.2.3. Their method for finding onset was based on that of Liebmann and Marengo (2001) and has three stages. Firstly harmonic analysis applied to the whole timeseries for each grid point is used to determine if one or two wet seasons are experienced per year. The start and end of the period when the wet season usually occurs is then found; this is termed the 'climatological water season'. The onset and cessation in each individual year is then found. The onset and cessation dates are determined by finding the minima and maxima, respectively, in the cumulative daily precipitation anomaly, which increases when the daily precipitation is above the climatological mean daily rainfall, and decreases when the daily precipitation is below the climatological mean daily rainfall.

When considering the Horn of Africa, Liebmann et al. (2012) defined the broad seasons when the long and short rains are expected to occur, as their method did not determine the seasons when rainfall occurs for regions with two wet seasons per year. They did not examine the onset and cessation over other regions that experience two wet seasons a year, such as the West Africa southern coastal region (coast of Ghana and the Ivory Coast; region 4 in Figure 2.4). Thus, in this study, an alternative method is proposed for the first time to find the two periods when the wet seasons usually occur over such regions. The onset and cessation for each individual season is then found using the same method as that used for finding one season.

The following 3 sub-sections detail this application of the method of Liebmann et al. (2012). Firstly, harmonic analysis used to determine the number of seasons is described, followed by the method used for regions with one wet season per year, and finally the new adaptation of the method of Liebmann et al. (2012) for two season regions.

2.2.2.1 Categorising the Seasonality

Harmonic analysis was used to define the number of wet seasons experienced per year. Here, we describe regions that experience one wet season per year as having an annual regime, and regions that experience two wet seasons per year as having a biannual regime. For the small area in Ethiopia that experiences three wet seasons per year, only the two longest were

considered, and it was classified as biannual. For each grid point, the amplitude of the first and second harmonics were computed. Figure 2.1a-b show the amplitude of the first and second harmonics respectively for the TARCATv2 dataset. The ratio of the amplitude of the second harmonic to the amplitude of the first harmonic (Figure 2.1c) was used to determine the seasonality (similar results were found for all six datasets; Figure S1 in Supplementary Information). A ratio greater than 1.0 indicated a biannual point, and a ratio less than 1.0 indicated a point with an annual regime. This contour is marked on Figure 2.1c as a dashed line. For locations which experience one short season with very low rainfall totals the second harmonic may fit the data better, thus giving a higher ratio even though there is just one wet season (Liebmann et al., 2012), therefore results over regions such as the Sahara need to be carefully analysed. The harmonic analysis approach is similar to that used in Liebmann et al. (2012) to determine the number of wet seasons per year over Africa, although they used threshold ratios of both 0.75 and 4.0 and monthly rather than daily precipitation data. The method has also been utilised for other applications; Yang and Slingo (2001) used Fourier analysis in their examination of the diurnal cycle in convection over the Tropics.

Visually, all the datasets appear to show the same patterns and identify broadly similar regions as biannual in agreement with other studies (e.g. the Horn of Africa (Camberlin et al., 2009; Yang et al., 2015a), a zonal equatorial strip extending from Uganda to Equatorial Guinea (Diem et al., 2014), and a small region on the southern West African coastline (Sultan and Janicot, 2003; Liebmann et al., 2012; Herrmann and Mohr, 2011; Sylla et al., 2010)) suggesting that this method is successfully identifying regions with two wet seasons per year. Herrmann and Mohr (2011) defined the number of seasons using monthly precipitation and temperature data and also found a small region on the southern West African coastline and the Horn of Africa have two wet seasons, although they defined the equatorial strip as humid with no seasonal cycle, whereas here it has been defined as having two seasons. Nicholson (2000) highlighted a much wider area as having two seasons than that found here yet identified areas with a biannual regime having a rainfall maxima in the austral or boreal summer, rather than in transition seasons, as would be expected (Washington et al., 2013). Comparison of the region shown as having a rainfall maxima in transition seasons in Nicholson (2000) with the area that experiences a biannual regime found here gives much better agreement. Figure 2.1c also shows a high ratio over parts of the Sahara and north Africa, but this is due to low rainfall, as described above. ARCV2, TARCATv2, TRMM and ERA-I also identify the south west tip of Africa as biannual; this is again thought to be due to the dry climate (Herrmann and Mohr, 2011; Nicholson, 2000).

The ratio maps for the six datasets were compared using Pearson Pattern Correlation (PPC) and Mean Absolute Error (MAE). MAE values are between 0.6-0.7, with all datasets performing similarly. The PPC coefficients are between 0.16-0.63, with all but the correlation between GPCP and ARCV2 (0.16) significant at the 99% level. Examining the pattern correlation for the amplitude of the first and second harmonics individually gave higher correlations, with values of 0.84-0.96 for the first harmonic, and 0.63-0.87 for the second harmonic. In summary, using harmonics to determine the number of wet seasons has produced results similar to those in other studies, and all the datasets give consistent results showing a small region on the southern West African Coastline, the Horn of Africa and the equatorial strip as the biannual regions.

2.2.2.2 Diagnosing onset and cessation for annual regimes

The method used to determine the onset and cessation at grid points with an annual regime described here is as in Liebmann et al. (2012). Initially, the period of the year when the wet season occurs, termed the 'climatological water season', must be determined, to account for those seasons that span calendar years. First the climatological mean rainfall for each day of the calendar year, Q_i , where i goes from 1 January to 31 December, is computed (red line in Figure 2.2), and the climatological annual mean rainfall \bar{Q} (mm/day). From this the climatological cumulative daily rainfall anomaly on day d , $C(d)$, is found:

$$C(d) = \sum_{i=1 \text{ Jan}}^d Q_i - \bar{Q} \quad (2.1)$$

where i ranges from 1 January to the day (d) for which the calculation applies. In this example, $C(d)$ is calculated for each day from 1 January to 31 December. Figure 2.2 shows ($Q_i - \bar{Q}$)

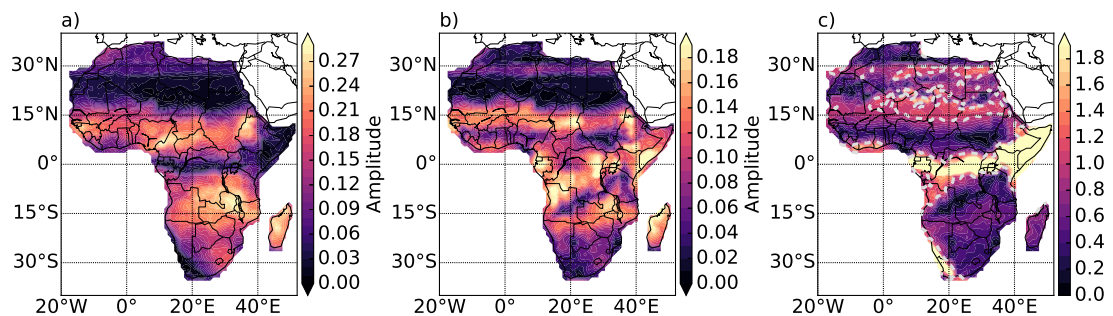


Figure 2.1 Amplitude of the harmonics at frequency of one (a) and two (b) cycles per year for each grid point in TARCATv2 (1984-2014). The ratio of the amplitudes (b/a) is shown in (c). The dashed contour in (c) marks where the ratio is equal to 1.0.

as a blue line, and $C(d)$ as a green line. The day of the minimum in C marks the beginning of the climatological water season, d_s , and the maximum marks the end, d_e .

In the second stage the onset dates are calculated individually for each year, by computing the daily cumulative rainfall anomaly on day D , $A(D)$:

$$A(D) = \sum_{j=d_s-50}^D R_j - \bar{Q} \quad (2.2)$$

where R_j is the rainfall on day j , and j ranges from $d_s - 50$ to the day being considered (D). $A(D)$ is calculated for each day from $d_s - 50$ to $d_e + 50$ for each year. The day after the minimum in $A(D)$ is the onset, as after this the rainfall is persistent in occurrence, duration and intensity (Diaconescu et al., 2015) and the day of the maximum (after the minimum) is the cessation date. Since the climatological water season may potentially span multiple calendar years the onset and cessation is not computed for the first and last year of each record.

2.2.2.3 Diagnosing the onset and cessation for biannual regimes

For points where there are two wet seasons per year, a different method is required in order to determine the periods of the year when wet seasons, or 'climatological water seasons',

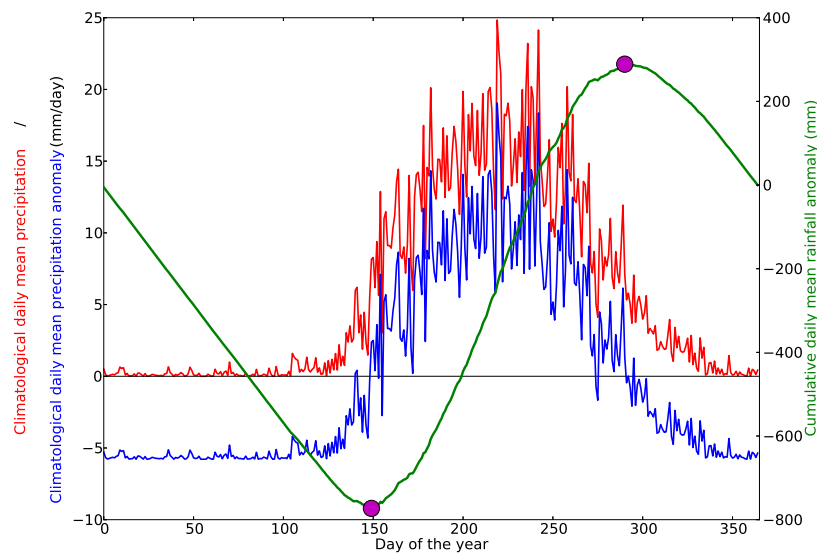


Figure 2.2 Climatological daily mean rainfall for each day of the year (red), climatological daily mean rainfall anomaly (blue) and climatological cumulative daily mean rainfall anomaly (green) for 9.5 ° N, 14.5° W from GPCP averaged over 1997-2014. The magenta dots mark the extent of the 'climatological water season'.

occur (Figure 2.3). This part of the method is proposed for the first time in this paper. The climatological cumulative daily rainfall anomaly $C(d)$ (green line in Figure 2.3, calculated in the same way as above) for each point is smoothed using a 30 day running mean ($S(d)$, purple line). Minima/maxima in the smoothed curve are detected by identifying days where $S(d)$ is lower/higher than the 4 preceding days and lower/higher than the 4 following days (Figure 2.3a). A number of periods were considered, and 4 days was chosen as it gave enough minima and maxima to identify the season, but did not erroneously place minima and maxima mid-season. For each minima, the first following maxima is located, and is assumed to end that season. The two longest seasons are assumed to be the two seasons of interest. Thus in Figure 2.3, the two main seasons are selected and the other minima and maxima found by the method are discarded. This gives two season start and end dates, d_{s1} , d_{e1} , d_{s2} and d_{e2} .

These seasons are then considered separately, and the individual onset and cessation dates are found using the second part of the one season method:

$$A(D) = \sum_{j=d_{s1}-20}^D R_j - \bar{Q} \quad (2.3)$$

where R_j is the rainfall on day j , and j ranges from $d_{s1} - 20$ to the day being considered (D). $A(D)$ is calculated for each day from $d_{s1} - 20$ to $d_{e1} + 20$, and for each day from $d_{s2} - 20$ and $d_{e2} + 20$, for each year. A shorter period of 20 days (as opposed to 50 used above) was used to ensure the correct season was captured, as the intervening dry periods between multiple wet seasons may be shorter than 100 days, for example, over the West Africa southern coastal region the 'little dry season' occurs during July and August only. Minima and maxima in $A(D)$ were again used to identify onset and cessation dates.

The first and second seasons were objectively split using the start date of the 'climatological water seasons'; the season that started between 31 May and 27 October was considered to be the second rainy season, and the other was considered to be the first rainy season. The long length of this window is designed to capture the start of the second season over West Africa in August -September and the onset over Kenya in October. Over Kenya and East Africa these are referred to as the 'short' rains and 'long' rains respectively, and this terminology is used when discussing this area.

2.2.3 Regions

Africa was divided into a number of regions (Figure 2.4). Regions were chosen such that they experienced an annual or biannual regime consistently across all datasets; grid points

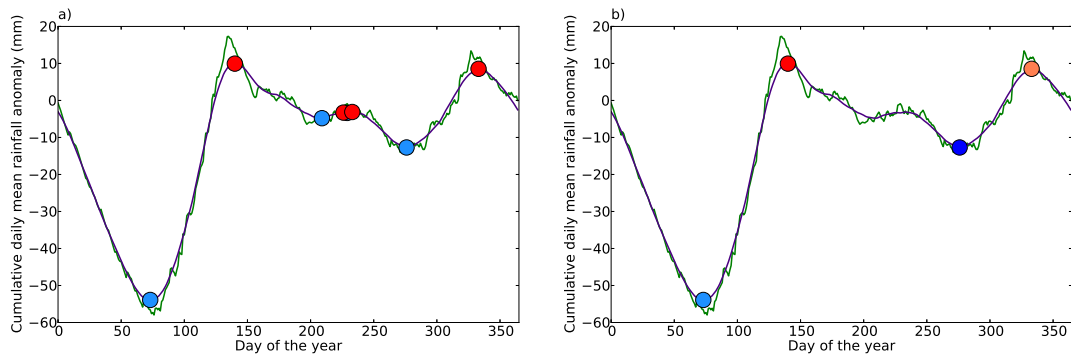


Figure 2.3 Climatological cumulative daily mean rainfall anomaly (green) and climatological cumulative daily mean rainfall anomaly smoothed using a 30 day running mean (purple) for 34.5° E, 3.5° N from GPCP averaged over 1997-2014. The blue (red) dots in (a) mark the minima (maxima) found using the method detailed in section 2.2.2.3. The light and dark blue dots in (b) mark the beginning of the two seasons, while the red and orange dots mark the end of the two seasons.

with conflicting definitions are shaded in pink in Figure 2.4 and have not been included. Two regions have been excluded; north of 15° N is predominantly arid over the Sahara Desert, so there is no pronounced wet season, and the Mediterranean region shows very large differences between the datasets (shaded in dark purple in Figure 2.4) due to the dry climate resulting in few datasets giving values here (see Figs S2 and S3 in Supplementary Information). The biannual region over the Democratic Republic of the Congo, Uganda and Gabon has also not been considered (shaded in light purple in Figure 2.4); this region is known to be humid, and therefore may not exhibit a dry season in all years (Herrmann and Mohr, 2011) and shows large variation between the different datasets (see section 2.4). Seasonality is less important in such regions, due to higher rainfall totals and more continuous precipitation. A small area covering southern Gabon and the Republic of the Congo, shown in orange as it has an annual regime, was not included as it is separated from region 12 by grid points with conflicting definitions. The regions were also chosen to contain broadly contemporaneous onset and cessation dates. Regions 1-3, 5-7, and 11-17 experience an annual regime (orange in Figure 2.4) and regions 4 and 8-10 experience a biannual regime (yellow in Figure 2.4). The mean spatial standard deviation for onset and cessation over each region was computed to confirm spatial homogeneity in each region. With the exception of region 16 (covering central and eastern South Africa), all regions had mean spatial standard deviation for onset of less than 30 days, and less than 20 days for cessation. Plotting median cessation against median onset showed good clustering of points by region (not shown), with some outliers for region 16. Thus, the regions were considered satisfactory for this analysis of continental scale patterns, with extra consideration required for region 16. While the majority of South Africa experiences a single wet season during austral summer, the south coast of South Africa

experiences rainfall throughout the calendar year, and the western part receives winter rainfall (Engelbrecht et al., 2015; Weldon and Reason, 2014). While exclusion of regions containing conflicting definitions (pink in Figure 2.4) removes much of the winter rainfall regime, the large variability is likely to be a consequence of the inclusion of differing rainfall regimes. Region 4 is referred to throughout as the West African southern coastal region.

2.3 Physical Relevance of the Seasonality Metric

Previous work has demonstrated the stability of the method described in section 2.2.2.2 for capturing onset and cessation dates (Liebmann et al., 2012; Boyard-Micheau et al., 2013). This is further discussed in section 2.4. Here we assess the physical relevance of this quantity as a metric for seasonality of African rainfall. Firstly, we examine the agreement between our results and two of the main physical drivers of African rainfall, namely seasonal progression of the rainband associated with the Intertropical Convergence Zone (ITCZ) and the West African Monsoon. Secondly, the consistency with agriculturally based definitions of the seasonal cycle is assessed, via comparison with local, threshold-based onset methods which have been

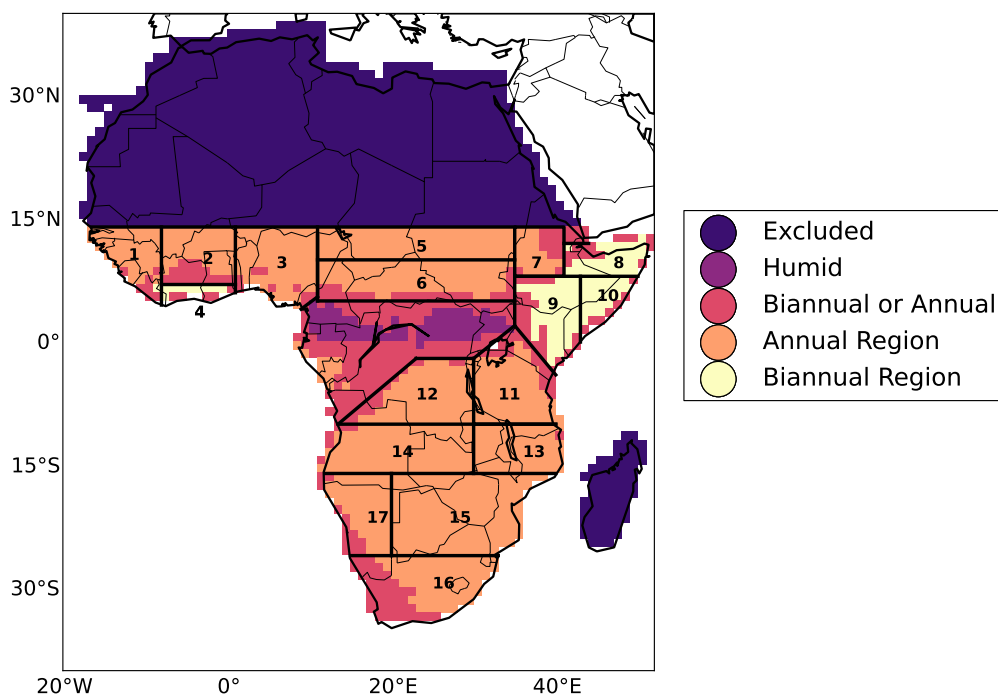


Figure 2.4 Regions used for analysis (1-17). Dark purple indicates areas excluded, pink indicates regions that are defined as annual and biannual in different datasets and light purple indicates the humid region of central Africa. Orange regions are annual regime regions and yellow regions are biannual regions.

designed with agricultural applicability in mind.

2.3.1 Movement of the ITCZ/ Tropical Rain Belt

Seasonal progression of the rainband associated with the ITCZ, or tropical rain belt, is the main driver of the seasonal cycle of precipitation for the majority of Africa. Our results for the climatological seasonal cycle are compared against published literature on the ITCZ and Tropical Rain Belt. The focus is predominantly on regions with a biannual regime.

Figure 2.5 shows the onset of the second and first rains plotted with the onset of the southern and northern single wet seasons respectively, and the cessation of the second and first rains plotted with the cessation of the northern and southern single seasons respectively. The contour marked shows the position of the annual/biannual boundary. The progression of the tropical rain belt appears to be spatially continuous with no marked artificial shifts (e.g. along the annual/biannual boundary) and no large spurious discrepancies between neighbouring grid points. This demonstrates that the onset dates identified by the biannual method are compatible with those found using the method for annual regimes. However, rapid progressions (or 'jumps') that are present in reality are captured (Hagos and Cook, 2007).

During the austral spring the tropical rain belt travels south, bringing the second rainy season and then the wet season over southern Africa. Figure 2.5d shows a continuous progression from the onset of the second rains over central Africa and the Democratic Republic of the Congo into the rest of southern Africa, beginning on 27 August on average at 20.5°E, 0.5°S, and later onset in the east and over the Horn of Africa, with onset occurring on 8 October (on average) at 43.5°E, 4.5°N, consistent with the pattern found in Liebmann et al. (2012). The end of the northern wet season progresses zonally southward with the cessation of the second rains following in a similar manner (Figure 2.5b). The onset of the first rains over the West Africa southern coastal region in the late boreal spring merges well with the onset of the wider West African Monsoon (Figure 2.5a), and the cessation of the first rains follows the retreat of the rainfall over southern Africa, starting at the Zimbabwe, Mozambique, South Africa border on the 4 March, and reaching Equatorial Guinea (10.5°E, 1.5°N) on 23 May (Figure 2.5c). Both the zonal pattern of onset over West and central Africa, and the radial pattern over southern Africa are well matched and consistent with the first rains onset and cessation.

Figure 2.6 contains the onset and cessation for the 17 regions shown in Figure 2.4. These results are consistent with published onset and cessation dates in the literature for East Africa (Ngetich et al., 2014; Camberlin et al., 2009), the West Africa southern coastal region

(Thorncroft et al., 2011; Adejuwon and Odekunle, 2006; Nguyen et al., 2011; Sultan and Janicot, 2003; Nicholson, 2013) and southern Africa (Shongwe et al., 2015; Kniveton et al., 2009).

2.3.2 Consistency with West Africa Monsoon Dynamics

In West Africa the seasonal cycle is driven by the monsoon. Figure 2.6a shows the mean onset and cessation for regions 1-6 (see Figure 2.4) from all six datasets. Region 4 (West Africa southern coastal region) experiences two wet seasons per year, 1-3 and 5-6 experience an annual regime.

The onset of the first rains and cessation of the second rains over the West Africa southern coastal region merges well with the wider onset and cessation over West Africa (Figure 2.5a-b). The onset of the West African Monsoon is comprised of two stages; the pre-onset and onset (Sultan and Janicot, 2003). During late boreal spring the Intertropical Front (ITF), which

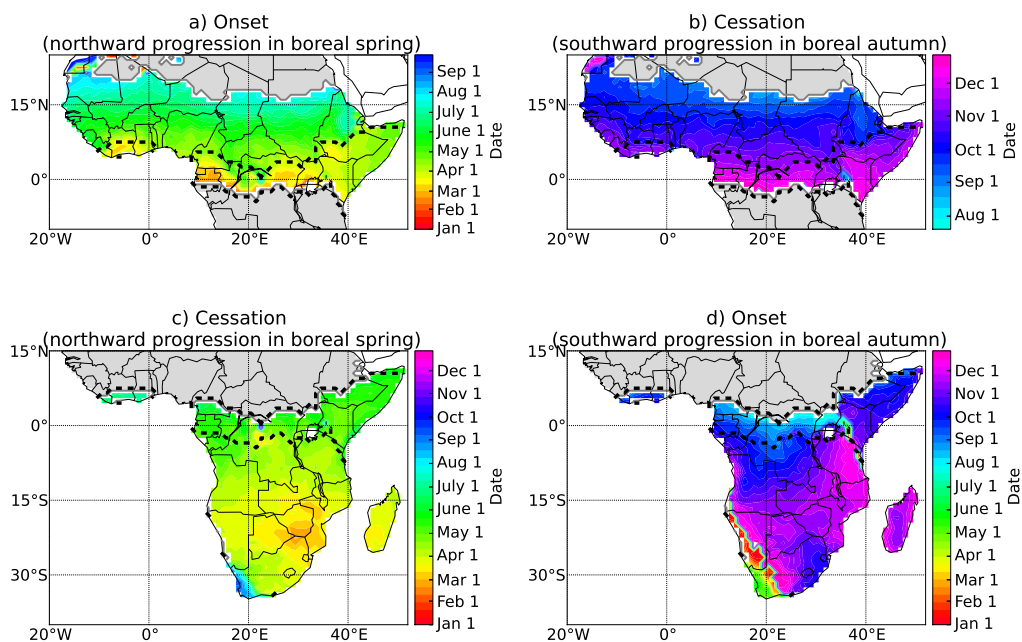


Figure 2.5 Southward and northward progression of onset and cessation across the annual/biannual boundaries. a) shows the northward progression of onset in boreal spring from onset of the first/long rains into onset of the West African Monsoon. b) shows the southward progression of cessation in boreal autumn from the cessation of the West African Monsoon into the end of the second/short rains. d) shows the southward progression of onset in boreal autumn, from the onset of the second/short rains into the onset of the annual rains over southern Africa. c) shows the northward progression of cessation in boreal spring from the end of the annual rains over southern Africa into the end of the first/long rains. These were computed using the GPCP dataset over 1998-2013. Grey indicates regions not considered for these plots.

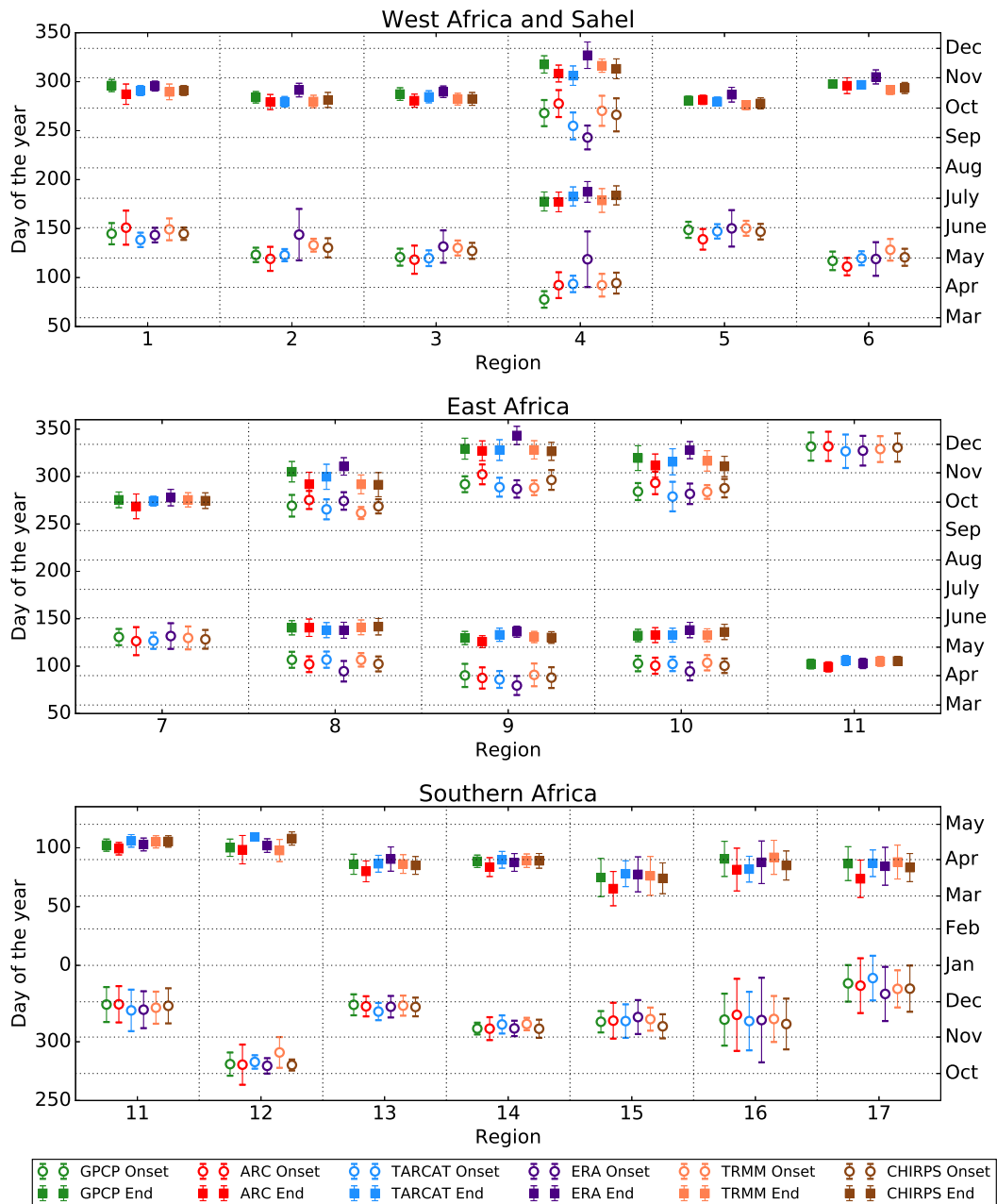


Figure 2.6 Mean and standard deviation of the mean onset and cessation date for each dataset over the regions in Western (regions 1-6), Eastern (regions 7-11) and Southern Africa (regions 11-17) Africa (a,b,c respectively).

marks the northern limit of the south-westerly monsoon winds, migrates northward, while the ITCZ remains south of West Africa. This initiates local convection, and the beginning of the first wet season on the southern coastline, around early April. Onset over region 4 is around 17 March - 27 April, consistent with the mid-April onset of the coastal phase found in Thorncroft et al. (2011).

Later, during the boreal summer, the ITCZ abruptly shifts north, bringing the onset of the monsoon rains across the rest of West Africa. At this time, there is a decline in the rainfall along the coast, known as the 'little dry season', which occurs from mid-July into August (Adejuwon and Odekunle, 2006). After the onset in region 4, onset commences in the surrounding regions (1-3, 5-6) and the first wet season over the West Africa southern coastal region ends around 25 June - 5 July (Figure 2.6a). Adejuwon and Odekunle (2006) found the start of the 'little dry season' over SW Nigeria between 15 and 25 July, Sultan and Janicot (2003) showed it beginning around early July at 5°N, and Nguyen et al. (2011) found the demise of the coastal rainfall occurred on 26 June, consistent with the dates shown in Figure 2.6a. Successfully capturing the 'little dry season' is a strength of this method. At the end of the boreal summer, as the monsoon retreats equatorward, the wet season terminates over West Africa and the coastal region experiences a second rainfall peak from August/September until early November (Sultan and Janicot, 2003; Nicholson, 2013; Thorncroft et al., 2011).

Figure 2.6a shows that as the monsoon season ends over regions 1-3 and 5-6, a second wet season occurs over the West Africa southern coastal region. Zhang and Cook (2014) found monsoon demise over the Sahel ranging from 5 October to 30 October, consistent with the October cessation dates found for regions 1-3 and 5-6 in Figure 2.6a. They also noted a later demise in western coastal Sahel, in comparison with central and eastern regions, also apparent in our results, which can be seen by comparing the cessation dates over Sierra Leone with the same latitude in Nigeria (Figure 2.5b). The second wet season over the West Africa southern coastal region starts around 30 August - 3 October, consistent with Sultan and Janicot (2003) who find a start around August/September and Adejuwon and Odekunle (2006) who find the end of the 'little dry season' between 29 August and 8 September. The similarity between our results and those of Sultan and Janicot (2003) is particularly noteworthy, given their use of station-based rainfall. The end of this second wet season marks the end of the West African Monsoon, around 1 - 22 November (Figure 2.6a), which can be seen in Figure 2.5b.

2.3.3 Comparison with other methods for identifying the onset

The previous sub-sections have demonstrated that this method identifies seasons that are consistent with dynamical drivers of African rainfall. In order to evaluate consistency with agricultural definitions of the seasonal cycle, we compare our results against two other onset methods, calibrated locally and designed to identify the start of the growing season.

1. The first method is that of Marteau et al. (2009), which is based on a threshold of 20mm being exceeded over 1-2 days, with no 7 day dry period in the following 20 days.
2. The second method is a combination of Issa Lélé and Lamb (2010) and Yamada et al. (2013), which requires a rainfall rate of large enough magnitude to be societally useful (3-4mm/day) over a longer period (14 days).

This comparison was completed over all grid points in 9°N - 15°N and 0° - 20°W, which is the area used in Marteau et al. (2009). Since both local onset methods do not consider the period prior to 1 May, the same limit was applied to all methods, for the purpose of this comparison. The agreement between the two local onset methods was good, with a PPC coefficient of 0.97, and an MAE value of 12.5 days (on average). Agreement with the method presented here was also good, with correlation values of 0.84 and 0.9 for Marteau et al. (2009) and Issa Lélé and Lamb (2010) respectively. The MAE values were 16.8 days and 8.41 days (on average) for Marteau et al. (2009) and Issa Lélé and Lamb (2010) respectively. This indicates that the onset dates given here do coincide with indigenous methods. The similarity of values found when comparing the two local methods and those when this method was used confirm that the differences are not much larger when the method of cumulative anomalies is used.

In this section it has been demonstrated, through comparison with known physical drivers of African seasonal rainfall, and previously used onset methods, that the method for determining the onset and cessation of the wet season detailed above is able to capture the correct physical progression of the seasonal rainfall across both annual and biannual regions of Africa.

2.4 Evaluation over a range of datasets

This method is designed to account for systematic bias in variability and amount, so that identified discrepancies between datasets relate primarily to differences in their representation of the seasonality of rainfall. In this section we assess these features by comparing onset and cessation dates from six datasets of African precipitation. Mean onset and cessation dates and their temporal variability across all datasets are displayed in Figure 2.6 for Western,

Eastern and Southern Africa. Temporal variability in onset and cessation is quantified as the interannual standard deviation of the mean date across each region for each dataset, depicted in Figure 2.6 as error bars. Figures containing the mean onset and cessation for each of the six datasets are included in Supplementary Information; the median value across all six datasets are shown in Figure 2.7, Figure 2.8a-b and Figure 2.8c-d for annual regimes, the first/long rains and the second/short rains respectively. On Figures 2.7- 2.8 crosses indicate grid points where more than one of the dataset means were outside the range (median \pm 1 standard deviation), where the standard deviation is defined uniquely for each grid point, and is the mean standard deviation of onset/cessation over all six datasets. Regions where the standard deviation of daily rainfall was less than 1 mm/day were excluded, as this indicates a dry regime with no marked wet and dry seasons. Annual and biannual regimes have been considered separately.

2.4.1 Annual Rainfall Regime

Figures 2.6 and 2.7 generally indicate good agreement between the onset and cessation dates in the different datasets. The pattern over the coast of south west South Africa and Namibia is one region of difference between the datasets (Figure 2.7); the datasets differ here in their annual/biannual categorization, hence it is shaded pink in Figure 2.4 and has not been included in the regional analysis. In general, Figure 2.7a indicates an onset date in January for the northern part of this coastal strip, and April-May for the southern part consistent with the rainfall maxima in May-June and March for the southern and northern parts of this region, respectively, found in Nicholson (2000). The Mediterranean coastline and

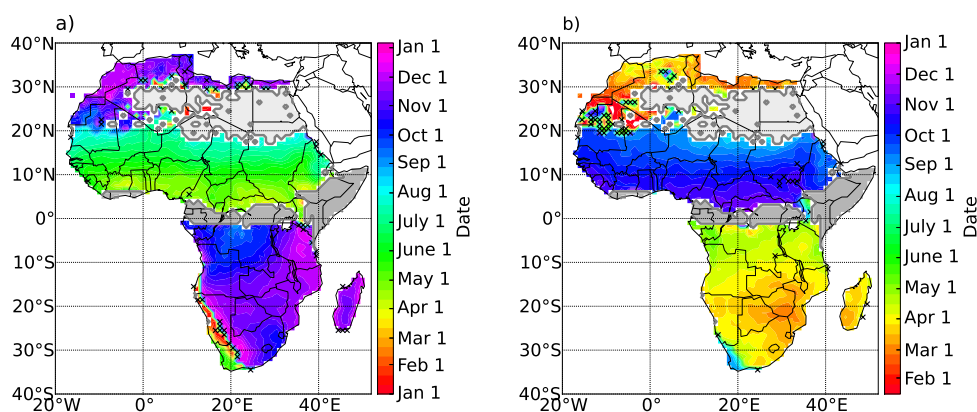


Figure 2.7 Median of the mean onset (a) and mean cessation (b) date for annual regime regions over all datasets. Stippling indicates where there is more than one mean value outside the median \pm one standard deviation, where the standard deviation used is the mean of the standard deviation in onset/cessation at that grid point over all six datasets. Dark grey indicates biannual regions, pale grey indicates dry regions.

parts of the Sahara contain regions of disagreement, where the wet season is poorly defined. Mean onset for annual regions (regions 1-3, 5-7, 11-17; Figure 2.6) shows some inter-dataset variation between the onset dates, including a later onset over region 2 in West Africa in ERA-I (see section 2.4.3) and TRMM appears to have a later mean onset over region 12, but for the most part, the mean onset date for each region is fairly consistent for the different datasets. Consistent spatial patterns across the datasets are confirmed by high (>0.82) PPC coefficients (below diagonal in Table 2), found to be statistically significant at the 99% level, despite the high autocorrelation (Wilks, 2011; Adams and Lawrence, 2014). MAE values (above diagonal in Table 2) confirm the good agreement with values of 10-17 days with the highest MAE values associated with ERA-I. Interannual variability (Figure 2.6) is generally consistent across datasets, with the largest values consistently found over regions 15, 16 and 17. Although the southwest coastal strip is excluded (shaded pink in Figure 2.4), this is likely the result of the inclusion of different rainfall regimes and drier climates, especially across South Africa (Engelbrecht et al., 2015; Weldon and Reason, 2014).

Good agreement is also apparent in cessation dates from different datasets over regions with an annual regime (Figure 2.6 and Figure 2.7b). Notable exceptions include early cessation in ARCV2 over regions 15 and 17, and to a lesser extent over regions 1, 7, 13, and 14, and late mean cessation in ERA-I over regions 2, 5 and 6. The individual mean cessation plots confirm the early cessation in ARCV2 over southern Africa, (see Figure S3b, Supplementary Information). High (>0.96), statistically significant (at 99% level) PPC coefficients (below diagonal in Table 3) confirm consistent spatial patterns, and good agreement is demonstrated in low MAE values of 5-10 days (above diagonal in Table 3). Interannual variability is generally lower for cessation than onset (Figure 2.6), and is again generally consistent across datasets, with the largest values over regions 15-17.

Overall, there is good agreement between the onset and cessation found in the different datasets in regions with an annual regime, demonstrating that all the datasets used contain

	TARCATv2	ARCV2	GPCP	TRMM	CHIRPS	ERA-I
TARCATv2	-	14.02	11.51	14.27	11.16	16.38
ARCV2	0.89	-	17.71	17.97	15.68	17.16
GPCP	0.91	0.82	-	13.69	10.64	15.37
TRMM	0.90	0.85	0.88	-	10.97	15.17
CHIRPS	0.92	0.85	0.90	0.91	-	11.20
ERA	0.86	0.87	0.86	0.87	0.93	-

Table 2.2 Comparison of mean onset date between the six datasets over annual regime regions. Below the diagonal is the Pearson Pattern Correlation (PPC) coefficient and above the diagonal is the Mean Absolute Error (days).

	TARCATv2	ARCv2	GPCP	TRMM	CHIRPS	ERA-I
TARCATv2	-	8.21	6.41	7.67	5.65	8.91
ARCv2	0.99	-	8.85	10.49	7.39	10.29
GPCP	1.00	0.97	-	6.85	5.12	7.39
TRMM	0.99	0.96	0.98	-	5.04	8.71
CHIRPS	1.00	0.99	1.00	1.00	-	7.36
ERA	0.99	0.99	0.99	0.99	1.00	-

Table 2.3 Comparison of mean cessation date between the six datasets over annual regime regions. Below the diagonal is the Pearson Pattern Correlation (PPC) coefficient and above the diagonal is the Mean Absolute Error (days).

a consistent representation of the seasonal cycle, as defined using the method above. This suggests that all the different satellite based precipitation datasets are accurately capturing the same patterns of annual rainfall progression over Africa. The reanalysis dataset (ERA-I) has been found to have some discrepancies over certain regions (e.g. region 2, see section 2.4.3), but mostly shows good agreement with the observational datasets.

2.4.2 Biannual Rainfall Regime

For the most part, the datasets agree well for the biannual regions (Figure 2.8), with central Africa exhibiting the largest disagreement, while the Horn of Africa and the West Africa southern coastal region contain few points of disagreement. Because this is the first time this method has been applied to biannual rainfall, the next sections provide discussion of the three regions that experience more than one season per year, namely, central Africa, East Africa and the West Africa southern coastal region.

2.4.2.1 Central Africa

The majority of regions of disagreement in Figure 2.8 reside within inland equatorial Africa, with the disagreement in timing of the onset and cessation here related to several factors. Firstly, central Africa experiences a humid climate, with an ill-defined dry season (Herrmann and Mohr, 2011), although some studies point out that there are maxima of rainfall in November and March/April (Washington et al., 2013; Nikulin et al., 2012). In regions, such as this, that are humid all year round, studies of rainfall seasonality are of limited interest. Differences between rainfall estimations in observational datasets over central Africa may result from variations in the inclusion of rain gauge measurements (Maidment et al., 2015). ERA-I overestimates rainfall over central Africa when compared with both Global Precipitation Climatology Centre precipitation dataset (GPCC) (Paeth et al., 2011; Dee et al., 2011) and GPCP (Nikulin et al., 2012). In addition to large rainfall magnitude differences

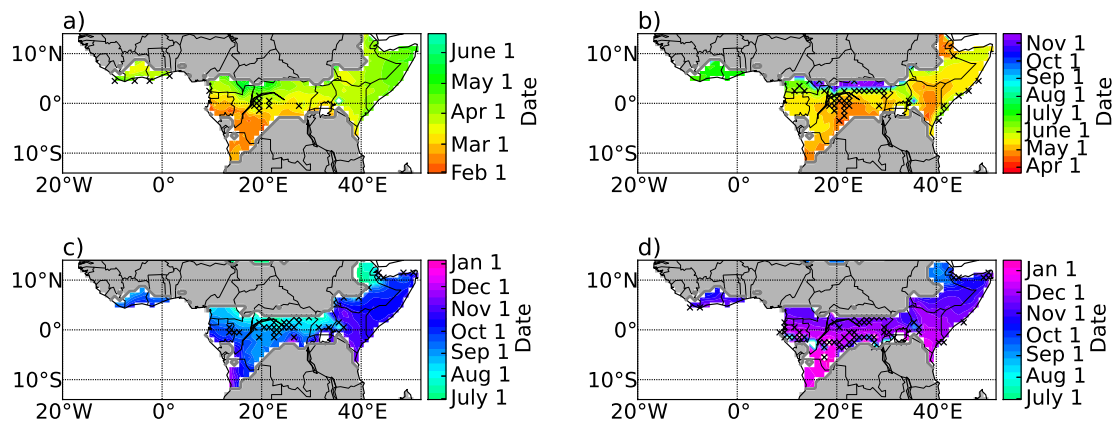


Figure 2.8 Median of the mean onset and cessation dates for the first/long (a-b) and second/short (c-d) rains over all datasets. Stippling indicates where there is more than one mean value outside the median \pm one standard deviation, where the standard deviation used is the mean of the standard deviation in onset/cessation at that grid point over all six datasets. Grey indicates annual regimes.

(Washington et al., 2013), studies have also reported on discrepancies in the phase of the annual rainfall pattern over central Africa. Sylla et al. (2010) found ERA-I does not correctly represent the double peaked seasonal structure and December - January dry season over North and South Equatorial Central Africa respectively. Over the Congo Basin, Washington et al. (2013) showed that TRMM, TAMSAT and ERA-I all capture the double peaked pattern, but all three exhibited timing differences. Overall, disagreement in onset and cessation dates found over this region is likely due to significant differences in the datasets.

2.4.2.2 East Africa

Figure 2.8 only exhibits disagreement over East Africa (here taken to comprise regions 8-10) on coastlines or the biannual/annual boundary regions, where the two seasons may be less well defined. Figure 2.6b supports this conclusion of good agreement between the datasets for the long rains over regions 8-10, both in terms of the mean date, and the consistently low interannual variability. The PPC coefficients and MAE values for both onset and cessation confirm this; MAE values range between 3 and 11 days (3 - 6 days if ERA-I is excluded) and PPC coefficients are all above the threshold to be significant at the 95% confidence level (results not shown).

The differences are larger for the short rains (Figure 2.8c-d, Figure 2.6b), but mostly small in magnitude. For the cessation, all the datasets but ERA-I are consistent in terms of mean cessation date and interannual variability, confirmed by MAE values of 4 - 8 days when

ERA-I is excluded (4 - 32 days with ERA-I), and PPC coefficients above the threshold to be significant at the 95% confidence level (results not shown). For the onset, ARCV2 seems to give marginally later onset dates, possibly due to the underestimation of ARCV2 rainfall over the Ethiopian Highlands and the surrounding region, particularly from June - September (Awange et al., 2016; Young et al., 2014). Young et al. (2014) found over eastern Ethiopia ARCV2 contained the lowest rainfall for the June-December period, when compared with gauges, TRMM, CMORPH and TAMSAT, and only exhibited a marginal increase in rainfall during the short rains season in south-eastern Ethiopia. Despite this, the PPC coefficients for the onset are above the threshold to be significant at the 95% confidence level and MAE values range between 6 - 13 days, indicating that ARCV2 is not a large outlier.

2.4.2.3 West Africa Southern Coastal Region

Agreement of onset/cessation dates is generally reasonable over the West Africa southern coastal region (Figure 2.8), but larger variations are found for the second season (Figure 2.6a). For the first season, the main difference is in the onset; GPCP and ERA-I give mean onset dates of 18 March and 24 April respectively, with the others all occurring between 1 April and 3 April. ERA-I also contains large interannual variability in the onset (Figure 2.6a). MAE values range from just 5 - 10 days when GPCP and ERA-I are excluded, but increase to 5 - 17 days and 5 - 40 days when just GPCP and both GPCP and ERA-I are included, respectively. Agreement in cessation is better, with MAE values of 2 - 11 days for all datasets (results not shown).

For the onset of the second season, ERA-I gives the earliest cessation date on 30 August, followed by TARCATv2 on 10 September, with the other datasets giving mean onset dates between 22 September and 3 October (Figure 2.6a). This large difference in onset date is found in the MAE values with values of 4 - 10 days when TARCATv2 and ERA-I are excluded, but increasing to 21 days when TARCATv2 is included and 33 days when ERA-I is included. Cessation is only marginally less variable, with earliest dates in TARCATv2 and ARCV2 at the beginning of November, and latest cessation in ERA-I at the end of November. MAE values range between 3 - 11 days when ERA-I is excluded, and 3 - 20 days when ERA-I is included (results not shown).

The results here are less consistent than those for East Africa and for annual regimes, with larger differences found between the TARCATv2, ERA-I and GPCP datasets. Differences in TARCATv2 are not unexpected, given the overall rainfall underestimation in TARCATv2 along the West African Coastline (Maidment et al., 2014; Tarnavsky et al., 2014). Diaconescu et al.

(2015) found GPCP had more days with rainfall >10mm and longer continuous wet periods over this region than TRMM, ARCV2 and ERA-I, which may be related to the earlier onset found in the first rains in GPCP. ARCV2 exhibits larger variability over region 1; timeseries in the Supplementary Information (Figure S6c) attributes this to an excursion in both onset and cessation in ARCV2 over 2001-2007, likely due to a dry bias during 2001-2007 and may relate to inhomogeneity in the rain gauge record (Maidment et al., 2015). Generally, the largest differences over the West Africa southern coastal region are related to ERA-I, and are explored in section 2.4.3.

2.4.3 Differences between ERA-I and other datasets over West Africa

ERA-I is a reanalysis dataset, hence rainfall is calculated differently to observational datasets. While ERA-I assimilates observations, model parametrisations are required to generate cloud and rainfall, and changes in observing systems can introduce spurious variability in the hydrological cycle (e.g. Dee et al., 2011). In general, reanalysis data would not be expected to exactly represent observational data. For the most part, Figures 2.6-2.8 indicate ERA-I performs well over southern Africa, exhibits some timing differences over Eastern Africa, and contains notable disagreements over Western Africa. Given the nature of the dataset, we therefore have low confidence in the variability in ERA-I onset/cessation dates over West Africa, which are at odds with the other datasets.

Timeseries for regions 2 and 4 (Figure 2.9) indicate a trend toward later onset by ERA-I (first rains in region 4), which explains the large variability shown in Figure 2.6a. In addition, ERA-I exhibits later cessation (second rains in region 4, Figure 2.6a); Figure 2.9 confirms that this bias is present throughout the timeseries for region 2, but only prior to 2000 for region 4 (second rains). The 'little dry season' (the period between the two wet seasons over region 4) is much shorter in ERA-I than the other datasets.

Other studies have indicated that precipitation amount and variability in ERA-I differs from observational datasets over West Africa (and other areas e.g. central Africa, Nikulin et al., 2012; Sylla et al., 2010). Although the large scale features of the West African Monsoon are captured, a lack of northward propagation of precipitation results in an ERA-I overestimation of precipitation along the coast, and an underestimation further north (Diaconescu et al., 2015; Paeth et al., 2011; Nikulin et al., 2012; Hill et al., 2016). A weaker first rainfall maxima along the coast (Diaconescu et al., 2015; Nikulin et al., 2012), matched by a shorter first season resulting from the later onset in our results, suggests this rainfall overestimation is associated with the second wet season. The failure of ERA-I to propagate the rain band

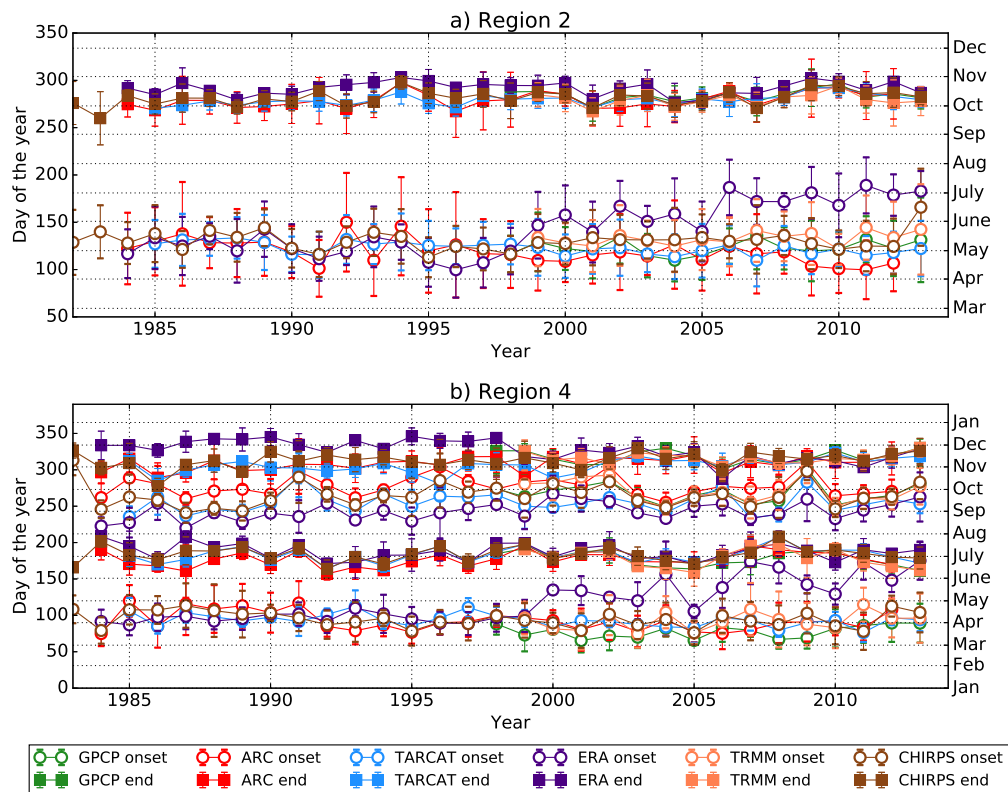


Figure 2.9 Timeseries of mean onset and cessation over regions 2 and 4 (a-b respectively). Different colored lines indicate different datasets. The error bars show the standard deviation in onset/cessation across the region at each time.

north over the Sahel, and consequential southerly location of the rainfall maxima (compared with observations, Nikulin et al., 2012), results in the reduced ‘little dry season’ and earlier onset of the second season found here. The later end of the second season is due to the overestimation of rainfall in this region (Nikulin et al., 2012).

Additionally, ERA-I fails to reproduce the observed interannual variability in precipitation (Sylla et al., 2010), with Nikulin et al. (2012) identifying an artificial declining trend in precipitation, consistent with the progressively later onset in ERA-I found in our results, which gave rise to larger interannual variability.

Given the method described here is able to capture the physical progression of the ITCZ throughout Africa (section 2.3), including the behavior associated with the West African Monsoon, these discrepancies in ERA-I indicate that this reanalysis dataset is not correctly representing the West African Monsoon and ‘little dry season’, as found in other studies (Nikulin et al., 2012).

2.5 Example application; Interpretation of Interannual Variability over East Africa

Consistency with known physical drivers (section 2.3), and good agreement across datasets (section 2.4), establishes confidence in the method. An example of how the method can be used to analyse interannual variations in onset and cessation over East Africa, detailed in this section, highlights potential applications and usability.

Over East Africa seasons of reduced length indicate lower rainfall (Philippon et al., 2015; Camberlin et al., 2009) and correspond with well-known drought years. A very brief short rains season in 2010 (Region 9: Figure 2.10a, Regions 8 and 10: Figure S7) reflects the failure of the 2010 short rains, which, coupled with the reduced long rains in 2011 (Figure 2.10a, S7), led to drought and famine over East Africa (Lott et al., 2013; Yang et al., 2014; Hoell and Funk, 2014). Failure of the 2005 short rains (Hastenrath et al., 2007) is also discernible in Figure 2.10a.

Despite the lower interannual variability in the long rains (compared with the short rains, Camberlin et al., 2009), dry long rains in 1984, 1993 and 2000, and wetter long rains in 1990 (Philippon et al., 2015) are apparent as shorter and longer seasons respectively in Figure 2.10a (and S7). Additionally, the premature end of the long rains in 2004, and early beginning in 2010 is also found by various Kenyan Institutes (USAID FEWS NET, 2004; Kenya Food Security Steering Group (KFSSG), 2010). Correct representation of previously identified rainfall features in the timeseries (Figure 2.10a and S7) for all datasets confirms the method is accurately identifying interannual fluctuations in the wet seasons, and overall, all six datasets have a good representation of the interannual variability in the biannual regions of East Africa.

East African rainfall responded strongly to the 1997-98 El Niño event, with weaker short rains in 1996 and long rains in 1997, followed by heavier short rains in 1997 immediately preceding the peak of the event, which generated floods across the region (Black et al., 2003). Immediately following the peak, the 1998 long rains were wetter than usual, followed by drier short rains in the boreal autumn (Hoell and Funk, 2014; Black et al., 2003; Philippon et al., 2015). Overall, it is expected that positive phases of the El Niño Southern Oscillation (ENSO) result in enhanced rainfall, while negative phases result in lower rainfall (Black et al., 2003). Reduced short rain seasons in 1996 and 1998 for regions 8-10, with a longer season in 1997 (Figure 2.10a and Figure S7), imply that patterns recorded here match expected behaviour across the Horn of Africa. El Niño conditions in 1986 and 1987 also resulted in reduced short rains, consistent with Philippon et al. (2015).

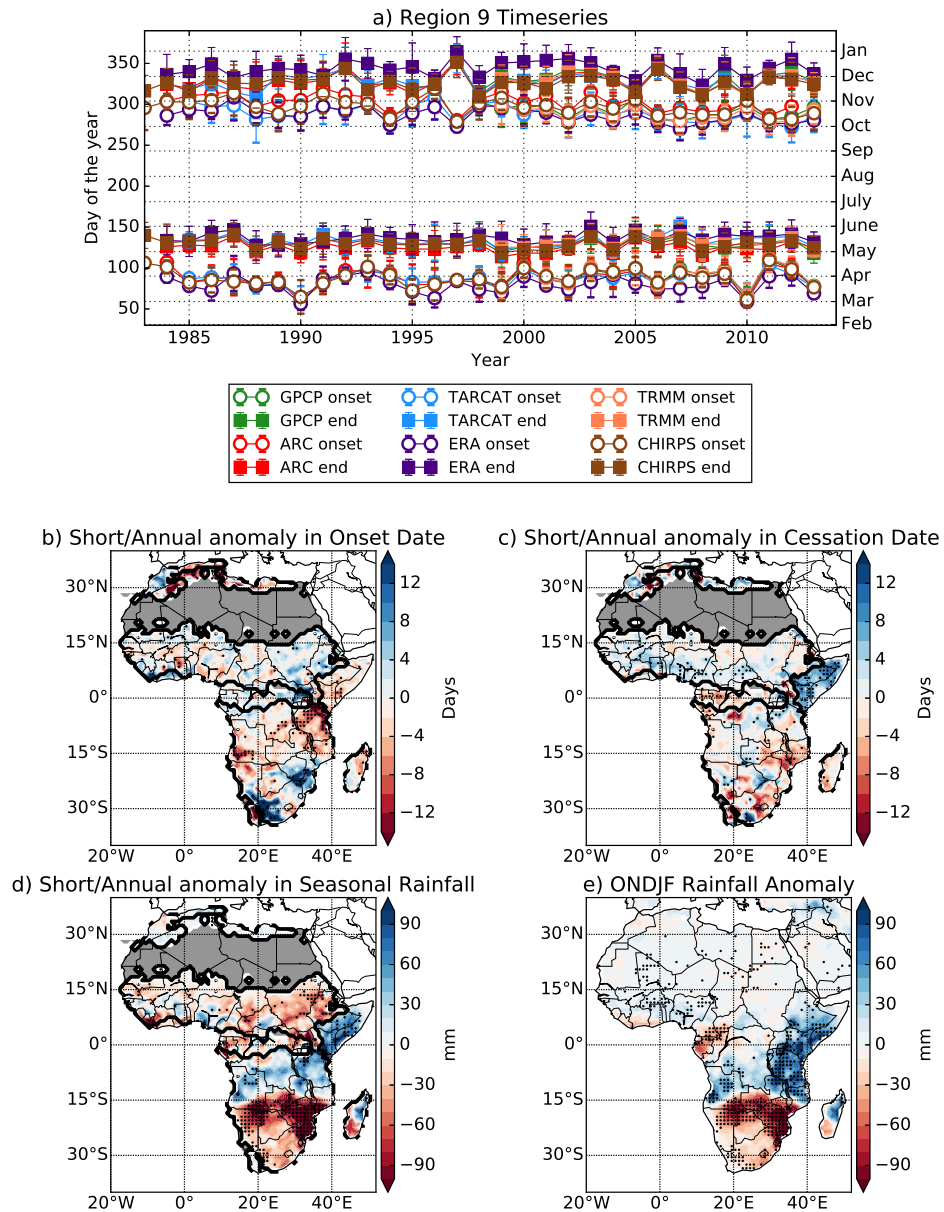


Figure 2.10 Impact of El Niño on onset/cessation. a) Timeseries of mean onset and cessation for long/short rains (bottom/top) over region 9. The error bars show the standard deviation in onset/cessation across the region at each time, with different datasets shown in different colors. b-d) Composite of onset, cessation, and wet season rainfall respectively in El Niño years for annual rains and short rains, minus the mean over 1982-2013, computed using CHIRPS data. The black contour marks the biannual/annual boundary. The El Niño years included were 1982, 1986, 1987, 1991, 1994, 1997, 2002, 2004, 2006 and 2009. The grey area indicates a dry regime. e) ONDJF rainfall anomaly in El Niño years (CHIRPS). Stippling indicates a statistically significant difference in El Niño years (t-test, 5% significance level).

One advantage of a continental-scale method for determining onset and cessation, applicable to annual and biannual regimes, is the ability to analyse the wider scale variations in seasonality. As an example, and following the findings above, the impact of El Niño upon both the annual rains and short rains was assessed (Figure 2.10b-e). The well-documented boreal winter dipole in rainfall anomaly, with higher rainfall totals over 0-15°S and the Horn of Africa, and the opposite between 15°S and 30°S (Figure 2.10e) (Cook, 2001; Camberlin et al., 2001; Kyte et al., 2006) is clearly captured in the seasonal rainfall (rainfall between onset date and cessation date) for short rains and annual regimes (Figure 2.10d). The anomaly is more pronounced over the Horn of Africa in Figure 2.10d compared to Figure 2.10e, demonstrating the value of the method extension for biannual regimes. Lower rainfall over 15°S and 30°S is collocated with later onset dates (Figure 2.10b), and a consequentially shorter season. Higher rainfall to the north is related to longer seasons; however, this results from an earlier onset over the annual regime region (Figure 2.10b), with onset of the annual rains 9 days earlier over region 11 (Tanzania) in El Niño years, but a later cessation of the short rains (7 days later on average) across the Horn of Africa (Figure 2.10c). In addition, the rainfall anomaly extends across the continent, but the onset responses are more pronounced east of 20°E. Over West Africa and the Sahel rainfall variations are not clearly associated with changes in seasonal timing. Overall, Figure 2.10 shows how applying this method over the whole of Africa clearly highlights the spatial patterns in rainfall teleconnections with El Niño.

2.6 Discussion and Conclusions

A modified method for determining the onset and cessation of the wet season over Africa was proposed and assessed using six observational and reanalysis datasets of African precipitation. The compatibility with known physical drivers of African seasonal rainfall, strong agreement between the different satellite-based precipitation datasets, in both the mean and temporal variations, and consistent features found across both rainfall regimes, establish confidence that this method (section 2.2) successfully captures the annual progression of rainfall across Africa and the beginning and end of the wet season for both regions with one wet season per year, and regions with two wet seasons per year. The onset and cessation are key parameters in understanding the impact of changes in the seasonal cycle on agriculture (Boyard-Micheau et al., 2013), and thus this method provides a foundation on which variability and change in the growing season can be investigated. Its dependence solely on daily rainfall and mean climatology, and proven ability to capture physical patterns, also makes it a suitable metric for analysis of variability and change in rainfall dynamics.

The following conclusions have been reached:

- Patterns of onset and cessation dates, produced by this method were found to be consistent with known physical drivers of African seasonal precipitation, namely, the ITCZ and the West African Monsoon, as well as agricultural onset methods. Continuous progression of onset and cessation dates across annual/biannual boundaries and consistency between both the detection methods for annual and biannual regions increase confidence in the method. Correct capturing of the 'little dry season' along the West Africa southern coastal region (Adejuwon and Odekunle, 2006) is a strength of this method.
- Patterns of onset and cessation are as found by Liebmann et al. (2012) and others (Oguntunde et al., 2014; Tadross et al., 2005; Mugalavai et al., 2008; Ngetich et al., 2014). Over West Africa, onset and cessation progress in a zonal manner (Oguntunde et al., 2014; Fitzpatrick et al., 2015), whereas over southern Africa onset spreads south east and north west simultaneously, and cessation expands radially from the Zimbabwe/ Mozambique/ South Africa border (Tadross et al., 2005).
- Satellite-based datasets generally agreed in their representation of the seasonal cycle in African rainfall, indicated by PPC coefficients and MAE values, particularly for regions with an annual rainfall regime and the biannual region of East Africa.
- The largest discrepancies were found in central Africa due to general dataset disagreement resulting from the low rain gauge density and generally humid climate with lack of pronounced dry seasons (Washington et al., 2013; Maidment et al., 2015; Herrmann and Mohr, 2011). In regions, such as this, where there is rain all year round, this type of analysis is, in any case, of limited interest.
- TARCAV2, GPCP and ARCV2 exhibit differences in the timing of the two wet seasons over the West Africa southern coastal region. TARCAV2 is known to have discrepancies in this region (Maidment et al., 2014; Tarnavsky et al., 2014) and differences have also been found in GPCP (Diaconescu et al., 2015). The excursion in ARCV2 over 2001-2007, which leads to larger variability, is likely due to a dry bias during 2001-2007, possibly related to inhomogeneity in the rain gauge record (Maidment et al., 2015).
- Timing errors in the ERA-I reanalysis over the West Africa southern coastal region and East Africa, and a trend towards later onset over West Africa not seen in observational

datasets, suggest that, while ERA-I has a good representation of the seasonal cycle over annual regime regions, its capturing of biannual seasonal regimes is less robust. ERA-I discrepancies over West Africa are well established (Diaconescu et al., 2015; Paeth et al., 2011; Nikulin et al., 2012), and may indicate that the model precipitation field is not reliable here, consistent with the discussion of spin up in the hydrological cycle in Dee et al. (2011), and Allan et al. (2014).

- Agreement of East African timeseries with observed rainfall features further corroborates the ability of the two season method to correctly identify the seasons and confirms accurate rainfall representation, especially in the satellite-based datasets. The strong response to multiple El Niño events over the Horn of Africa further demonstrates the strength of this method in correctly capturing interannual variations in rainfall seasonality, and the wider scale responses (Figure 2.10) highlight further utility for meteorological analysis, and some degree of potential predictability of this method.

This method proposed here has many advantages. Studies examining onset on a national scale often use an agricultural definition of the format 'the first wet day of N consecutive days receiving at least P millimetres without a dry spell lasting n days and receiving less than p millimetres in the following C days' (Boyard-Micheau et al., 2013). However, as demonstrated by the differences in parameters used by Mugalavai et al. (2008) and Ngetich et al. (2014) when examining maize growth in Kenya, these are only locally applicable. In addition, datasets with different climatologies and rainfall amounts will give inconsistent onset and cessation dates, or will require bias correcting. While such methods have value for community level decision support, they cannot be used continent-wide to examine long term changes in risk. However, the agreement between the method presented here and agriculturally motivated measures of seasonality suggest that this method could be used to assess agricultural risk continent-wide. The low spatial density of weather stations means use of methods exploiting other meteorological variables, such as potential evapotranspiration (PET) (Cook and Vizzy, 2012) or wind shear (Omotosho, 1992) are not suitable when examining observational datasets. In contrast, the method used here is universally applicable, as its single parameter is the local annual daily mean precipitation which is defined uniquely for each grid point, thus accounting for regions with different rainfall totals, and datasets with different rainfall biases.

Often, prior to the date when the wet season fully commences, heavy rainfall events can occur which are then followed by a prolonged dry period. This is termed a 'false onset', as it appears that the wet season has begun. They present a large agricultural risk, as planting at the time of the false onset can lead to significant crop loss if the plants do

not survive the intervening dry period (Marteau et al., 2009; Osorio and Galiano, 2012). Certain onset methods, such as methods based on thresholds of the cumulative percentage mean rainfall (Odekunle, 2006), or the method of Cook and Vizio (2012), comparing daily precipitation with PET, do not take into account such events. The method presented here takes into consideration false onsets, without the use of a fixed dry period (for example 20-30 days, Fitzpatrick et al., 2015). A high rainfall event, followed by a prolonged dry period (characteristic of a false onset) would give a positive anomaly followed by a prolonged period of negative anomalies, resulting in the cumulative daily rainfall anomaly falling below its previous minima (before the large rainfall event). Thus, using the absolute minima as the onset removes the impact of false onsets.

There are some limitations, namely, the method requires consistent above average precipitation, giving a pronounced increase in the cumulative daily precipitation anomaly. Intermittent or light rainfall at the beginning and end of the wet season will be represented as a negative daily rainfall anomaly, therefore these periods will not be considered as part of the wet season, potentially giving a reduced season length. Since onset/cessation can only be identified once the rainfall season is over, current applicability from an operational perspective is limited. However, the ability to highlight patterns in onset and cessation dates and their triggers will provide valuable information for forecast users. In addition, the method does not take into account locations that experience a major change in seasonal cycle from year to year. While the removal of regions with conflicting biannual/annual definitions should remove any impacts in these results, it should be taken into consideration for certain regions in future studies. Although all comparisons completed in this study, with both local onset methods and other papers, showed good agreement, comparison with other onset/cessation dates was not completed for all regions.

The results presented here raise important questions on the meaning of comparison metrics for datasets of African precipitation. Most studies comparing datasets of precipitation compare absolute amounts of rainfall (Maidment et al., 2014; Awange et al., 2016; Novella and Thiaw, 2013). Here, it has been demonstrated that datasets with contrasting rainfall quantities may exhibit good agreement in their representation of the seasonal cycle. The importance of the timing of the seasonal cycle in agricultural practice (Oguntunde et al., 2014) means good representation in datasets is crucial, and suggests that a comparison of the seasonality of datasets should be included in intercomparison studies.

In conclusion, this paper has applied a consistent method of assessment of seasonality to six datasets of African precipitation. The results demonstrate strong agreement in the

representation in the seasonal cycle in all the five satellite-based datasets, with moderate agreement in the reanalysis dataset, and the robustness of the method of cumulative daily mean precipitation anomalies to determine the onset and cessation of the wet season(s) and capture the correct physical progression of the seasonal rains. This demonstrates that this method is suitable for use in further studies, including climate change analysis and model verification.

Acknowledgments

The authors would like to thank Rory Fitzpatrick and three anonymous reviewers for their reviews which lead to significant improvements of the paper. Caroline M. Dunning was supported with funding from a Natural Environment Research Council (NERC) PhD Studentship through the SCENARIO Doctoral Training Partnership, Grant No. NE/L002566/1. Emily C.L. Black was supported by the National Centre for Atmospheric Sciences climate division core research programme. Richard P. Allan's contribution to the research leading to these results has received funding from the National Centre for Earth Observation and the European Union 7th Framework Programme (FP7/2007-2013) under Grant Agreement no. 603502 (EU project DACCIWA: Dynamics-aerosol-chemistry-cloud interactions in West Africa). All observational and reanalysis datasets exploited are publicly available datasets. ARCv2 data can be obtained from <ftp://ftp.cpc.ncep.noaa.gov/fews/fewsdata/africa/arc2/bin/>. The TARCATv2 dataset is available from the TAMSAT website (<http://www.met.reading.ac.uk/tamsat/data>). The CHIRPS dataset, produced by the Climate Hazards Group, is available at http://chg.geog.ucsb.edu/data/chirps/#_Data. GPCP daily data is available from <http://precip.gsfc.nasa.gov/>. ERA-I data was sourced from the ECMWF using <http://apps.ecmwf.int/datasets/data/interim-full-daily/levtype=sfc/>. The TRMM 3B42 data was obtained from <http://pmm.nasa.gov/data-access/downloads/trmm>.

Chapter 3:

Identification of deficiencies in seasonal rainfall simulated by CMIP5 climate models

To address the overarching aim to 'improve capability for robust projection of user-relevant rainfall characteristics over Africa', projections from climate models are utilised (§5). Here, the representation of the seasonality of rainfall over Africa in climate models has been evaluated, to give an indication of the utility of climate models for such analysis (§1.3.2).

This advances previous model evaluation studies, the majority of which focussed on monthly data or averaged the seasonal cycle over large spatial areas (§1.3.2, §3.1). This chapter also presents an application of the method described in §2, which for the first time permits a multi-model comparison of rainfall seasonality in Africa. By characterising the seasonal cycle in terms of regime, progression and timing, more information is provided on model deficiencies. This chapter addresses the second aim to 'Evaluate and identify deficiencies in representation of seasonality over Africa by climate models'.

Additionally, in §3.4 causes of a model deficiency are discussed. This analysis is extended in §4.

This chapter has been published in Environmental Research Letters (Dunning et al., 2017) and the Supplementary Information can be found at <http://stacks.iop.org/ERL/12/114001/mmedia>.

Identification of deficiencies in seasonal rainfall simulated by CMIP5 climate models

Caroline M. Dunning, Richard P. Allan, Emily C.L. Black

Abstract

An objective technique for analysing seasonality, in terms of regime, progression and timing of the wet seasons, is applied in the evaluation of CMIP5 simulations across continental Africa. Atmosphere-only and coupled integrations capture the gross observed patterns of seasonal progression and give mean onset/cessation dates within 18 days of the observational dates for 11 of the 13 regions considered. Accurate representation of seasonality over central-southern Africa and West Africa (excluding southern coastline) adds credence for future projected changes in seasonality here. However, coupled simulations exhibit timing biases over the Horn of Africa, with the long rains 20 days late on average. Although both sets of simulations detect biannual rainfall seasonal cycles for East and Central Africa, coupled simulations fail to capture the biannual regime over the southern West African coastline. This is linked with errors in the Gulf of Guinea sea surface temperature (SST) and deficient representation of the SST/rainfall relationship.

3.1 Introduction

The timing and seasonality of precipitation is of critical importance to the many African stakeholders who depend upon the seasonal rains for agricultural and domestic purposes. Failure or delays in these rains can lead to significant socio-economic impacts (Vizy et al., 2015). Future changes in climate will be felt not only through changes in mean precipitation, but also through altered seasonality, which in turn influences the growing season and crop yields (Vizy et al., 2015), the length of the malaria transmission season (Tanser et al., 2003), the supply of hydroelectric power (Yamba et al., 2011; van Vilet et al., 2016) and surface water supplies (de Wit and Stankiewicz, 2006). Producing reliable projections of the impact of climate change in a range of sectors therefore requires an accurate representation of seasonality within the climate projections being utilized.

Seasonality is sensitive to changes in atmospheric circulation patterns (Shongwe et al., 2009; Lee and Wang, 2014) and diagnosing and interpreting such changes requires a robust understanding of the dynamics and drivers of the seasonal cycle. In order to use Global Climate Models (GCMs) to investigate the physical mechanisms driving the seasonal cycle of precipitation, and assess the reliability of future impact projections, it is necessary that GCMs

are able to represent the seasonality of African precipitation.

In this study we take a continental scale approach to the assessment of the seasonality of African precipitation in Atmospheric Model Intercomparison Project (AMIP) and historical experiments as part of the Coupled Model Intercomparison Project Phase 5 (CMIP5) simulations (Taylor et al., 2012). An objective technique is applied using cumulative rainfall anomaly to calculate the onset and cessation of wet seasons (Liebmann et al., 2012; Dunning et al., 2016). This technique enables examination of the nature of the seasonal cycle, in terms of the number of wet seasons experienced per year (seasonal regime), the patterns of rainfall advance and retreat, and the timing of the wet seasons.

This paper aims to address three main questions:

- Can models realistically represent contrasting annual and biannual seasonal precipitation regimes across the continent?
- How well is the seasonal progression of rainfall represented, including spatial patterns of rainfall advance and retreat throughout the year?
- How well is the timing of the rainy seasons captured?

Many previous studies examining the representation of African precipitation in CMIP models have assessed mean rainfall amount and interannual variability for fixed seasons (Kumar et al., 2014; Lee and Wang, 2014; Mehran et al., 2014; Maidment et al., 2015). Those studies that do consider the seasonal cycle of precipitation either take averages over large areas, smoothing out much of the variability, and neglecting the seasonal progression of the rains (Dike et al., 2015) or use metrics such as seasonality skill score (Koutroulis et al., 2016), sum of squared errors (Yamana et al., 2016), or space-time root-mean-square error (Flato et al., 2013) which primarily focus on long-term monthly data. The methodological approach used here enables comparison between models, notwithstanding timing discrepancies. Additionally, the proven agricultural relevance of this onset/cessation metric means this evaluation of climate models is informative for impact studies (Dunning et al., 2016).

Studies that examine the onset and cessation of rainfall in climate models, taking into account the seasonal progression of rains, have previously focused on specific regions such as East Africa (McHugh, 2005; Yang et al., 2015b), Southern Africa (Dedekind et al., 2016) and the Sahara (Liu et al., 2002). The continental approach taken here complements these regional studies, providing insight into the links between timing biases in different regions and the links with large-scale progression of the wet season across regions. Several of the previous studies into seasonality have used regional climate models, such as the CORDEX regional

models (West Africa: Mounkaila et al. (2015), Southern Africa: Shongwe et al. (2015), East Africa: Endris et al. (2013)). While these models are valuable in providing regional detail, they are driven at their lateral boundaries by GCMs, and therefore understanding the seasonality in GCMs remains of key importance. Furthermore, some impact projections use GCMs, and few conduct thorough assessments of the representation of precipitation seasonality, potentially using models with significant deficiencies in seasonality representation (Yamba et al., 2011; Hamududu and Killingtveit, 2012; Caminade et al., 2014; van Vilet et al., 2016). The United Nations Development Programme (UNDP) Climate Change Country Profiles contain multi-model mean projections of annual and seasonal temperature and precipitation for a range of developing countries and were designed to facilitate climate change assessment with minimal computational expense (McSweeney et al., 2010), and are currently utilised in both agricultural (Adhikari et al., 2015) and ecological (Laloë et al., 2014) sectors. However, the same set of 15 GCMs are used for all countries, and hence multi-model mean projections in the locally-defined seasonal means may be inaccurate if the models used contain seasonal cycle timing biases.

This study presents, for the first time, a continent-wide evaluation of climate model representation of African rainfall seasonality. It aims to better characterise the representation of the seasonal cycle in terms of regime, progression and timing, in order to provide more detail on model deficiencies and their causes, and to facilitate better application of such models for climate change impact assessments.

3.2 Methods and Data

In order to assess rainfall seasonality in terms of seasonal regime (annual or biannual), progression and timing, we apply the method of Dunning et al. (2016) which extends the methodology of Liebmann et al. (2012). Firstly, at each grid point the ratio between the amplitude of the first and second harmonics is computed to determine whether an annual (one wet season/year) or biannual (two wet seasons/year) regime dominates. Secondly, the period of the year when the wet season occurs is determined by identifying the minima and maxima in the climatological cumulative daily mean rainfall anomaly, to account for seasons that span multiple calendar years. Dunning et al. (2016) introduces a method for doing this for biannual regimes, accompanying the method for annual regimes in Liebmann et al. (2012). Following the identification of the climatological seasons, onset and cessation dates are calculated for each season and year individually by identifying the minima and maxima in the daily cumulative rainfall anomaly over that season. The climatological cumulative daily mean rainfall anomaly and daily cumulative rainfall anomaly are computed independently for each climate model

and dataset. Onset and cessation dates are not calculated for the first or last years of each dataset. The approach was found to be applicable for datasets with contrasting rainfall biases, producing contemporaneous onset/cessation dates (Dunning et al., 2016), and thus can be applied to model simulations without the need for bias correction. The method also permits seasons to span different time periods thus enabling the examination of timing differences and comparison of wet seasons that do not coincide exactly across models and observations. By comparison with agricultural onset methods proposed by Marteau et al. (2009), Issa Lélé and Lamb (2010), and Yamada et al. (2013), Dunning et al. (2016) demonstrate the relevance of this method to agricultural stakeholders.

For calculation of onset and cessation dates, daily precipitation data is required. 46 models were chosen from the CMIP5 generation of models (Taylor et al., 2012), based on the availability of daily precipitation for an AMIP simulation (which applies observed sea surface temperature (SST) and sea ice and realistic radiative forcings) or CMIP5 historical simulation (which includes a fully coupled ocean and is driven by historical radiative forcings) from the British Atmospheric Data Centre (BADC). 28 AMIP simulations were used over 1979-2008 and 39 CMIP historical simulations were used over 1979-2005 (some variations in dates; Table S1 in Supplementary Information). Models, name of institute and horizontal resolution are listed in Table S1. Only the first ensemble members (r1i1p1) are considered since differences across ensemble members were found to be minimal, and much smaller than the inter-model differences. To allow construction of multi-model means, the data were re-gridded using bilinear interpolation to the GPCP 1DD $1^{\circ} \times 1^{\circ}$ grid. For some models this is a large increase in resolution; results were compared using a $2^{\circ} \times 2^{\circ}$ grid for the CMIP historical simulations and found to be unchanged. Following re-gridding, onset and cessation dates were calculated. For the individual model results in the Supplementary Information, the method is applied at native resolution (Table S1).

In order to compare rainfall over the southern West African coastline and SSTs over the Gulf of Guinea (section 3.4), monthly SST data was obtained for 37 of the 39 historical simulations from BADC. Monthly HadISST observed SST and monthly AMIP forcing SST data were obtained at $1^{\circ} \times 1^{\circ}$ horizontal resolution.

A reference dataset was required for comparison, to facilitate the assessment of the ability of CMIP5 model simulations to represent seasonality over Africa. Inaccuracies in ERA-Interim reanalysis precipitation data have been identified (Hill et al., 2016; Dunning et al., 2016) and thus reanalysis data was not used. To account for uncertainties in some datasets (Maidment et al., 2014) five different satellite based precipitation datasets available at daily resolution

were exploited (Table S2): the African Rainfall Climatology version 2 (ARCV2) precipitation dataset (Novella and Thiaw, 2013), the Climate Hazards Group InfraRed Precipitation with Stations (CHIRPS) dataset (Funk et al., 2015), the Global Precipitation Climatology Project 1 Degree Daily (GPCP 1DD) product (Huffman et al., 2001), the TAMSAT (Tropical Applications of Meteorology using SATellite data and ground-based observations) African Rainfall Climatology and Timeseries (TARCATv2) dataset (Maidment et al., 2014; Tarnavsky et al., 2014; Maidment et al., 2017) and the Tropical Rainfall Measuring Mission (TRMM) Multisatellite Precipitation Analysis (TMPA) 3B42 research derived daily product (Huffman et al., 2007). Temporal coverage and horizontal resolution are shown in Table S2. They were all re-gridded to the $1^\circ \times 1^\circ$ GPCP 1DD grid for all analysis (including Supplementary Information).

For analysis of timing, Africa was divided into a number of regions (Figure S1). These were chosen to primarily exhibit an annual or biannual regime and contain broadly similar onset and cessation dates. The area north of 15°N was not included in the analysis due to the dry climate. The GPCP annual/biannual categorisation was used as a basis for the region mask; model simulation grid-points were considered as belonging to a region if they fell within the correct geographical area and had the correct annual/biannual categorisation. Hence Figure S1 shows the maximum possible extent of the regions; for some models fewer points were included if they had an incorrect categorisation.

Figure 3.1 illustrates the application of the Dunning et al. (2016) method over the Horn of Africa and the Sahel (region map: Figure S1/Figure 3.4b). Average rainfall rate in each of the four/two seasons is calculated for the long term climatology (all available years; coupled: 1980-2004, atmosphere-only: 1980-2007, observations: 1982-2013) for standard meteorological seasons (Horn of Africa: Short Rains October-December, Long Rains March-May; Sahel: Wet Season July-September, Dry Season October-June; hashed bars) and when the seasons are determined dynamically for each model and year (solid bars) using the method of Dunning et al. (2016) which allows seasons to shift in space and time from year to year and across different models. Rainy seasons are differentiated more clearly from the dry seasons when the seasons are determined dynamically, as the method accounts for interannual variability in seasonal timing and model timing biases. This better seasonal distinction is obtained for all regions (Figure S2-3) with wet/dry season difference in average rainfall rate 33% larger when seasons are defined dynamically (annual regions). This demonstrates the advantage of examining seasonality using a method that objectively identifies wet seasons in models, and would enable the analysis of future changes in seasonality, while accounting for errors in the mean state.

The socio-economic importance of the East African long rains, necessitates extensive climate model analysis of this season, where use of a method that better distinguishes the long rains (as seen in Figure 3.1a) would facilitate more meaningful model analysis and inter-model comparison (Lyon and DeWitt, 2012; Tierney et al., 2015). Due to prior assessment (Flato et al., 2013; Kumar et al., 2014; Koutroulis et al., 2016) the magnitude of the seasonal cycle is not explicitly examined here, however, similar average rainfall rates (Figure 3.1 and S2-3) indicates agreement in seasonal cycle amplitude across observations, atmosphere-only, and coupled simulations for all regions.

3.3 Results

First the representation of annual and biannual seasonal regimes in the model simulations is examined. The multi-model mean ratio of the second harmonic to first harmonic for observations, atmosphere-only simulations and coupled simulations are shown in Figure 3.2a-c (individual model plots; Figure S4-S7). A ratio greater than 1.0 indicates a biannual regime, whereas a ratio of less than 1.0 indicates an annual regime.

In Africa the biannual regime covers three zones: the Horn of Africa (Camberlin et al., 2009; Yang et al., 2015a), a zonal equatorial strip from Equatorial Guinea to Uganda (Diem et al., 2014) and a small region on the South West Africa Coastline (hereafter referred to as SWAC) (Sultan and Janicot, 2003; Herrmann and Mohr, 2011) (Figure 3.2a). The

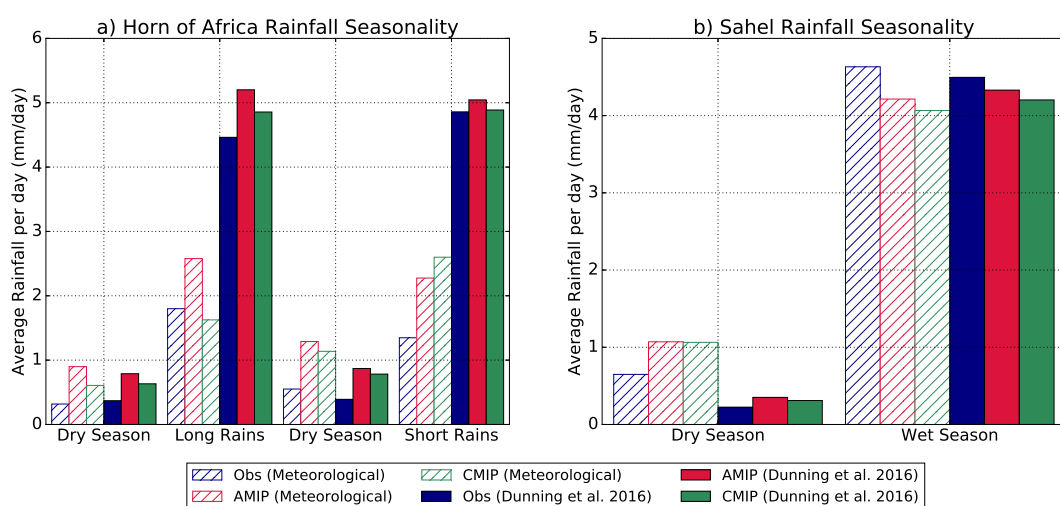


Figure 3.1 Average rainfall rate (mm/day) during the wet/dry seasons over the Horn of Africa (a) and the Sahel (b) when defined using meteorological seasons (dashed bars) and dynamically varying seasons (Dunning et al. (2016), solid). The same set of simulations was used for both meteorological and dynamically varying seasons. See Figure S1 for a map of the regions.

atmosphere-only simulations capture the biannual regime over these regions (Figure 3.2b), and while the area experiencing a biannual regime is larger than in the observations, there is good agreement between Figure 3.2a and 3.2b. While the coupled simulations capture the biannual regime for the Horn of Africa and the equatorial strip, the biannual regime over SWAC is not represented (Figure 3.2c). The lack of such a season over Nigeria in HadGEM2-ES has also been identified by Dike et al. (2015), but causes were not attributed. In both experiments an annual regime is found over southern Africa, West Africa and the Sahel, as in the observations.

Secondly, the representation of the spatial patterns of seasonal progression of precipitation is examined. Figure 3.3 shows the multi-model mean onset and cessation dates for both annual and biannual regimes. The patterns in observations (Figure 3.3a,d,g,j) are in agreement with those in Liebmann et al. (2012) and Dunning et al. (2016). The broadly meridional progression of onset and cessation dates across West Africa and the Sahel is represented by both multi-model means, with northward progression of onset in the boreal spring following on smoothly from the onset of the first/long rains (Figure 3.3a-c), and southward progression of cessation in the boreal autumn preceding the end of the second/short rains (Figure 3.3d-f). The later onset over northwest Senegal and surrounding areas in comparison with other points of the same latitude (Marteau et al., 2009) is also apparent in Figure 3.3a-c. Christensen et al. (2013) found models fail to capture central features of the West African Monsoon, yet we find realistic representation of the seasonal progression over West Africa. Over central and southern Africa, onset commences in the north-west and south-east, following the onset of the second/short rains; a pattern seen in observations, and both multi-model means. Figure 3.3j-l all exhibit the radial spreading of cessation, commencing on the Mozambique/ Zimbabwe/ South Africa

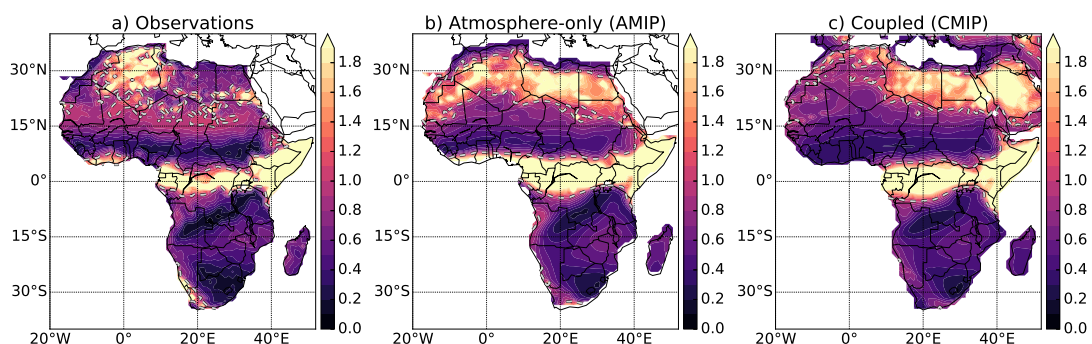


Figure 3.2 The mean ratio of the amplitude of the harmonic at two cycles/year to the amplitude of the harmonic at one cycle/year for (a) observations, (b) atmosphere-only (AMIP) and (c) coupled (CMIP historical) simulations. The dotted line shows where the ratio is equal to 1.0.

border, leading into the cessation of the first/long rains. The main difference is found over the south west tip of South Africa; the winter rainfall regime experienced here (as opposed to the summer regime experienced in the majority of the country, Weldon and Reason, 2014; Engelbrecht et al., 2015) covers a larger area in the coupled simulations (Figure 3.3i,l) than in atmosphere-only simulations and observations (Figure 3.3g,h,j,k). Dedekind et al. (2016) also found discrepancies over southern Africa where the summer rainfall peak was 2 months early in CCAM (AMIP). Correspondingly, individual models (Figure S8-23) demonstrate seasonal progression in agreement with that found in the observations.

The third aspect of seasonality examined was seasonal timing (Figure 3.4); full results for all models and regions (Figure S1) are in Figure S24-S26. The multi-model mean onset and cessation dates for five of the regions (Figure 3.4a) show the models generally simulate the wet season at the correct time of year. Notable differences include early onset over the Sahel (23 ± 15 days on average for atmosphere-only, 25 ± 18 days for coupled simulations, where the error relates to standard deviation across models), longer short rains over the Horn of Africa (cessation $\sim 16 \pm 11$ days later) and later long rains (onset/cessation $\sim 19 \pm 13$ days late for coupled simulations) over the same region. The late bias of the long rains in coupled simulations, with cessation in early June (on average) may explain some of the dry bias previously found in the long rains over East Africa in CMIP5 models (Yang et al., 2015b). The overestimation of the short rains, typically found in such models (Yang et al., 2015b), is replicated here in the combination of longer season length, of 14 ± 14 days longer for AMIP and 25 ± 15 days longer for CMIP historical simulations (Figure 3.4a), and similar average rainfall per day (Figure 3.1a).

Most coupled simulations do not capture the biannual regime over SWAC (Figure 3.2c), hence the mean onset and cessation dates for the annual regime over this region are shown in Figure 3.4a; while the season over SWAC is longer than is found over West Sahel, it is shorter than atmosphere-only and observations for SWAC, with onset occurring during the first rains, and cessation occurring during the second rains. Biannual onset and cessation dates for one of the two coupled simulations that simulate a biannual regime here (MIROC4h and BCC-CSM1-1-M) show good agreement with observations, but the onset dates are late in BCC-CSM1-1-M.

Mean onset and cessation dates were computed for each simulation for 13 regions with an annual regime (see Figure S1) and the Horn of Africa, and compared with mean observational onset and cessation dates. For atmosphere-only simulations the mean difference from observations for onset ranged between -18 ± 14 days to $+6 \pm 10$ days (negative values denote

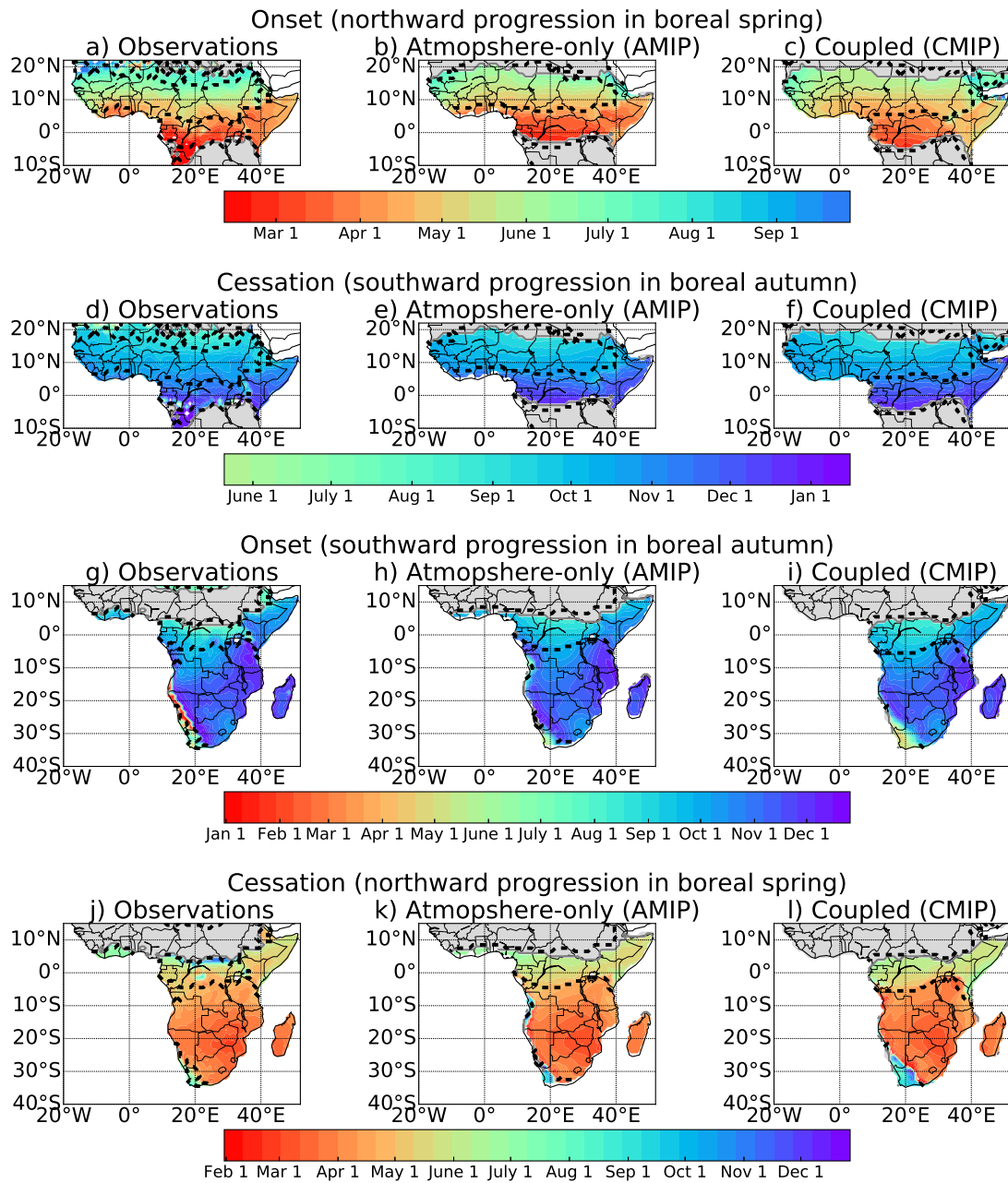


Figure 3.3 Seasonal progression of onset/cessation of wet seasons in observations (a,d,g,j) , atmosphere-only (AMIP) (b,e,h,k) and coupled (CMIP) simulations (c,f,i,l). Onset/cessation in annual regime regions is plotted with onset/cessation in biannual regions to demonstrate continuous progression across annual/biannual boundaries (denoted by dashed black lines). a-c) Northward progression of onset in boreal spring from first/long rains into West African Monsoon (WAM). d-f) Southward progression of cessation in boreal autumn from the WAM into end of second/short rains. g-i) Southward progression of onset in boreal autumn, from second/short rains into the annual rains over southern Africa. j-l). Northward progression of cessation in boreal spring from the end of the annual rains over southern Africa into first/long rains. Grey indicates regions not considered for these plots.

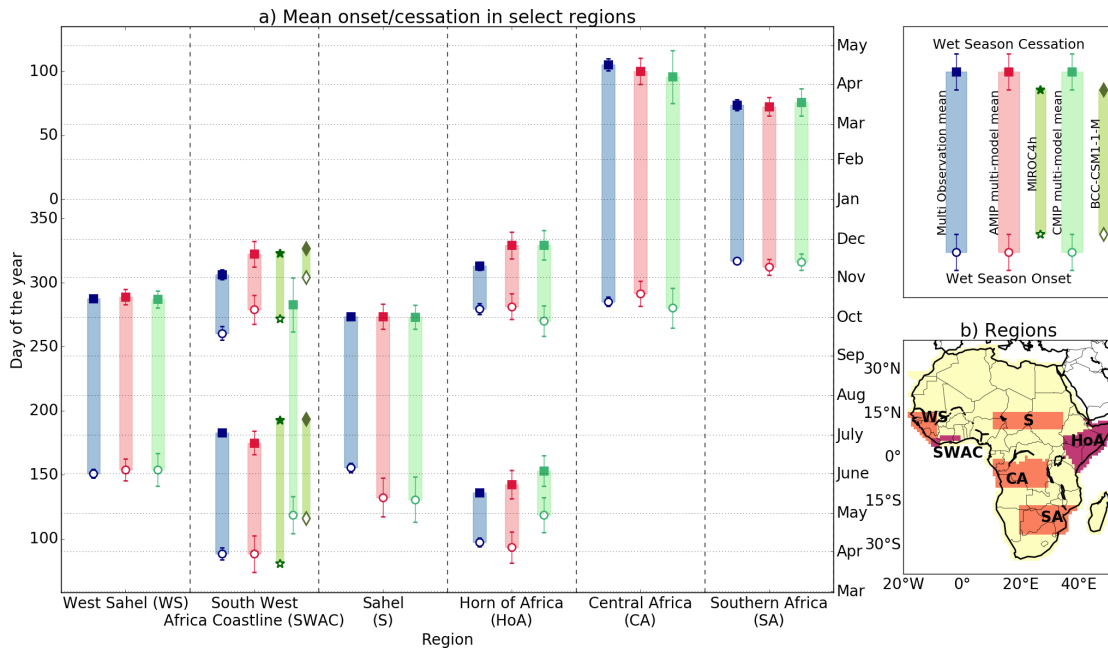


Figure 3.4 Mean onset (open circles) and cessation (filled squares) for selected regions (see b). Multi-model mean for observations, atmosphere-only (AMIP) and coupled (CMIP) simulations are plotted with the errorbars indicating standard deviation over individual model means for each region. Shaded bars indicate the period of the wet season. For SWAC the mean annual regime onset/cessation in coupled simulations is plotted, along with mean onset/cessation for MIRCOC4h and BCC-CSM1-1-M (coupled simulations), the only coupled simulations to capture a biannual regime here.

early onset, positive is late), with the onset over the Sahel exhibiting larger differences of -23 ± 15 days. Cessation dates exhibited smaller mean differences, with differences ranging between -5 ± 10 days to 8 ± 15 days for the different regions. For coupled simulations the mean difference from observations for onset ranged from -15 ± 10 days to $+3 \pm 13$ days, with larger differences over the Sahel (-25 ± 18 days) and over the west coast of southern Africa. The discrepancy over this southern region is likely to be related to overestimation of the area that experiences a winter rainfall regime shown in Figure 3.3, and exclusion of dry areas associated with the Namibian Desert (Liebmann et al., 2012; Engelbrecht et al., 2015). For cessation, differences from the observations are of similar magnitude, with differences ranging from -12 ± 10 days to $+15 \pm 11$ days, with the west coast of southern Africa again an outlier, showing a much higher value. Individual results for each model and region are included in the Supplementary Information.

Overall, Figures 3.2- 3.4 (and Figures S4-S23) indicate that the model simulations realistically capture the seasonal progression of the rainy seasons over Africa. However, coupled simulations overestimate the areal extent of the winter rainfall regime in South Africa, leading to large timing errors over South Africa (40-50 days on average, region 15 in Figure S24-S25) and importantly fail to capture the biannual regime over SWAC. The potential for detrimental

impacts of the intervening dry season on agricultural yields (Odekunle, 2007) coupled with high population density (GRUMP: Global Urban-Rural Mapping Project, 2000), and changing nature of the seasonality (Chineke et al., 2010), motivated further exploration of this misrepresentation (Section 3.4).

3.4 Simulation of the Little Dry Season in Southern Coastal West Africa

The biannual regime over SWAC comprises 4 seasons; a dry season from November-March, the first wet season from April-June and the second wet season from mid-September-October. These two wet seasons are separated by a break in the monsoon rains during July-August, known as the 'August Break' (Chineke et al., 2010) or 'Little Dry Season' (LDS) (Odekunle, 2010). The LDS can be a useful period for weeding and spraying of crops; when the LDS is too early, long or intense, yields can be reduced (Adejuwon and Odekunle, 2006). Both the mean annual cycle of precipitation in observations (blue line) and atmosphere-only (red line), over the LDS region (Figure 3.5b), show the biannual seasonal cycle. However, Figure 3.5b confirms that coupled simulations (green line) do not capture the correct seasonal cycle.

The misrepresentation of the Little Dry Season is related to the southward ITCZ bias in coupled simulations (Richter and Xie, 2008; Roehrig et al., 2013; Toniazzo and Woolnough, 2014; Monerie et al., 2017). This bias has been connected with the presence of warm Atlantic SST biases in the Gulf of Guinea (Vizy and Cook, 2001; Cook and Vizy, 2006; Roehrig et al., 2013), via influences on the meridional temperature gradient. Furthermore, the strength of the West African Monsoon is sensitive to SSTs in the equatorial cold tongue (Patricola et al., 2012), such that sporadic warming in this region resulting from Atlantic Niños (Nnamchi et al., 2015) weakens the monsoon circulation and monsoon rains are confined to the Guinea Coast (Chang et al., 2008). Hence, the failure of the coupled simulations to reproduce the eastern equatorial cold tongue in boreal summer (Richter and Xie, 2008; Patricola et al., 2012) may be associated with the restricted northward progression of the ITCZ. More locally, the reduction in rainfall during the LDS is accompanied by cool SSTs in the northern Gulf of Guinea, in particular, between 8°W-2°E, and 3°N to the West African coastline (Figure 3.5a, pink box), resulting from ocean upwelling (Odekunle and Eludoyin, 2008, Figure 3.5). Adejuwon and Odekunle (2006) proposed that the LDS was a consequence of these local cooler SSTs leading to the inter-tropical discontinuity (ITD) travelling further inland, while Odekunle and

Eludoyin (2008) suggested that cool SSTs increased static stability over this region, inhibiting convection.

The correct representation of the LDS in atmosphere-only simulations with prescribed SSTs and incorrect representation in fully coupled simulations (Figure 3.5b), combined with previous research (Adejuwon and Odekunle, 2006; Odekunle and Eludoyin, 2008), suggests an SST driver for the LDS. Thus the relationship between SSTs in the northern Gulf of Guinea region (8°W-2°E, and 3°N to the West African coastline; pink box in Figure 3.5a), and LDS rainfall is explored to determine if this could explain the misrepresentation (Figure 3.5). Observational datasets were used to determine the mean period of the LDS (2 July - 17 September), and the region influenced by this regime (SWAC; blue dots in Figure 3.5a). Linear regression was used to examine the relationship between LDS rainfall and July-August-September (JAS) SST (Figure 3.5c). Observations and atmosphere-only simulations exhibit the expected relationship with colder SST anomaly years resulting in lower LDS rainfall, yet coupled simulations fail to represent this association (Figure 3.5c). In addition, none of the coupled simulations realistically represent the SST seasonal cycle over the region of interest identified by Adejuwon and Odekunle (2006); the minima are in September rather than August, and the amplitude of the SST seasonal cycle is only ~55% of that in HadISST, at 2.3K compared with 4.3K in HadISST and 4.1K in AMIP.

The coupled historical simulations for MIROC4h and BCC-CSM1-1-M contain an LDS at a few coastal grid-points, evident in most ensemble members, and also exhibit SST anomalies in the lowest 10% for July and August, compared with all coupled simulations (brown/pale pink dashed line, Figure 3.5d).

These findings are consistent with the lack of a LDS in coupled simulations being related to unrealistic representation of the SST seasonal cycle, and an incorrect interannual relationship between SST and rainfall. The seasonal cycle of SST is an important driver of seasonality in rainfall, with previous studies identifying a significant influence of the decline in equatorial SST from April to July on the development of the monsoon (Okumura and Xie, 2004) and a delay in the phase of the Atlantic SST seasonal cycle resulting in an increase in late rainy season precipitation (Monerie et al., 2017). It may be inferred therefore that models that represent SST seasonality well are more likely than others to capture the seasonality of rainfall accurately. However, a good representation of SST is not the only factor in determining models' ability to capture rainfall. When analyzing the Atlantic ITCZ structure, Siongco et al. (2015) found that model horizontal resolution had a large influence on the marine ITCZ. MIROC4h and BCC-CSM1-1-M have higher spatial resolution than many of the other mod-

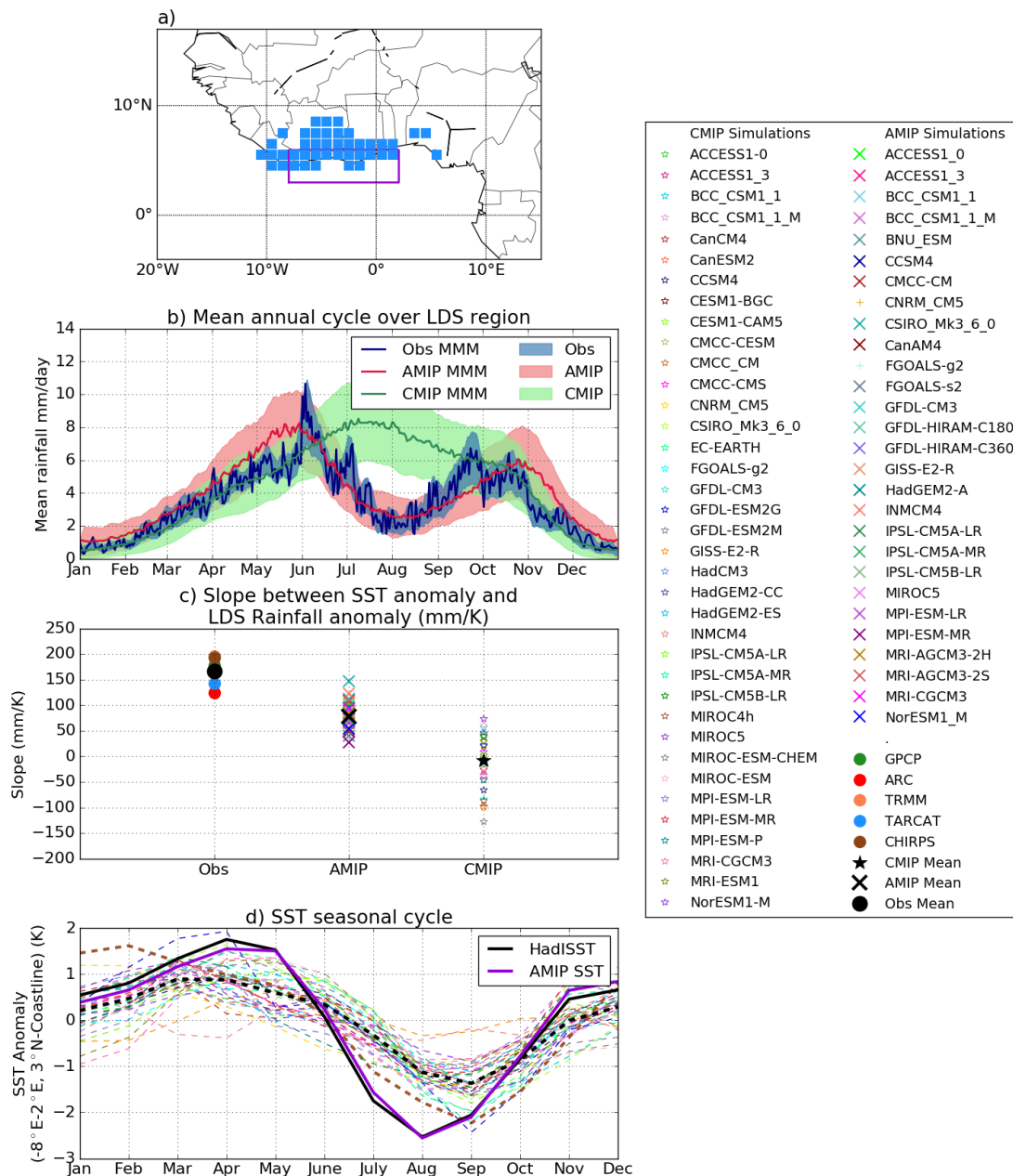


Figure 3.5 Rainfall and SST links over SWAC and neighbouring ocean. a) Location of the region that experiences the Little Dry Season (LDS; blue dots) and the SST region of interest (pink box). b) Mean annual cycle of rainfall in observations, atmosphere-only and coupled simulations over the LDS region (blue dots in a). c) Slope of the linear regression between interannual variations in LDS rainfall (rainfall during 2 July - 17 September) and July-August-September (JAS) SST. Filled symbols indicate statistical significance of the slope at the 95% significance level (crosses for AMIP). d) Seasonal cycle of SST in HadISST, AMIP and coupled simulations, with the black dotted line indicating the coupled multi-model mean. The anomalies are calculated relative to annual mean SST from each dataset/model simulation.

els used and better representation of the SST seasonal cycle, with lower SST anomalies in JAS. Yet, it would be over-simplistic to argue that resolution and accurate representation of SST alone determine models' ability to capture the LDS at a few grid points. Monerie et al. (2017) noted that the influence of SST varies across climate models, which may explain why some models with similar SST seasonal cycle and resolution (e.g. EC-Earth) do not contain an LDS. Of the 18 models analysed by Cook and Vizy (2006) only 4 correctly captured the relationship between Gulf of Guinea SST anomalies and West African Monsoon precipitation anomalies; hence even with the correct SST the coupled simulations may not produce a LDS due to inaccurate representation of the variability. Furthermore, the monsoon acts to cool SST (Okumura and Xie, 2004; Hagos and Cook, 2009); hence correct representation of SST seasonality is both a cause of and response to the accuracy of precipitation seasonality. The preceding discussion thus highlights two likely causes of model bias in the representation of the West African Monsoon and provokes a number of additional questions. Further detailed analysis of such mechanisms is merited, along with other LDS drivers, including the deflection of south-westerly winds to westerly winds (Olaniran, 1989), which could be addressed through idealized model integrations and further analysis of observations.

3.5 Conclusions

The representation of precipitation seasonality in atmosphere-only and coupled historical CMIP5 climate model simulations has been evaluated across Africa using observations and an objective methodology for quantifying seasonal characteristics (Liebmann et al., 2012; Dunning et al., 2016). Using this methodological approach demonstrates the presence of a biannual regime over regions with timing biases, where the use of standard meteorological seasons may suppress the perceived seasonal cycle, and thus can be used to compare model simulations, notwithstanding timing biases.

Overall, the CMIP5 simulations capture the gross seasonal cycle of African precipitation on a continental scale. The patterns of seasonal progression of the rainy season are well-represented, and the atmosphere-only simulations realistically simulate biannual rainfall regimes for the Horn of Africa, Equatorial Africa and a region on the southern West Africa coastline (SWAC). Patterns of seasonal progression over southern Africa are the consequence of interactions between the ITCZ, the South Atlantic Anticyclone, mid latitude westerlies and the Angola Low, where the tropical-extratropical cloud bands that bring summer rainfall across southern Africa form (Reason et al., 2006). The large-scale similarity in spatial rainfall progression patterns over Southern Africa across observations, atmosphere-only and coupled

integrations suggest that the models capture these interactions which lead to the non-zonal patterns observed in this region (Reason et al., 2006; Shongwe et al., 2009, 2015). Seasonal timing in atmosphere-only simulations demonstrates good agreement with observations (most mean onset/cessation dates agree within 18 days) although both sets of simulations exhibit an early onset of the wet season over the Sahel (~25 days early). Additionally, coupled simulations exhibit timing biases over the Horn of Africa (long rains ~20 days late).

Although the seasonal cycle is generally represented well in atmosphere-only model runs, in regions influenced by annually changing SST, SST biases in coupled simulations lead to errors in rainfall patterns. The incorrect annual seasonal regime found over SWAC (bimodal in observations) has been linked to an unrealistic seasonal cycle of SST and erroneous SST/rainfall relationships in this region. Additional work is merited to further elucidate exact mechanisms that determine the realistic representation of certain features and improve physical mechanisms represented by coupled simulations. Climate model projections should be treated with caution, and projections of future agriculture production in this region may be unrealistic, due to the significant impact of the LDS on crop yields (Adejuwon and Odekunle, 2006).

In conclusion, on a continental scale, the resemblance of spatial progression patterns thus adds credence to GCM future projections (Tierney et al., 2015). However, in regions where the rainfall seasonal cycle is not well captured, caution should be exercised when interpreting climate change projections for impact assessment. The information in Figures S24-26 on timing biases for individual models can be used to inform future studies on suitable model selection, reducing the inclusion of models with timing biases.

Acknowledgments and Data

The authors would like to thank two anonymous reviewers for their insightful and constructive comments.

We acknowledge the World Climate Research Programme's Working Group on Coupled Modelling, which is responsible for CMIP, and we thank the climate modeling groups (models listed in Table S1) for producing and making available their model outputs; for CMIP, the U.S. Department of Energy's PCMDI provided coordinating support and led development of software infrastructure in partnership with the Global Organization for Earth System Science Portals. Model data were sourced from the CMIP5 data portal (http://cmip-pcmdi.llnl.gov/cmip5/data_portal.html) and the British Atmospheric Data Centre (<http://badc.nerc.ac.uk/>).

All observational datasets exploited are publicly available datasets. ARCV2 data can be obtained from <ftp://ftp.cpc.ncep.noaa.gov/fews/fewsdata/africa/arc2/bin/>. The TARCATv2 dataset is available from the TAMSAT website (<http://www.met.reading.ac.uk/~tamsat/data>). The CHIRPS dataset, produced by the Climate Hazards Group, is available at http://chg.geog.ucsb.edu/data/chirps/#_Data. GPCP daily data are available from <http://precip.gsfc.nasa.gov/>. The TRMM 3B42 data were obtained from <http://pmm.nasa.gov/data-access/downloads/trmm>.

Monthly HadISST observed SST was obtained from the UK Met Office: <http://www.metoffice.gov.uk/hadobs/hadisst/data/download.html> and monthly AMIP forcing SST data was obtained from http://www-pcmdi.llnl.gov/projects/amip/AMIP2EXPDSN/BCS/amipbc_dwnld.php.

Caroline M. Dunning as supported with funding from a Natural Environment Research Council (NERC) PhD Studentship through the SCENARIO Doctoral Training Partnership grant NE/L002566/1. Richard P. Allan's contribution to the research leading to these results has received funding from the National Centre for Earth Observation and the European Union 7th Framework Programme (FP7/2007-2013) under grant agreement 603502 (EU project DACCIIWA: Dynamics-aerosol-chemistry-cloud interactions in West Africa). Emily Black's contribution to the research has been supported by the National Centre for Atmospheric Science (Climate division), the NERC/DFID BRAVE project (NE/M008983/1) the NERC/DFID HyCristal project (NE/M020371/1) and the Global Challenges Research Fund ERADACS project (NE/P015352/1).

Chapter 4:

The impact of air-sea coupling and ocean mean state biases on the representation of the seasonal cycle of precipitation over southern West Africa in climate models

In §3 a deficiency in the representation of the seasonal cycle over the southern West African coastline in coupled climate models is identified. It is found that coupled climate models do not capture the biannual rainfall regime and the Little Dry Season. Given the societal importance of this season (Adejuwon and Odekunle, 2006) and limited previous literature examining this season (Dike et al., 2015) in this chapter the processes important for this seasonal regime are explored. Thus this chapter addresses the third aim to 'Elucidate dynamical processes determining seasonality, its variability and climate model representation'.

In §1 the importance of understanding and interpreting the underlying physical mechanisms for the production of 'robust' projections is highlighted, thus this chapter is important in addressing the overall aim of this thesis to 'improve capability for robust projection of user-relevant rainfall characteristics over Africa'. At the current time no study has investigated the representation of the Little Dry Season in climate models, thus this analysis represents an important advancement of the literature.

This chapter will be submitted to Climate Dynamics and the Supplementary Information can be found in the Appendices (§ 7.1).

The impact of air-sea coupling and ocean mean state biases on the representation of the seasonal cycle of precipitation over southern West Africa in climate models

Caroline M. Dunning, Linda C. Hirons, Nicholas P. Klingaman, Richard P. Allan, Emily Black, and Andrew G. Turner

Abstract

The biannual seasonal rainfall regime over the southern coastline of West Africa is characterised by two wet seasons separated by the ‘Little Dry Season’ in July-August. Lower rainfall totals during this intervening dry season may be detrimental for crop yields, over a densely populated region with high societal dependence upon agricultural output. Coupled CMIP5 models do not correctly capture this seasonal regime, and instead generate a single wet season, peaking at the expected timing of the Little Dry Season. Hence the realism of future climate projections over this region is questionable. Here, the representation of the Little Dry Season in coupled model simulations is investigated, to elucidate factors leading to this misrepresentation. By using the Global Ocean Mixing Layer configuration of the Met Office Unified Model, the impact of coupled model ocean biases over different ocean basins can be examined while maintaining air-sea coupling. Coupled model Atlantic Ocean biases are found to be the cause of the incorrect seasonal regime over the southern West African coastline. The reduction in rainfall during the Little Dry Season in observations is associated with upper level descent and reduced ascent along the coastline. When coupled model Atlantic Ocean biases are introduced ascent over the coastline is deeper and rainfall totals are higher during July-August. Hence, this study indicates additional impacts of Atlantic Ocean biases in coupled climate models, and highlights model development required for production of meaningful climate change projections over this region.

4.1 Introduction

The southern coastline of West Africa is a highly populated region, with many dependent upon seasonal rainfall for crop irrigation and replenishment of drinking water supplies. While the majority of West Africa experiences one primary monsoonal wet season per year (Sultan and Janicot, 2003; Nicholson, 2013), a region on the southern West African coastline, encompassing parts of southern Ghana, Benin, Togo, Ivory Coast and SW Nigeria experiences two wet seasons per year (Herrmann and Mohr, 2011; Liebmann et al., 2012; Parker and Diop-Kane, 2017). The northward progression of the tropical rain belt in boreal spring brings

the first wet season from April-June; the second wet season in September and October is associated with the returning southward progression of the tropical rain belt in boreal autumn. Separating the two wet seasons is the 'Little Dry Season' (LDS): a period of lower and less frequent rainfall (Adejuwon and Odekunle, 2006; Odekunle and Eludoyin, 2008; Chineke et al., 2010; Parker and Diop-Kane, 2017). The length and severity of the LDS has important socio-economic implications: while a shorter and less intense LDS is useful for weeding and spraying crops with pesticide, a longer and more intense LDS can lead to crop failure (Adejuwon and Odekunle, 2006; Odekunle, 2007).

A number of interactions between the LDS and other meteorological phenomena have been proposed (Odekunle, 2007). Years with cooler than average sea surface temperatures (SSTs) over the Gulf of Guinea have an increased land-sea thermal contrast, strengthening the monsoon southwesterlies and shifting the tropical rain belt further inland, giving a more intense LDS (lower rainfall) (Adejuwon and Odekunle, 2006). More locally, anomalously cool SST (when compared with the latitudinal average) is consistently observed in July-September over the northern Gulf of Guinea (8°W-2°E, 3°N to the coastline, see Figure 4.1d-f), adjacent to the region that experiences the LDS (Parker and Diop-Kane, 2017), which increases static stability over the region, suppressing convection and limiting rainfall (Odekunle and Eludoyin, 2008; Odekunle, 2010). This cool SST results from local coastal upwelling (Parker and Diop-Kane, 2017), strengthened by the summer intensification of the eastward Guinea Current which leads to shoaling of the thermocline near the northern coast of the Gulf of Guinea, and the advection of cold coastally upwelled water by the South Equatorial Current (northward extension of the cold Benguela Current; Odekunle and Eludoyin, 2008). Odekunle (2007) identified strong relationships between SSTs in the Gulf of Guinea, the source regions of the Guinea and Benguela current and the LDS, with higher SSTs associated with higher rainfall during the LDS (i.e. less intense LDS). Parker and Diop-Kane (2017) highlighted the role of high pressure over the Gulf of Guinea and the St Helena high pressure cell: the effect of this high pressure extends to the coastal regions, where the associating sinking motion reduces convection during the LDS.

Coupled global climate models (CGCMs) are used for sensitivity tests that explore the physics of meteorological phenomena, as well as producing projections of future climate change. Many studies have identified and explored deficiencies in the representation of the West African monsoon in atmosphere-only climate model simulations (AGCMs) and CGCMs (Cook and Vizy, 2006; Roehrig et al., 2013; Flato et al., 2013). Most notably, the majority of models exhibit a southward shift of the main rain belt, with deficient rainfall over the Sahel

(Roehrig et al., 2013; James et al., 2017; Steinig et al., 2018). In addition, the large mesoscale propagating systems, which bring much of the boreal summer rainfall over West Africa and the Sahel (Mathon et al., 2002), are not well represented (Roehrig et al., 2013) and the Saharan Heat Low is generally weaker than found in reanalyses and placed too far southwest (Dixon et al., 2017a). Models also fail to reproduce important coupling between Sahel rainfall and large scale dynamics over West Africa, including the African Easterly Jet (Whittleston et al., 2017). Dunning et al. (2017) identified a deficiency in CGCMs' representation of the seasonal cycle of precipitation over the southern West African coastline. The AGCMs, forced by observed SSTs, correctly produced wet seasons in April-June and September-October, separated by the LDS. However, the CGCMs generated a single wet season, with a single rainfall peak in July-August, coincident with the observed LDS. They proposed that this was due to the incorrect SST seasonal cycle over the northern Gulf of Guinea in CGCMs. Over the northern Gulf of Guinea SST declines from April/May to August due to oceanic upwelling and transport of cool water by ocean currents (e.g. Figure 4.1a-f, Odekunle and Eludoyin, 2008). However, CGCMs do not capture this cooling, shown in Dunning et al. (2017), and Figure 4.1g-l, where the increasing warm bias over this region is apparent. This may be related to insufficient upwelling or low resolution of ocean model components leading to inaccurate representation of the Guinea Current. The misrepresentation of the seasonality over the southern West African coastline may bring into question the realism of climate projections in this region as well as the utility of CGCMs for establishing the driving mechanisms and exploring teleconnections. Failure to capture the LDS and associated processes may indicate more general difficulties with the representation of monsoon dynamics for example insufficient northward progression of the monsoon. Dike et al. (2015) also identified the lack of the LDS over Nigeria in one coupled climate model, but did not investigate this discrepancy further. While other studies have explored deficiencies in the representation of the wider West African Monsoon, few have explicitly investigated the representation of the LDS in global climate models (Dunning et al., 2017). Here, we aim to investigate possible factors that lead to this deficiency. Such factors may also influence model simulations in other regions where similar processes operate.

Adejuwon and Odekunle (2006), Odekunle and Eludoyin (2008) and Parker and Diop-Kane (2017) all highlight the role of cool SSTs in the Gulf of Guinea in the seasonal cycle of precipitation over the southern West African coastline and the LDS, via influences on the location of the tropical rain belt and static stability over the coastline. Locally, where warm onshore waters persist (e.g. to the east around the Niger Delta in Nigeria and off the coast of Liberia, e.g. Figure 4.1e-f) the LDS is weak or absent (Parker and Diop-Kane, 2017). At a larger scale, warm biases in tropical South Atlantic SSTs are ubiquitous across

the current generation of global climate models, due to errors in ocean upwelling, marine stratocumulus and equatorial winds (Richter et al., 2012; Găinușă-Bogdan et al., 2017). Due to the strong relationship between Atlantic SSTs and the West African Monsoon (Hagos and Cook, 2009), these biases have been associated with deficiencies in the representation of the West African Monsoon (Roehrig et al., 2013). Steinig et al. (2018) and Eichhorn and Bader (2017) found SST biases in the tropical Atlantic were related to precipitation biases over the Guinea coastline. Conversely, several studies including Hagos and Cook (2009) and Okumura and Xie (2004) note the influence of the West African monsoon on SST, and weaker winds associated with a deficient monsoon circulation may lead to reduced upwelling and warmer SST, reducing the land-sea thermal contrast and thus reducing the strength of the monsoon circulation. Dunning et al. (2017) found that the Coupled Model Intercomparison Project Phase 5 (CMIP5) historical simulations did not contain the correct magnitude of SST seasonal cooling from April/May to August over the northern Gulf of Guinea, and proposed that this resulted in the incorrect seasonality of precipitation over the southern coastline of West Africa, and lack of the LDS. However, there are many other differences between atmosphere-only and coupled climate model simulations in addition to SST that may affect the representation of the LDS, such as the inclusion of air-sea interactions, which has been shown to have significant impacts on the representation of other tropical phenomena, such as the Madden Julian Oscillation (DeMott et al., 2015).

In this study, we employ the UK Met Office Unified Model (MetUM) to investigate factors influencing the representation of the seasonal cycle of precipitation over the southern coastline of West Africa. In addition to standard atmosphere-only and coupled configurations, a novel aspect of the present work involves the application of the Global Ocean Mixed Layer configuration (Hirons et al., 2015). Using this configuration firstly enables us to cleanly identify the role of air-sea coupling on the representation of the LDS, and secondly to allow us to analyse the impact of different mean ocean states, while maintaining short timescale air-sea coupling. The potential mechanisms underlying the representation of the LDS are explored to understand the factors that influence the seasonal cycle over this region.

4.2 Model, Methods, Data

4.2.1 MetUM Simulations

We analyse atmosphere-only and fully coupled simulations from the MetUM Global Atmosphere version 6.0 (GA6, Walters et al., 2017) and MetUM Global Coupled Model version

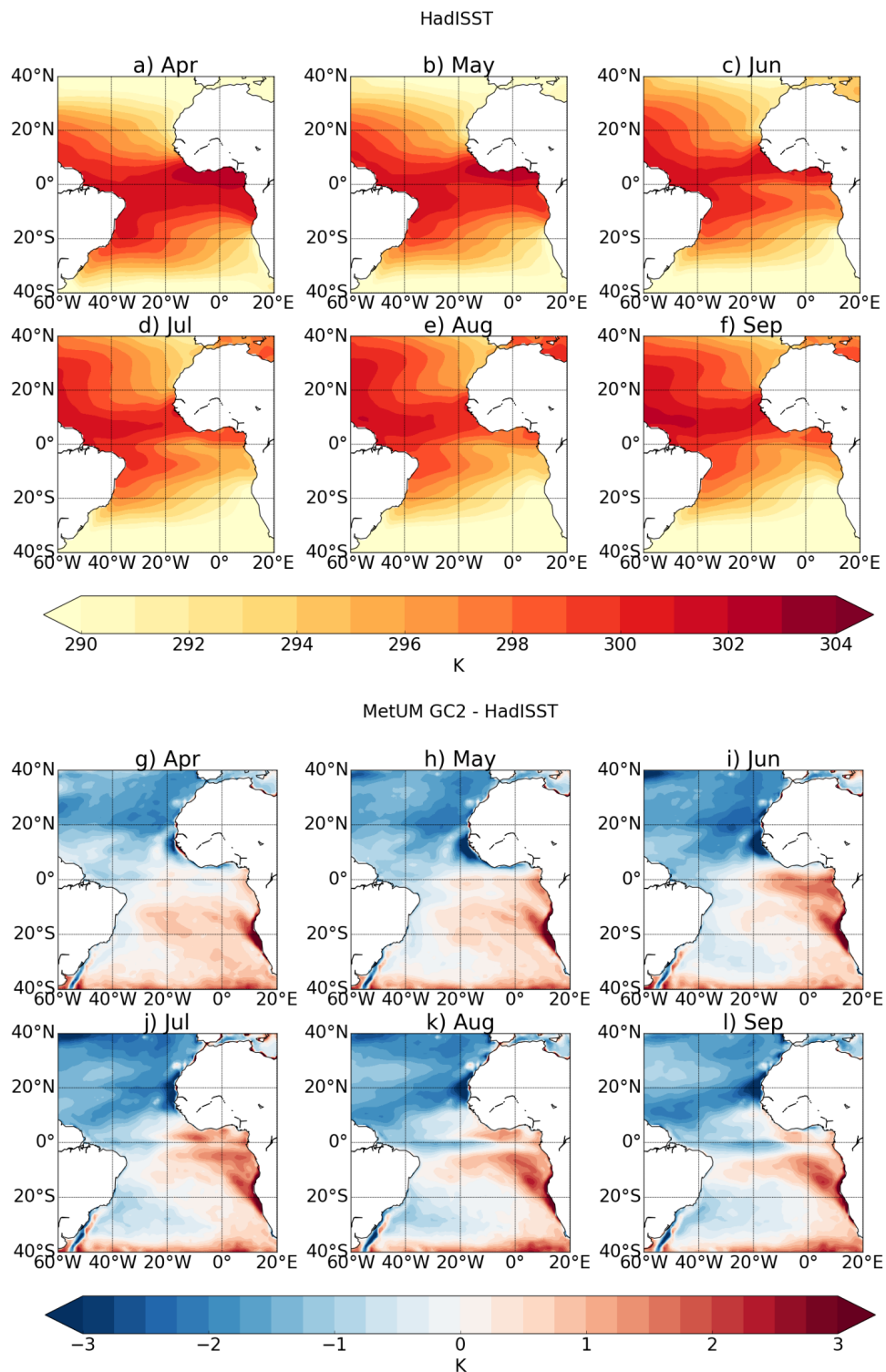


Figure 4.1 a-f) Mean monthly SST from HadISST for April-September. g-l) Difference between HadISST SST and annual mean surface temperature from MetUM GC2 (fully coupled configuration of the MetUM), at N216 resolution for April-September.

2.0 (GC2, Williams et al., 2015) respectively. See Table 4.1 for a full list of simulations used in this study. GA6 is forced using daily observed SST (Reynolds et al., 2007) and sea ice forcings (Taylor et al., 2012) (including interannual variability) and also includes an interactive land surface. GC2 consists of atmosphere, ocean, sea ice and land surface models, with fluxes of momentum, freshwater and heat exchanged between the atmosphere-land and ocean-ice components via the OASIS3 coupler (Ocean Atmosphere Sea Ice Soil, Valcke et al., 2003) with a 3 hour coupling period (Williams et al., 2015). To assess the impact of horizontal resolution, we use three GA6 simulations, at N96 ($1.88^\circ \times 1.25^\circ$), N216 ($0.83^\circ \times 0.56^\circ$) and N512 ($0.35^\circ \times 0.23^\circ$) horizontal resolution. All the simulations used have 85 levels in the vertical and a model lid at 85km. For GC2, the ocean vertical resolution is 75 levels in the ocean, with a 1m top level (Williams et al., 2015). For the N96 and N216 resolution GA6 simulations 26 years of data (1983-2008) are used, for the higher resolution N512 simulation 9 years (1982-1990) of data are used. For the GC2 simulations 28 years of data are used (nominal years 1983-2010); this simulation uses present-day greenhouse gas and aerosol forcing (no volcanic forcing) and thus these years do not correspond to observations.

We also use the Global Ocean Mixed Layer configuration of the UK Met Office Unified Model (MetUM-GOML). This comprises GA6 coupled to the Multi-Column K Profile Parametrisation Ocean (MC-KPP), which consists of a single oceanic column, with high vertical resolution (100 points in 1000m; top layer 1.2m thick) below each atmospheric grid point, with 3 hour coupling frequency. To represent the mean ocean advection (including upwelling), and account for biases in the surface fluxes, a seasonal cycle of depth-varying temperature and salinity corrections are applied to constrain the mean ocean state in MetUM-GOML to a reference climatology (e.g. observed ocean state or a coupled model ocean state). The 3D temperature and salinity corrections are computed from a 10-year relaxation simulation using MetUM-GOML, where MC-KPP profiles are constrained to the reference climatology with a relaxation timescale of 15 days. The daily mean seasonal cycles of the resulting temperature and salinity tendencies (smoothed with a 31-day running mean) are then applied to a free-running coupled MetUM-GOML simulation with no interactive relaxation. For full details of the simulation design, see Hirons et al. (2015). The structure of MetUM-GOML, with independent one-dimensional ocean columns, and temperature and salinity corrections used to constrain the ocean mean state, means it is very flexible. MetUM-GOML can be constrained to different ocean reference climatologies, regionally or globally, by changing the corrections applied, and independent ocean columns mean that both corrections and air-sea coupling can be applied selectively in time and space. Furthermore, the lack of three-dimensional ocean dynamics means MetUM-GOML is computationally inexpensive (Hirons et al., 2015).

Model Configuration	Ocean reference climatology or SST forcing data	Resolution	Years	Experiment Identifier
GA6	SST - Reynolds et al. (2007) Sea Ice - AMIP	N96,N216 N512	1983-2008 1982-1990	GA6-OBS
GC2	-	N96,N216	28	GC2-GC2
GOML	Met Office ocean reanalysis (1980-2007)	N96,N216	28	GOML-OBS
GOML	GC2 Mean ocean state (100 year average)	N96,N216	28	GOML-GC2
GOML	GC2 Mean ocean state (Atlantic) Met Office ocean reanalysis (Indian and Pacific)	N96	28	GOML-ATL-N96
GA6	GOML-OBS SST	N96,N216	28	GA6-GOML

Table 4.1 Table listing the experiments used in this analysis.

We use three sets of MetUM-GOML simulations (Table 4.1). The first set of simulations uses the observed mean ocean state from the Met Office ocean analysis (Smith and Murphy, 2007) as the reference climatology. The second uses the mean ocean state from the GC2 simulations as the reference climatology. These simulations were performed at both N96 and N216 horizontal resolution. For the third simulation the reference climatology was a hybrid of observations and GC2. GC2 mean ocean state was used over the Atlantic Basin (North Atlantic, North Sea, Mediterranean Sea, South Atlantic and Southern Ocean 67°W to 23°E, with the latitudinal extent determined by region of seasonally varying sea ice, see Figure 2 in Hirons et al., 2015), while observed mean ocean state was used for the Pacific and Indian Oceans. Each experiment is named using the model configuration used, the reference climatology, and the horizontal resolution, thus MetUM-GOML configuration constrained to GC2 mean ocean state at N96 resolution is labelled 'GOML-GC2-N96'. The vertical resolution is 85 levels in the atmosphere with the model lid at 85km; for the ocean MC-KPP is configured with a depth of 1000m over 100 vertical levels with vertical resolution of 1.2m at the surface (Hirons et al., 2015). 28 year simulations are analysed, with present-day greenhouse gas and aerosol forcing.

Using GOML enables us to cleanly separate the role of air-sea interactions and the role of mean state ocean biases on the representation of the seasonal cycle of precipitation over the southern West African coastline, within a coupled framework. Table 4.2 summarises the comparisons used in this study. Hirons et al. (2015) demonstrate that when MetUM-GOML is constrained to observations the SST biases are small (also seen in Figure 4.2b); thus by

analysing GOML-OBS the role of air-sea interactions can be examined in a model with a more accurate ocean mean state. However, Figure 4.2b shows that the inclusion of air sea coupling in GOML-OBS does result in some small SST biases. We performed a further GA6 simulation, forced with 31-day smoothed SSTs (including interannual variability) from GOML-OBS (GA6-GOML) to isolate the role of air-sea interactions, with identical mean SST.

Comparing GOML-OBS with GOML-GC2 explores the role of mean ocean state biases, while maintaining coupling and using the same model configuration. Figure 4.2a,c demonstrates that GOML-GC2 replicates the mean SST biases from GC2-GC2.

Finally, by analysing GOML-ATL-N96 and comparing it to GOML-OBS and GOML-GC2 it is possible to ascertain whether the differences between GOML-OBS and GOML-GC2 are associated with mean ocean biases in the Atlantic Ocean, or mean ocean biases in the Pacific and Indian Oceans. Mohino et al. (2011) identified interactions between the Pacific and Indian Oceans and the West African monsoon and rainfall over the Gulf of Guinea, which suggests that biases in the Pacific and Indian Oceans may affect the LDS. Figure 4.2d shows the difference in annual mean SST between GOML-ATL-N96 and observed SST. Over the South-East Tropical Atlantic a warm bias is apparent, which is present in GC2 (Figure 4.2a,c) and the majority of coupled climate models (Richter et al., 2012; Eichhorn and Bader, 2017; Steinig et al., 2018). Over the Indian and Pacific basins the differences in surface temperature are smaller, similar to Figure 4.2b.

4.2.2 Observations

The Global Precipitation Climatology Project (GPCP) 1 Degree Daily precipitation dataset combines thermal infrared and passive microwave satellite data with rain gauge data to produce daily rainfall estimates over both land and ocean (Huffman et al., 2001). GPCP data for 1997-2014 were used on the native $1^\circ \times 1^\circ$ grid.

For wind speed and mean vertical velocity, ERA-Interim (ERA-I) reanalysis data were used over 1983-2010. ERA-I is produced using the European Centre for Medium Range Weather

Comparison	Impact of
GOML-OBS vs GA6-GOML	Air Sea Coupling
GOML-GC2 vs GOML-OBS	Mean Ocean State (Global)
GOML-ATL-N96 vs GOML-GC2-N96	Mean Ocean State (Atlantic)
GOML-ATL-N96 vs GOML-GC2-N216	Mean Ocean State (Atlantic) and horizontal resolution

Table 4.2 Experiment comparisons used in this study, and the impacts revealed.

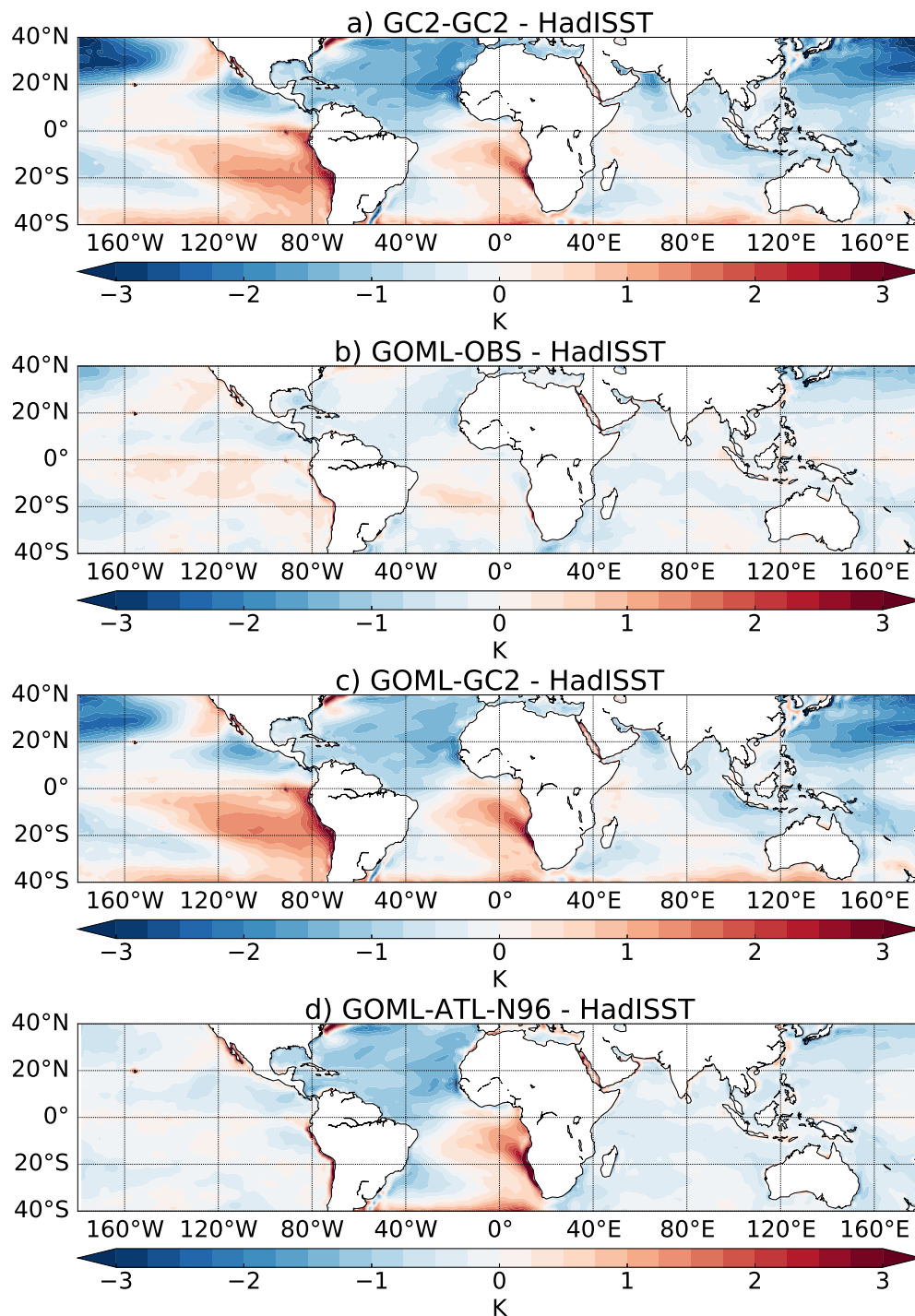


Figure 4.2 Difference between HadISST SST and annual mean surface temperature from a) GC2-GC2, b) GOML-OBS, c) GOML-GC2, at N216 resolution and d) GOML with observed ocean (Indian and Pacific) and GC2 mean ocean state over the Atlantic (GOML-ATL-N96), at N96 resolution.

Forecasts' (ECMWF) Integrated Forecast System combined with data assimilation for the global atmosphere at 0.75° resolution (Dee et al., 2011). Six-hourly eastward (u), northward (v) and vertical (ω) winds were averaged to produce monthly means. For the vertical profiles (Figure 4.9), 12-hourly total precipitation was averaged to produce monthly means.

Monthly HadISST observed SST data was obtained from the UK Met Office at $1^\circ \times 1^\circ$ horizontal resolution for 1983-2010.

4.2.3 Methods

As in Liebmann et al. (2012) and Dunning et al. (2016), harmonic analysis was used to categorise the seasonal regime at each grid point as either an annual regime (one wet season, no LDS) or a biannual regime (two wet seasons). The amplitude of the first and second harmonics at each grid point are computed using daily rainfall, and the ratio is calculated. If the amplitude of the second harmonic is greater than the first (ratio >1.0), then the grid point experiences a biannual regime, whereas if the amplitude of the first harmonic is greater (ratio <1.0) then the grid point experiences an annual seasonal regime.

The region that experiences the LDS (Figure 4.4a, purple crosses) was defined as grid points within 20°W - 10°E , 0° - 15°N that exhibited a biannual regime (according to GPCP data). This method picks out points that exhibit a notable LDS in the majority of years; points where there is a LDS occasionally or where it has only a short duration (e.g. less than a month) are not identified.

In section 4.4 the mean monthly position and width of the Tropical Rain Belt (TRB) is compared across the simulations, and with observations. The monthly mean location of the TRB is defined using a method for identifying the location of the InterTropical Convergence Zone (ITCZ; Shonk et al., 2018). Mean monthly rainfall is computed for each month at each grid point over 30°S - 30°N . For each month and longitude, the latitude of the rainfall centroid is computed, using only latitudes where the rainfall is above half the maximum rainfall rate. The latitude of the rainfall centroid is taken to be mean latitudinal position of the TRB. The width of the TRB was defined using a 3mm/day threshold.

4.3 Performance of MetUM and horizontal resolution

Figure 4.3 shows the seasonal rainfall and 10m winds. The seasonal meridional progression of the main tropical rain belt is apparent, with the rain belt positioned over the northern Gulf of Guinea and southern West African coastline in boreal spring and autumn, and travelling

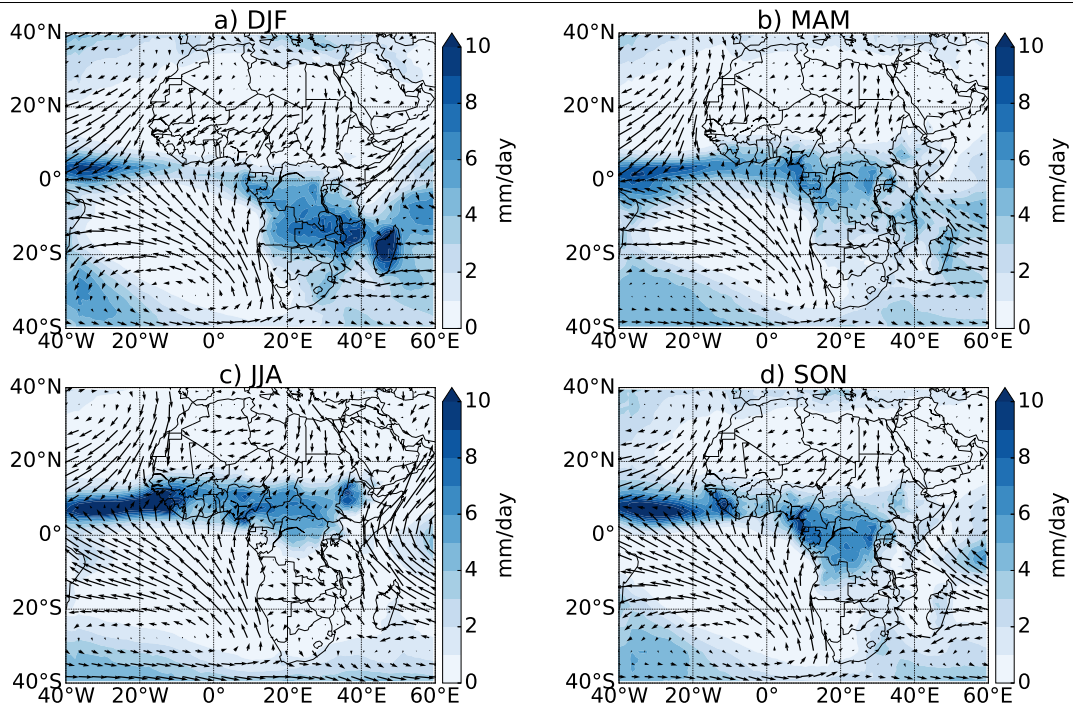


Figure 4.3 Seasonal mean rainfall (GPCP) and 10m winds (ERA-I).

further north over the Sahel in boreal summer. The south-westerly monsoon winds and north-easterly Harmattan winds are also apparent.

We first assess whether the MetUM exhibits the same behaviour as other CMIP atmosphere-only and coupled simulations, as found in Dunning et al. (2017); specifically does GA6 (atmosphere-only) capture the correct seasonal cycle including the Little Dry Season and does GC2 (fully coupled simulation) contain one season per year, with the peak in July-August. We also investigate which resolution is most suitable for this analysis.

GA6-OBS correctly captures the first wet season and the Little Dry Season (LDS) at all resolutions (Figure 4.4). However, the magnitude of the second season is much lower than observed, particularly in the N96 simulation. GC2-GC2 contains one wet season per year, with the peak of the wet season in July-August, in agreement with the coupled simulations from CMIP5 (Dunning et al., 2017). Thus the MetUM can be used to investigate this discrepancy further.

Rainfall bias maps for June-August (JJA) and September-November (SON, see Supplementary Information Figure 7.1, 7.2) show that while GA6-OBS and GC2-GC2 both contain rainfall across West Africa in JJA, moving south in SON, they both exhibit a dry bias over the Sahel in JJA and over West Africa south of 15°N in SON. The JJA bias has also been identified in other studies (Williams et al., 2015; Walters et al., 2017). Thus this suggests that the underestimation of the second wet season in Figure 4.4 is indicative of wider scale

biases in model representation of the monsoon, in both atmosphere-only and coupled simulations. In particular the presence of a dry bias in SON, without a neighbouring wet bias suggests that this error is related to rainfall amplitude, not a spatial displacement. Stratton et al. (2018) found that using a convection-permitting simulation of the MetUM reduced the JJA rainfall bias, due to better representation of westward propagating mesoscale convective systems and more rainfall at higher rain rates. In this study the focus is on the differences between atmosphere-only and coupled simulations and impacts upon the southern West African coastline, hence the factors leading to this bias are not explored further.

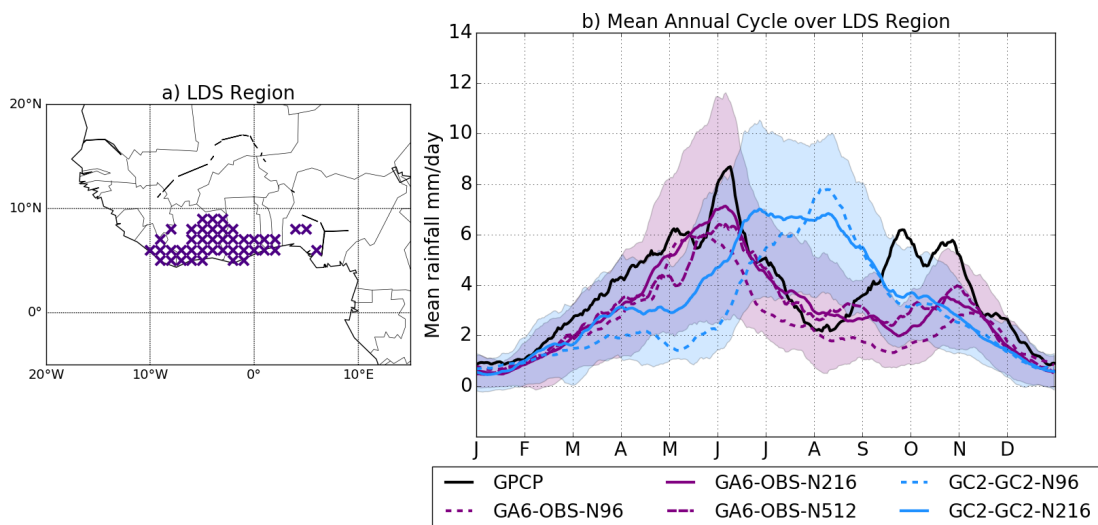


Figure 4.4 Panel (b) shows the mean annual cycle of precipitation over the LDS region (shown in panel a) in GA6-OBS at N96, N216 and N512 resolution and GC2-GC2 at N96 and N216 resolution. For the time periods used see Table 4.1. The black solid line shows the mean seasonal cycle from GPCP over 1997-2014.

Horizontal resolution improves the representation of the seasonal cycle in the LDS region from N96 to N216 (Figure 4.4). The rainfall maxima are higher at N216, closer to the GPCP rainfall totals. None of the simulations correctly capture the magnitude of the second wet season. N512 resolution shows little benefit over N216.

Figure 4.5 shows the region that experiences a biannual regime in the GA6-OBS and GC2-GC2 simulations (red), defined using harmonic analysis (ratio threshold of 1.0, see section 4.2.3), at different resolutions, compared with GPCP (black dashed line). Liebmann et al. (2012) use a threshold of 0.75 to maximise the region with a biannual regime, hence regions where the ratio is greater than 0.75 are marked in blue. White indicates that an annual regime is experienced (ratio less than 0.75). Both the GA6-OBS N216 and GA6-OBS N512 simulations contain a zonal band that experiences a biannual regime, similar to that found in the GPCP precipitation data. In the N96 simulation this band is split, with a biannual seasonal regime seen at only a few longitudes. For GC2 the band is split in both the N96 and N216

simulations, with a biannual regime not captured between 10°W and 0°. Figure 4.5 suggests that the N216 simulation captures the seasonal cycle better than the N96 simulation does, but the difference between the N216 and N512 simulation is minimal. Vellinga et al. (2016) found that higher resolution MetUM simulations capture the westward propagating, intense convection systems over West Africa that bring much of the seasonal rainfall, while in lower resolution simulations rainfall is weaker and occurs synchronously across the Sahel. Additionally, using higher resolution enables the model physics to better represent the processes and interactions between rainfall and dynamics, leading to more realistic representation of strong rainfall events and decadal trends (Vellinga et al., 2016), although they also found greatest benefit at N512, not N216. Throughout the remainder of this study N216 resolution is chiefly used (except for GOML-ATL-N96); when N96 is used this will be indicated in the experiment identifier, otherwise N216 should be assumed.

4.4 Effect of Air-Sea Interactions and Ocean Mean State

Comparing GA6-GOML and GOML-OBS (and GA6-OBS) cleanly identifies the impact of including air-sea coupling (see Section 4.2.1, Table 4.2). The seasonal cycle of precipitation over the LDS region (Figure 4.4a) from these three simulations is shown in Figure 4.6a. All three simulations show similar seasonal cycles, and show good agreement with GPCP from January-August and December, but underestimate the second wet season during September-

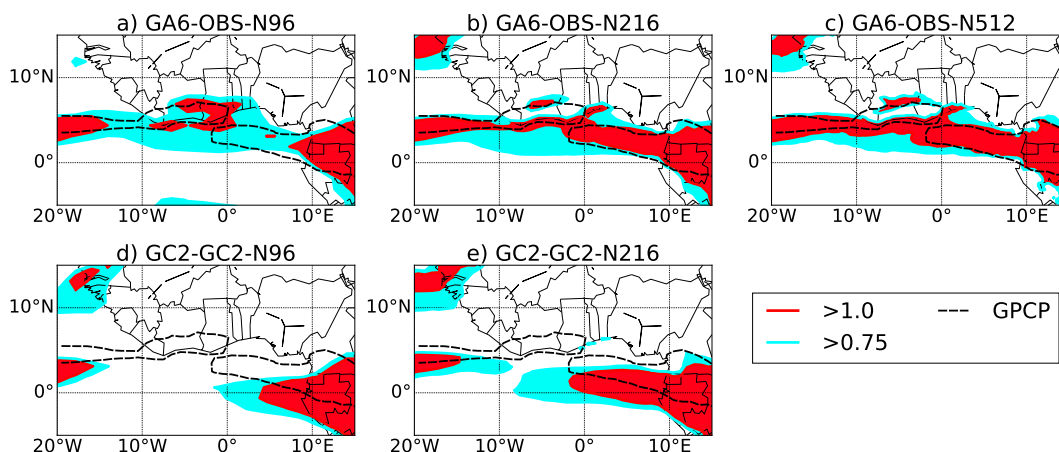


Figure 4.5 Ratio of the amplitude of the second harmonic to the amplitude of the first harmonic at each grid point across West Africa for 3 GA6-OBS simulations at N96 (1983-2008), N216 (1983-2008) and N512 (1982-1990) resolution and 2 GC2-GC2 simulations at N96 and N216 resolution. In general, a high ratio (greater than 1.0) indicates a biannual seasonal cycle, while a low ratio (less than 1.0) indicates an annual seasonal cycle. The black contour shows the location of where the ratio is equal to 1.0 when GPCP data is used, and demarcates the region that experiences a biannual regime. White indicates the ratio is less than 0.75 (annual regime).

November. The correlation matrix shown in Figure 4.6b shows strong correlations, with coefficients greater than 0.9, between the three seasonal cycles, and statistically significant positive correlation with GPCP, with coefficients greater than 0.81. Some slight differences between GA6-OBS and GA6-GOML (Figure 4.6) suggest that small SST biases in GOML-OBS influence the precipitation seasonal cycle here. Including air-sea coupling, while maintaining the same mean SST, has a minimal impact on the representation of the seasonal cycle over the LDS region. Including thermodynamic air sea coupling also does not improve the intensity of the second wet season.

Comparing GOML-GC2 to GOML-OBS isolates the effect of the ocean mean states on the seasonal cycle of precipitation over the southern West African coastline (see Section 4.2.1, Table 4.2). Both GC2-GC2 and GOML-GC2 misrepresent the seasonal cycle, with one wet season per year, with the peak in rainfall occurring when the LDS should occur (Figure 4.6a), hence the inclusion of coupled model mean ocean state biases leads to the incorrect seasonal cycle. Figure 4.6a shows that the difference between GOML-GC2 and GOML-OBS is much greater than the difference between GOML-OBS and GA6-OBS, indicating that GC2 mean ocean biases have a bigger impact on the seasonal cycle in the LDS region than the inclusion of air-sea coupled physics.

The seasonal cycle from GOML-ATL-N96 (Figure 4.6a) shows similar patterns to GOML-GC2, with one wet season per year, peaking in July/August, during the observed LDS. GOML-ATL-N96 underestimates rainfall relative to GOML-GC2-N216, but has similar rainfall totals to GOML-GC2-N96 (Figure 4.6a), suggesting this underestimate is related to horizontal resolution rather than differences in the mean ocean state.

The correlation of the mean annual rainfall cycle across the simulations (Figure 4.6b) demonstrates that the agreement is greatest between the simulations with the same mean ocean state; strong correlations are found between GA6-OBS and GOML-OBS, and between GC2-GC2 and GOML-GC2, with correlation coefficients greater than 0.95. Conversely, agreement is much lower between simulations with the same model but different ocean states (GOML-OBS and GOML-GC2) and GA6-OBS and GC2-GC2, with correlation coefficients in the range 0.49-0.62. For the GOML-ATL-N96 simulation, Figure 4.6b indicates better agreement between GOML-ATL-N96 and either GOML-GC2-N96 or GOML-GC2-216 (correlation coefficients of 0.974 and 0.931 respectively), than between GOML-ATL-N96 and GOML-OBS (correlation coefficient of 0.304). Thus we surmise that the incorrect representation of the seasonal cycle of rainfall over the southern West African coastline in GOML-GC2 is related to Atlantic Ocean mean state biases.

The incorrect seasonal cycle for simulations with coupled model mean ocean state in the Atlantic (GC2-GC2, GOML-GC2 and GOML-ATL-N96, Figure 4.6a) can be partitioned into a number of components: a late onset and deficient rainfall in May; excess rainfall in July-August, during the peak of the LDS; and insufficient rainfall in October (seen in all simulations). The first two factors, which are not exhibited in GA6-OBS and GOML-OBS, will be explored further.

In order to compare the location of the rainfall in different simulations, Figure 4.7a,e shows the mean monthly position of the TRB (see section 4.2.3 for definition), in May and August (Figure 4.7b,f shows the mean position averaged over 3 longitude ranges). Figure 4.7c,g shows the mean position of the northern and southern limits of the TRB, defined using a 3mm/day threshold (Figure 4.7d,h shows the mean northern and southern limits averaged over 3 longitude ranges). As in Figure 4.6, the GOML simulations are similar to the GA6 and GC2 simulations with the same mean ocean state; GOML-ATL-N96 is similar to GOML-GC2 and GC2-GC2. In May and August all simulations place the TRB south of the observed position in GPCP, especially in those simulations with GC2 ocean state in the Atlantic (GC2-GC2, GOML-GC2 and GOML-ATL-N96).

In May, the mean position of the TRB is just south of the coastline in GPCP (Figure 4.7a). The mean TRB position in GA6-OBS and GOML-OBS is just south of the GPCP mean position (Figure 4.7a-b), with GC2-GC2, GOML-GC2 and GOML-ATL-N96 placing the TRB further south, just north of the equator. The northern and southern limits (solid and dashed lines

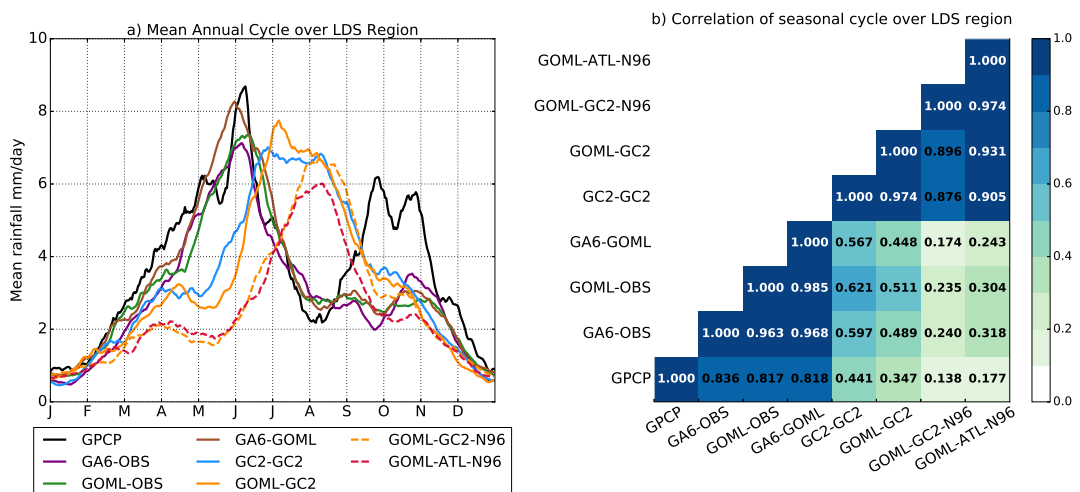


Figure 4.6 a) Mean annual cycle of precipitation over the LDS region (Figure 4.4a) using the simulations listed in Table 4.1. The black solid line shows the mean seasonal cycle from GPCP over 1997-2014. b) Pearson correlation coefficient between the mean seasonal cycle over the LDS region from the different simulations.

respectively; Figure 4.7c-d) confirm this southward bias, with the TRB over approximately 0°N-10°N in GPCP, GA6-OBS, and GOML-OBS, and over approximately 5°S to the coastline in GC2-GC2, GOML-GC2 and GOML-ATL-N96, consistent with the lower rainfall in May over the southern West Africa coastline region (Figure 4.6). Previous studies suggest that the southward bias in mean TRB position is related to warm SST biases in the Gulf of Guinea (Roehrig et al., 2013, Figure 4.1), which will be discussed more in Section 4.4.1. Consistent results across GOML-GC2 and GOML-ATL-N96 confirm this bias is related to Atlantic Ocean mean state biases.

In August, the TRB is positioned over Burkina Faso in GPCP, while GA6-OBS and GOML-OBS exhibit a southward shift, with the TRB positioned over northern Ghana and Ivory Coast (Figure 4.7e). Again, GC2-GC2 and GOML-GC2 place the TRB even further south, with GOML-ATL-N96 exhibiting an additional southward bias (Figure 4.7e-f). The position of the northern boundary is the same in four simulations (GA6-OBS, GC2-GC2, GOML-OBS and GOML-GC2), passing through Senegal, Southern Mali and along the southern boundary of Niger (Figure 4.7g-h). The key difference between these simulations is related to the position of the southern boundary, which leads to the differences in mean position (Figure 4.7e-f). In GPCP, GA6-OBS, and GOML-OBS the southern limit of the TRB crosses the coastline at the Liberia/Ivory Coast border, lies over the middle of the Ivory Coast and Ghana, and crosses the coastline again near Togo. Thus the southern part of the Ivory Coast and Ghana are outside the southern limit of the TRB in August, consistent with the low rainfall in August (Figure 4.6a), and the correct representation of the LDS. In GC2-GC2, GOML-GC2 and GOML-ATL-N96 the southern limit of the TRB is south of the coastline at all longitudes between 20°W and 10°E, consistent with the high rainfall over the southern West Africa coastline region and the incorrect representation of the LDS. The different positions of the southern boundary over the LDS region (10°W-2°E) can clearly be seen in Figure 4.7h. This indicates that the incorrect representation of the LDS in simulations with GC2 SST biases is not solely related to an overall southward shift of the TRB, but may also be related to more local factors (see Section 4.4.2), including differences in patterns of ascent and descent. GOML-ATL-N96 exhibits a southward shift in both the northern and southern boundaries, which is related to horizontal resolution (see Supplementary Information for Figure 4.7 replicated at N96 (Figure 7.3)).

In the next sections May and August are considered separately, and factors related to the rainfall biases in these months are presented.

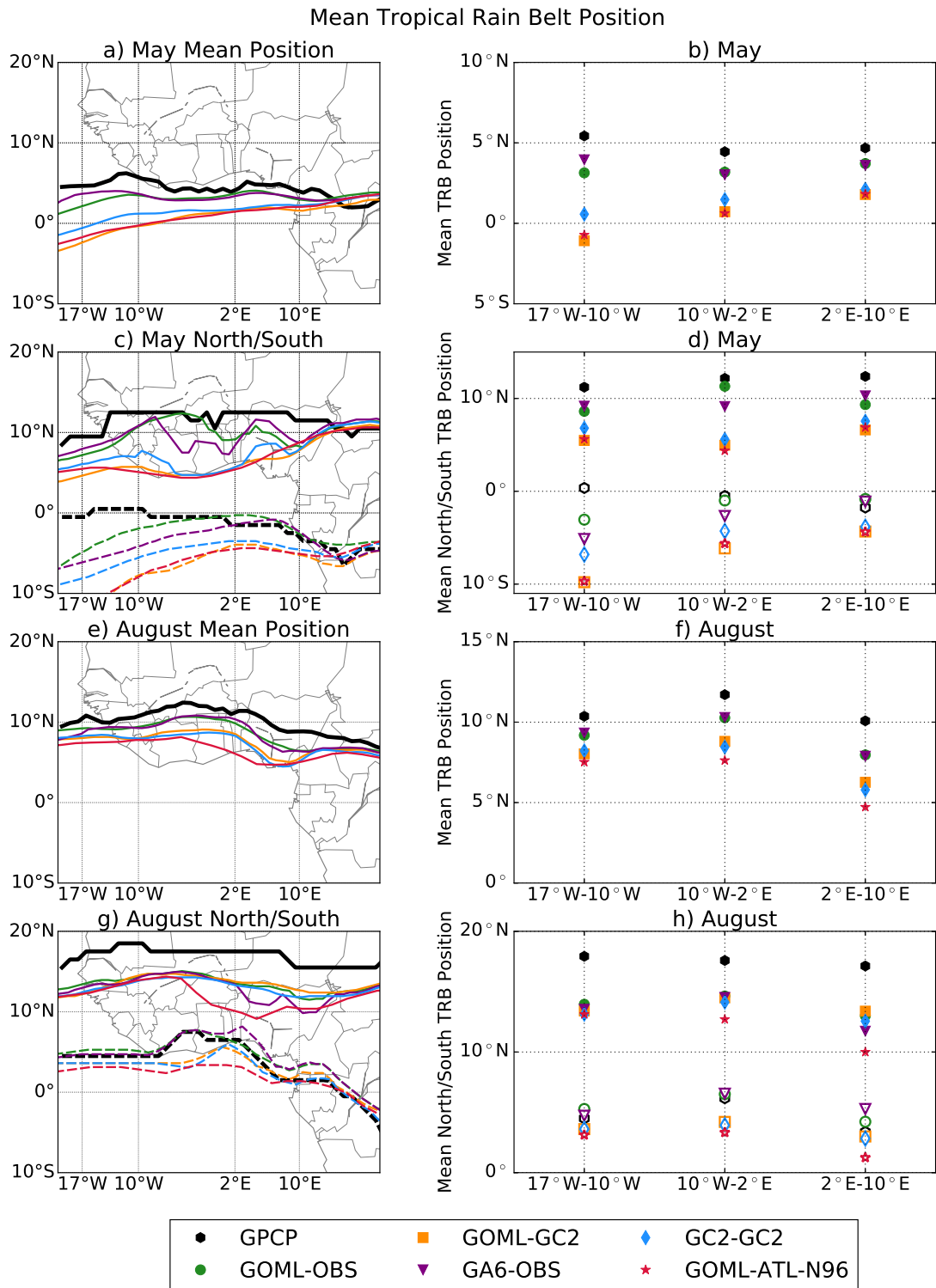


Figure 4.7 Mean monthly position of the Tropical Rain Belt (a,b,e,f) and mean position of the northern and southern limits of the Tropical Rain Belt (c,d,g,h) for May and August. The mean monthly position is calculated by identifying the rainfall centroid using the top 50% of rainfall at each longitude (a,b,e,f). The northern and southern limits are defined using a threshold of 3mm/day. Different coloured lines are for different simulations. The right column shows the mean position averaged over 17°W-10°W, 10°W-2°E and 2°E-10°E. Dashed lines/open symbols indicate the southern boundary. For details of dates and simulations see Table 4.1.

4.4.1 Southward Bias in the TRB position in May

In May, simulations with GC2 mean ocean state (GC2-GC2, GOML-GC2, and GOML-ATL-N96), which includes a warm bias over the southern tropical Atlantic, underestimate the rainfall over the LDS region (Figure 4.6a) due to a southward bias in the position of the tropical rain belt (Figure 4.7a-d).

A number of studies have identified a southward bias in the ITCZ in global climate models, and associated this with SST biases over the tropical Atlantic (Richter and Xie, 2008; Richter et al., 2012; Roehrig et al., 2013; Toniazzo and Woolnough, 2014). Coupled climate models, including GC2 (Figure 4.2), exhibit severe warm biases in the tropical Atlantic, with a large warm bias in the south east tropical Atlantic, peaking at the Angola/Namibia Coastline and extending north-west towards the equator, covering much of the basin (Eichhorn and Bader, 2017). Furthermore, coupled climate models fail to capture the equatorial cold tongue that forms in the eastern equatorial Atlantic during boreal summer (Figure 4.1); combined with the cold bias to the west, this leads to a reversal of the equatorial zonal SST gradient (Richter et al., 2012). Improved representation of Atlantic SSTs (Eichhorn and Bader, 2017), and in particular the Atlantic Cold Tongue, improves the onset and seasonal evolution of the West African Monsoon (Steinig et al., 2018), as colder SSTs in the eastern Atlantic cold tongue region enhance the land-sea temperature contrast and strengthen the monsoon flow (Okumura and Xie, 2004; Chang et al., 2008).

GOML-GC2 and GOML-ATL-N96 show a cold SST bias north of the equator and warm bias south of the equator in May (Figure 4.1, Figure 4.8) which is likely to contribute to the southward bias in the position of the TRB by altering the interhemispheric temperature gradient. A warmer southern hemisphere atmosphere (and cooler northern hemisphere) increases northward cross-equatorial atmospheric energy transport, which induces a southward moisture flux anomaly, which pushes the tropical rain belt south (Hwang and Frierson, 2013; Hawcroft et al., 2017).

ERA-I and HadISST exhibit a northwest-southeast temperature gradient across the tropical Atlantic, with south-easterly winds from the cooler waters off the Angola/Namibia Coastline towards the warmer western equatorial Atlantic (Figure 4.8a). The same pattern is found in GOML-OBS, with small biases (Figure 4.8b). GOML-GC2 and GOML-ATL-N96 (Figure 4.8c,d) contain a north-south temperature gradient in the equatorial region, demonstrated by the warm bias in the east and cool in the west, with associated northwesterly wind anomalies between 0°S and 5°S. These wind biases are also likely to be linked to the southward shift of the TRB. Although the investigation of the relationship between Atlantic SST

biases, wind biases and precipitation biases has been the focus of many studies (Okumura and Xie, 2004; Richter and Xie, 2008; Richter et al., 2012, 2014), establishing causal mechanisms remains a challenge, as in other basins (Shonk et al., 2018).

Richter and Xie (2008) and Richter et al. (2012) argue that the westerly bias in surface winds over the Atlantic during boreal spring, also present in atmosphere-only simulations, is the cause of Atlantic SST biases, since weakened easterlies are associated with a deeper thermocline in the east and reduced equatorial upwelling which inhibits equatorial cold tongue formation. Similarly, Figure 4.8b shows small north-westerly wind biases in the western equatorial Atlantic in May. The eastern warming and western cooling in turn induces westerly wind biases via a Bjerknes feedback mechanism (Richter and Xie, 2008). Richter et al. (2012) propose that this westerly wind bias originates from excess convection over tropical Africa, and reduced convection over South America, which initiates a pressure gradient that drives the westerly wind anomalies (Richter and Xie, 2008). In addition, Richter et al. (2014) highlighted the role of latitudinal position of the boreal spring ITCZ on equatorial surface winds, with a southward shift of the ITCZ linked to the westerly wind bias at the surface. The same pattern of biases is seen in Figure 4.8 (and Figure 4.7), which may suggest the same processes and feedbacks are active in GOML-GC2 (and GOML-ATL-N96). Additionally, other studies have noted the role of the West Africa Monsoon winds on the SST, as the cross-equatorial southerlies induce Ekman equatorial upwelling south of the equator that cools the eastern equatorial Atlantic (Okumura and Xie, 2004; Hagos and Cook, 2009). Reduced cross-equatorial southerlies, as seen in Figure 4.8c,d, will therefore also act to reduce equatorial upwelling in fully coupled simulations, contributing to the warm bias.

The results here demonstrate that mean ocean state biases in the Atlantic lead to a southward shift of the TRB in boreal spring, related to changes in the meridional temperature gradient, and equatorial wind biases, which also affect and respond to the position of the tropical rain belt. Further investigation is required to investigate the complex interplay of factors, including precipitation, wind and SST biases that develop over the Atlantic during boreal spring in coupled simulations.

4.4.2 Overestimation of rainfall during the August LDS

Vertical cross sections of zonal wind and vertical velocity were used to compare the location of regions of ascent and descent and rainfall in the GOML simulations with ERA-I reanalysis over the LDS region (Figure 4.9). For August, ERA-I and GOML-OBS show similar patterns, also in agreement with Nicholson (2009), Nicholson (2013) and James et al. (2017).

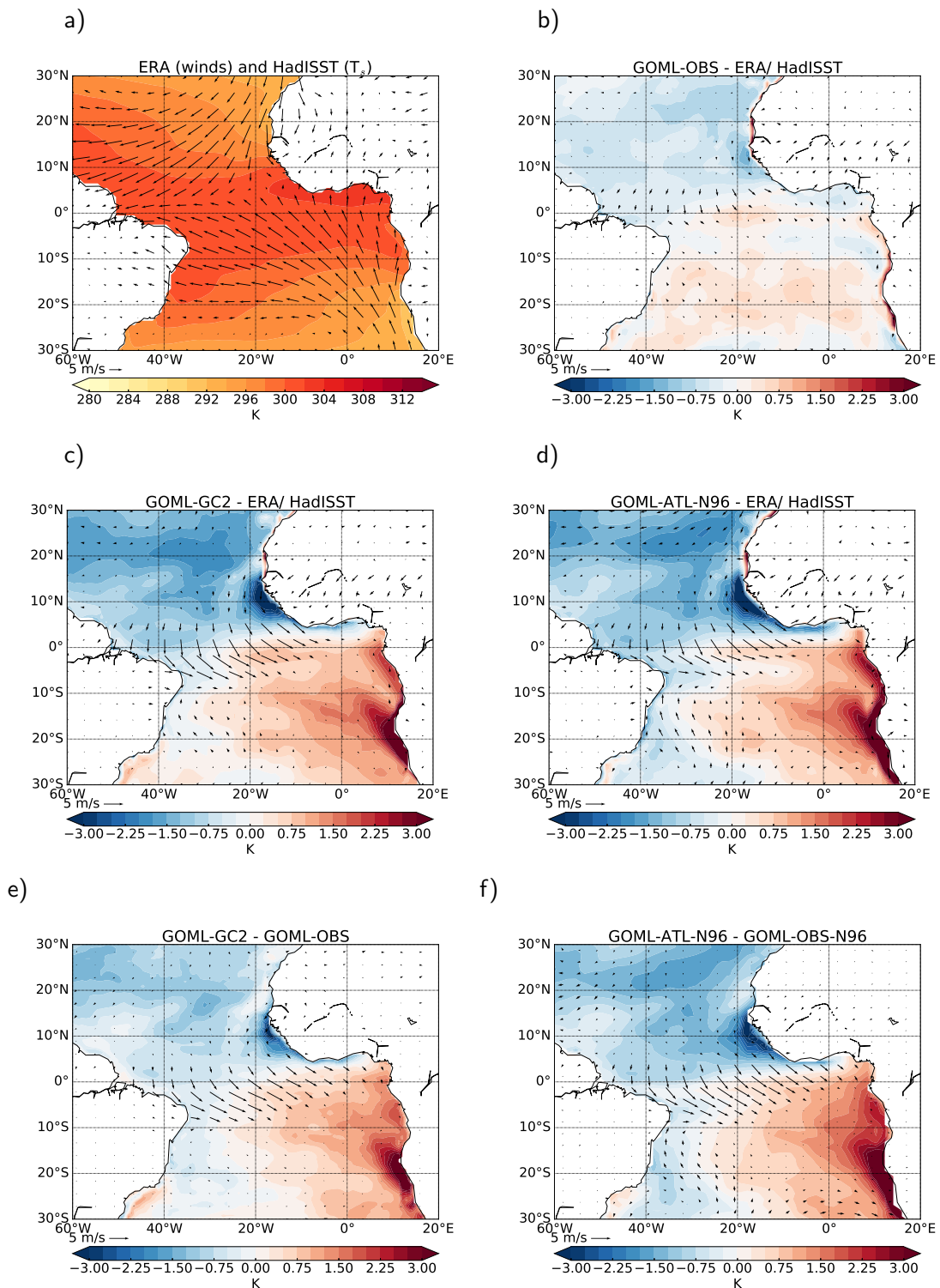


Figure 4.8 Mean 10m wind (vectors) and surface temperature (coloured contours) in May in a) ERA/HadISST (winds/surface temperature respectively). Difference between ERA-I and b) GOML-OBS, c) GOML-GC2, and d) GOML-ATL-N96. e) shows the difference between GOML-GC2 and GOML-OBS and f) shows the difference between GOML-ATL-N96 and GOML-OBS-N96.

Two regions of ascent are identified: one centred around 20°N (shifted slightly south in GOML-OBS) and another deeper region centred around 10°N. The ascent at 20°N corresponds to the surface ITCZ (Nicholson, 2009), while the most of the rainfall is associated with the ascent at 10°N, just north of the coastline. Both ERA-I and GOML-OBS have a weaker, more southerly rainfall peak compared with GPCP (dashed black line). The southward shift of the northern region of shallow ascent in all GOML simulations when compared with ERA-I may indicate that the surface ITCZ does not propagate far enough north, and this may be related to the dry bias over the Sahel in JJA seen in both GA6-OBS and GC2-GC2 (see Supplementary Information, Figure 7.1) and the southward shift of the TRB in Figure 4.7.

Descent over the northern Gulf of Guinea (Figure 4.9a-b), which encroaches onto the southern West African coastline, caps the shallow ascent along the coastline, and gives lower rainfall totals here. ERA-I and GOML-OBS show reduced precipitation along the coast, associated with the LDS, associated with shallower ascent at the coast due to upper level descent. While GOML-GC2 and GOML-ATL-N96 (Figure 4.9c-d) also capture the two main regions of ascent, they do not capture the region of descent encroaching onto the coastline. The ascent at the coastline is deeper, associated with a second rainfall peak on the coast, consistent with earlier results showing rainfall along the coastline in August in GOML-GC2 and GOML-ATL-N96 (Figure 4.6a). The ascent in GOML-ATL-N96 at 10°N is weaker than in GOML-GC2, but this is a consequence of resolution rather than ocean mean state biases (see Supplementary Information, Figure 7.4). All simulations show a southward shift in the position of the African Easterly Jet (AEJ) compared to ERA-I: while in ERA-I (and Nicholson, 2013) the axis of the AEJ is north of the main region of ascent, the GOML simulations show the axis of the AEJ co-located with the ascent at 10°N. James et al. (2017) also identified a southward shift in the AEJ in GC2. Again, this is consistent with the southward shift of the TRB in Figure 4.7 in all simulations. This supports the conclusion from Figure 4.7 that the LDS in August, in both observations and model simulations, is associated with local factors, rather than southward shifts of the rain belt dependent on mean ocean state, as GOML-OBS, GOML-GC2 and GOML-ATL-N96 all contain the southward shift in the AEJ axis. The stronger AEJ in GOML-ATL-N96 compared with GOML-GC2 and GOML-OBS is not a consequence of resolution (see Supplementary Information, Figure 7.4), and is driven by other factors.

Figure 4.9 suggests that the descent above 500hPa and limited ascent along the coastline is associated with reduced rainfall over the coastline during August in ERA-I and GOML-OBS. In GOML simulations with coupled model mean ocean state over the Atlantic (GOML-GC2

and GOML-ATL-N96) the region of descent is shifted south, and the ascent along the coastline is deeper, and higher rainfall is seen along the coastline. Parker and Diop-Kane (2017) state that high pressure over the Gulf of Guinea extends onto the coastline in July-August, with the associated descent inhibiting rainfall, leading to the LDS. Over the northern Gulf of Guinea GOML-GC2 and GOML-ATL-N96 exhibit lower mean sea level pressure in August, compared with GOML-OBS/GOML-OBS-N96 (result not shown). Although it was not quantitatively shown, Odekunle and Eludoyin (2008) and Odekunle (2010) also proposed that increased static stability over the coastline limits convection and leads to the reduced rainfall associated with the LDS. They suggest that this increased static stability results from the cool SSTs along this coastline during the boreal summer, resulting from local upwelling and the advection of cold upwelled waters from other regions. Similarly, Parker and Diop-Kane (2017) note that the LDS is weak or absent where warm onshore waters persist, for example, to the east around the Niger Delta in Nigeria and off the coast of Liberia. Upwelling between the Liberia/Ivory Coast border and Ghana is a consequence of the non-linear dynamics of the Guinea Current and its detachment from the coast, while upwelling east of Ghana is driven by local winds (Djakouré et al., 2017), hence reduced upwelling in coupled models is consistent with poor representation of the Guinea Current and the westerly wind biases present over this region from June-August (result not shown).

Figure 4.9 demonstrates that when GOML is constrained to the observed ocean state, with the cool SSTs in August (Figure 4.1d-f), upper level descent reduces rainfall along the coastline, whereas the introduction of GC2 mean ocean state biases, including a warm anomaly over the northern Gulf of Guinea (Figure 4.1j-l), leads to ascent along the coastline and the lack of the LDS in those simulations. However, as Figure 4.1 and Figure 4.2 show, differences in SST between GOML-OBS and GOML-GC2 (and GOML-OBS and GOML-ATL-N96) are not limited to the northern Gulf of Guinea, and other GC2 mean ocean biases may also play a role. Further investigation, with additional simulations, is required to elucidate specific regions of influence and mechanisms.

4.5 Discussion and Conclusions

Several configurations of the Met Office Unified Model (MetUM) were used to explore factors that influence the representation of the seasonal cycle of precipitation over the southern coastline of West Africa, which is unrealistically represented in coupled climate model simulations (Dunning et al., 2017). In addition to atmosphere-only (GA6) and fully coupled (GC2) configurations, we analyse simulations with the Global Ocean Mixed Layer (GOML)

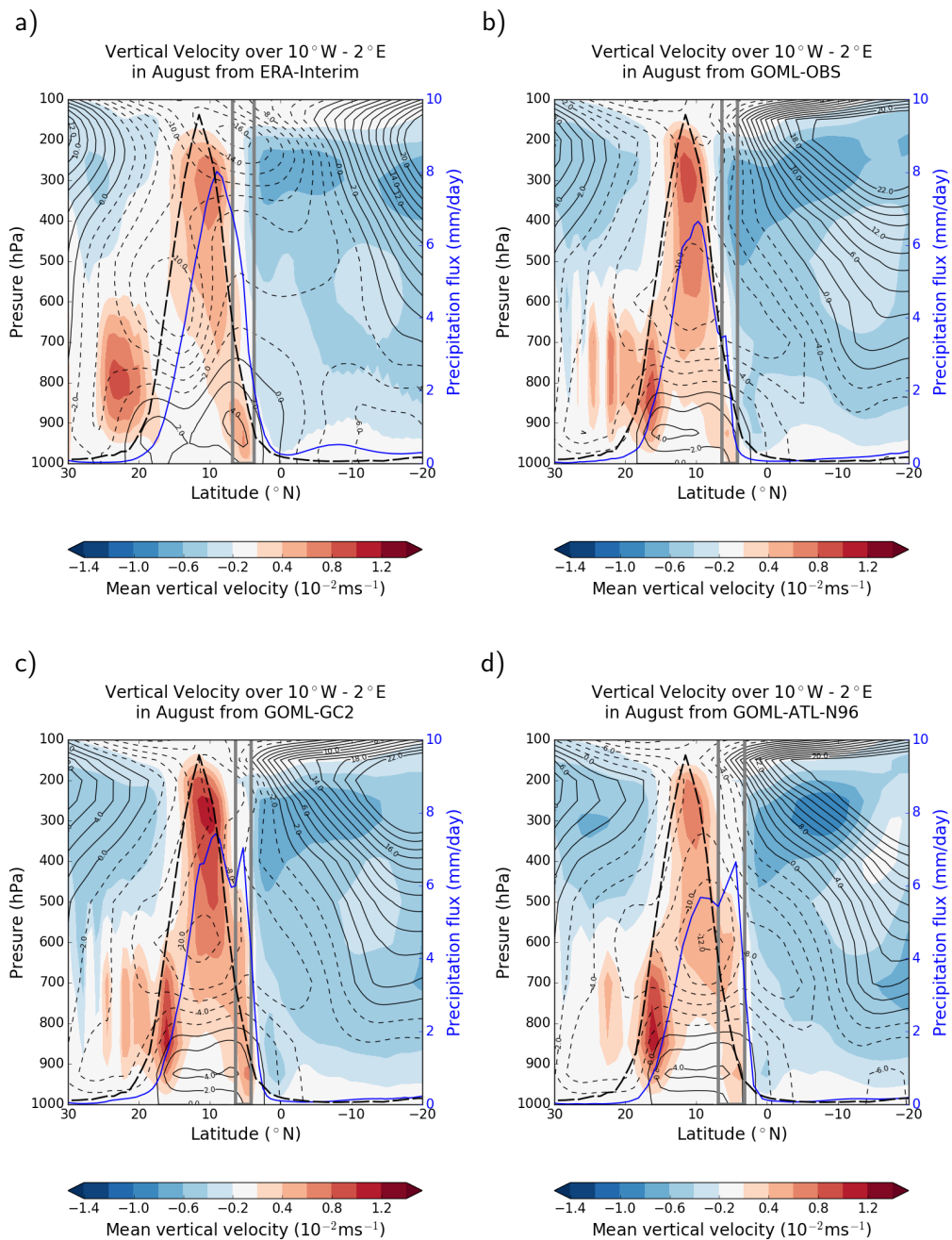


Figure 4.9 Vertical cross section of the mean vertical velocity in August (coloured contours), mean zonal wind velocity (solid/dashed contours for positive/negative values respectively) and mean precipitation (solid blue line) from ERA-I (a), GOML-OBS (b), GOML-GC2 (c) and GOML-ATL-N96 (d) averaged over 10°W to 2°E. The dashed black line shows the GPCP precipitation. The grey lines mark the coastline region (where land sea fraction is between 5% and 95%). For details of dates and simulations see Table 4.1.

configuration, which enables us to cleanly isolate the role of air-sea interactions, and examine the impact of different ocean state climatologies, while maintaining air-sea coupling (Hirons et al., 2015).

We have shown differences in the balance of ascent and descent over the southern West African Coastline in simulations that correctly or incorrectly represent the LDS, adding support to previous studies that suggested that the seasonal reduction in rainfall observed over the southern West African coastline during the LDS is related to increased static stability, which prevents the development of convection and thus inhibits precipitation (Odekunle and Eludoyin, 2008).

All simulations underestimated rainfall over the southern West African coastline in October. This meant that the second wet season, following the LDS, was not captured by any of the model simulations. The presence of this bias in both GA6-OBS and GC2-GC2 demonstrates that this bias is not a consequence of mean ocean state biases nor the inclusion of air-sea coupling. James et al. (2017) show that GC2 also contains a dry bias across West Africa in SON. This bias may be related to the dry bias that occurs further north across the Sahel in June-August in GC2 (James et al., 2017), which is also present in atmosphere-only simulations (Williams et al., 2015), including GA6 and the previous version, GA4 (Walters et al., 2017). Stratton et al. (2018) performed a convection-permitted simulation using the MetUM across Africa and found that the JJA dry bias was reduced, as the convection-permitted simulation contained a realistic westward propagation of mesoscale convective systems, and produced more precipitation, and more at higher rain rates.

The warm SST biases over the south-east tropical Atlantic in GC2 are prevalent in many coupled climate models (Richter et al., 2012; Toniazzo and Woolnough, 2014; Siongco et al., 2015). Other studies have identified the detrimental effect of these biases for the representation of the West African Monsoon and Sahel precipitation, of reducing precipitation over the Sahel (Roehrig et al., 2013; Eichhorn and Bader, 2017; Steinig et al., 2018). Here we have shown that these biases lead to an inaccurate representation of the seasonality of precipitation over a densely populated part of West Africa, where the seasonal rainfall is of high socio-economic importance. These biases inhibit accurate projections of future changes in rainfall amount and timing for the region that experiences the LDS. Further work is required to improve the representation of SST in the Atlantic, which will facilitate greater understanding of future changes in many aspects of the West African Monsoon.

The pattern of SST and surface wind biases apparent in Figure 4.8 are similar to those found by Richter and Xie (2008) and Richter et al. (2012), who state that continental pre-

precipitation biases that initiate westerly wind biases across the equatorial Atlantic, reducing equatorial upwelling, are a source of the SST biases in the equatorial Atlantic. Additionally, reduced strength of cross-equatorial southerlies may reduce equatorial upwelling, and contribute to warm SST biases. Along the Guinea coastline, low horizontal resolution of ocean model components may result in poor representation of the Guinea Current and upwelling, resulting in the warm bias in this region. Establishing the origin of SST biases is beyond the scope of the present study, but further work should examine such processes.

The additional simulation performed with coupled model mean ocean state over the Atlantic, and observed mean ocean state over the Indian and Pacific Oceans demonstrates that the discrepancies in simulations using coupled model ocean state are related to Atlantic Ocean biases, and adds credence to the proposed mechanisms. Further investigation, with additional simulations for example with coupled model ocean biases just over the South-East Atlantic Ocean, or the northern Gulf of Guinea, or with biases only in certain seasons, are required to further elucidate specific regions of influence and mechanisms, but is beyond the scope of this study.

One notable caveat is that GOML does not simulate coupled modes of variability that rely on ocean dynamics (e.g. the El Niño Southern Oscillation, the Indian Ocean Dipole, Atlantic Niños). Thus we cannot capture any mean-state biases that are due to the rectification onto the mean state of erroneous teleconnections from these phenomena to West Africa. The similarity of GOML-GC2 and GC2-GC2 suggests that biases are linked to the mean state, not to variability, and thus this effect is small.

In summary, the overestimation of July-August rainfall in GOML-GC2 over the southern West African coastline is not due to air-sea coupled physics, but rather is linked to mean ocean state biases in the Atlantic. While horizontal resolution plays some role, it is not the primary cause of the biases in this region. The key conclusions are:

- The atmosphere-only configuration of the MetUM simulates two wet seasons over the southern coastline of West Africa, whereas the fully coupled configuration does not exhibit a biannual regime, and places the peak of the one annual wet season during the expected LDS period, similar to the results from CMIP5 coupled models (Dunning et al., 2017). However, the atmosphere-only configuration also underestimates the magnitude of the second wet season, which was not seen in the wider CMIP5 ensemble.
- The Global Ocean Mixed Layer (GOML) configuration allows one to include air-sea interactions while constraining the mean ocean state, which isolates the coupling without

introducing the wrong mean state with large systematic errors in SST. The inclusion of air-sea coupling has a minimal influence on the seasonal cycle of precipitation over the southern coastline of West Africa.

- Differences in the mean ocean state lead to differences in the seasonal cycle of precipitation over the southern West African coastline. When ocean mean state biases from a coupled climate model simulation (GC2) are introduced two wet seasons and the LDS are not captured, and rainfall is underestimated in late boreal spring and early boreal summer.
- The underestimation of rainfall in May in simulations with coupled model mean ocean state biases is related to a southward shift of the main tropical rain belt, associated with; warm SST anomalies in the south eastern tropical Atlantic; cool SST anomalies in the north and west; and north-westerly wind biases between 0°S and 10°S.
- In August, upper level descent caps the ascent along the coastline in reanalysis (ERA-Interim) and GOML-OBS, limiting the convection, resulting in the lower rainfall rates associated with the LDS. In GOML-GC2 and GOML-ATL-N96 the ascent along the coastline is not restricted, leading to greater depth of ascent and high rainfall rates. A number of studies have proposed that the cool SSTs near the Guinea coastline in boreal summer (see Figure 4.1) increase static stability, which inhibits convection and leads to the LDS (Odekunle and Eludoyin, 2008; Odekunle, 2010). Here it is found that the introduction of coupled model SST biases, including a warm anomaly along the Guinea Coast in August, leads to enhanced ascent and rainfall in the LDS region.
- The GOML-ATL-N96 simulation, with coupled model ocean state over the Atlantic, and observed mean ocean state elsewhere, exhibits similar behaviour to the simulations with the coupled model ocean state globally, indicating that the discrepancies discussed above are related to biases over the Atlantic Ocean and not remote teleconnections from the Indian or Pacific Oceans.

In conclusion, mean ocean state biases over the Atlantic Ocean in GOML-GC2 (and GOML-ATL-N96) result in inaccurate representation of the seasonal cycle of precipitation over the southern West African coastline, including the failure to correctly capture the Little Dry Season. This may suggest that the failure to capture the correct seasonal cycle in GC2 and other coupled climate models is associated with SST biases over the Atlantic Ocean, however, the coupled nature of the system renders it impossible to separate forcing from response, and the biases could be result of a different chain of processes. Further work is required to robustly

identify the mechanisms via which the mean ocean state biases and the rainfall seasonality interact, and identify the sources of the SST biases and model modifications which could potentially act to reduce such biases.

Chapter 5:

Later wet seasons with more intense rainfall over Africa under future climate change

Low adaptive capacity and high societal dependence on seasonal rainfall results in elevated vulnerability to the impacts of climate change across much of Africa. Hence the overall aim of this thesis is 'To improve capability for robust projection of user-relevant rainfall characteristics over Africa', by producing projections of user-relevant rainfall characteristics over Africa. In §2 a methodology of quantifying user-relevant rainfall was presented and found to be applicable to datasets with contrasting rainfall biases, and in §3 it is shown that this methodology identifies the wet season in climate model output and thus can be used to produce future projections. §3 also concludes that accurate representation of seasonality over central-southern Africa and West Africa (excluding southern coastline) adds credence for future projected changes in seasonality here.

Thus, in this chapter the methodology developed in §2 is applied to projections of precipitation under future climate scenarios to investigate changing characteristics of African wet seasons, addressing the final aim to 'Interpret projected future changes in seasonal characteristics', advancing previous studies that presented changes in rainfall totals for fixed meteorological seasons or average results over large spatial areas (§5.1). In addition to projections of changes in seasonal timing and total seasonal rainfall, changes in measures of rainfall intensity are presented and processes that give rise to the observed changes are explored.

This chapter is under review at Journal of Climate and the Supplementary Information can be found in the Appendices (§ 7.2).

Later wet seasons with more intense rainfall over Africa under future climate change

Caroline M. Dunning, Emily C.L. Black, Richard P. Allan

Abstract

Changes in the seasonality of precipitation over Africa have high potential for detrimental socio-economic impacts due to high societal dependence upon seasonal rainfall. Here, for the first time we conduct a continental scale analysis of changes in wet season characteristics under the RCP 4.5 and RCP 8.5 climate projection scenarios across an ensemble of CMIP5 models using an objective methodology to determine the onset and cessation of the wet season. A delay in the wet season over West Africa and the Sahel of over 5-10 days on average, and later onset of the wet season over Southern Africa is identified, and associated with increasing strength of the Saharan Heat Low in late boreal summer, and a northward shift in the position of the tropical rain belt over August-December. Over the Horn of Africa rainfall during the 'short rains' season is projected to increase by over 100mm on average by the end of the 21st century under an RCP 8.5 scenario. Average rainfall per rainy day is projected to increase, while the number of rainy days in the wet season declines in regions of stable or declining rainfall (West and Southern Africa) and remains constant in Central Africa, where rainfall is projected to increase. Adaptation strategies should account for shorter wet seasons, increasing intensity and decreasing rainfall frequency, which will have implications for crop yields and surface water supplies.

5.1 Introduction

Africa is acutely vulnerable to the effects of climate change. The large proportion of the population dependent upon rain-fed agriculture for their source of income and subsistence means that future changes in rainfall over Africa have high potential for detrimental socio-economic consequences. In particular, the timing of the seasonal cycle determines the length of the growing season and agricultural yields (Vizy et al., 2015), and affects the transmission period of a number of vector borne diseases (Tanser et al., 2003). Understanding future changes in the seasonal cycle of precipitation over Africa is crucial for establishing appropriate adaptation strategies. In order to assess and interpret future projections of rainfall, we require an improved understanding of the drivers and physical mechanisms behind future changes in seasonality. For the most part, coupled climate models have been found to accurately represent the seasonal cycle of precipitation over Africa (Dunning et al., 2017), affording the

opportunity to investigate future projections and the associated driving mechanisms.

The combination of increased atmospheric water vapour in a warming climate (Held and Soden, 2006; Allan et al., 2010; Chou et al., 2013) with changes in atmospheric circulation, leads to a complex pattern of change in rainfall over the Tropics, with changes in seasonality accompanying changes in rainfall amount. Studies documenting recent enhancements in the seasonal cycle of precipitation, with wet seasons getting wetter and dry seasons getting drier (Chou et al., 2013), and a widening of the tropical belt (Seidel et al., 2008) altering the seasonal progression of the tropical rain belt (Birner et al., 2014), imply changing rainfall seasonality in the tropics (Feng et al., 2013), which will continue under future climate change (Marvel et al., 2017).

Previous studies have examined the changes in annual or seasonal rainfall totals over Africa (Hulme et al., 2001; Lee and Wang, 2014; Tierney et al., 2015; Lazenby et al., 2018). Collins et al. (2013) found increases in rainfall across central equatorial Africa in boreal winter (December-January-February, DJF), particularly over East Africa, with decreases over north-east Africa and southern Africa for the end of the 21st Century (2081-2100). In March-April-May (MAM) Collins et al. (2013) again shows increases in rainfall over central Africa and decreases over northern and southern Africa. Patterns of change are similar in June-July-August (JJA) and September-October-November (SON) with increases over North and North West Africa and decreasing rainfall over southern Africa (Collins et al., 2013).

However, the societally important rainfall, that which impacts agricultural yields and affects the transmission of vector borne diseases, occurs during the wet season which may not coincide with fixed meteorological seasons (Cook and Vizzy, 2012). For example, over the Horn of Africa the second wet season (short rains) occurs in October-December (Camberlin et al., 2009; Shongwe et al., 2011; Yang et al., 2015a). In addition, climate model simulations may contain timing biases, such as over East Africa where the first wet season (long rains; March-May) is late in coupled model simulations (Dunning et al., 2017). Furthermore, other metrics are of high importance to agriculturists in addition to the total amount of seasonal rainfall. The timing of the wet season, and particularly the onset, determines planting dates and thus has large impacts upon agricultural yields (Kniveton et al., 2009).

Some studies have postulated on changes in onset and cessation of the wet season by analysing changes in rainfall amounts in the transition seasons or the months at the beginning and end of the wet season (Biasutti and Sobel, 2009; Seth et al., 2013; Sylla et al., 2015), for example, Shongwe et al. (2009) identified a decline in austral spring (SON) rainfall over southern Africa and associated this with a delay in wet season onset, and Biasutti (2013)

found declining rainfall in the onset months (June-July) and increasing rainfall in the demise months (September-October) implying a delay in the rainy season over West Africa. However, these studies offer no quantitative assessment of how the seasonal timing is changing and do not take into account model timing biases. Furthermore, Monerie et al. (2016) found that the delay in cessation of the West African monsoon was not correlated with the mean late monsoon precipitation change, although we would expect changing onset and cessation dates to be related to changing rainfall at the beginning and end of the wet season. Studies looking at the changing nature of seasonal timing by quantitatively calculating onset and cessation dates tend to focus on the national to regional scale (Vizy et al., 2015) or average the results over large spatial areas, such as in Christensen et al. (2013) where future projections of onset date, retreat date and duration are averaged over a North Africa and Southern Africa region, masking spatial variability. Marvel et al. (2017) examined changes in the seasonal cycle of zonal mean precipitation, and found a later onset at tropical latitudes; however zonal averaging masks spatial variability, especially as the progression of rainfall is not always zonally contiguous (Liebmann et al., 2012; Dunning et al., 2016).

Cook and Vizy (2012) analysed future projections of the growing season in Africa in a single regional climate model, run with 6 ensemble members, with the boundary conditions determined using output from 9 climate model simulations from the CMIP3 generation of models. The number of growing season days is calculated by comparing precipitation to potential evapotranspiration, with start and end dates computed over select regions. They find a longer growing season in the central and eastern Sahel, and reductions in length of the growing season over southern Africa and parts of the western Sahel. The increased resolution of the CMIP5 ensemble enables analysis, previously only possible in regional models, to be carried out in global models. There is thus an opportunity to advance Cook and Vizy (2012)'s results by examining changes across a number of global climate models from the CMIP5 generation of models, enabling the robustness of changes to be examined, using a methodology applicable across an ensemble of climate models, regardless of differences in their basic state. Furthermore, we further their discussion on the mechanisms behind future changes in seasonality.

We use an objective method for identifying the onset and cessation of the wet season, and for the first time investigate changes in characteristics of African wet seasons under climate change across a large ensemble of CMIP5 models at a continental scale. Decomposing the annual cycle into a measure of seasonal timing and rainfall amount enables us to quantify changes in both these aspects of seasonality, for regions with both one and two wet seasons

per year. In addition, changes in measures of rainfall intensity are also considered. This analysis is conducted across continental Africa, enabling us to relate changes in seasonal timing with changes in the meteorological systems that drive the seasonal cycle of rainfall over Africa.

5.2 Methods and Data

5.2.1 Model output and observational data

Daily precipitation data from 29 models used in the fifth phase of the Coupled Model Intercomparison Project (CMIP5, Taylor et al., 2012) was used to compute onset and cessation dates over a recent period (1980-1999), a mid-21st Century period (2030-2049) and a period at the end of the 21st Century (2080-2099). The CMIP5 simulations include fully coupled ocean and are designed to represent observed radiative forcings over the historical period while future projections use the Representative Concentration Pathway (RCP) 4.5 and RCP 8.5. The RCPs comprise scenarios of future changes in greenhouse gas emissions and short-lived species, and land use change, used as a basis for assessing possible climate impacts (Van Vuuren et al., 2011; Thomson et al., 2011). RCP 4.5 is considered an intermediate mitigation scenario, with emissions peaking around 2040, and radiative forcing stabilising at 4.5 Wm^{-2} at 2100, while RCP 8.5 is a high emissions scenario, with emissions rising throughout the 21st century, leading to a radiative forcing of 8.5 Wm^{-2} at 2100 (Van Vuuren et al., 2011; Thomson et al., 2011; Riahi et al., 2011). These two scenarios were chosen to span a range of medium to high emissions future projections. Models were chosen based on the availability of daily rainfall data for the required periods from the British Atmospheric Data Centre (BADC). Table S1 contains a full list of models, name of institute and horizontal resolution. Due to the fact that different models have different numbers of ensemble members, and the small number of available ensemble members, only the first ensemble member (r1i1p1) are used.

Trends from the CMIP5 simulations are compared with those from the atmosphere-only simulations from the Atmospheric Model Intercomparison Project (AMIP); daily rainfall from 28 model simulations over 1979-2008 was utilised (see Table S1 in Dunning et al. (2017) for a full list of models used).

To produce the multi-model means data were regridded using bilinear interpolation to a $1^\circ \times 1^\circ$ grid. For timeseries, variables were averaged over the domain used and no interpolation was applied.

To investigate dynamical aspects of changes (Saharan Heat Low strength index and An-

gola Low index) monthly geopotential height data (at 850 hPa and 925 hPa) was obtained for the 29 CMIP5 models for the historical simulation over 1980-2099 and the RCP 4.5 and RCP 8.5 simulations over 2080-2099. Other variables were also obtained from BADC, including surface temperature, 850hPa temperature (used for calculation of potential temperature), mean pressure at sea level, and relative humidity, specific humidity and u and v winds at 925hPa for the same scenarios and periods.

Dunning et al. (2017) examined the representation of African rainfall seasonality in CMIP5 models, using the same method for categorising seasonal regimes and calculating onset/cessation dates as is used here. The main biases identified include timing biases over the Horn of Africa and an overestimation of the areal extent of the winter rainfall regime over south-west Africa. Furthermore, Dunning et al. (2017) found that the coupled simulations failed to capture the biannual regime over the southern West African coastline. However, for the most part Dunning et al. (2017) reported that coupled climate models capture the observed patterns of seasonal progression and give onset and cessation dates within 18 days of the observational dates, and thus can be used to produce projections of changing seasonality.

In order to compare trends in AMIP and CMIP5 simulations with observed trends, a reference dataset was required. TAMSATv3 (Tropical Applications of Meteorology using SATellite data and ground-based observations version 3) daily rainfall estimates are produced using thermal infrared imagery (TIR) from Meteosat (provided by The European Organisation for the Exploitation of Meteorological Satellites) (Schmetz et al., 2002). Rainfall estimates are calculated using a time invariant calibration, based on rainfall observations from a consistent rain gauge network (Tarnavsky et al., 2014; Maidment et al., 2014, 2017). The temporal consistency of both the gauge measurements used and the calibration, and long time coverage (1983 onwards) makes this dataset suitable for analysis of trends. Datasets which merge in rain gauge observations are not suitable, as the changing rain gauge coverage can result in spurious rainfall trends (Maidment et al., 2015). Rainfall data from TAMSATv3 was used for 1984-2016 and bilinearly interpolated to a $1^\circ \times 1^\circ$ grid. Other datasets were also considered; results produced using the Climate Hazards Group InfraRed Precipitation with Stations (CHIRPS) daily precipitation dataset (Funk et al., 2015) are included in the Supplementary Information for comparison. For the identification of the position of the tropical rain belt daily rainfall data over land and ocean was required, thus daily precipitation data from the Global Precipitation Climatology Project (GPCP) was used over 1997-2014 (at $1^\circ \times 1^\circ$ resolution, Huffman et al., 2001).

5.2.2 Methodology for identifying onset and cessation of rainfall seasons

Onset and cessation dates were calculated using the methodology of Dunning et al. (2016) which extends the methodology of Liebmann et al. (2012). For analysis of changes in onset and cessation dates the method is applied separately to the three time periods used (recent period, mid 21st Century and end of the 21st Century).

The method has three stages; full details of the method can be found in Dunning et al. (2016). Firstly, the seasonal regime at each grid point is categorised as being a dominantly annual regime (one wet season/ year) or biannual regime (two wet seasons/year). This is achieved by computing the ratio of the amplitude of the second harmonic to the first harmonic. Next, in order to account for wet seasons that span the end of the calendar year, the period of the year when the wet season occurs, termed the climatological water season, is determined, by identifying the minima and maxima in the climatological cumulative daily mean rainfall anomaly. The climatological cumulative daily mean rainfall anomaly is calculated by first computing the climatological mean rainfall for each day of the calendar year, Q_i , and the long-term climatological daily mean rainfall, \bar{Q} . Using this, the climatological cumulative daily rainfall anomaly on day d , $C(d)$, is:

$$C(d) = \sum_{i=1 \text{ Jan}}^d Q_i - \bar{Q} \quad (5.1)$$

where i ranges from 1 January to the day (d) for which the calculation applies. The minima and maxima in C are used to define the beginning and end of the climatological water season. For locations with a biannual regime the method extension presented in Dunning et al. (2016), not included in the original method of Liebmann et al. (2012), is used to identify the climatological period of the two wet seasons. Finally, onset and cessation dates are calculated for each season and year individually. The daily cumulative rainfall anomaly is computed for each season; onset is defined as the minima in the daily cumulative rainfall anomaly and cessation is defined as the maxima. The period between the minima and maxima is a period when the rainfall is persistent in occurrence, duration, and intensity (Diaconescu et al., 2015). Due to seasons spanning the end of the calendar year, onset and cessation dates are not calculated for the first or last years of each dataset.

In order to produce the timeseries over 1950-2090 the method was modified. The original method does the annual/biannual categorisation over the entire period and also determines the timing of the climatological water season (the period of the year when the wet season occurs) over the entire period. While this is suitable for 20 year periods, it is not suitable for a 140 year

period, where we may expect shifts in the seasonal cycle. In order to overcome the issue of changing annual/biannual categorisation, maps were produced showing regions where models showed a change in annual/biannual categorisation (Figure S3). The West Africa (10°W - 9°E , 7°N - 13°N) and Southern Africa (20°E - 35°E , 10°S - 20°S) regions for timeseries were chosen such that almost no models showed a change in regime (Figure S3). The Central Africa region was chosen to cover the area that showed a large increase in wet season rainfall, with a few models showing a change in regime. The multi-model-mean annual seasonal cycle over the region exhibits an annual regime for both 1980-1999 (historical simulation) and 2080-2099 (RCP 8.5) and thus it was deemed that an annual regime could be assumed for the entire time period over this region (Figure S3). For the Horn of Africa region (land points in 35°E - 51°E , 3°S - 12°N) a biannual seasonal regime was assumed and the two season method was used. If the method could not identify two wet seasons per year then the point was excluded for that year.

The second issue, that of the timing of the climatological water season (period of the year when the wet season occurs), was resolved by determining the period of the climatological water season for each year individually, using a 20 year period centred on the year in question. For example, for 1950, daily rainfall data from 1940-1959 were used to determine the beginning and end of the climatological water season. Onset and cessation dates were then calculated in the same way as described above. This adjustment should take into account any shifts in timing of the wet season.

This onset/cessation methodology identifies the period when the rainfall is persistent in occurrence, duration, and intensity, relative to the mean climate (Diaconescu et al., 2015) and has been used in a number of studies (Boyard-Micheau et al., 2013; Diaconescu et al., 2015; Monerie et al., 2016; Liebmann et al., 2017). The lack of dependence on a particular threshold facilitates the production of contemporaneous onset/cessation dates across datasets with contrasting rainfall biases (Liebmann et al., 2012; Dunning et al., 2016), enabling application to climate model simulations without the need for bias correction (Dunning et al., 2017) as the cumulative rainfall anomaly is calculated separately for each model and grid point. However, because it is a relative measure a systematic increase in rainfall will lead to no change in onset and cessation date, whereas using methods based on exceeding a rainfall threshold (e.g. Marteau et al. (2009); Issa Lélé and Lamb (2010)) would show a change in onset and cessation. Such methods, however, cannot be applied to climate model output, due to biases both in rainfall amount and occurrence, rendering methods that look for 'no dry spell of 7 days in the next 20 days' useless. This justified applying the cumulative rainfall anomaly

method of Dunning et al. (2016), following on from Liebmann et al. (2012), which identifies changes in timing of the most persistent period of rainfall. While this method was shown to have good agreement with local indigenous methods for the present climate (Dunning et al., 2016) the same cannot be assumed for future climates. However, shifts in the timing of the periods of persistent rainfall are likely to relate to changes in timing of agricultural wet seasons, and identifying the wettest periods allows us to look at changes in physical drivers leading to these changes. The aliasing of changes in rainfall amount into changes in onset and cessation should be taken into consideration, and seasonal cycles were checked to ensure that the changes were realistic.

Frequency and occurrence of rainfall within the wet season is also investigated. A threshold of 1mm per day was used to define a rainy day (also used in CLIMDEX indices; see <https://www.climdex.org/indices.html>); for each year and model the number of days over this threshold within the wet season (between onset and cessation) was counted, and the rainfall on these days was averaged to give the number of rainy days, and average rainfall per rainy day respectively. While some models (in particular those with higher spatial resolution, Zhang et al., 2016) may give more realistic current distributions and future changes in the frequency and occurrence of rainfall within the wet season, we have used all of the 29 CMIP5 models used in this study to produce these metrics, as present performance does not necessarily translate into more reliable future projections (Rowell et al., 2016) and extensive model evaluation would be required in order to justify the exclusion of models.

5.2.3 Characterisation of dynamical drivers

In order to assess changes in the seasonal progression of the Tropical Rain Belt, a method for defining the location of the InterTropical Convergence Zone (ITCZ) in terms of the peak rainfall was used (Shonk et al., 2018). Firstly, the mean daily rainfall is computed for each day of the year at each grid point. Only the region between 30°N and 30°S is considered. For each longitude and day the range of latitudes where the rainfall is greater than half of the maximum rainfall rate is considered; within this range the latitude of the rainfall centroid is taken to be the mean location of the ITCZ/ TRB. Two other definitions were also used in the analysis to establish robustness (see Supplementary Information) - the latitude of the maximum rainfall for each longitude and the latitude of the rainfall centroid (not limited to top 50%). Shonk et al. (2018) found that the definition based on the rainfall centroid of the top 50% gave a smoothly varying quantity, while the method based on maximum rainfall can exhibit large variations. Similar methods were also used by d'Orgeval et al. (2006) and

Monerie et al. (2013) to analyse changes in progression of rain belts across Africa.

The Saharan Heat Low (SHL) and Angola Low (AL) are important drivers of rainfall seasonality and variability over West Africa and the wider Sahel (Lavaysse et al., 2009) and Southern Africa (Munday and Washington, 2017) respectively. An index was required for quantifying the strength of the SHL and AL to establish whether changes in the strength of the SHL or AL will influence changing seasonality. Munday and Washington (2017) identified the AL as the lowest 5% of December-January-February (DJF) mean geopotential height (at 850hPa) over southern Africa (5°E-55°E, 0°-35°S). The strength of the AL is defined as the mean geopotential height within this mask, with lower geopotential height values indicating a stronger AL. Lower level atmospheric thickness is commonly used to determine the location and strength of the SHL (Lavaysse et al., 2009); Dixon et al. (2017a) and Dixon et al. (2017b) identified the location of the SHL to be where the low-level atmospheric thickness (925-700hPa) is greater than a 90% threshold over West Africa (0°-40°N, 20°W-30°E). The value of the 90% detection threshold quantifies the strength of the SHL; a higher value indicates higher temperatures and a stronger SHL. With future climate change we expect increasing lower tropospheric temperatures, resulting in higher lower level atmospheric thickness (implying a stronger SHL) and higher geopotential height (implying a weaker AL). Therefore, in order to compare the changing strengths of the SHL and AL, using a metric that takes into account background changes in the meteorological variable used, and uses the same variable to determine the strength of the SHL and AL would be more suitable.

An alternative methodology has been utilised by Biasutti et al. (2009) and Dixon et al. (2017a) for quantifying the strength of the SHL; comparing low-level geopotential heights averaged across the Sahara (20°N-30°N, 10°W-35°E) with the average geopotential height across the entire tropics (20°S-20°N). This comparison gives a climatological index of the local regional monsoon circulation, and in the summer months describes the strength of the SHL, while also accounting for background/large-scale changes in geopotential height. Dixon et al. (2017a) found strong correlation between this index and the index based on lower level atmospheric thickness in July-September. Here we used (15°N-30°N, 15°W-30°E) instead, to exclude the boreal summer low over Saudi Arabia, and ensure the region contained the SHL in the boreal summer months. A similar region was defined over Southern Africa, where Munday and Washington (2017) identified the AL to be; 8°S-30°S, 10°E-35°E and compared with the average geopotential height across the entire tropics (20°S-20°N) to give an index for the AL. The methods of Lavaysse et al. (2009) and Munday and Washington (2017) were used to establish the location of the SHL and AL in present and future climates; as both features

are strongly constrained by topography (Chauvin et al., 2010; Evan et al., 2015; Munday and Washington, 2017) no large shifts in location are expected and thus such metrics can be utilised (see Supplementary Information).

Biasutti et al. (2009) and Dixon et al. (2017a) used geopotential height at 925 hPa for the SHL while Munday and Washington (2017) used 850 hPa for the AL due to lower levels intersecting with topography in some CMIP5 models. Here geopotential height at 925 hPa was used for the SHL and 850hPa geopotential height was used for the AL. The Supplementary Information includes results for both 850hPa and 925hPa geopotential height for both regions and consistent results were obtained (Figure S16-17). Dixon et al. (2017a) noted that this metric describes the strength of the regional monsoon circulation, and only describes the strength of the low during the summer months, when the low is within the regions defined; when discussing results the distinction between the strength of the regional monsoon circulation and strength of the SHL/AL will be noted.

5.3 Changing Rainfall Seasonality and Characteristics

Figure 5.1 shows the median change in onset, cessation, wet season length and seasonal rainfall from 1980-1999 to 2080-2099 (RCP 8.5 scenario) across 29 CMIP5 models. For the RCP 4.5 scenario, a mid-range scenario with a smaller climate change signal than RCP 8.5, consistent spatial patterns of change were found, although generally of smaller magnitude (see Supplementary Information). Spatial patterns were also consistent for the mid-century period, though changes were very small (results not shown). Wet season onset is projected to get later across much of West Africa and the southern Sahel, and over a north-west/south-east orientated strip across southern Africa, with the largest changes of over 12 days on average over parts of Angola, Zimbabwe and Mozambique (8 days for RCP 4.5). West of 0°W, and at all longitudes between 10°N and 20°S, more than 75% of the CMIP models used agree that the onset will get later. In the regions with an annual regime 0°-20°N, Figure 5.1b shows cessation of the wet season getting later, which combined with Figure 5.1a, indicates the wet season over West Africa and the Sahel is shifting later in the calendar year, with little change in length, confirmed in Figure 5.1c. Across West Africa and the Sahel, there is good model agreement (>75% of models) that cessation will get later. This is consistent with the increase in late wet season rainfall found in other studies (Biasutti and Sobel, 2009; Biasutti, 2013; Seth et al., 2013; Monerie et al., 2016). Sylla et al. (2015) found the largest reduction in rainfall in the pre-monsoon and mature monsoon phase west of 5°W and Monerie et al. (2017) also found a decrease in precipitation over the western Sahel; this is in agreement with the

largest delay in onset west of 0-5°W presented in Figure 5.1a . Cook and Vizy (2012) found a reduction in the number of growing season days west of 0°W associated with a delay in onset, where Figure 5.1 also shows onset getting later and a reduction in season length, however Cook and Vizy (2012) also found increases in spring rainfall to the east of this, with an earlier onset, not found in this study or others (Biasutti and Sobel, 2009; Lee and Wang, 2014; Seth et al., 2013; Sylla et al., 2015). Across West Africa and the Sahel they find delays in the end date of 8-10 days on average, in agreement with the results in Figure 5.1. Dunning et al. (2017) found that the coupled CMIP5 models did not capture the correct seasonal regime over the southern West African coastline, thus results there should be viewed with caution.

Over Southern Africa, the later onset results in a shorter wet season, with a reduction in

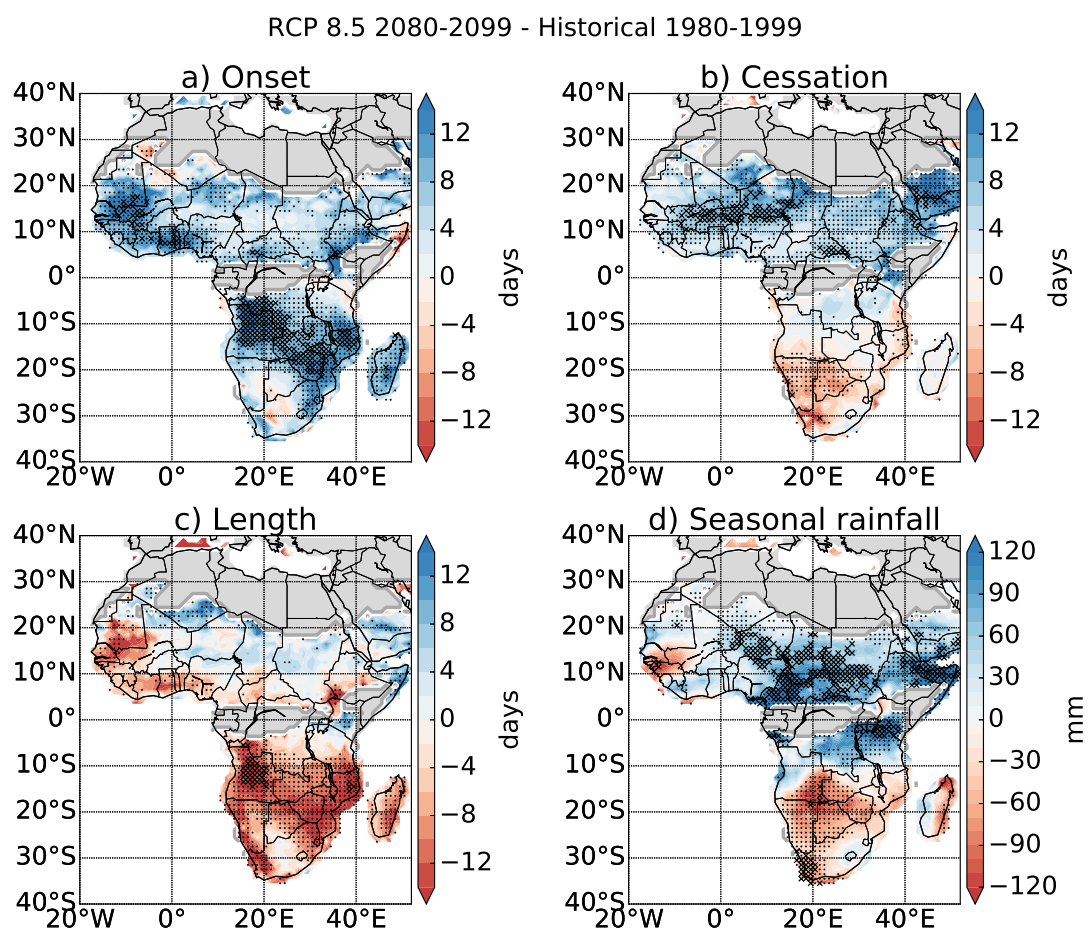


Figure 5.1 Median Change in a) Onset, b) Cessation, c) Season Length and d) Wet Season Rainfall in 29 CMIP5 simulations from 1980-1999 (historical simulation) to 2080-2099 (RCP 8.5 scenario). Blue colours indicate the onset/cessation getting later while red colours indicate onset/cessation getting earlier. Crosses indicate where 75% of the simulations agree on the sign of the change, and more than 50% of the models show a statistically significant change (Mann Whitney U test, 5% significance level). Dots indicate where 75% of the simulations agree on the sign of the change. Grey regions indicate regions where <5 models produce onset/cessation dates due to a dry climate or two wet seasons per year.

total wet season rainfall centred on the Angola/ Namibia/ Botswana/ Zambia border, with more than 75% of the models agreeing on a reduction in rainfall. Similarly, Cook and Vizi (2012) found a reduction in growing season days across Angola and southern Democratic Republic of the Congo associated with a decline in austral spring rainfall leading to a later onset. Figure 5.1b shows earlier cessation over Namibia and Botswana, but very few models indicate a statistically significant change here. Shongwe et al. (2009) also identified a decline in austral spring rainfall over Mozambique and Zimbabwe, which they associated with a delay in the onset. To the north of the equator, in central regions, wet season rainfall is projected to increase, with strong model consensus and the largest statistically significant changes found over Cameroon, southern Chad and the surrounding regions, with average increases greater than 75mm over 15°E-30°E, 5°N-11°N (50mm for RCP 4.5), also found by Cook and Vizi (2012). Little change in total wet season rainfall is found west of 5°E. Over northern Tanzania there is little change in seasonal timing, but an increase in total wet season rainfall.

The central equatorial region and Horn of Africa experience two wet seasons per year; projections for the 'long rains' (boreal spring wet season) and 'short rains' (boreal autumn wet season) are shown in Figure 5.2. Earlier cessation of the long rains and later onset of the short rains implies a longer boreal summer dry season; however these changes are less than a week on average and only statistically significant over small areas. The most notable changes are for the short rains; Figure 5.2d,h shows the end of the short rains occurring over 8 days later on average (similar value for RCP 4.5), and substantial increases in rainfall amount, similar to the findings in Shongwe et al. (2011) and Cook and Vizi (2012). There is strong model consensus, with more than 75% of the models agreeing on later cessation and heavier rainfall across the region. Coupled climate simulations for the historical period overestimate the short rains and underestimate the long rains relative to observations; thus projections of increasing short rains should be viewed with caution (Tierney et al., 2015; Yang et al., 2015b; Dunning et al., 2017). The pattern of surface warming in the Indian Ocean shows greater warming in the northwest Indian Ocean compared to the south east Indian Ocean (Zheng et al., 2013), implying an increasingly positive Indian Ocean Dipole (IOD) (results not shown). Positive IOD leads to increased rainfall over East Africa, particularly during the short rains (Black et al., 2003; Shongwe et al., 2011), which may contribute to the longer and wetter short rains in Figure 5.2. Further south, Funk et al. (2008) found that warming of the Indian Ocean disrupted onshore moisture transports leading to reduced growing season rainfall over South-East Africa. Shongwe et al. (2009) also found a substantial weakening of moisture transport from the Indian Ocean along the south-east coast of southern Africa, related to reduced austral spring rainfall and a later onset. Thus, the pattern of warming in

RCP 8.5 2080-2099 - Historical 1980-1999

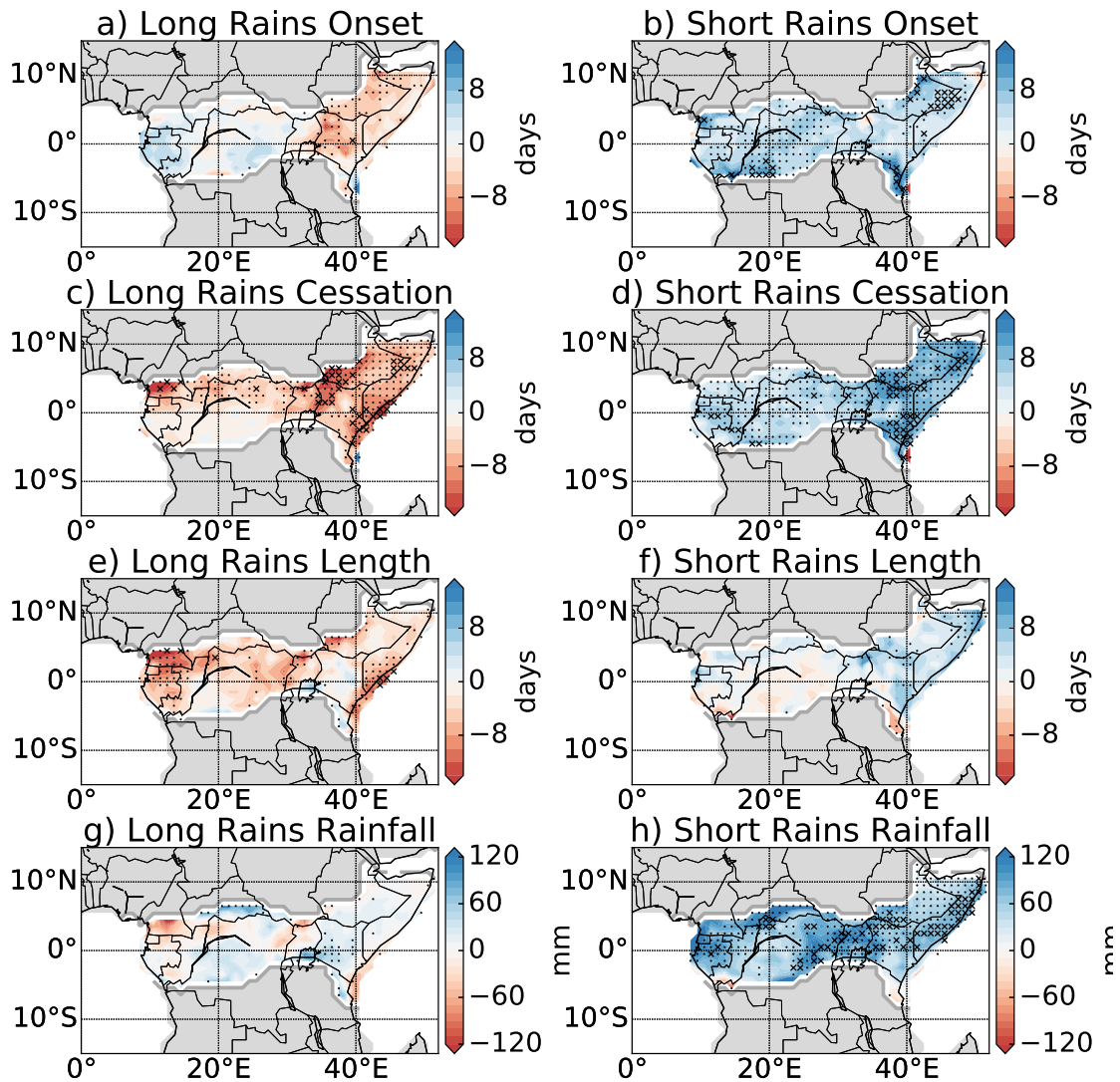


Figure 5.2 Median Change in Onset (a-b), Cessation (c-d), Season Length (e-f) and Wet Season Rainfall (g-h) for the Long (boreal spring, left) and Short (boreal autumn, right) Rains in 29 CMIP5 simulations from 1980-1999 (historical simulation) to 2080-2099 (RCP 8.5 scenario). Blue colours indicate the onset/cessation getting later while red colours indicate onset/cessation getting earlier. Crosses indicate where 75% of the simulations agree on the sign of the change, and more than 50% of the models show a statistically significant change (Mann Whitney U test, 5% significance level). Dots indicate where 75% of the simulations agree on the sign of the change. Grey regions indicate regions where <5 models produce onset/cessation dates due to a dry climate or one wet season per year.

the Indian Ocean may enhance the short rains over the Horn of Africa (Figure 5.2), and lead to later onset and reduced rainfall over Southern Africa (Figure 5.1). However, Lazenby et al. (2018) did not find sufficient evidence of a link between changing OND rainfall over Southern Africa and changing SST gradients.

In addition to the onset and cessation, the manner in which precipitation occurs also impacts agriculturalists and other stakeholders. Long, dry periods can reduce soil moisture and harden the surface layer, thus when heavy rainfall events do occur a smaller fraction infiltrates into the root layer and increased runoff leads to soil erosion (Black et al., 2016). Additionally, heavy rainfall can adversely affect crops such as coffee and cocoa, where intense rainfall may lead to the damage of the flowers (Rosenthal, 2011; Frank et al., 2011; Hutchins et al., 2015). Figure 5.3 shows the change in average rainfall per rainy day and number of rainy days in the wet season (where a rainy day is any day with rainfall ≥ 1 mm during the wet season), in addition to changes in onset and total wet season rainfall over part of Southern Africa (20°E-35°E, 10°S-20°S). While there is only a small change in total seasonal rainfall (Figure 5.3b), there is a significant decrease in the number of rainy days (10 fewer per wet season on average in 2090 compared to 1980-2000), and increase in the average rainfall per rainy day (increase of >0.75 mm/day on average in 2090 compared to 1980-2000; Figure 5.3c-d). Similarly, Sillmann et al. (2013) found a decline in the number of heavy precipitation days, more consecutive dry days and a higher percentage of rainfall coming from very wet days over this region. The observations exhibit much interannual variability, with none of the trends statistically significant at the 5% level (Wald Test, with the null hypothesis that the slope is zero). Over 1985-2007, timeseries from TAMSATv3 and the coupled simulations all show increasing rainfall per rainy day (TAMSATv3 - 0.30 mm/day/decade), in agreement with future trends. While overall there is a slight increase in the number of rainy days, there are large interannual variations. Precipitation estimates based on infrared radiation, such as TAMSATv3, do not capture daily extremes well, so may not simulate this aspect of climate change accurately (Maidment et al., 2014, 2017). Similar patterns of increasing intensity under future climate change are found over West Africa (20°E-35°E, 10°S-20°S, Figure S4), with increasing rainfall per rainy day over 1985-2007 in TAMSATv3, AMIP and the coupled simulations, with trends ranging from 0.09mm/day/decade to 0.12mm/day/decade, and future projections of decreasing numbers of rainy days, with decreases of 5-10 rainy days on average in 2090 compared to 1980-2000. Increasing rainfall per rainy day may explain the non-statistically significant change in rainfall over Mauritania and Senegal (Figure 5.1d), despite the statistically significant reduction in season length (Figure 5.1c), associated with the later onset (Figure 5.1a). Central Africa (15°E-30°E, 5°N-11°N) exhibits increasing average

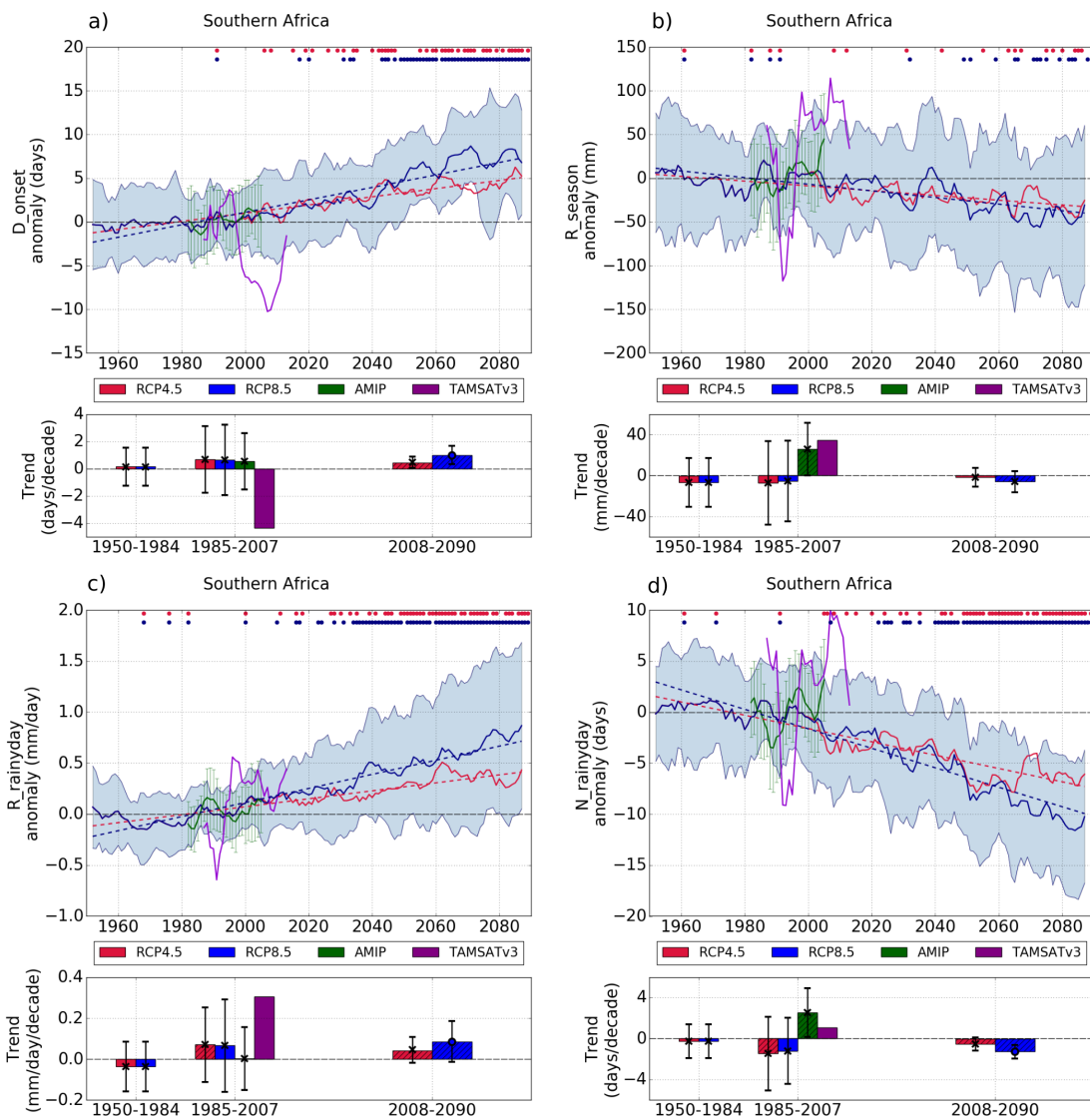


Figure 5.3 Timeseries of a) Onset, b) Total Wet Season Rainfall, c) average rainfall per wet season rainy day ($\geq 1\text{mm}$) and d) number of rainy days ($\geq 1\text{mm}$) in the wet season over a region in Southern Africa ($20^{\circ}\text{E}-35^{\circ}\text{E}$, $10^{\circ}\text{S}-20^{\circ}\text{S}$). The red and blue lines are the multi-model mean (over 29 CMIP5 models) after a 5 year running mean was applied, for RCP4.5 and RCP8.5 respectively over 1950-2090. The blue shaded area indicates the spread of model projections (\pm one standard deviation for RCP8.5 simulations - the spread for RCP4.5 was similar). The green line (with error bars) is the multi-model mean (\pm one standard deviation) for the AMIP simulations (1979-2008). The purple line is produced using TAMSATv3 precipitation (1985-2015). The dots indicate when the range of values from 29 models for that year are significantly different from the range for 1980-2000 at the 5% level, using a Mann Whitney U and t-test. The bar charts indicate the trend over different periods; 1950-1984, 1985-2007 (AMIP and observations period) and 2008-2090. The height of the bars indicates the trend of the multi-model mean; hatching indicates the trend is significantly different from 0 at the 5% level (Wald Test). The circle/cross and errorbar indicate the mean and standard deviations of the trend from the 29 models; a circle indicates over 50% of the models show a trend significantly different from 0 at the 5% level. Multi-model mean timeseries are computed after a 5 year moving average has been applied, and a 5 year moving average is also applied to the observation timeseries; trends are computed using the unsmoothed data.

rainfall per day, both over the observational and future period, and little long term change in number of rainy days (Figure S5), consistent with the increase in seasonal rainfall shown in Figure 5.1d. Other studies have identified similar trends over Southern Africa (Sylla et al., 2015; Pohl et al., 2017) and at wider scales (Cubasch et al., 2001); here we have identified that the same changes occur within the wet season, with the change in number of rainy days potentially important for determining changes in overall seasonal rainfall.

Figure 5.4 shows the observed and projected changes in cessation of the wet season over West Africa (10°W - 9°E , 7°N - 13°N) and Central Africa (15°E - 30°E , 5°N - 11°N), and cessation of the 'short' rains (boreal autumn wet season over the Horn of Africa; land points in 35°E - 51°E , 3°S - 12°N). Dunning et al. (2016) showed that the cessation of the short rains follows on from the cessation of the main wet season over West Africa and the Sahel, associated with the southward retreat of the rain belt in boreal autumn. The projections indicate cessation shifting later in all three regions in the future with multi-model mean changes of up to 10 days (Figure 5.4). Observed trends from TAMSATv3 and AMIP simulations also show cessation getting later, with particularly strong trends in TAMSATv3 over the Central Africa region, with trends of around 5 days/decade over 1985-2007 (Figure 5.4b). Agreement between future projections, AMIP and observed trends adds credence to future projections.

Timeseries for the West African region shows the best AMIP/TAMSATv3 agreement compared to the other regions with trends of 1.8 days/decade and 2.5 days/decade over 1985-2007 respectively. Some of this trend is likely to be attributable to the recent rainfall recovery over Sahel region, following the devastating drought in the 1980s (Biasutti et al., 2009; Nicholson, 2013; Evan et al., 2015), but it is also strongly influenced by decadal climate variability (Maidment et al., 2015). Figure 5.4c shows cessation of the short rains getting later by 4.2 days/decade over 1985-2007 (TAMSATv3), with much interannual variability. Agreement of future projections with past trends may add additional confidence to future projections, though the trends in TAMSATv3 and AMIP are larger than those from the coupled simulations in all three regions, they are more likely to reflect internal climate variability not represented by ensemble mean simulations.

In summary, CMIP5 projections show changes in the seasonal timing of the wet season over Africa. A delay in the wet season is projected over West Africa and the Sahel, with recent trends showing the cessation of the wet season getting later. Over Southern Africa a later onset results in a shorter wet season, and reduced total wet season rainfall. Increasing rainfall is projected for the 'short rains' over the Horn of Africa, with a later end to the season. Model agreement, with >75% of the models agreeing on the sign of the change indicates robustness,

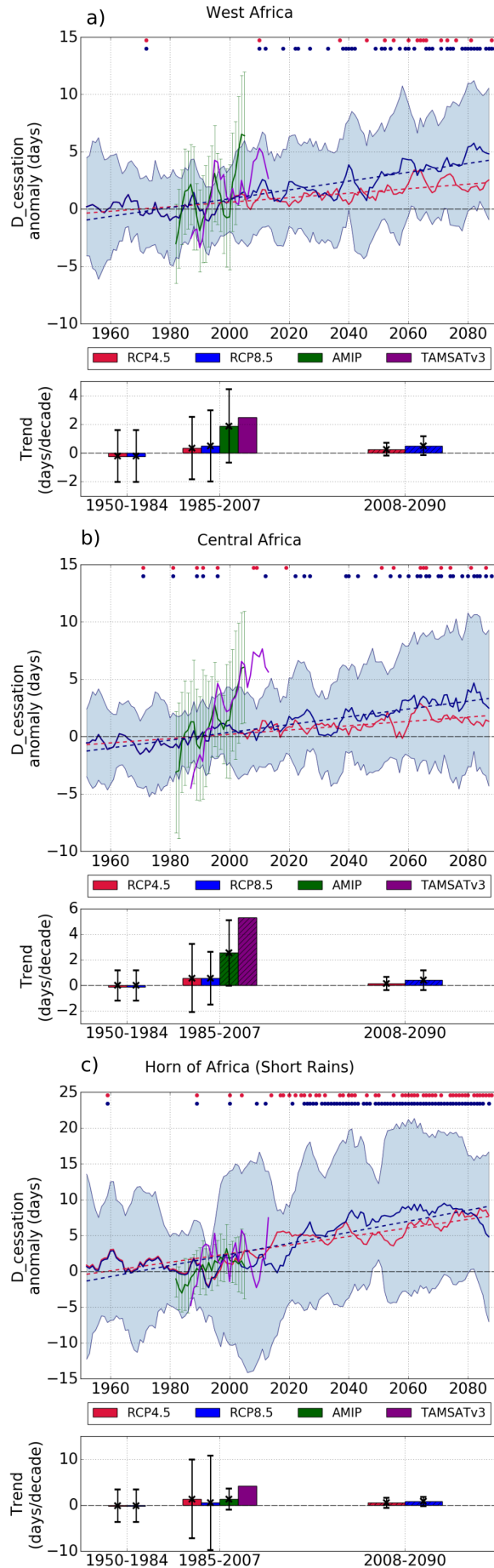


Figure 5.4 As Figure 5.3 but for cessation over regions in a) West Africa (10°W-9°E, 7°N-13°N) and b) Central Africa (15°E-30°E, 5°N-11°N) which experience one wet season per year, and c) cessation of the short rains over the Horn of Africa (land points in 35°E-51°E, 3°S-12°N).

and agreement with observations and AMIP adds credence. Within the wet season average rainfall per rainy day is projected to increase, while the number of rainy days is projected to decline in regions of stable or declining rainfall and remain constant in Central Africa, where rainfall is projected to increase. In the next section possible drivers of such changes will be explored.

5.4 Drivers leading to Later Onset/Cessation of Wet Seasons

The seasonal progression of rainfall over Africa is driven by complex interaction of a number of factors (Nicholson, 2000; Sultan and Janicot, 2003; Lavaysse et al., 2009; Nicholson, 2013; Lazenby et al., 2016; Munday and Washington, 2017; Nicholson, 2017). In this section we investigate changes in a number of mechanisms that drive the seasonal progression of rainfall at the continental scale. In particular, the seasonal progression of the tropical rain belt, and the strength of the Angola Low and Saharan Heat Low are explored. The northward and southward progression of the tropical rain belt, following the maximum incoming solar radiation is one of the major drivers of the seasonal cycle of precipitation across Africa. The Saharan Heat Low and Angola Low form over northern and southern Africa respectively during the local summer, and cyclonic circulation associated with these features leads to significant transport of moisture onto the continent from the neighbouring oceans (Nicholson, 2013; Lazenby et al., 2016). Comparing responses across the ensemble of CMIP5 models, and inspecting outliers, enables us to utilize the CMIP5 ensemble as a 'testbed' to examine mechanistic hypotheses.

The trend of cessation getting later over West Africa and the Sahel, onset getting later over Southern Africa, combined with the later shift of the short rains suggests a change in the progression of the tropical rain belt during the second half of the calendar year. Separate studies have identified factors suggesting both the later shift of cessation over the Sahel (Biasutti and Sobel, 2009; Seth et al., 2013; Monerie et al., 2016) and later onset over South East Africa (Shongwe et al., 2009). Seth et al. (2013) found a redistribution of monsoon rainfall from early to late in the monsoon season, with a reduction in early season rainfall the consequence of an enhanced convective barrier resulting from reduced moisture availability. Dwyer et al. (2014) found a global amplification and phase delay of the seasonal cycle of precipitation, with the delay attributed to changes in the seasonality of the circulation. In this section we investigate factors affecting the delay in the cessation over West Africa and the Sahel, and onset over Southern Africa.

Firstly, the method of Shonk et al. (2018) was used to identify the mean position of the tropical rain belt (TRB) in CMIP5 simulations (see section 5.2.3) to assess whether a change in seasonal progression of the TRB was observed. Figure 5.6a-b shows the mean seasonal progression of the TRB and change over 0°E - 35°E . The analysis was repeated using two other definitions for TRB (latitude of maximum rainfall and latitude of rainfall centroid not limited to top 50%; see section 5.2.3); the same results were obtained, suggesting that the analysis is robust to TRB definition (see Supplementary Information). Figure 5.6a demonstrates fairly good agreement between the seasonal progression of the TRB in observations and CMIP5 models; the main difference is between January and March/April. Under RCP 8.5 the southward progression of the TRB shifts later in the year; the TRB is on average 0.8 - 1.2° north of its position in the historical simulation from August to December, or when viewed from a single latitude the passage of the TRB occurs up to 15 days later. This is consistent with the trends seen in onset and cessation (Figure 5.1- 5.2); a later southward progression leads to a later cessation over West Africa and later onset over Southern Africa. Using similar methods d'Orgeval et al. (2006) also found a northward shift in the location of the rain belt in October and Monerie et al. (2013) identified a northward shift from August-November, when considering the region from 0°E - 25°E , 10°S - 21°N . Analysis with an observational dataset (GPCP) confirms that later southward progression of the TRB is associated with later cessation and onset over West Africa and the Sahel, and Southern Africa respectively (see Supplementary Information and Figure S11). Identifying the position of the TRB over 0°E - 35°E required daily rainfall data over land and ocean, thus GPCP 1DD data was used for this analysis (Huffman et al., 2001). Maidment et al. (2014) showed high correlation between GPCP and TAMSAT rainfall, and Dunning et al. (2016) shows good agreement between onset/cessation dates produced using TAMSAT and GPCP 1DD.

The later onset over West Africa is mostly significant west of 0°W (Figure 5.1). The change in position of the TRB was analysed separately over this region. Between 16°W and 0°W a southward shift in the mean position of the TRB is apparent from January-June under the RCP scenarios compared with historical (1980-1999, see Supplementary Information). This is consistent with the later onset in Figure 5.1a. Other studies have linked reduced early season precipitation over West Africa with lower relative humidity resulting from reduced moisture convergence (Seth et al., 2013) related to south-westerly flow anomalies carrying more moisture to the east (Cook and Vizi, 2012, see Supplementary Information).

During the boreal summer high insolation and low evaporation over the Sahara leads to the formation of an intense heat low (Lavaysse et al., 2009; Dixon et al., 2017a), termed

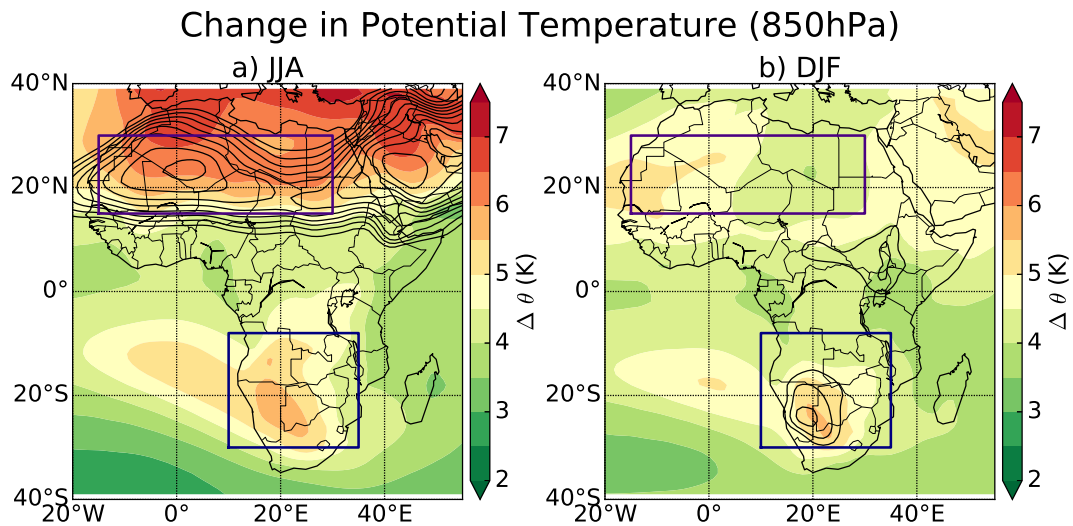


Figure 5.5 Multi-model mean change in potential temperature (850hPa) for RCP 8.5 2080-2099 - historical 1980-1999 in a) JJA and b) DJF. Contours show the multi-model mean potential temperature (850hPa) in the historical simulation (1980-1999), increasing in steps of 1 K from 308 K. The purple and navy boxes indicate the regions used to compute the strength of the SHL and AL respectively.

the ‘Saharan Heat Low’ (SHL), with high surface temperatures and low surface pressures (Lavaysse et al., 2009; Parker and Diop-Kane, 2017). The associated cyclonic circulation increases the north easterly Harmattan flow and south westerly monsoon flow (Lavaysse et al., 2009; Nicholson, 2013; Parker and Diop-Kane, 2017), that transports moisture rich air into the Sahel region, fuelling convection and precipitation (Dixon et al., 2017b) and thus forms a key part of the West African Monsoon (Chauvin et al., 2010; Nicholson, 2013). Variations in both the strength and position of the SHL have been shown to affect the onset of the monsoon and total seasonal rainfall (Lavaysse et al., 2009; Biasutti and Sobel, 2009; Chauvin et al., 2010; Park et al., 2016; Dixon et al., 2017a), as well as intraseasonal variations, including monsoon ‘bursts’ (Nicholson, 2013; Parker and Diop-Kane, 2017). Future projections indicate strengthening and deepening of the SHL leading to increasing Sahel rainfall (Biasutti and Sobel, 2009; Monerie et al., 2016; Vizy and Cook, 2017).

The Angola Low (AL) forms over a plateau region in southern Angola/ northern Namibia in austral summer, at the southern limit of a trough of low pressure trough extending from Ethiopia, through Central Africa, associated with the intertropical convergence zone (Reason et al., 2006; Munday and Washington, 2017). Variations in the strength of the AL have been associated with interannual precipitation variability over Southern Africa (Cook et al., 2004; Munday and Washington, 2017). Increased westerlies from the south-east Atlantic, associated with strengthened AL circulation, increase low-level moisture in this region, increasing the formation of tropical-extratropical cloud bands and precipitation (Cook et al., 2004; Reason

et al., 2006; Lazenby et al., 2016; Munday and Washington, 2017). Conversely, Cook et al. (2004) found that dry late summers (January-March) were associated with a decrease in the strength of the AL.

Given the important role that the SHL and AL play in driving rainfall seasonality and variability over West Africa and the wider Sahel (Lavaysse et al., 2009) and Southern Africa (Munday and Washington, 2017) respectively, their influence in a changing climate was investigated. A metric based on the methodology of Biasutti et al. (2009) and Dixon et al. (2017a) was used to quantify changes in the strength of the SHL and AL (see section 5.2.3). This index describes the strength of the regional circulation throughout the year; during the boreal/austral summer it describes the strength of the SHL/AL respectively (Dixon et al., 2017a). The location of the two regions used to define the strength of the SHL and AL is shown in Figure 5.5, with the colours showing the multi-model mean increase in 850 hPa potential temperature over JJA (a) and DJF (b). The largest increases in temperature are found across North Africa, north of 20°N in JJA. Over the AL region a smaller increase in potential temperature is found in both JJA and DJF.

Comparison of the relative strength of the SHL and AL in the historical and future simulations shows an increase in the strength of the SHL in June-September, with the largest increases toward the end of the boreal summer (Figure 5.6c,e) as found in Biasutti et al. (2009). Recent increasing greenhouse gas concentrations have been shown to act to strengthen the West African Monsoon circulation and the SHL (Dong and Sutton, 2015), with continuing emissions likely to contribute to future strengthening. The magnitude of the increase in strength of the AL in austral summer is similar to the increase in strength of the southern regional circulation throughout the entire year, and is of lower magnitude than the increase in strength of the SHL in the late boreal summer months (Figure 5.6c-e). This is consistent with the increases in potential temperature seen in Figure 5.5.

Thus we postulate that the increase in strength of the SHL, associated with higher surface temperatures, lower surface pressure and lower geopotential height over the region, toward the end of the boreal summer, is causing the TRB to move further north in July and August (Figure 5.6a-b). This in turn delays the southward progression, thus giving a later cessation of the wet season over West Africa and the Sahel, and is one of the factors contributing to the later short rains over the Horn of Africa, and later onset of the main wet season over Southern Africa. The changes associated with the strengthening of the SHL (higher surface temperatures, lower surface pressure (Figure 5.7) and lower geopotential height), toward the end of the boreal summer, favour moisture convergence over the northern part of

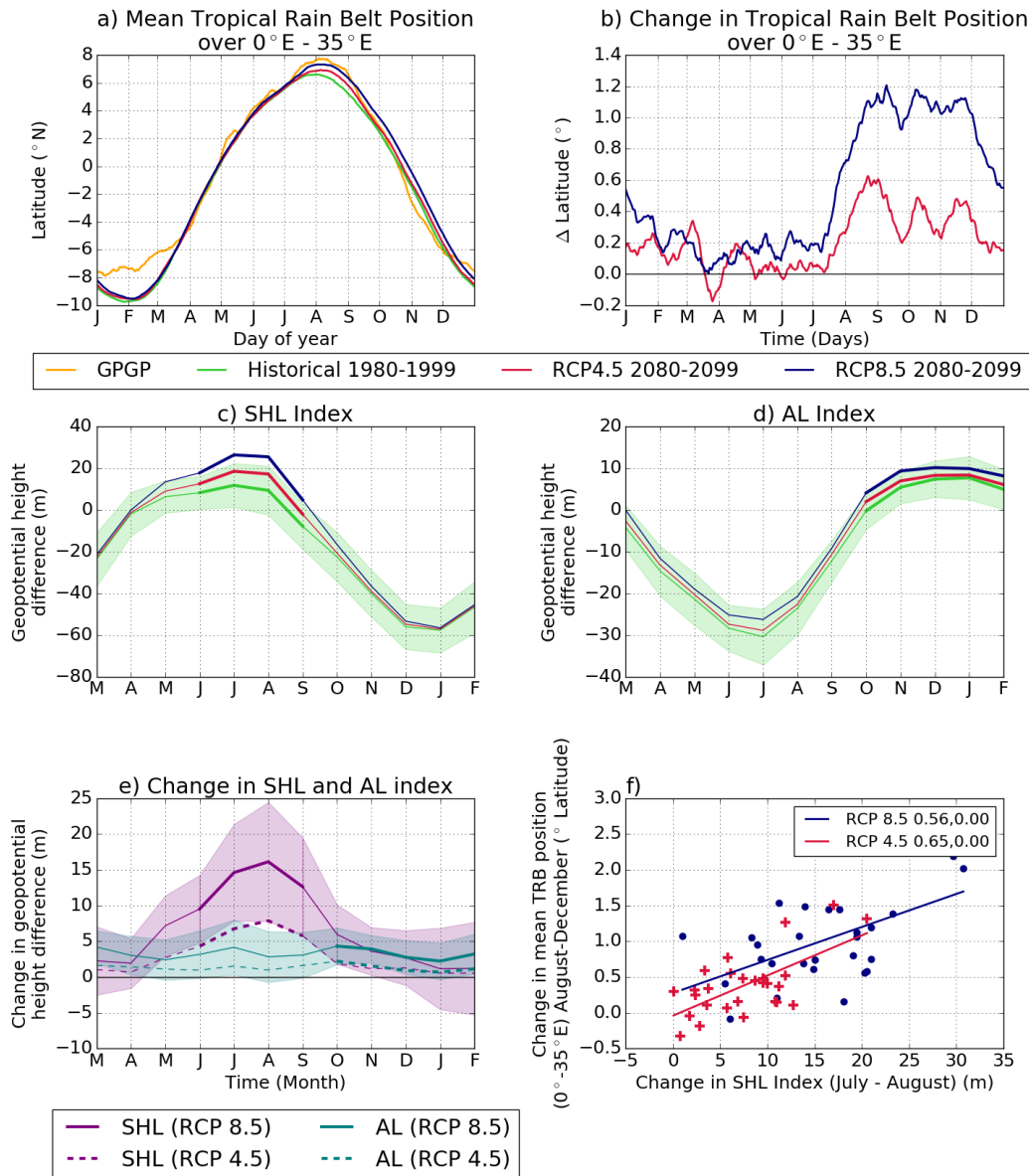


Figure 5.6 Mean Tropical Rain Belt position (a) and change in position of the TRB (b) in RCP 4.5 and RCP 8.5 simulations over 29 CMIP5 models for 2080-2099 compared with historical 1980-1999 (and GPCP over 1997-2014 for a), averaged over $0^{\circ}\text{E}-35^{\circ}\text{E}$, produced using the method of Shonk et al. (2018) on a daily basis and smoothed using a 15 day running mean. Regional circulation index for the northern region (including SHL, c) and southern region (including AL, d) for historical, RCP 4.5 and RCP 8.5 simulations over 29 CMIP5 models for 1980-1999 and 2080-2099. The green shaded area indicates the range across the 29 CMIP5 models for the historical simulation. The thicker lines indicate when the SHL/AL is within the region, and the regional circulation index also describes the strength of the SHL/AL. e) Change in strength of the regional circulation North/SHL (purple) and South/AL (teal) from historical 1980-1999 to RCP 4.5 (dashed) and RCP 8.5 (solid) (2080-2099). Again, thicker lines indicate when the SHL/AL is within the region, and the regional circulation index also describes the strength of the SHL/AL. The shading shows the model spread (\pm one standard deviation) for RCP 8.5. f) Mean change in position of TRB over $0^{\circ}\text{E}-35^{\circ}\text{E}$ (August-December) is plotted against change in change in SHL index for RCP 4.5 and RCP 8.5; the values in the legend indicate the Pearson correlation coefficient (r value, p value). EC-EARTH is excluded from (f).

Africa; Figure 5.7 shows greater transport of moisture into the Sahel region, both southerly from the Gulf of Guinea and northerly from the Mediterranean, and northward anomalies around the equator. Monerie et al. (2016) also found a northward shift of the monsoon, and increased moisture transport from the Mediterranean Sea. This is likely to be linked to later cessation over this region found in Figure 5.1b. Additionally, there is less moisture transport into southern Africa, with reduced relative humidity in August-October (Figure 5.7). Seth et al. (2013) associated later onset over Southern Africa with reduced boundary layer moisture availability at the end of the dry season, resulting from reduced moisture convergence and lower evaporation. Thus, changes in moisture transport associated with changes in the strength of the SHL may influence relative humidity over Southern Africa and delay the start of the wet season, although other drivers, including changes in pressure and surface temperatures over the neighbouring oceans are also likely to play a role (Funk et al., 2008; Shongwe et al., 2009; Lazenby et al., 2018).

In order to test this hypothesis, the increase in strength of the SHL in 29 CMIP5 models is plotted against the mean change in TRB position (Figure 5.6f). Models with a larger increase in strength of the SHL in July-August also exhibited a larger northward shift in the position of the TRB in August - December, and conversely, models with a smaller amplification of the SHL such as EC-Earth have a smaller change in TRB position (Figure 5.6f) with the correlation coefficient statistically significant at the 5% level. In their analysis of one regional climate model, Cook and Vizu (2012) related a deepening of the SHL with increased south westerly monsoon flow and a delay in the wet season over the Sahel; we have extended this by testing the hypothesis quantitatively across the CMIP5 ensemble.

The drivers of variability in the SHL and Sahel precipitation have been explored in a number of studies. Rowell (2003) and Park et al. (2016) identified the Mediterranean Sea as being a key region of influence on Sahel precipitation, with higher SSTs over the Mediterranean leading to more rainfall over the Sahel via an increased southward moisture flux. Monerie et al. (2016) identified this southward moisture flux from the Mediterranean as being a key source of moisture for the increased precipitation over the Sahel in the late monsoon season (September). We find a strong correlation between the July-August increase in temperature over the Mediterranean Sea (from 1980-1999 to 2080-2099) and the July-August increase in strength of the Sahara Heat Low (over the same period) with a correlation coefficient of 0.74 (correlation across the 29 CMIP5 models, results not shown). The warming over the Mediterranean during July-August in EC-Earth is in the lowest 10% of the 29 CMIP5 models used in this analysis, which may partly explain the different patterns seen in this model.

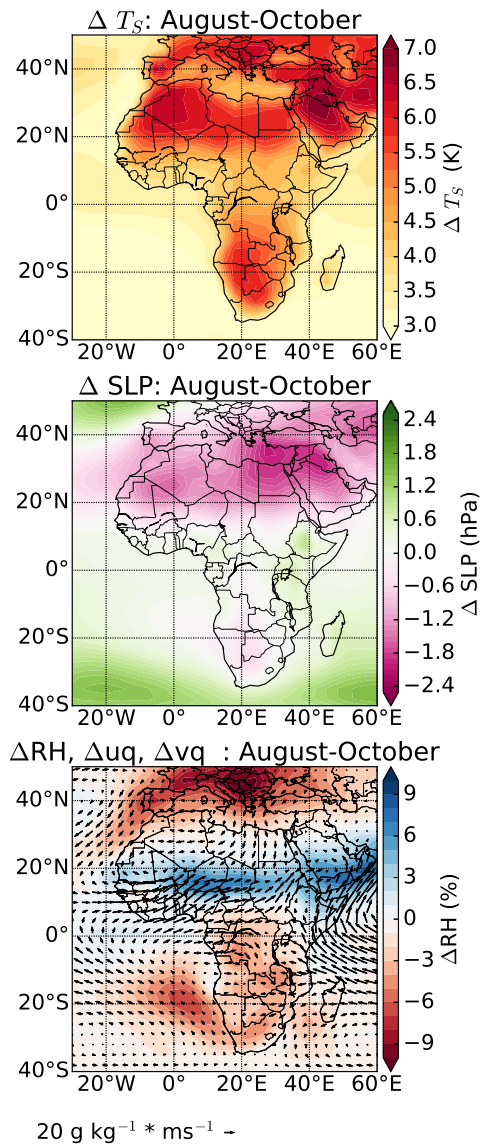


Figure 5.7 Multi-model mean change in surface temperature (top, K), air pressure at sea level (middle, hPa) and relative humidity (%) and moisture flux ($g\ kg^{-1} \times ms^{-1}$) at 925hPa (bottom) from 1980-1999 (historical) to 2080-2099 (RCP8.5 simulation) over August-October.

Enhanced temperatures over the Sahara act to deepen the SHL and enhance monsoon flow, bringing more moisture into the region. Water vapour is a greenhouse gas, leading to further temperature increases (Evan et al., 2015; Vizy and Cook, 2017). Again, warming in EC-Earth in July-August is in the lowest 10% for July-September over North Africa ($10^{\circ}W-60^{\circ}E$, $20^{\circ}N - 50^{\circ}N$), furthermore, EC-Earth also doesn't capture the boreal summer amplified warming over North Africa, Southern Europe, the Mediterranean Sea and central Asia compared with the global temperature increase seen in other CMIP5 models. Thus, some of the seasonal response may therefore be related to the amplification of land sea temperature contrast simulated by climate models (Sutton et al., 2007; Joshi et al., 2008; Lambert et al., 2011). Variations in the strength of the SHL have also been linked to variations in dust aerosol (Alamirew et al., 2018) and greenhouse gas concentrations (Dong and Sutton, 2015), with increasing concentrations of greenhouse gases acting to strengthen the SHL. While increasing

dust concentrations cool the surface via scattering of shortwave radiation (Konare et al., 2008; Solmon et al., 2008), dust aerosol warms the lower troposphere as a whole due to absorption of shortwave and longwave radiation, such that the net effect at the top of the Saharan residual layer is a warming, which will act to strengthen the Saharan Heat Low (Alamirew et al., 2018). While Konare et al. (2008) and Solmon et al. (2008) both associated increased atmospheric dust with reduced precipitation over the region, the large atmospheric radiative convergence from dust and heating of the planetary boundary layer identified by Alamirew et al. (2018) may suggest that the impact of dust is larger than previously estimated, and precipitation responses should be investigated further.

In summary a northward shift in the mean position of the tropical rain belt in August-December (and consequent later southward progression of the tropical rain belt) and later onset/cessation of the wet season has been linked with increasing strength of the Saharan Heat Low. Simulations with stronger amplification of the heat low experience a greater delay in the southward progression of the Tropical Rain Belt.

5.5 Conclusions

In conclusion, an objective methodology has been used to investigate changes in the characteristics of African wet seasons under climate change across 29 CMIP5 models. Additionally, changes in large scale drivers of the seasonal cycle of precipitation over Africa are investigated to explore the physical mechanisms underlying future changes.

Our key findings are:

- A pattern of increasing rainfall intensity was identified, with higher average rainfall per rainy day found across regions of West Africa, Southern Africa and Central Africa. Combined with a decline in the number of rainy days this leads to little change, or a slight decline in the total wet season rainfall over West and Southern Africa. Over Central Africa the combination of increasing rainfall per rainy day with little change in the number of rainy days leads to increases in the total seasonal rainfall.
- Large parts of Southern Africa are projected to experience a later onset date, with changes of around 12 days over Angola, as well as a shorter wet season and less wet season rainfall.
- Over the Horn of Africa, which experiences two wet seasons per year, the second wet season ('short rains') is projected to end over a week later, with a large increase in

seasonal rainfall.

- Over West Africa/ the Sahel both onset and cessation are projected to get later, with the entire wet season shifting 5-10 days later in the calendar year, and little overall change in the length of the wet season.
- The southward retreat of the tropical rain belt is projected to shift later in the calendar year, consistent with the trends of later cessation over West Africa and the Sahel, later short rains and later onset over Southern Africa. On average the tropical rain belt is projected to be 0.8-1.2° north of its previous position over August-December.

Large increases in surface temperature over the Sahara and North Africa during the boreal summer months lead to an intensification of the Saharan Heat Low. Smaller changes are identified in the strength of the Angola Low. Thus it is proposed that the higher temperatures and lower surface pressure and geopotential height means that the tropical rain belt travels further north and stays north longer, delaying the southward retreat, although other factors (including changing SST) are also likely to alter rainfall seasonality further south. Across the 29 CMIP5 models used we found strong correlation between the increase in strength of the SHL and the shift in the TRB position, with models that had a larger increase in the strength of the SHL exhibiting a larger shift in the position of the TRB. A number of other factors may also play a role, but the analysis of these factors is beyond the scope of this study.

Previously, Cook and Vizy (2012) analysed future projections of the growing season across Africa in a single regional climate model, and proposed that delay in the wet season over the Sahel was related to the deepening of the SHL. We found consistent results, and tested the SHL/ wet season delay hypothesis quantitatively across the CMIP5 ensemble, and found it to be robust.

Further analysis is required to explore inter-model differences, and the impacts of other drivers. For example, a number of studies have identified the role of warming in the Western Indian Ocean on moisture transport over Southern Africa (Funk et al., 2008; Shongwe et al., 2009), although Lazenby et al. (2018) found no robust link between austral spring rainfall and changing SST gradients. They commented on the potential role of South Atlantic high pressure as a driver of changing onset (Reason et al., 2006), but did not investigate this further. Seth et al. (2013) associated spring precipitation decreases across Southern Africa with declining moisture convergence and reduced evaporation. In this study, we found no robust link between an increase in the strength of the Angola Low and changing seasonality. Thus, investigating the role of other drivers, including pressure patterns over the South Atlantic

and different patterns of Indian Ocean warming on the seasonal cycle of precipitation would be interesting extension. Fully understanding inter-model differences in projected changes in the Saharan Heat Low would also advance this work further.

Dunning et al. (2017) identified some discrepancies in the representation of the seasonal cycle in coupled CMIP5 simulations; namely timing biases over the Horn of Africa and an overestimate of the short rains, an overestimate of the region experiencing a winter rainfall regime over south-west Africa and an incorrect seasonal cycle over the southern West African coastline. Thus future projections for these regions should be viewed with caution. Model improvements, that reduce such biases in coupled simulations are needed to produce reliable future projections over such regions.

In conclusion, future climate change will lead to a shift in the timing of wet seasons over Africa, with a delay in the wet season over West Africa and the Sahel, and later onset leading to a reduction in season length over Southern Africa. This may have implications for crop development, as a shorter growing season may mean that crops do not reach full maturity. Additionally, increasing intensity of rainfall may adversely affect crops, particularly at certain times during coffee development. Further work is required to investigate additional drivers, and their interactions, as well as attribution of inter-model differences.

Acknowledgments and Data

We acknowledge the World Climate Research Programme's Working Group on Coupled Modelling, which is responsible for CMIP, and we thank the climate modeling groups (models listed in Table S1) for producing and making available their model outputs; for CMIP, the U.S. Department of Energy's PCMDI provided coordinating support and led development of software infrastructure in partnership with the Global Organization for Earth System Science Portals. Model data were sourced from the CMIP5 data portal (http://cmip-pcmdi.llnl.gov/cmip5/data_portal.html) and the British Atmospheric Data Centre (<http://badc.nerc.ac.uk/>).

All observational datasets exploited are publicly available datasets. The TAMSATv3 dataset is available from the TAMSAT website (<http://www.met.reading.ac.uk/~tamsat/data>). GPCP daily data (Supplementary Information) are available from <http://precip.gsfc.nasa.gov/>. The CHIRPS dataset, produced by the Climate Hazards Group, is available at http://chg.geog.ucsb.edu/data/chirps/#_Data.

Caroline M. Dunning is supported with funding from a Natural Environment Research Council (NERC) PhD Studentship through the SCENARIO Doctoral Training Partnership grant NE/L002566/1. Richard P. Allan's contribution to the research leading to these results

has received funding from the National Centre for Earth Observation and the European Union 7th Framework Programme (FP7/2007-2013) under grant agreement 603502 (EU project DACCIWA: Dynamics-aerosol-chemistry-cloud interactions in West Africa). Emily Black's contribution to the research has been supported by the National Centre for Atmospheric Science (Climate division) ACREW project, which is supported by NERC and the Global Challenges Research Fund. She also gratefully acknowledges support from the NERC/DFID BRAVE project (NE/M008983/1), the NERC/DFID HyCristal project (NE/M020371/1) and the Global Challenges Research Fund project, SatWIN-ALERT (NE/R014116/1).

Chapter 6:

Conclusions

In this thesis a framework was developed to objectively analyse the seasonal progression of rainfall and its characteristics over Africa, of fundamental importance to societies. Central to this was the development of a methodology to characterise the rainfall regime and identify the onset and cessation date of the wet season. This framework was then utilised to assess the representation of seasonality in coupled climate models and interpret future projections, with additional analysis of important driving mechanisms. This addressed the overall aim: '*To improve capability for robust projection of user-relevant rainfall characteristics over Africa*'.

In this chapter, the major outcomes of the thesis are discussed, highlighting how the aims and objectives presented in Chapter 1 have been addressed, potential applications and key implications.

6.1 Scientific Advances

6.1.1 Development and application of a framework for objectively characterising seasonal rainfall

A framework has been developed for identifying the onset and cessation date of wet seasons, using a new methodology for regions with two wet seasons per year, and applied to multiple satellite-based rainfall datasets (Chapter 2) and climate model output (Chapters 3 and 5). The results demonstrate strong agreement in the representation in the seasonal cycle in the five satellite-based datasets used. Most notably, results show that this methodology robustly identifies the wet season for multiple rainfall regimes and is also applicable across datasets with contrasting rainfall biases (Chapter 2). Comparison with local indigenous methods demonstrates that this metric is societally relevant. Therefore this framework can be used

to compare the characteristics of rainy seasons across models and datasets where the wet seasons do not coincide exactly. It was also used to characterise observed rainfall seasonality and explore interannual variability. Thus the first aim, of “developing a method to capture and characterise seasonality in rainfall” has been addressed. Such a framework advances the methodological approach used in previous studies, such as Cook and Vizy (2012) and Liebmann et al. (2012) as it enables continental scale analysis of seasonal characteristics, with a consistent methodology across regions with both one and two wet seasons per year, and gives comparable onset/cessation dates across multiple datasets.

A framework for effectively and objectively identifying the wet seasons has a number of useful applications. In Chapter 2 the methodology is used to explore the interaction between the El Niño Southern Oscillation and precipitation seasonality over East and Southern Africa. It was found that El Niño conditions were associated with later cessation of the short rains over the Horn of Africa, and earlier onset of the primary austral summer wet season over Tanzania. Both of these regions experienced higher seasonal rainfall totals during El Niño years. Conversely, over southern Africa lower rainfall totals are observed in El Niño years, with no consistent anomaly in seasonal timing. This may have implications for seasonal forecasting and predictability, as the findings indicate that onset and cessation over East Africa are related to large scale modes of climate variability and SST.

Given the substantial climate model biases present across Africa, including biases in rainfall amount and timing, a framework that accurately identifies the wet season enables improved model and observational inter-comparison and production of future projections. For example, Levy et al. (2013) found that accounting for biases in the model mean state reduced the spread in model projections. For East Africa, model timing biases complicate the analysis of long term trends in rainfall. Many studies have highlighted the disparity in the recent observed decline in the East African Long Rains and future projections of increasing Long Rains (Rowell et al., 2015b), defining the long rains as occurring in March-May. In this thesis, a timing bias was identified over the Horn of Africa in coupled climate models, with the long rains 20 days late on average (Chapter 3). This indicates that sampling March-May conditions alone is inadequate for analysing changes in the Long Rains in climate models. Furthermore, characterisation of the seasonal cycle in Chapter 2 demonstrated that the peak of the long rains occurs from late March - mid May over the Horn of Africa. Hence applying this method both across datasets and models, and for trend analysis, facilitates a more complete comparison of wet seasons. Applying this methodology to future projections, no statistically significant change in long rains rainfall is found over the 21st Century (Chapter 5), although

poor representation of the present day climate may cast doubt on the robust nature of these projections.

In Chapter 5 the method was used to diagnose future projections of changes in wet seasons (see § 6.1.3). The application of this methodology highlighted good model agreement in changes in seasonal timing and rainfall amount, with more than 75% of the models agreeing on the sign of the change across large areas; agreement was likely improved due to the use of this method.

Overall, a methodology has been developed that accurately and objectively identifies the wet season for multiple rainfall regimes across contrasting datasets. Such a methodology has a wide range of potential applications, extending beyond meteorological analysis (see § 6.3).

6.1.2 Investigation of model biases

For the first time, a continent-wide evaluation of climate model representation of African rainfall seasonality was conducted by applying the methodology developed in Chapter 2 to atmosphere-only and coupled simulations. The representation of African rainfall seasonality in climate models was generally accurate, with atmosphere-only and coupled simulations capturing the gross observed patterns of seasonal progression and mean onset/cessation dates within 18 days of the observational dates for 11 of the 13 regions considered. However, some deficiencies were noted, over the Horn of Africa and the southern West African coastline (Chapter 3), where the biannual regime is not captured in coupled climate models. This addressed the second aim to “evaluate and identify deficiencies in representation of seasonality over Africa by climate models”. While biases in rainfall amount during the Long and Short rains over the Horn of Africa had been identified in previous studies (Tierney et al., 2015; Yang et al., 2015b), timing biases had not previously been examined. Very few studies have examined the representation of the biannual regime over the Southern West African coastline and LDS (Dike et al., 2015). Due to the societal importance of this season and the lack of research examining the physical mechanisms and climate model representation of this season, this is investigated further in Chapter 4.

Comparison between AMIP and CMIP models (Chapter 3) suggests that the misrepresentation over the Southern West African coastline is related to SST biases over the Gulf of Guinea; further analysis in Chapter 4 using the Global Ocean Mixed Layer configuration of the Met Office Unified Model (MetUM-GOML) demonstrated that mean ocean state biases over the Atlantic Ocean lead to this misrepresentation. Warm SST biases in the southern tropical Atlantic are ubiquitous across the current generation of coupled global climate mod-

els (Găinușă-Bogdan et al., 2017) and influence rainfall over the Atlantic and West Africa. Tropical Atlantic SST biases have been found to affect the position and structure of the ITCZ over the Atlantic, with warm biases leading to a southward shift of the rainfall (Toniazzi and Woolnough, 2014; Eichhorn and Bader, 2017), although no previous studies have specifically examined the impact of Atlantic SST biases on the LDS. A number of causes of this SST bias have been proposed (Richter and Xie, 2008; Toniazzi and Woolnough, 2014; Găinușă-Bogdan et al., 2017) and further work is ongoing to investigate the complex interplay of precipitation, wind and SST biases over the Atlantic Ocean (Shonk et al., in prep).

Previous studies (e.g. Odekunle and Eludoyin, 2008) propose that an increase in static stability over the southern West African coastline during August leads to the reduction in rainfall associated with the LDS; in Chapter 4 it is shown that upper level descent encroaching onto the coastline is important for the August rainfall reduction. Combined with establishing the important role of SST biases discussed above, the aim to “Elucidate dynamical processes determining seasonality, its variability and climate model representation” has been addressed.

Regarding East Africa, Chapter 3 shows that the short rains are overestimated with the cessation over two weeks later than observed, on average, and onset too early. The overestimation of the short rains has also been identified in previous studies (Tierney et al., 2015; Yang et al., 2015a,b). The future projections in Chapter 5 show an increase in short rains rainfall under future climate change, and the cessation getting later by up to 10 days. Thus the future trends could be interpreted as an amplification of the current model biases, and may be a model artefact rather than a robust change. Additional analysis should be conducted to establish the robustness of this trend (see § 6.3).

Coupled climate model biases in the representation of seasonality over East Africa are also related to SST biases; Yang et al. (2015b) find that the bias in the seasonal cycle of East African precipitation in coupled climate model simulations is driven by biases in the near surface moist static energy, which is modulated by the SST bias over the western Indian Ocean. Thus, the results in chapters 3 and 4 demonstrate the important role of coupled model SST biases on the seasonal cycle of precipitation over parts of Africa, and the need to reduce such model biases.

6.1.3 Interpretation of future projections

In Chapter 5 the methodology is applied to projections of precipitation under future climate change scenarios to investigate the changing characteristics of African wet seasons. The physical processes and mechanisms associated with such changes are also investigated.

While a number of studies have investigated changing African rainfall under future climate change, this represents the first quantitative assessment of changing seasonality across the continent. Onset of the main wet season is projected to get later over southern Africa, with shifts of over 12 days over parts of Angola, Zimbabwe and Mozambique, with less seasonal rainfall south of 10°S. A key finding is that over West Africa and the Sahel cessation is projected to get later, with shifts of over 5-10 days, associated with a strengthening of the Saharan Heat Low and delayed southward progression of the tropical rainy belt. Rainfall is also projected to increase in intensity, with higher rainfall per rainy day and fewer rainy days, consistent with previous findings (Christensen et al., 2013). This addresses the final aim to “Interpret projected future changes in seasonal characteristics”.

Pohl et al. (2017) also find fewer rainy days over southern Africa and a reduction in seasonal mean rainfall south of 10°S, however, model agreement is improved here compared with their study, presumably due to accurate identification of the wet season in each model, relative to the model's mean climate. Shongwe et al. (2009) also propose that lower austral spring rainfall over southern Africa leads to later onset; here an objective methodology has been used to quantify the change in onset date (largest changes of over 12 days). Lau and Kim (2015) find increased dryness over Southern Africa and other regions along the polar flank of the climatological subtropics, and link this to changes in the Hadley Circulation, strengthened by atmosphere-land interactions, indicating that this change may be indicative of larger scale climatic shifts. This reduction in the seasonal rainfall has implications for those who depend on the seasonal rainfall, as crop water requirements for current staple crops may no longer be met, and there may be reduced availability of drinking water, and water for construction and energy generation. Suitable adaptation measures should be developed to help mitigate the impact of such changes.

In their analysis of changes in the global monsoon, Lee and Wang (2014) found an increase in northern hemisphere monsoon precipitation (also reported by Christensen et al., 2013) and delay in the withdrawal of the northern hemisphere monsoon. Similarly, Dwyer et al. (2014) find that CMIP5 models project an amplification and phase delay of the seasonal cycle of tropical precipitation. For the Indian Monsoon, an increase in monsoon rainfall is projected, due to increasing moisture over the Indian Ocean (Turner and Annamalai, 2012). Christensen et al. (2013) also show the retreat of the Indian Monsoon getting later. Thus, the delay in the main wet season over West Africa and the Sahel, increase in rainfall over Central Africa, and increase and delay in the short rains over East Africa reported in Chapter 5 is consistent with these larger scale changes.

In addition to changes in timing of the seasonal rains, the results in Chapter 5 show that rainfall is projected to increase in intensity, with higher rainfall per rainy day and fewer rainy days. Increasing temperatures lead to increasing lower tropospheric water vapour, governed by the Clausius-Clapeyron relation; while this does not determine changes in global mean precipitation due to energy balance constraints, the intensity of the heaviest rainfall events will increase with the availability of moisture (Allen and Ingram, 2002), although Taylor et al. (2017) find that recent increasing frequency of high intensity Sahelian storms is related to changes in the land-sea temperature gradient, not moisture. A similar pattern of increasing intensity and fewer wet days is also reported in the most recent IPCC report, which shows an increase in simple daily precipitation intensity index and seasonal maximum consecutive dry days for the summer season over the global monsoon domain (Christensen et al., 2013). A similar pattern of fewer wet days and heavier rainfall events is also identified by Sharmila et al. (2015) for the Indian Monsoon. In Chapter 5 it is also noted that an increase in rainfall per rainy day is found everywhere, whereas a decline in the number of rainy days is only found in regions of stable or declining rainfall; over central Africa where rainfall is projected to increase, the number of rainy days remains constant. Such high intensity rainfall can have detrimental impacts on fragile crops and degrade soil quality via increasing runoff and soil erosion. Agricultural practices may need to adapt in order to overcome potential difficulties, including better soil management practices and more resilient crop varieties.

Chapter 5 argues that the shift in timing over West Africa and the Sahel, and later onset over Southern Africa, is linked with an increase in the strength of the Saharan Heat Low, and a northward shift in the position of the tropical rain belt during the second half of the calendar year. This suggests that changes over North Africa have implications for rainfall seasonality across the continent, highlighting the importance of conducting meteorological analysis at the continental scale, as well as at the regional scale and accounting for the impact of remote as well as local drivers.

6.2 Limitations

A number of limitations are discussed in each chapter. In this section some of the main limitations in addressing the overall aims of this thesis are highlighted and discussed.

The first limitation relates to the method developed in Chapter 2. The method captures the peak of the wet season by identifying the minima and maxima in the cumulative daily rainfall anomaly. Liebmann et al. (2012) also noted that performance of the method is limited

if there is no clear wet season and light and/or intermittent rainfall instead. In such cases, there is no clear global minima and maxima associated with the onset and cessation; thus the methodology may return a very short wet season, or onset/cessation dates that are not representative of the wet season experienced. While additional measures were applied to ensure that the onset was not at the very end of the climatological water year, and the cessation occurred after the onset, additional methodological development is required to remove years without a well-defined wet season or instead calculate a meaningful onset/cessation date for such years. Over much of continental Africa the precipitation seasonal cycle is dominated by one or two main wet seasons per year, so for the most part this limitation should not have a sizable impact, except over very humid regions with year round rainfall, or very dry regions where the wet season is very short or often fails. Over such regions the timing of the wet seasons is less relevant for society or model intercomparisons. Additional analysis should also examine how often such seasons occur both in observations and in climate model simulations in order to understand the spatial and temporal extent of this limitation.

Additionally, just two seasonal regimes were identified; annual and biannual, and inter-annual variability in the seasonal regime was not accounted for. Additional work should look at defining additional regimes and considering variability in the seasonal regime. Herrmann and Mohr (2011) found that in regions with single wet seasons there was high interannual stability in the seasonal regime, but greater variability was found in regions with multiple wet seasons and transition zones. Decreasing stability in the seasonal regime under climate change would have large societal implications due to increasing uncertainty of the nature of the seasonal cycle. However, this element of societally important precipitation change has not been investigated in this thesis, which is a noteworthy limitation given the aim to improve capability for robust projections of user-relevant rainfall characteristics over Africa.

Another limitation of the method is highlighted in Chapter 5, where the method is used to interpret future climate projections. As noted in § 5.2, the methodology identifies the peak of the wet season, relative to the mean climate. Thus a systematic increase in rainfall will yield no change in seasonal timing. Additionally, an increase in rainfall solely at the beginning of the wet season may result in a change in cessation date, despite no change in rainfall at the end of the wet season, as the climatological daily mean rainfall will have increased. This is particularly acute in regions with two wet seasons per year as changes in one season can affect the onset/cessation dates of the other season. For example, the large increase in short rains rainfall over East Africa acts to increase the climatological daily mean rainfall, which may result in a change in the onset/cessation dates of the long rains. In Chapter 5 this has

been accounted for by analysing the mean seasonal cycle to confirm that changes in seasonal characteristics were robust and accurate. However, this does affect the analysis of the East African long rains. In particular, this may limit the ability to produce 'robust projections', as stated in the main aim of this thesis, as projections over regions with two wet seasons per year may not be fully representative. Further development of the method, removing the aliasing of changes in rainfall amount and potentially separating the year in regions with two distinct wet seasons would be a valuable extension.

It is noted in Chapters 2, 3 and 5 that the method is of limited use over the south west coast of Southern Africa due to the existence of multiple rainfall regimes over a small spatial extent. The Namib Desert and south west coastline experience a dry climate, Cape Town and the surrounding areas experience a winter rainfall regime while the south coast has rainfall year round (Weldon and Reason, 2014; Engelbrecht et al., 2015). The methodology will not work for regions with very low rainfall or regions with year round rainfall (i.e. no well-defined wet season). In Chapter 3 it was found that the coupled models overestimated the spatial extent of the region that experiences a winter rainfall regime. However, comparisons of timing over South Africa were limited because of the multiple rainfall regimes. This means that deficiencies in the representation of the seasonal cycle over this region in coupled climate models cannot be fully characterised, limiting the ability to address aim 2, and robust projections over this region cannot be produced, limiting the ability to address aim 4. Higher resolution satellite data and rain gauge data should be used to explore the contrasting seasonal regimes over this region in more detail.

These methodological issues mainly limit the ability to address aim 1 'Develop a method to capture and characterise seasonality in rainfall' and aim 4 'Interpret projected future changes in seasonal characteristics', but also impact the ability to conduct model evaluation over parts of Southern Africa.

Due to time and computational limitations, the simulation of MetUM-GOML constrained to coupled model ocean state over the Atlantic Ocean, and observed mean ocean state elsewhere (GOML-ATL, see § 4.2) used lower horizontal resolution (N96). Consequently, when comparing GOML-ATL-N96 with the other simulations, the effects of varying horizontal resolution also had to be considered. Furthermore, Vellinga et al. (2016) found that lower resolution MetUM simulations were not able to represent the westward propagating, intense convection systems associated with a large proportion of the boreal summer rainfall received over West Africa, and instead rainfall in lower resolution simulations occurs synchronously across the region, with lower rainfall intensities than observed. The results presented in Chapter 4 also show

lower rainfall totals when N96 resolution is used compared with N216 horizontal resolution. While this simulation serves the required purpose in Chapter 4, confirming that differences in the representation of the seasonal cycle of precipitation over the southern West African coastline are due to mean ocean state biases in the Atlantic, not the Indian or Pacific Oceans, completing this simulation at N216 resolution would yield a more consistent comparison.

In Chapters 3 and 4 the role of SST biases on the representation of the seasonal cycle over the southern West African coastline was identified. The analysis of surface fluxes and the temperature constraints applied was limited, and thus the GOML simulations were not used to explore the source of these Atlantic SST biases. The GOML simulations used here were constrained to a mean seasonal cycle, therefore some large scale modes of climate variability, including ENSO, are not represented. While this did not restrict the analysis undertaken, it may have significant limitations for other applications. The main limitation for this thesis is the time and computational requirements, which limits the number of available simulations (see § 6.3).

6.3 Future Work

§ 6.2 highlighted additional method development that would increase the applicability and robustness of the onset/cessation methodology. Extending the method to better account for non-distinct wet seasons and suitably accounting for changes in rainfall amount would be valuable areas for future work. This thesis has also identified other interesting areas for future research which are presented below:

Applications of the Methodology:

In addition to numerous applications for meteorological analysis, this framework also has applications for ecological research, as the timing and duration of seasonal precipitation influences the dynamics of ecosystems and wildlife populations (Brawn et al., 2017), as well as agro-meteorology and decision making. Taylor et al. (in prep) have used the methodology to investigate the impacts of rainfall on kestrel populations in eastern Mauritius, and found that when breeding attempts overlap with the start of the wet season they suffer reduced success, possibly due to flooding of nests and difficulty finding food (Senapathi et al., 2011). The methodology has also been used for agricultural decision support. Additionally, it is currently being adapted for use in operational forecasting systems including Rainwatch and TAMSAT-ALERT (Asfaw et al., in review), providing up-to-date information on the likelihood that the season has started. While in this thesis the methodology was only applied to Africa, it could

be applied to any region with a well-defined wet season.

Little Dry Season Analysis:

In Chapter 3 a misrepresentation of the precipitation seasonal cycle over the southern West African coastline in coupled climate models is identified and linked to SST biases; in Chapter 4 additional simulations demonstrate that Atlantic Ocean mean state biases lead to this misrepresentation. Very few studies have investigated the representation of this seasonal regime in climate models, or completed detailed analysis of the driving mechanisms. Additional simulations, produced using MetUM-GOML, with coupled model SST biases over restricted parts of the Atlantic would help to further elucidate regions of influence and driving mechanisms of the LDS. For example, just imposing coupled model SST biases over the northern Gulf of Guinea and analysing the balance of ascent and descent along the coastline would indicate whether lower rainfall during the LDS is related to local SST or remote factors. Alternatively, just imposing coupled model SST biases over the southern Atlantic (warm bias) without the cold bias in the northern Atlantic would provide additional information on the role of the meridional temperature gradient. Performing these simulations at N216 resolution would help to separate the role of mean ocean state biases and the role of resolution.

Many studies have discussed factors influencing the warm SST biases in the southern Atlantic; including biases in atmospheric model components, exacerbated in coupled configurations (Richter and Xie, 2008; Găinușă-Bogdan et al., 2017) and oceanic processes (Toniazzo and Woolnough, 2014). Further work should investigate the complex interplay of precipitation, wind and SST biases over the Atlantic Ocean (Shonk et al., in prep). In particular, analysing the surface fluxes and temperature tendencies that were used to constrain GOML to different ocean states may identify how the SST biases develop, and through what mechanism.

The nature of the GOML framework means that it can be applied to any atmospheric model, not just the MetUM (Hirons et al., 2015). Running simulations using this configuration with an atmospheric model that does not underestimate rainfall across West Africa during October may yield interesting results and confirm the role of SST biases on the LDS.

Variability:

While adaptation strategies may help to mitigate against the impacts of a shift in the timing of onset/cessation, increasing interannual variations in onset timing and seasonal rainfall accumulation may be harder to plan for, particularly given low seasonal forecasting skill across much of Africa. In Chapter 2 interannual variations in onset and cessation are presented for select regions, using observations, but the representation of variability in atmosphere-only and

coupled climate model simulations was not investigated, and future projections of changing variability were not produced. Similarly, Cook and Vizzy (2012) did not consider changing interannual variability in their analysis of changing growing season characteristics across Africa, and Christensen et al. (2013) did not include changes in interannual variability in their projections of changes in onset and cessation date of the monsoon. When considering changes in the growing season over Malawi, Vizzy et al. (2015) did examine changing variability in the onset and demise date, but results were inconclusive.

Investigating changes in interannual variability in seasonal timing and amount would have important societal applications.

Identification of rainfall regimes:

Harmonic analysis was used to identify regions with one or two wet seasons per year, with a threshold used to categorise the regions. The same methodology was used by Liebmann et al. (2012). While the regions identified exhibited good agreement with published literature, they were not compared against agricultural farming practices to establish societal relevance. Additionally, this metric did not produce useful results when endeavouring to analyse shifting rainfall regimes under climate change (results not shown). Herrmann and Mohr (2011) used monthly rainfall and temperature data to classify 8 different seasonality classes across Africa, and analysed the stability of such regimes.

Further work could use additional harmonics (i.e. not just first and second) to identify different seasonal regimes using daily rainfall i.e. single wet season with multiple peaks, two equal wet seasons, two unequal wet seasons etc. Obtaining information on farming practices in different regions would indicate regions where the farming is in one/two seasons and may establish societal relevance of this metric. Furthermore, producing a more detailed categorisation with more rainfall regime categories may yield additional insight into changing rainfall regimes across Africa under climate change, a topic on which there is limited literature, to complement the changes in seasonal timing presented in Chapter 5.

Drivers of Future Climate Change:

In Chapter 5 it is proposed that the strong boreal summer increase in temperature over North Africa, and increase in the strength of the Saharan Heat Low affects the southward progression of the tropical rain belt, leading to a later cessation over West Africa and the Sahel, later cessation of the short rains over the Horn of Africa, and later onset of the wet season over Southern Africa. Further work should investigate the inter-model and inter-annual relationship between onset/cessation and the Saharan Heat Low, and the presence of such

a relationship in observations. In addition other drivers of changing rainfall seasonality have been proposed, including warming SSTs in the West Indian Ocean, a shift in the mean position of the Indian Ocean Dipole, and altering onshore moisture transports. While previous studies have discussed the role of the Saharan Heat Low and Indian Ocean SSTs on the seasonal cycle of rainfall over Africa (Biasutti and Sobel, 2009; Shongwe et al., 2009; Cook and Vizy, 2012), they have not directly related changes in onset/cessation date with changes in these drivers, or assessed the relative influence of the different factors. Further research should investigate the role of different factors on future rainfall seasonality.

In addition, as noted in § 6.1.2, coupled climate models overestimate the East African short rains (Chapter 3, Tierney et al., 2015; Yang et al., 2015b) and also project future increases in short rains rainfall (Chapter 5, Shongwe et al., 2011). Further analysis should identify the causes of the current model biases, and establish the processes leading to the future increase, to establish whether the projections are robust or simply an amplification of current model biases.

Inconsistent Model Outliers:

In Chapter 5 a different climate change signal is found in EC-Earth compared to the other CMIP5 models in July-August; the warming over North Africa and the Mediterranean is much lower than the other models, surface pressure increases rather than decreases and there is no increase in strength of the Saharan Heat Low. Other studies examining the Saharan Heat Low (Dixon et al., 2017b) and changes in the West African Monsoon (Monerie et al., 2016) have not included this model. Further work should explore inconsistent model outliers, and elucidate the factors and model components that lead to this difference, as this may help to identify important processes and mechanisms.

6.4 Conclusions

Building on and advancing previous work, a framework for investigating the seasonality of African rainfall has been developed and applied to characterise rainfall seasonality in observations, evaluate representation in climate model simulations and interpret projections of future changes.

Firstly, a methodology has been developed that determines the onset and cessation dates of wet season(s) over Africa for regions with one or two wet seasons per year, and tested across multiple datasets (Chapter 2). Compatibility with known rainfall drivers, consistency with indigenous methods and strong agreement across datasets confirms the method is correctly

capturing the correct seasonal progression of rainfall, and can be applied across datasets with contrasting rainfall biases. The method is then used to characterise the continuous seasonal progression of rainfall across regions with one/two wet seasons per year and interannual variability. In particular, El Niño conditions are associated with later cessation of the short rains over East Africa (7 days on average) and higher seasonal rainfall, and earlier onset of the wet season over Tanzania.

Secondly, this methodology is used to evaluate the representation of the seasonality of African precipitation in atmosphere-only and coupled simulations, produced as part of CMIP5 (Chapter 3). For the most part, atmosphere-only and coupled simulations capture the seasonal progression of the rainy seasons over Africa, with the biannual regimes over Central Africa and the Horn of Africa captured, realistic spatial patterns of wet season progression and mean onset/cessation dates within 18 days of the observational dates for the majority of the regions considered. However, coupled simulations exhibited timing biases over the Horn of Africa and failed to capture the biannual regime over the southern West African Coastline.

Simulations using the Global Ocean Mixed Layer configuration of the Met Office Unified Model demonstrated that the inclusion of biases over the Atlantic Ocean in coupled simulations leads to the inaccurate representation of the seasonal cycle over the southern West African Coastline in the MetUM, not the inclusion of air-sea coupling (Chapter 4). The balance of ascent/descent along the coastline is found to be important for the reduced rainfall associated with the LDS.

Finally, changes in wet season characteristics under the RCP4.5 and RCP8.5 climate projection scenarios were analysed (Chapter 5). Increasing strength of the Saharan Heat Low and a northward shift in the position of the tropical rain belt over August-December is associated with a delay in the wet season over West Africa and the Sahel, later onset of the wet season over southern Africa and later short rains over the Horn of Africa. Total rainfall accumulation during the short rains is projected to increase by over 100mm by the end of the 21st Century. In addition, a pattern of increasing rainfall intensity is identified with higher average rainfall per rainy day, and fewer rainy days.

The framework and methodology developed and utilised in this thesis realistically identifies the wet season in both observational datasets and climate model simulations and thus has many potential applications, including model and dataset inter-comparison, meteorological analysis of wet season characteristics and dynamics, and ecological research. Work is also currently ongoing to explore the operational utility of the method. The model deficiencies identified further highlight the importance of reducing biases over the Atlantic Ocean in

coupled climate model simulations.

In conclusion, since future changes in climate are likely to inflict detrimental impacts on agriculture and many other sectors, the research documented in this thesis and additional future analysis will be valuable for investigating the societal implications of ongoing climate change across Africa and for developing effective adaptation measures to reduce risk to society.

Chapter 7:

Appendices

7.1 Appendix 1: Supplementary Information for ‘The impact of air-sea coupling and ocean mean state biases on the representation of the seasonal cycle of precipitation over southern West Africa in climate models’

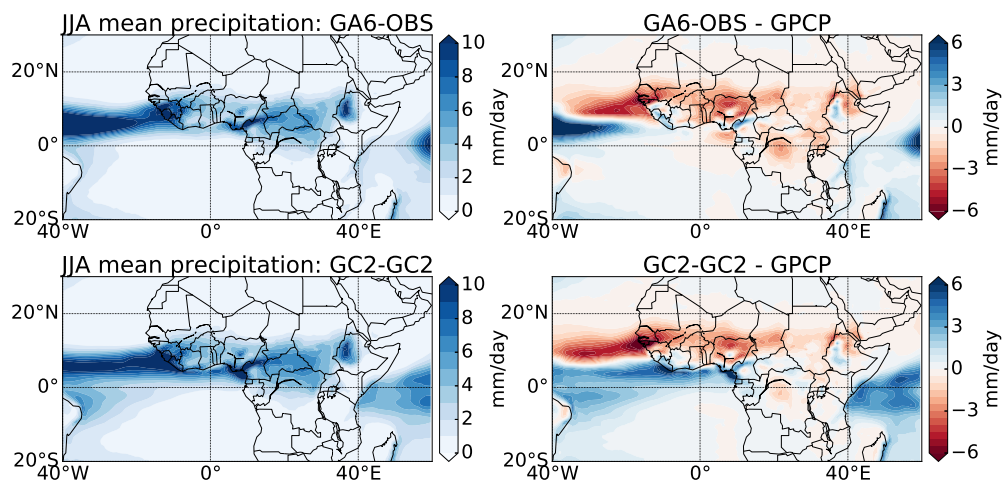


Figure 7.1 JJA rainfall (left) and bias when compared with GPCP (right) in GA6-OBS and GC2-GC2. For details of dates and simulations see Table 4.1.

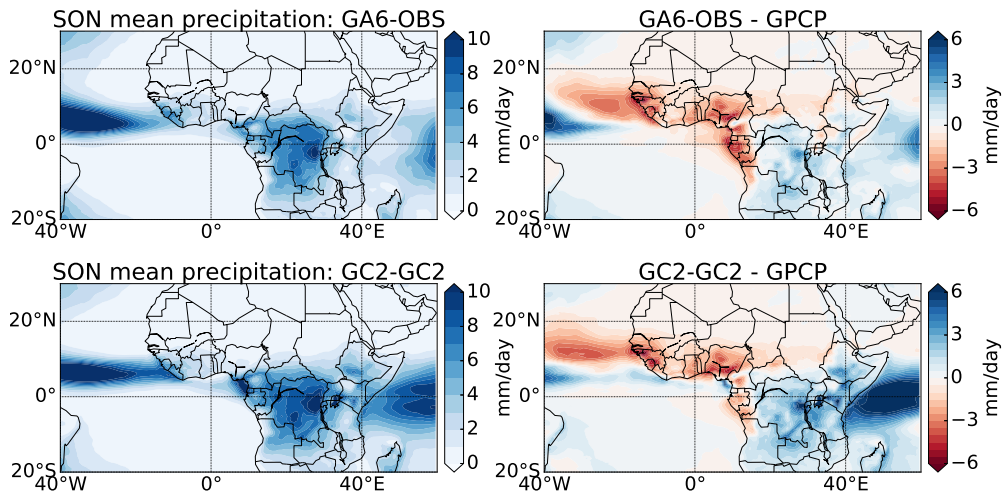


Figure 7.2 SON rainfall (left) and bias when compared with GPCP (right) in GA6-OBS and GC2-GC2. For details of dates and simulations see Table 4.1.

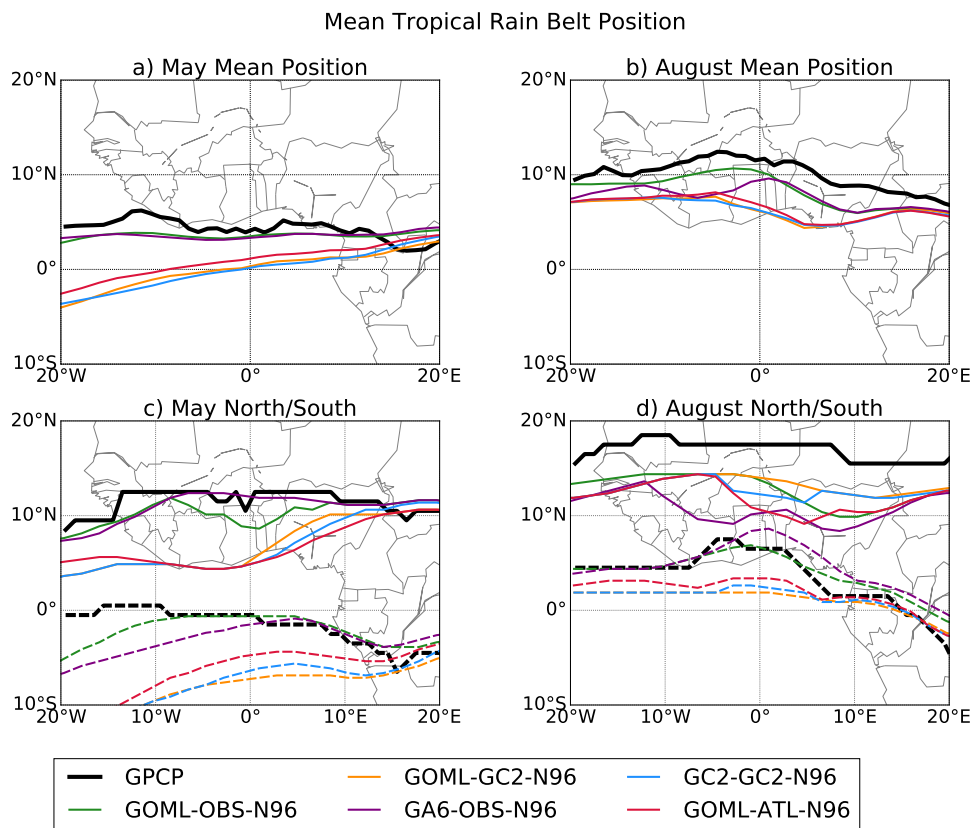


Figure 7.3 Mean monthly position of the Tropical Rain Belt (a-b) and mean position of the northern and southern limits of the Tropical Rain Belt (c-d) for May and August using simulations at N96 horizontal resolution. The mean monthly position is calculated by identifying the rainfall centroid using the top 50% of rainfall at each longitude (a-b). The northern and southern limits are defined using a threshold of 3mm/day. Different coloured lines are for different simulations (N96 resolution). For details of dates and simulations see Table 4.1.

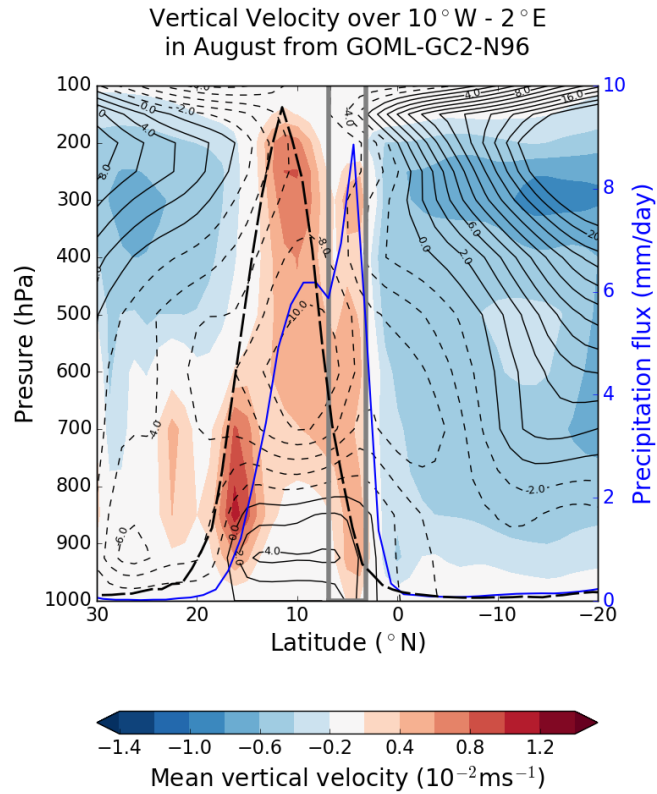


Figure 7.4 Vertical cross section of the mean vertical velocity in August (coloured contours), mean zonal wind velocity (solid/dashed contours for positive/negative values respectively) and mean precipitation (solid blue line) from GOML-GC2-N96 averaged over 10°W to 2°E. The dashed black line shows the GPCP precipitation. The grey lines mark the coastline region (where land sea fraction is between 5% and 95%). For details of dates and simulations see Table 4.1.

7.2 Appendix 2: Supplementary Information for ‘Later wet seasons with more intense rainfall over Africa under future climate change’

This Supplementary Information contains Figures S1- S17 and Table S1.

- **Median Change in Onset/Cessation for RCP 4.5: Figure S1- S2.** Figure 1 and 2 from the main paper repeated for RCP 4.5 scenario.
- **Changes in Seasonal Regime: Figure S3.** Assessment of whether the spatial extent of the region experiencing a biannual regime will change and definition of regions used for timeseries.
- **Timeseries: Figure S4- S8.** Timeseries of onset, cessation, total wet season rainfall, average rainfall per wet season rainy day and number of rainy days in the wet season over West Africa, Central Africa, Southern Africa and for the long and short rains over the Horn of Africa. These timeseries include observed trends produced using CHIRPS daily precipitation data (Funk et al., 2015) as well as TAMSATv3; for the most part good agreement is found between the two observational datasets.
- **Determining the Position of the Tropical Rain Belt: Figure S9.** Different methods for determining the position of the tropical rain belt are investigated to ensure results are robust to choice of method.
- **Relationship between Tropical Rain Belt Location and Onset/Cessation in Observations: Figure S10.** GPCP data is used to confirm that years when the southward retreat of the tropical rain belt is later/earlier have later/earlier onset and cessation.
- **Location of Saharan Heat Low and Angola Low: Figure S11- S14 .** Assessment to ascertain whether the Saharan Heat Low and Angola Low are likely to change location in the future.
- **Sahara Heat Low Index and Angola Low Index: Figure S15- S16.** Repetition of results using 925 hPa geopotential height in addition to 850 hPa geopotential height to ensure robustness.
- **Sensitivity of SHL/AL index to region used: Figure S17.** SHL and AL results are repeated using modified regions to ensure the results are robust to the region used.
- **Table of CMIP5 models used: Table S1**

7.2.1 Median Change in Onset/Cessation for RCP 4.5

In the paper Figure 1-2 depicts the median change in onset/cessation etc for the RCP 8.5 scenario, with a period at the end of the 21st century (2080-2099) compared with a period at the end of the 20th Century (1980-1999). The results are repeated here for the RCP 4.5 scenario (Figure S1- S2). The same patterns of change are found, with onset getting later over West Africa and Southern Africa, cessation getting later over the Sahel, and the short rains getting later with more rainfall. The magnitude of change is much smaller, and very few changes are statistically significant. This is expected given that RCP 4.5 is a medium emissions scenario and RCP 8.5 is a high emissions scenario (Van Vuuren et al., 2011).

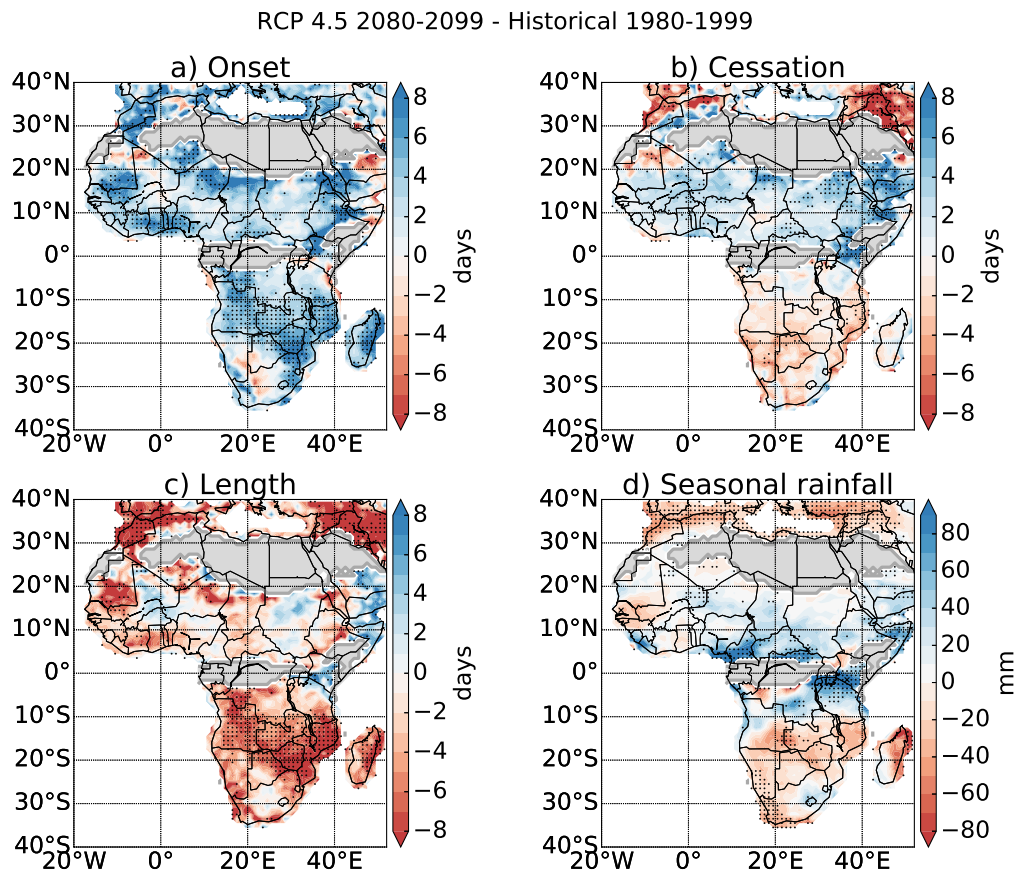


Figure S1 Median Change in a) Onset, b) Cessation, c) Season Length and d) Wet Season Rainfall in 29 CMIP5 simulations from 1980-1999 (historical simulation) to 2080-2099 (RCP 4.5 scenario). Blue colours indicate the onset/cessation getting later while red colours indicate onset/cessation getting earlier. Crosses indicate where 75% of the simulations agree on the sign of the change, and more than 50% of the models show a statistically significant change (Mann Whitney U test, 5% significance level). Dots indicate where 75% of the simulations agree on the sign of the change. Grey regions indicate regions where <5 models produce onset/cessation dates due to a dry climate or two wet seasons per year.

RCP 4.5 2080-2099 - Historical 1980-1999

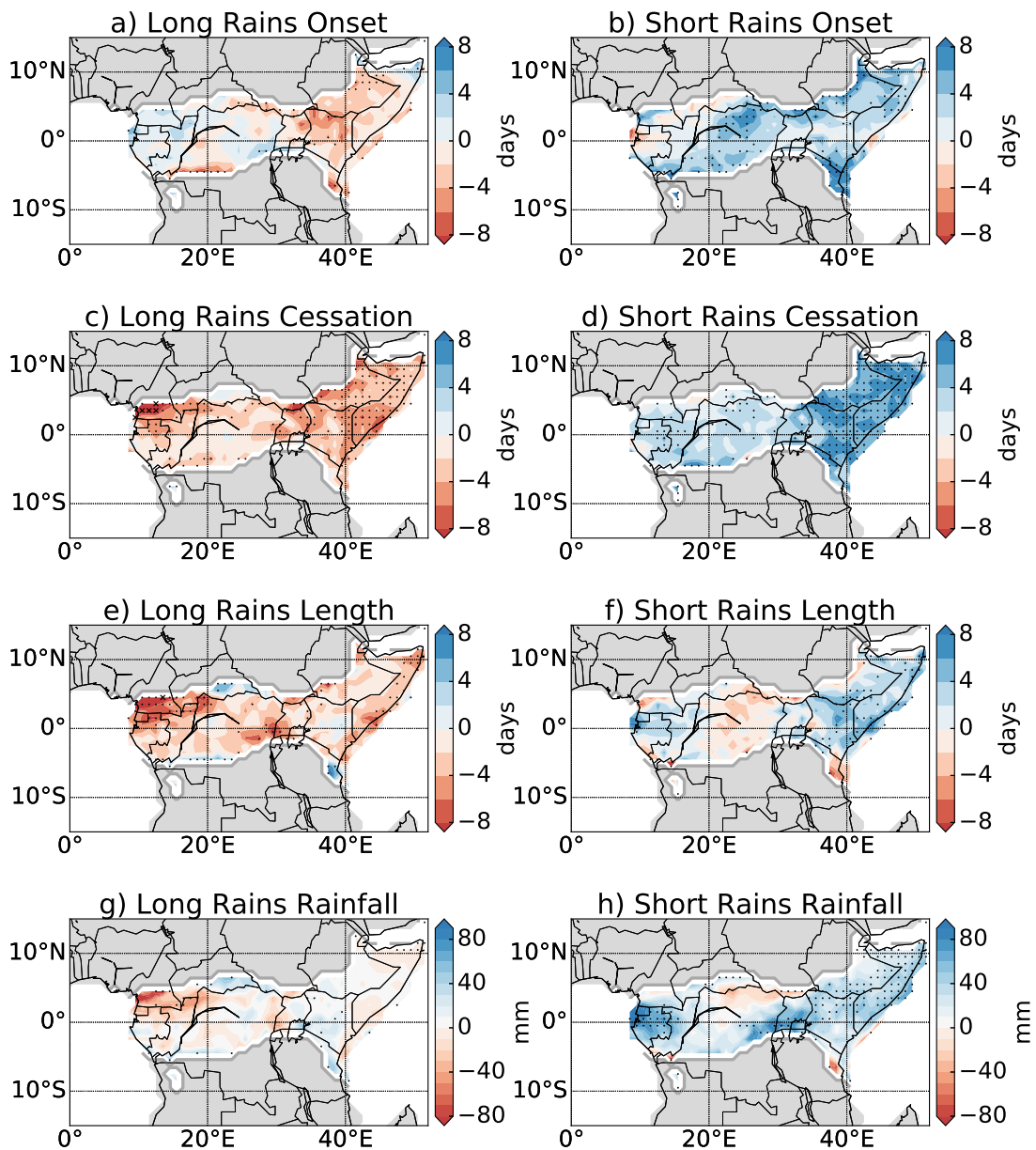


Figure S2 Median Change in Onset (a-b), Cessation (c-d), Season Length (e-f) and Wet Season Rainfall (g-h) for the Long (boreal spring, left) and Short (boreal autumn, right) Rains in 29 CMIP5 simulations from 1980-1999 (historical simulation) to 2080-2099 (RCP 4.5 scenario). Blue colours indicate the onset/cessation getting later while red colours indicate onset/cessation getting earlier. Crosses indicate where 75% of the simulations agree on the sign of the change, and more than 50% of the models show a statistically significant change (Mann Whitney U test, 5% significance level). Dots indicate where 75% of the simulations agree on the sign of the change. Grey regions indicate regions where <5 models produce onset/cessation dates due to a dry climate or one wet season per year.

7.2.2 Changes in Seasonal Regime

Harmonic analysis is used to categorise regions that experience one or two wet seasons per year for the 29 CMIP5 historical simulations over the period 1980-1999, and 29 CMIP5 RCP8.5 simulations over the period 2080-2099 and compared to ascertain whether some locations will experience a change in the seasonal regime, and whether the spatial extent of the region that experiences a biannual regime will change.

At each grid point, the number of models that show an annual/biannual regime was computed for the historical simulation (1980-1999) and the RCP 8.5 simulation (2080-2099). The difference was calculated and is shown in Figure S3. Looking at the central equatorial region, where the biannual regime is currently experienced, Figure S3 appears to suggest that the biannual regime is shifting northward. Between 0° and 10°N fewer models are showing an annual regime under RCP8.5 (Figure S3a) and more models are showing a biannual regime (Figure S3b). Conversely, between 0° and 10°S (and in the central Horn of Africa), Figure S3 shows more models exhibiting an annual regime under RCP 8.5, and fewer models exhibiting a biannual regime. However, for the most part less than a third of the models show a change in regime and mean annual seasonal cycles do not show large shifts in the seasonal regime (results not shown). In conclusion, while changes in the harmonic ratio under RCP 8.5 suggest that the biannual regime over the equatorial region is shifting northward, the annual cycle of precipitation exhibits small changes in the shape of the seasonal cycle and there are no large changes in seasonal regime.

The regions for the West Africa and Southern Africa timeseries were chosen such that very few models showed a change in regime. The locations of the regions used for all the timeseries are shown in Figure S3.

7.2.3 Determining the Position of the Tropical Rain Belt

In order to look at the changing position and progression of the tropical rain belt (TRB) a method for determining the location of the TRB was required. In Shonk et al. (2018) 3 methods for determining the location of the InterTropical Convergence Zone (ITCZ) are discussed; all 3 methods are based solely on rainfall and are therefore suitable for this application. All 3 methods use rainfall between 30°S-30°N for the calculation. The first method (max rainfall) uses the latitude of the maximum rainfall at each longitude to be the location of the ITCZ (Figure S9a,d). The second method uses the latitude of the rainfall centroid at each longitude (Figure S9b,e). The third method uses the latitude of the rainfall centroid, calculated using just the top 50% of the rainfall, at each longitude (Figure S9c,f). Shonk et al. (2018) found

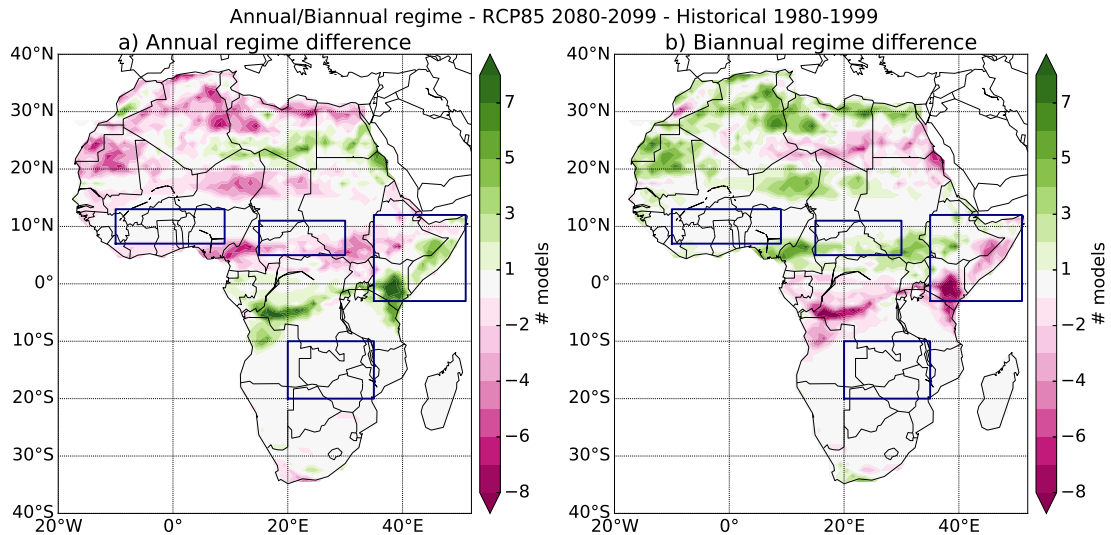


Figure S3 Change in number of models that contain an annual (a) or biannual (b) regime at each grid point in RCP 8.5 (2080–2099) compared with historical simulation (1980–1999). The categorisation of annual/biannual regimes was based on harmonic analysis (see section 5.2 and Dunning et al. (2016)). The boxes indicate the regions used for timeseries (Figure 3–4, S4–S8).

the third method gave a smoothly varying quantity, and used this method in their analysis. In this work we also use the same method. Figure S9 shows the results are the same for all 3 methods, with a northward shift in the second half of the calendar year. The method using the rainfall centroid calculated using all rainfall also shows a northward shift in the first half of the calendar year. This confirms that the result is robust to different methods.

7.2.4 Relationship between Tropical Rain Belt Location and Onset/Cessation in Observations

We postulate the later cessation found over West Africa and the Sahel, later onset over Southern Africa and later short rains over the Horn of Africa is related to a later southward progression of the tropical rain belt. This relationship was investigated using observational data. For this analysis we required daily precipitation data covering both land and oceans, thus the TAMSATv3 data could not be used. Instead, daily data from the Global Precipitation Climatology Project was used over 1997–2014 (Huffman et al., 2001). Onset and cessation dates were computed using the method of Dunning et al. (2016) for 1998–2013 (first and last years not included) and the position of the tropical rain belt (TRB) was calculated using the method of Shonk et al. (2018), which looks for the rainfall centroid in the top 50% of the rainfall.

Years were ranked based on the position of the TRB over 0° – 35°E for 1 August – 31

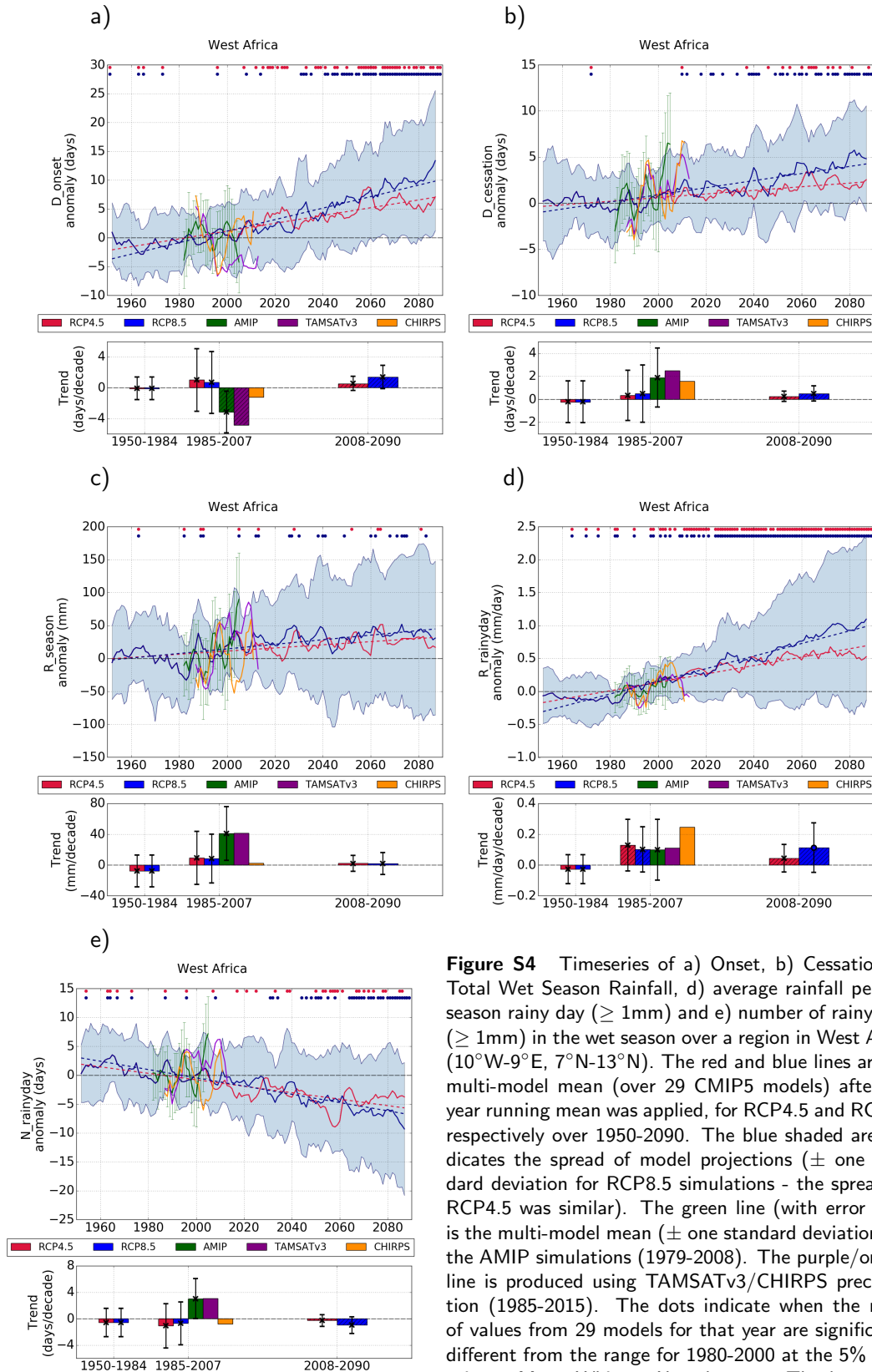


Figure S4 Timeseries of a) Onset, b) Cessation, c) Total Wet Season Rainfall, d) average rainfall per wet season rainy day ($\geq 1\text{mm}$) and e) number of rainy days ($\geq 1\text{mm}$) in the wet season over a region in West Africa (10°W - 9°E , 7°N - 13°N). The red and blue lines are the multi-model mean (over 29 CMIP5 models) after a 5 year running mean was applied, for RCP4.5 and RCP8.5 respectively over 1950-2090. The blue shaded area indicates the spread of model projections (\pm one standard deviation for RCP8.5 simulations - the spread for RCP4.5 was similar). The green line (with error bars) is the multi-model mean (\pm one standard deviation) for the AMIP simulations (1979-2008). The purple/orange line is produced using TAMSATv3/CHIRPS precipitation (1985-2015). The dots indicate when the range of values from 29 models for that year are significantly different from the range for 1980-2000 at the 5% level, using a Mann Whitney U and t-test. The bar charts indicate the trend over different periods; 1950-1984, 1985-2007 (AMIP and observations period) and 2008-2090. The height of the bars indicates the trend of the multi-model mean; hatching indicates the trend is significantly different from 0 at the 5% level. The circle/cross and errorbar indicate the mean and standard deviations of the trend from the 29 models; a circle indicates over 50% of the models show a trend significantly different from 0 at the 5% level.

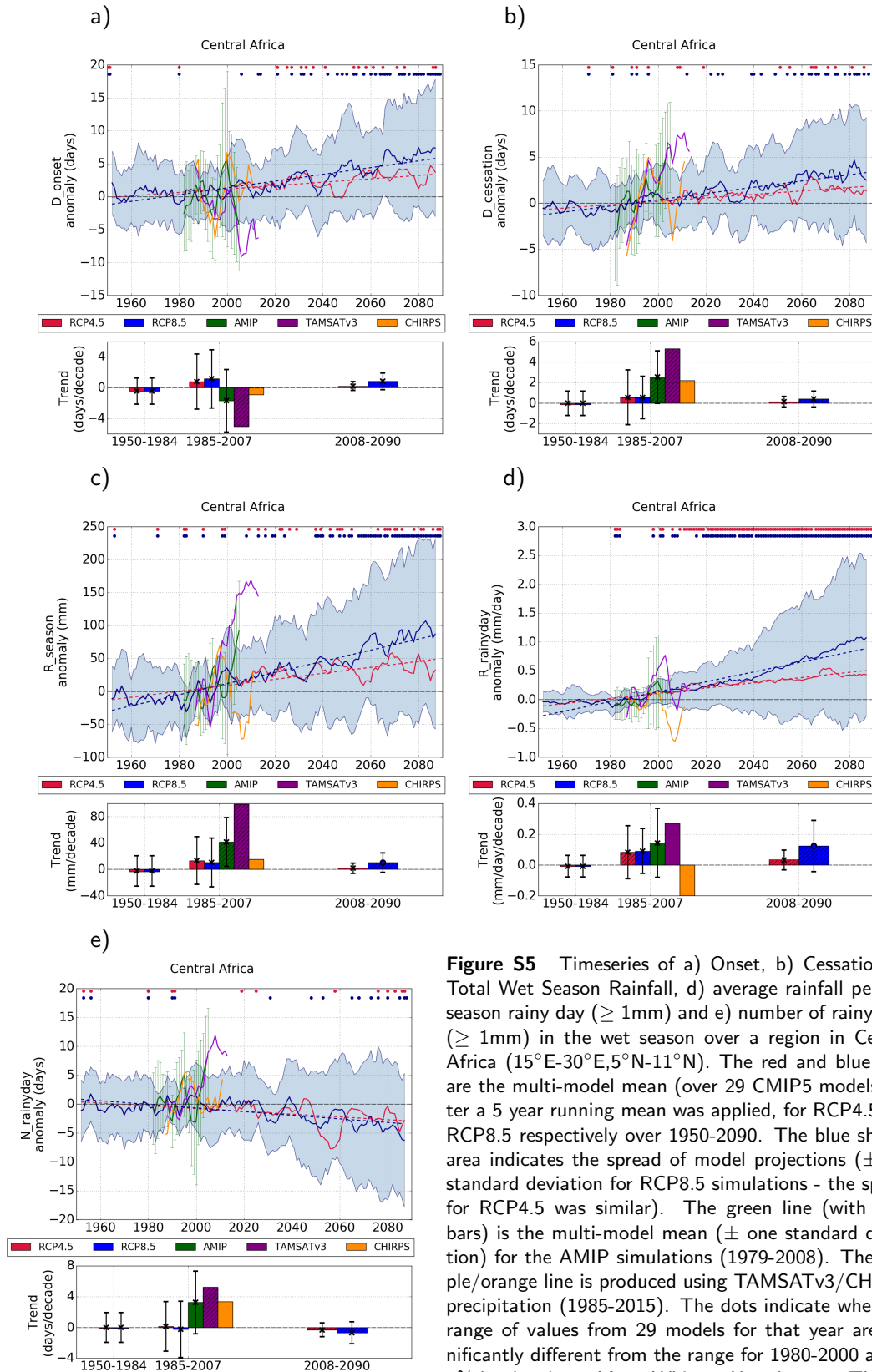


Figure S5 Timeseries of a) Onset, b) Cessation, c) Total Wet Season Rainfall, d) average rainfall per wet season rainy day ($\geq 1\text{mm}$) and e) number of rainy days ($\geq 1\text{mm}$) in the wet season over a region in Central Africa (15°E - 30°E , 5°N - 11°N). The red and blue lines are the multi-model mean (over 29 CMIP5 models) after a 5 year running mean was applied, for RCP4.5 and RCP8.5 respectively over 1950-2090. The blue shaded area indicates the spread of model projections (\pm one standard deviation for RCP8.5 simulations - the spread for RCP4.5 was similar). The green line (with error bars) is the multi-model mean (\pm one standard deviation) for the AMIP simulations (1979-2008). The purple/orange line is produced using TAMSATv3/CHIRPS precipitation (1985-2015). The dots indicate when the range of values from 29 models for that year are significantly different from the range for 1980-2000 at the 5% level, using a Mann Whitney U and t-test. The bar charts indicate the trend over different periods; 1950-1984, 1985-2007 (AMIP and observations period) and 2008-2090. The height of the bars indicates the trend of the multi-model mean; hatching indicates the trend is significantly different from 0 at the 5% level. The circle/cross and errorbar indicate the mean and standard deviations of the trend from the 29 models; a circle indicates over 50% of the models show a trend significantly different from 0 at the 5% level.

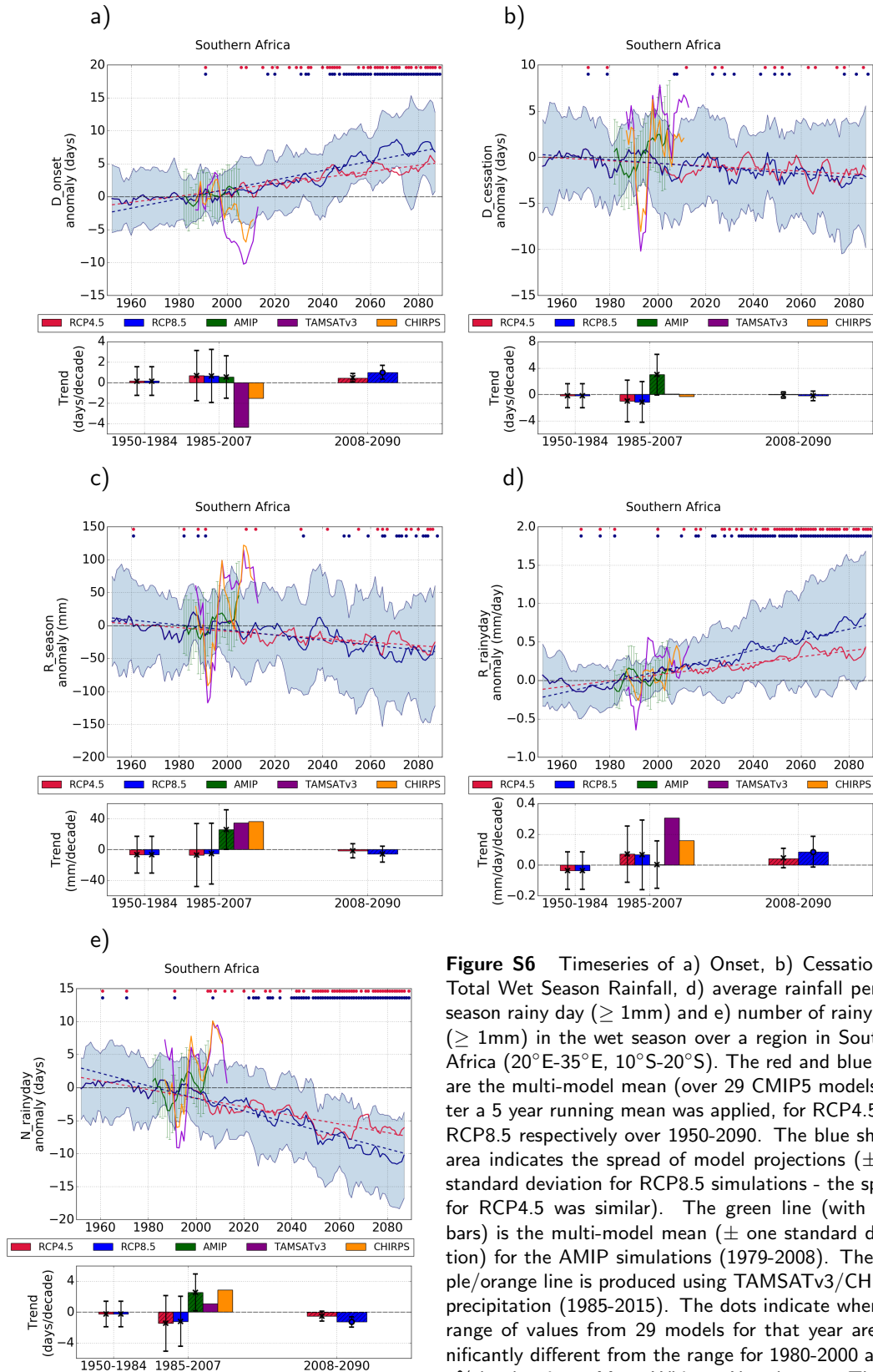


Figure S6 Timeseries of a) Onset, b) Cessation, c) Total Wet Season Rainfall, d) average rainfall per wet season rainy day ($\geq 1\text{mm}$) and e) number of rainy days ($\geq 1\text{mm}$) in the wet season over a region in Southern Africa ($20^{\circ}\text{E}-35^{\circ}\text{E}$, $10^{\circ}\text{S}-20^{\circ}\text{S}$). The red and blue lines are the multi-model mean (over 29 CMIP5 models) after a 5 year running mean was applied, for RCP4.5 and RCP8.5 respectively over 1950-2090. The blue shaded area indicates the spread of model projections (\pm one standard deviation for RCP8.5 simulations - the spread for RCP4.5 was similar). The green line (with error bars) is the multi-model mean (\pm one standard deviation) for the AMIP simulations (1979-2008). The purple/orange line is produced using TAMSATv3/CHIRPS precipitation (1985-2015). The dots indicate when the range of values from 29 models for that year are significantly different from the range for 1980-2000 at the 5% level, using a Mann Whitney U and t-test. The bar charts indicate the trend over different periods; 1950-1984, 1985-2007 (AMIP and observations period) and 2008-2090. The height of the bars indicates the trend of the multi-model mean; hatching indicates the trend is significantly different from 0 at the 5% level. The circle/cross and errorbar indicate the mean and standard deviations of the trend from the 29 models; a circle indicates over 50% of the models show a trend significantly different from 0 at the 5% level.

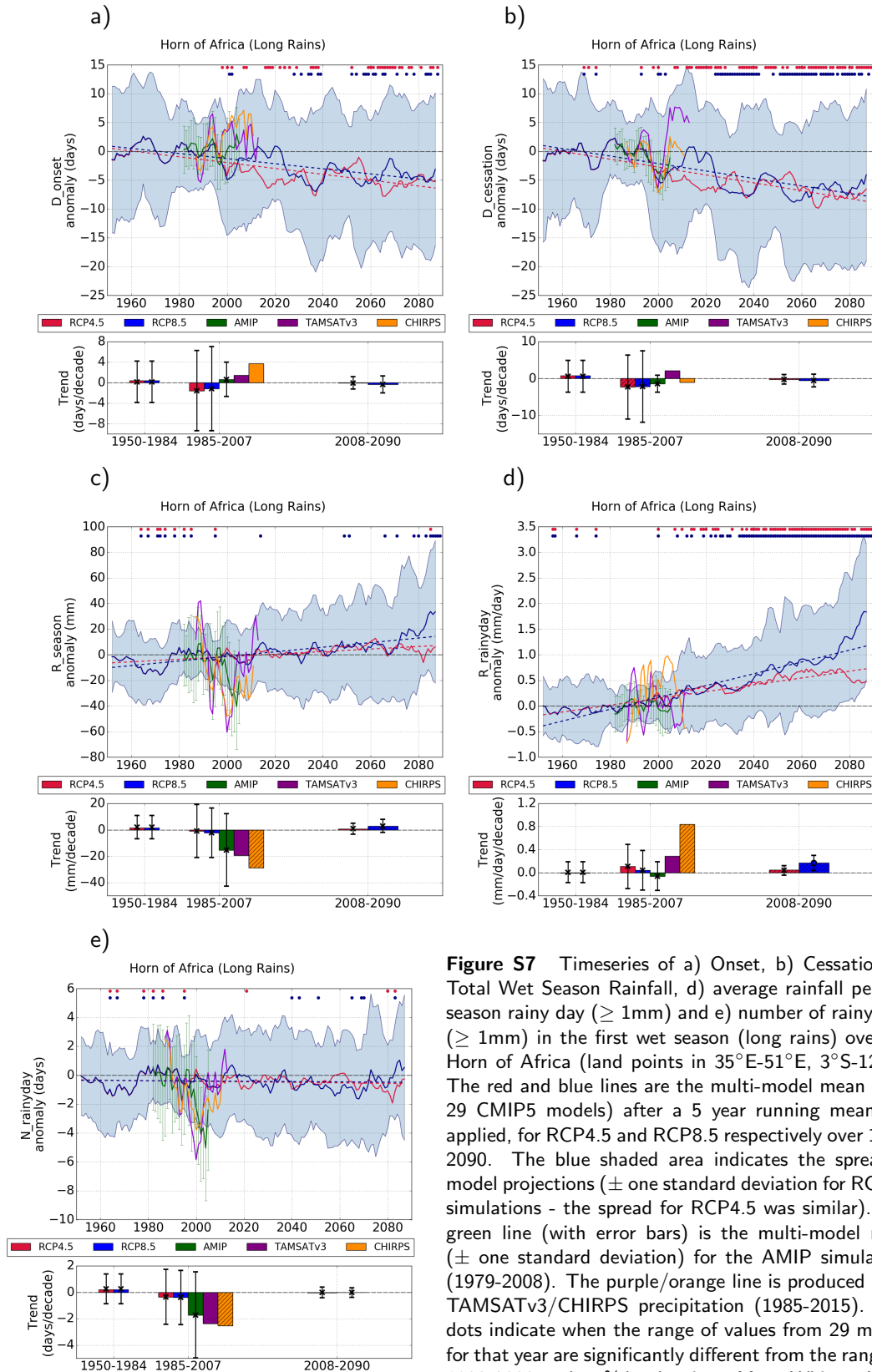


Figure S7 Timeseries of a) Onset, b) Cessation, c) Total Wet Season Rainfall, d) average rainfall per wet season rainy day ($\geq 1\text{mm}$) and e) number of rainy days ($\geq 1\text{mm}$) in the first wet season (long rains) over the Horn of Africa (land points in $35^{\circ}\text{E}-51^{\circ}\text{E}$, $3^{\circ}\text{S}-12^{\circ}\text{N}$). The red and blue lines are the multi-model mean (over 29 CMIP5 models) after a 5 year running mean was applied, for RCP4.5 and RCP8.5 respectively over 1950-2090. The blue shaded area indicates the spread of model projections (\pm one standard deviation for RCP8.5 simulations - the spread for RCP4.5 was similar). The green line (with error bars) is the multi-model mean (\pm one standard deviation) for the AMIP simulations (1979-2008). The purple/orange line is produced using TAMSATv3/CHIRPS precipitation (1985-2015). The dots indicate when the range of values from 29 models for that year are significantly different from the range for 1980-2000 at the 5% level, using a Mann Whitney U and t-test. The bar charts indicate the trend over different periods; 1950-1984, 1985-2007 (AMIP and observations period) and 2008-2090. The height of the bars indicates the trend of the multi-model mean; hatching indicates the trend is significantly different from 0 at the 5% level. The circle/cross and errorbar indicate the mean and standard deviations of the trend from the 29 models; a circle indicates over 50% of the models show a trend significantly different from 0 at the 5% level.

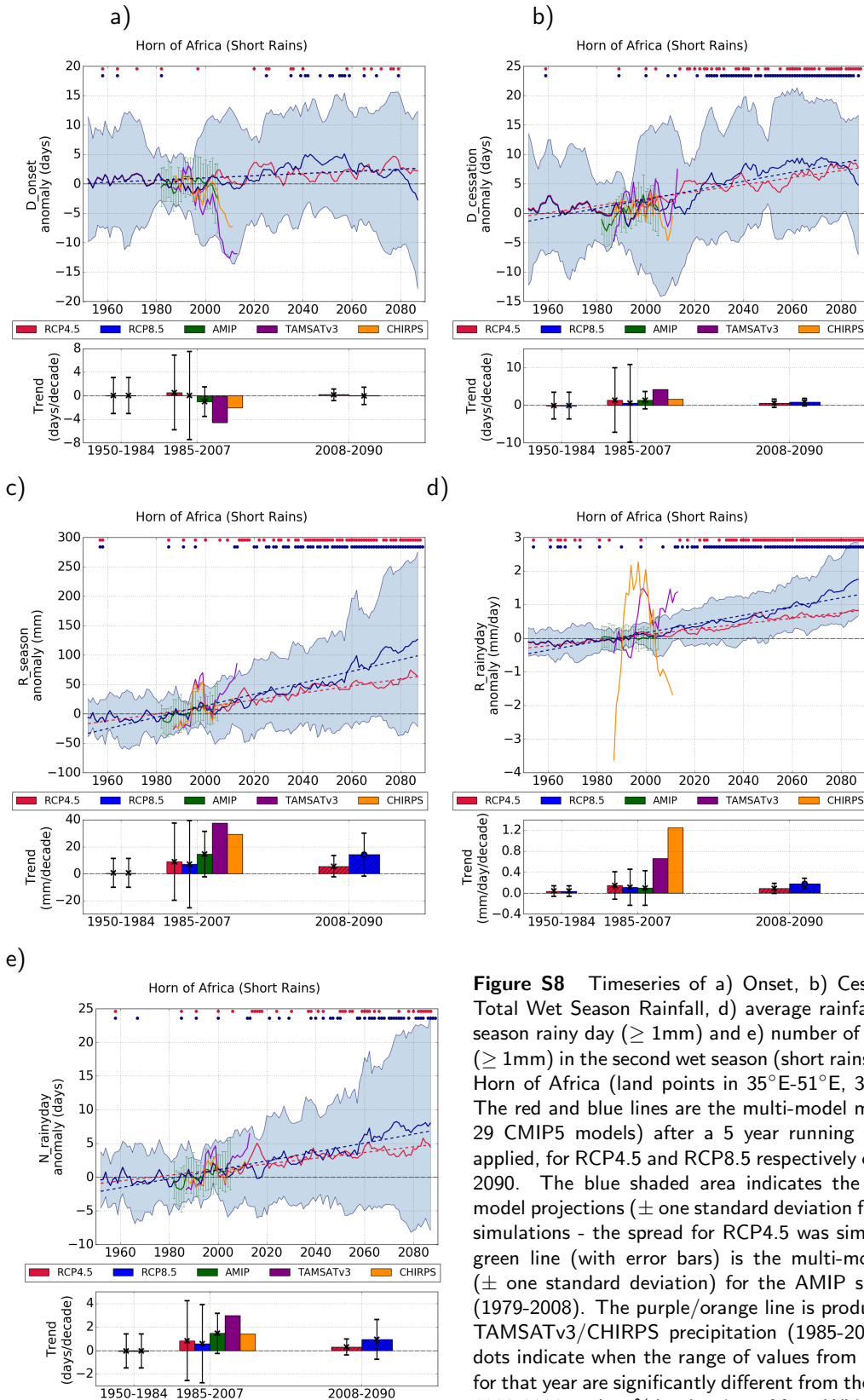


Figure S8 Timeseries of a) Onset, b) Cessation, c) Total Wet Season Rainfall, d) average rainfall per wet season rainy day ($\geq 1\text{mm}$) and e) number of rainy days ($\geq 1\text{mm}$) in the second wet season (short rains) over the Horn of Africa (land points in $35^{\circ}\text{E}-51^{\circ}\text{E}$, $3^{\circ}\text{S}-12^{\circ}\text{N}$). The red and blue lines are the multi-model mean (over 29 CMIP5 models) after a 5 year running mean was applied, for RCP4.5 and RCP8.5 respectively over 1950-2090. The blue shaded area indicates the spread of model projections (\pm one standard deviation for RCP8.5 simulations - the spread for RCP4.5 was similar). The green line (with error bars) is the multi-model mean (\pm one standard deviation) for the AMIP simulations (1979-2008). The purple/orange line is produced using TAMSATv3/CHIRPS precipitation (1985-2015). The dots indicate when the range of values from 29 models for that year are significantly different from the range for 1980-2000 at the 5% level, using a Mann Whitney U and t-test. The bar charts indicate the trend over different periods; 1950-1984, 1985-2007 (AMIP and observations period) and 2008-2090. The height of the bars indicates the trend of the multi-model mean; hatching indicates the trend is significantly different from 0 at the 5% level. The circle/cross and errorbar indicate the mean and standard deviations of the trend from the 29 models; a circle indicates over 50% of the models show a trend significantly different from 0 at the 5% level.

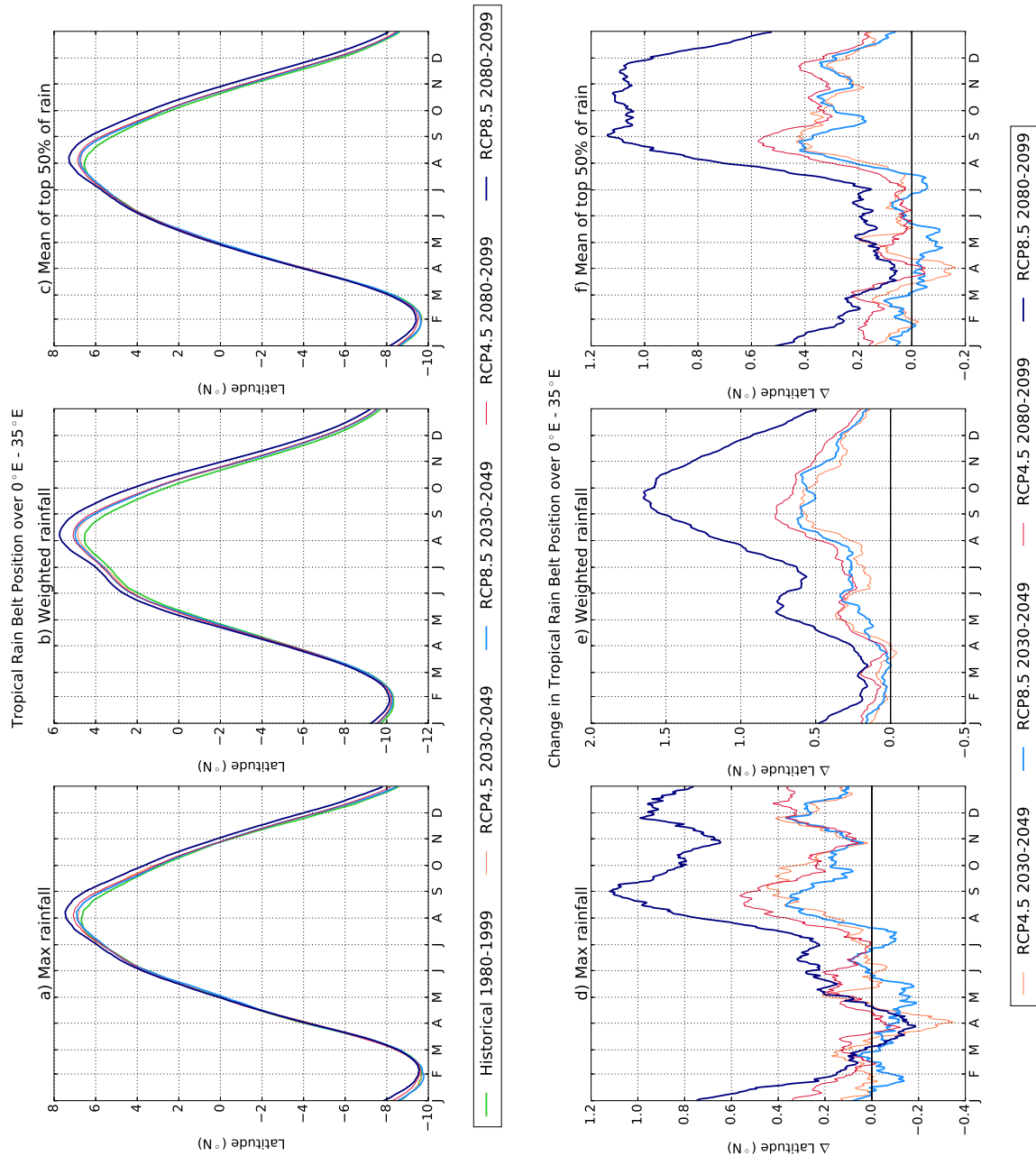


Figure S9 Mean tropical rain belt (TRB) position (a-c) for historical, RCP 4.5 and RCP 8.5 scenarios over 3 time periods and change relative to the historical period (d-f), calculated using 3 methods. Results here were smoothed using a 30 day moving average. a,d) Max rainfall uses the latitude of the maximum rainfall at each longitude to define the position of the TRB. b,e) Weighted rainfall takes the location of the rainfall centroid over 30°S-30°N for each longitude to be the position of the TRB. c,f) 'Mean of top 50% of rainfall' calculates the latitude of the rainfall centroid using just the top 50% of rainfall, at each longitude. The third definition is recommended by Shonk et al. (2018), and is the definition used.

December. Years below the 25th percentile (lowest 4 years, TRB south) and years above the 75th percentile (highest 4 years, TRB north) were chosen to represent years with early/late southward retreat respectively. Figure S10a-b) shows the position of the tropical rain belt in the early and late years, compared with the middle 50th percentile, and confirms that years where the TRB is shifted north/south in the second half of the calendar year have been selected. This is especially apparent in Figure S10b.

Figure S10c-f) shows the onset anomalies for the main wet season over Southern Africa and the short rains (c,e) and cessation anomalies for the wet season over West Africa and the Sahel and the short rains (d,f) in years below the 25th percentile (c-d) and years above the 75th percentile (e-f). In years where the TRB is shifted north in the second half of the calendar year, i.e. the southward retreat of the TRB is later (e-f) the anomalies show later onset and cessation, with a mean anomaly of around 5 days and over 60% of grid points exhibiting a positive anomaly. Conversely, in years when the TRB is south, and the southward retreat is earlier (c-d) the anomalies show earlier onset and cessation.

Although this analysis is conducted over only 16 years, the results suggest that shifts in the position of the tropical rain belt are related to changes in onset and cessation, with a later southward progression of the tropical rain belt leading to later cessation over the Sahel, later short rains and later onset over Southern Africa.

7.2.5 Location of Saharan Heat Low and Angola Low

The methods of Dixon et al. (2017a) (based on Lavaysse et al. (2009)) and Munday and Washington (2017) were used to determine if the Saharan Heat Low (SHL) and Angola Low (AL) are likely to shift spatially under future climate change.

Dixon et al. (2017a) and Lavaysse et al. (2009) determine the location of the SHL using the low-level atmospheric thickness (LLAT), defined as the difference between the geopotential heights at 700 hPa and 925 hPa. Here we have used the difference between 700 hPa and 850 hPa to be the LLAT, due to the 925 hPa level intersecting with the surface in some CMIP5 models. Values over West Africa (0° - 40° N, 20° W- 30° E) greater than the 90% level of each month's cumulative distribution function of LLAT are deemed to be within the SHL.

For each month the location of the SHL is determined, and the frequency of occurrence is computed for each model for the historical (1980-1999) and RCP 8.5 (2080-2099) simulations. Figure S11 shows the multi-mean mean frequency of occurrence for the historical simulation (black contours) and RCP 8.5 (colouration), with Figure S12 showing the difference. Overall Figures S11-S12 demonstrate that there is very little change in the location of the SHL; no

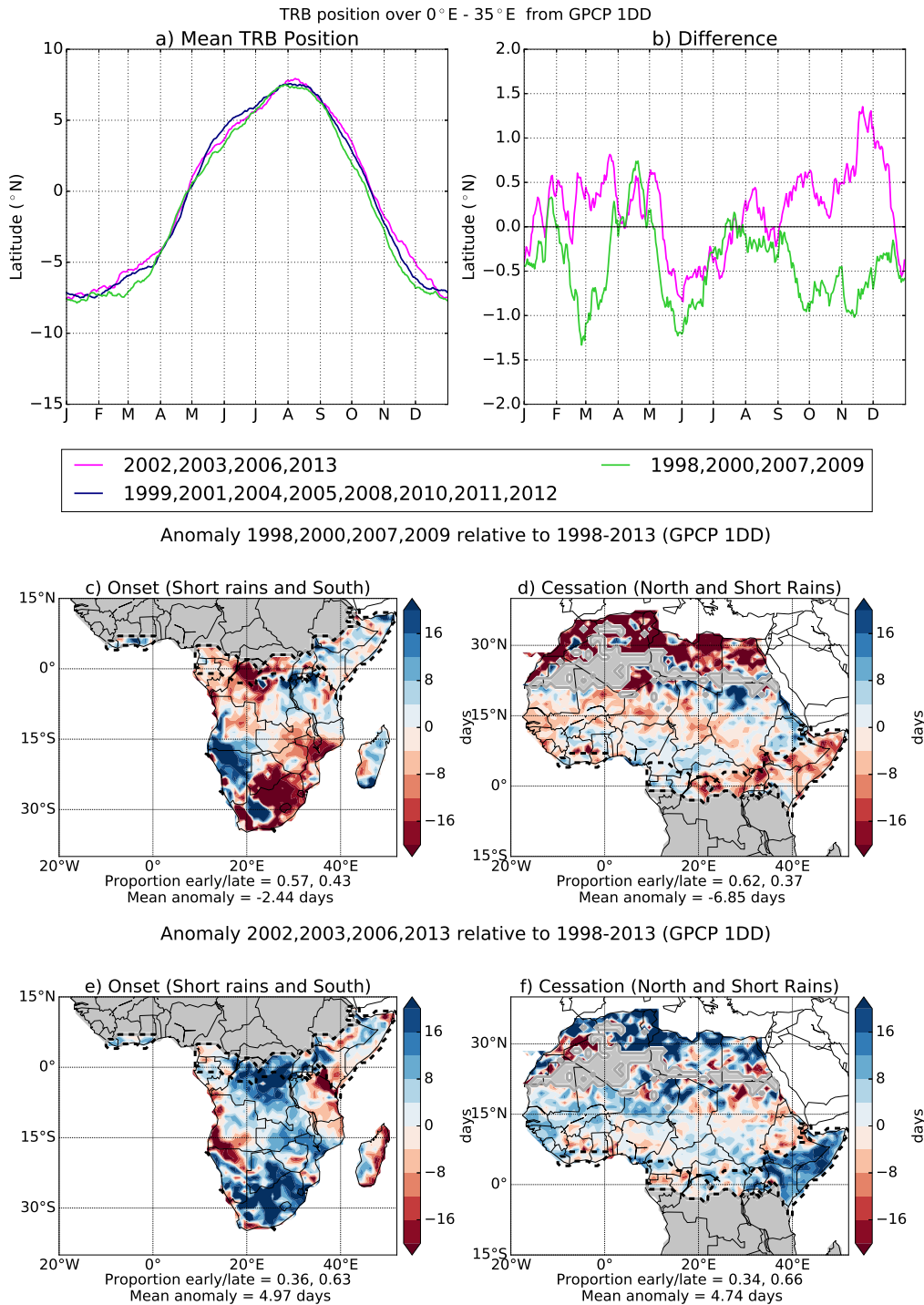


Figure S10 a-b) Mean Tropical Rain Belt (TRB) position (and difference) for 1998-2013 using GPCP 1DD data. Years were separated into early/late southward retreat by examining the mean TRB position (averaged over 0°-35°E) from 1 August - 31 December. Years below the 25th percentile and above the 75th percentile are averaged and shown in green and pink respectively. Years between the 25th and 75th percentiles are averaged and shown in blue. b) shows the difference in early/late years compared to the middle 50th percentile. c-d) Anomaly in 'early years' (those below the 25th percentile) compared to normal/late years in 1998-2013. c) Short rains onset and onset over Southern Africa. d) Cessation over Sahel and cessation of short rains. Proportion early/late shows the proportion of grid points that exhibit a negative/positive (early/late) anomaly respectively. The mean anomaly is computed across all grid points. e-f) as c-d) but for 'late years' (those above the 75th percentile) compared to normal/early years.

difference is visually evident in Figure S11, and Figure S12 only contains a small northward shift. This is expected as the Saharan Heat Low is strongly constrained by topography with the Atlas Mountains to the north and Hoggar mountains to the east (Lavaysse et al., 2009; Chauvin et al., 2010; Evan et al., 2015).

Munday and Washington (2017) define the Angola Low to be the lowest 5% of December-January-February 850 hPa geopotential height over 5°E - 55°E , 0° - 35°S . In the same way as for the SHL, the frequency of occurrence is computed for each model for the historical (1980-1999) and RCP 8.5 (2080-2099) simulations; Figure S13 shows the historical and RCP 8.5 location of the AL, with Figure S14 showing the change. There is very little change in the location of the AL, with no difference discernible in Figure S13, and a slight southward shift in Figure S14. Again the Angola Low is linked to topography, and forms over the plateau region with the Angolan and Namibian Highlands to the west (Munday and Washington, 2017).

The negligible change in location means that the method used for determining the strength of the SHL and AL based on geopotential anomalies over a Saharan region and a southern Africa region is appropriate, as the lows are in the same position in present and future climates.

7.2.6 Sahara Heat Low Index and Angola Low Index

In the paper we use an index for the strength of the Angola Low and Saharan Heat Low based on 850 hPa geopotential height. In Dixon et al. (2017a) the same index was used for the Saharan Heat Low, but geopotential height at 925 hPa was used. For our analysis it was decided to use 850 hPa due to the intersection of topography with the 925 hPa level in some of the CMIP5 models used. Here the results are repeated with the 925 hPa geopotential height to ensure robustness. The same results are found when 925 hPa (Figure S16) and 850 hPa (Figure S15) are used; the strength of the Saharan Heat Low increases towards the end of the boreal summer, the Angola Low exhibits a smaller increase in strength throughout the year.

7.2.7 Sensitivity of SHL/AL index to region used

To ensure that the results for the AL and SHL are not dependent upon the regions used, the analysis was repeated for modified regions. Figure S17 shows the change in strength of the SHL and AL when modified regions are used; the location of the new regions is marked in Figure S17 using dashed lines. While the absolute values are different when compared with Figure S15, Figure S17 shows an increase in the strength of the SHL in the boreal summer

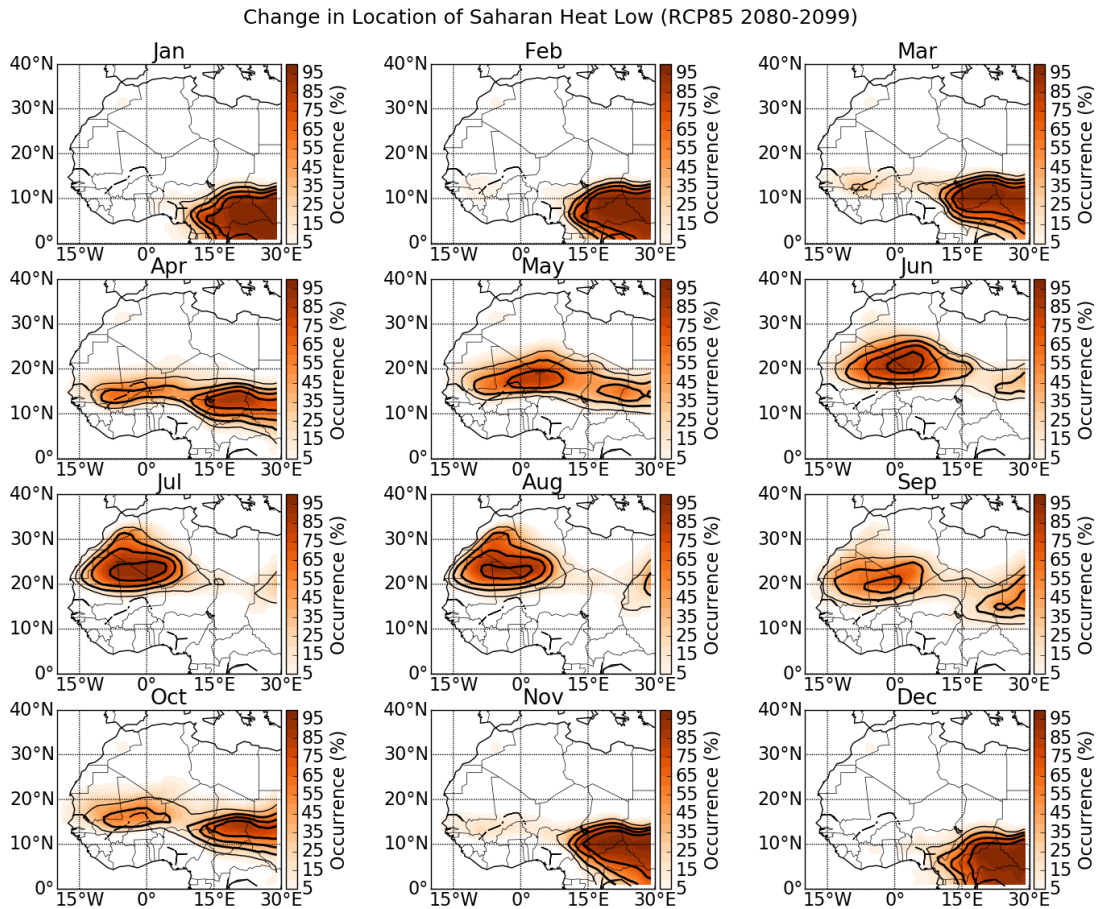


Figure S11 Seasonal progression of the position of the Saharan Heat Low. Colouration/contours show the average heat low occurrence frequency for the RCP 8.5 (2080-2099)/historical (1980-1999) simulations respectively. These frequencies represent how often the detection algorithm (> 90 th percentile of lower-level atmospheric thickness) locates the heat low at each grid point. The frequency is computed for each model individually; the multi-model mean is shown here. The narrow contour indicates an occurrence frequency of 20%; the thicker contours are for 40, 60 and 80%.

months, and a smaller increase in the strength of the AL. Thus we can conclude that the results are robust to the region selected.

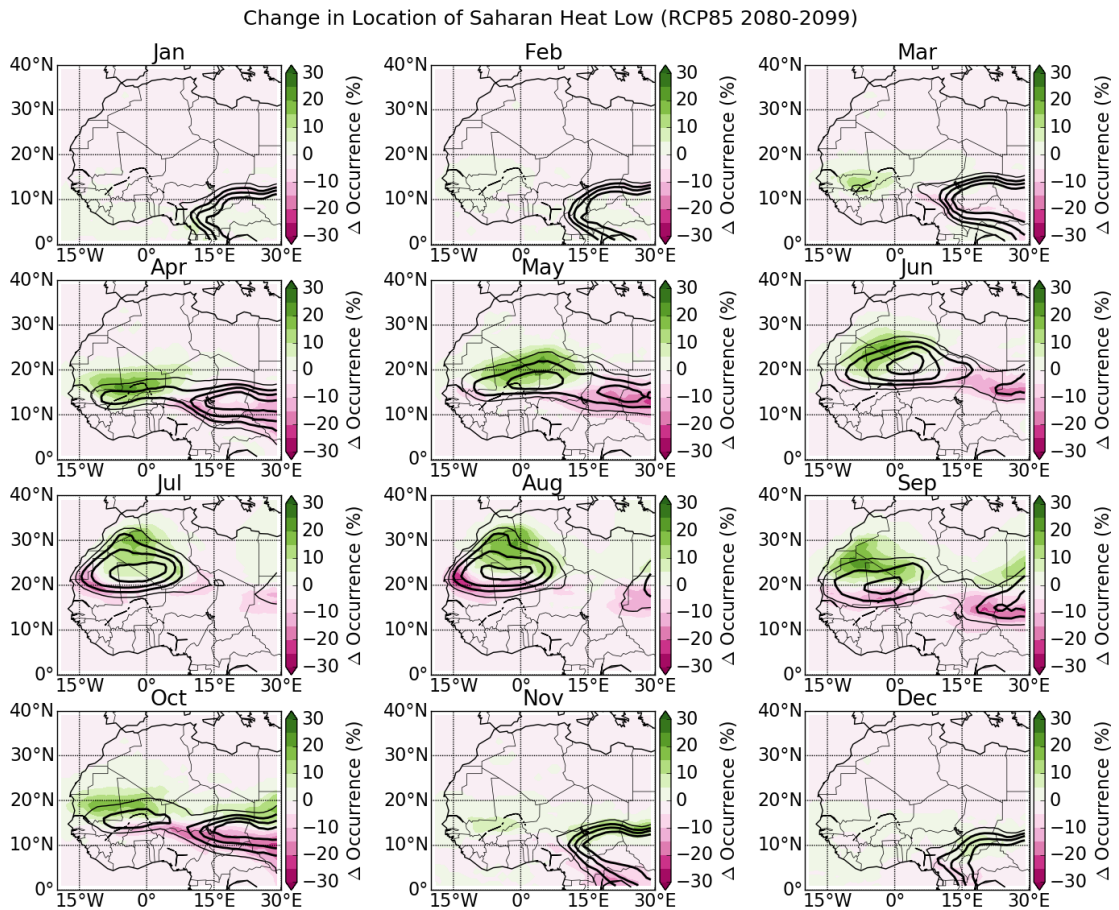


Figure S12 Change in monthly position of the Saharan Heat Low. Colouration shows the change in average heat low occurrence frequency for the RCP 8.5 simulation (2080-2099) compared to historical (1980-1999) simulation. Contours show the average heat low occurrence frequency for the historical (1980-1999) simulation. These frequencies represent how often the detection algorithm (> 90 th percentile of lower-level atmospheric thickness) locates the heat low at each grid point. The frequency is computed for each model individually; the multi-model mean is shown here. The narrow contour indicates an occurrence frequency of 20%; the thicker contours are for 40, 60 and 80%. Green colours indicate increasing frequency of occurrence, while pink colours indicate decreasing frequency of occurrence.

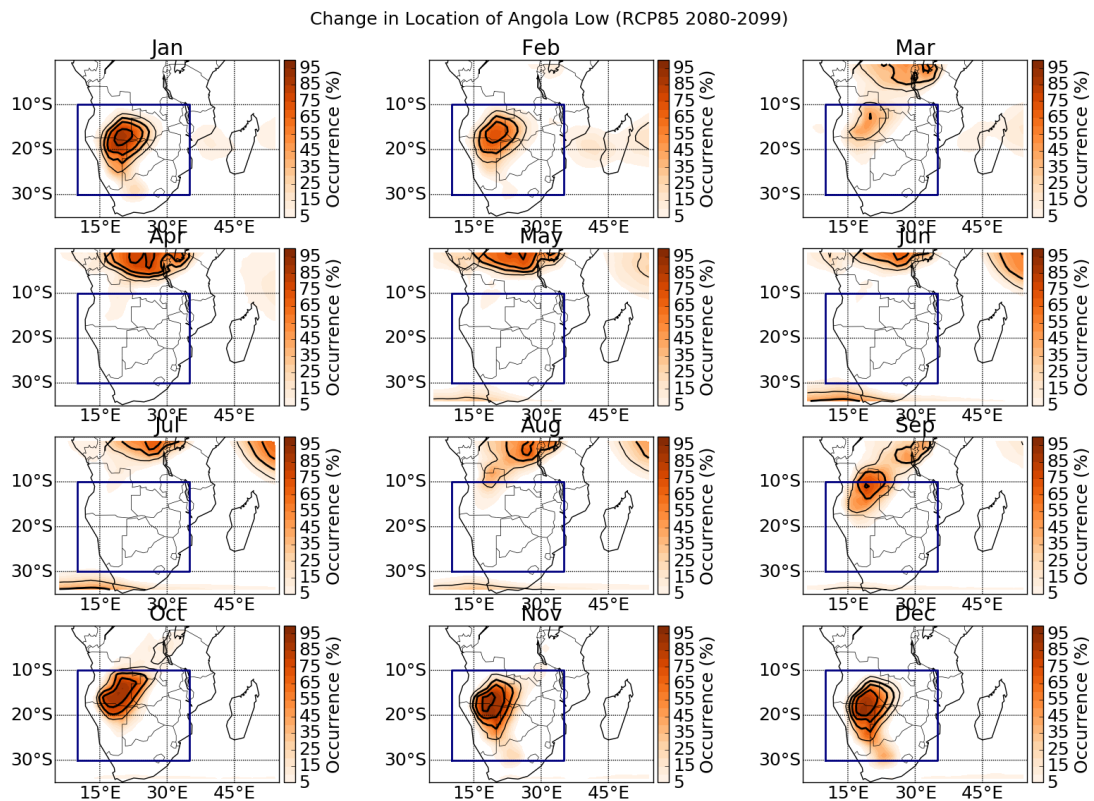


Figure S13 Seasonal progression of the position of the Angola Low. Colouration/ contours show the average heat low occurrence frequency for the RCP 8.5 (2080-2099)/ historical (1980-1999) simulations respectively. These frequencies represent how often the detection algorithm (< 5 th percentile of 850hPa geopotential height) locates the heat low at each grid point. The frequency is computed for each model individually; the multi-model mean is shown here. The narrow contour indicates an occurrence frequency of 20%; the thicker contours are for 40, 60 and 80%. The navy box shows the region used for the Angola Low strength index.

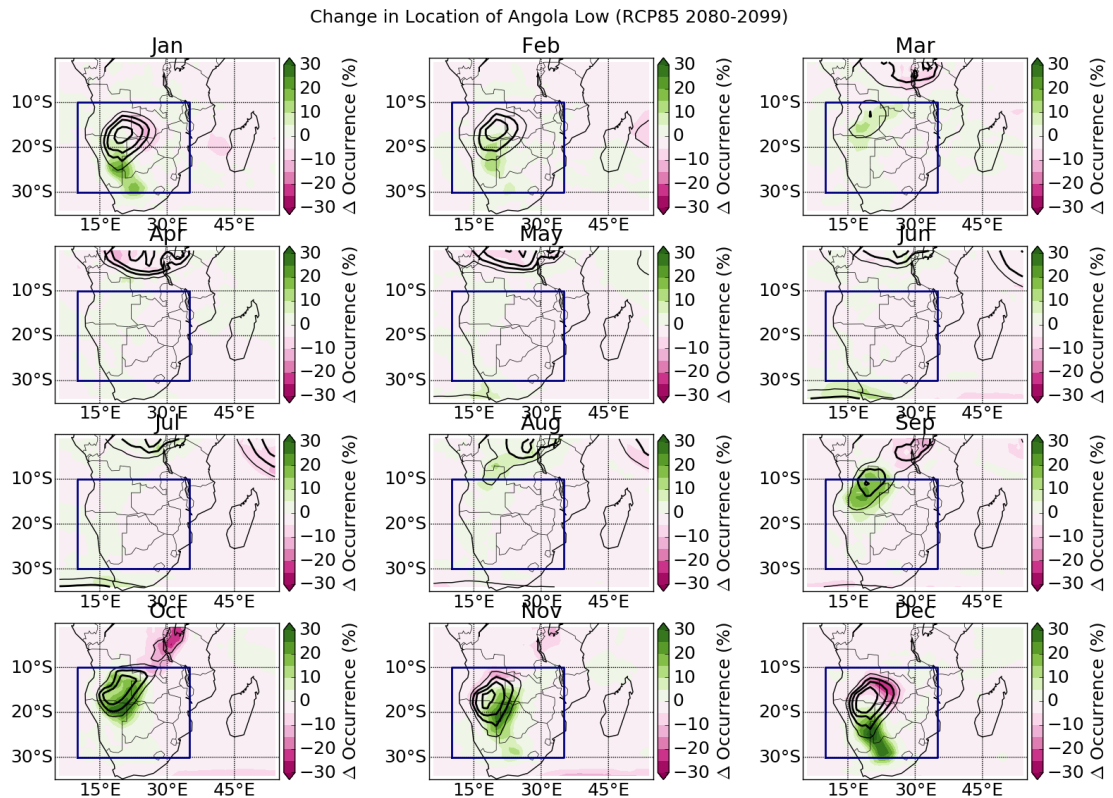


Figure S14 Change in monthly position of the Angola Low. Colouration shows the change in average heat low occurrence frequency for the RCP 8.5 simulation (2080-2099) compared to historical (1980-1999) simulation. Contours show the average heat low occurrence frequency for the historical (1980-1999) simulation. These frequencies represent how often the detection algorithm (< 5 th percentile of 850hPa geopotential height) locates the heat low at each grid point. The frequency is computed for each model individually; the multi-model mean is shown here. The narrow contour indicates an occurrence frequency of 20%; the thicker contours are for 40, 60 and 80%. Green colours indicate increasing frequency of occurrence, while pink colours indicate decreasing frequency of occurrence. The navy box shows the region used for the Angola Low strength index.

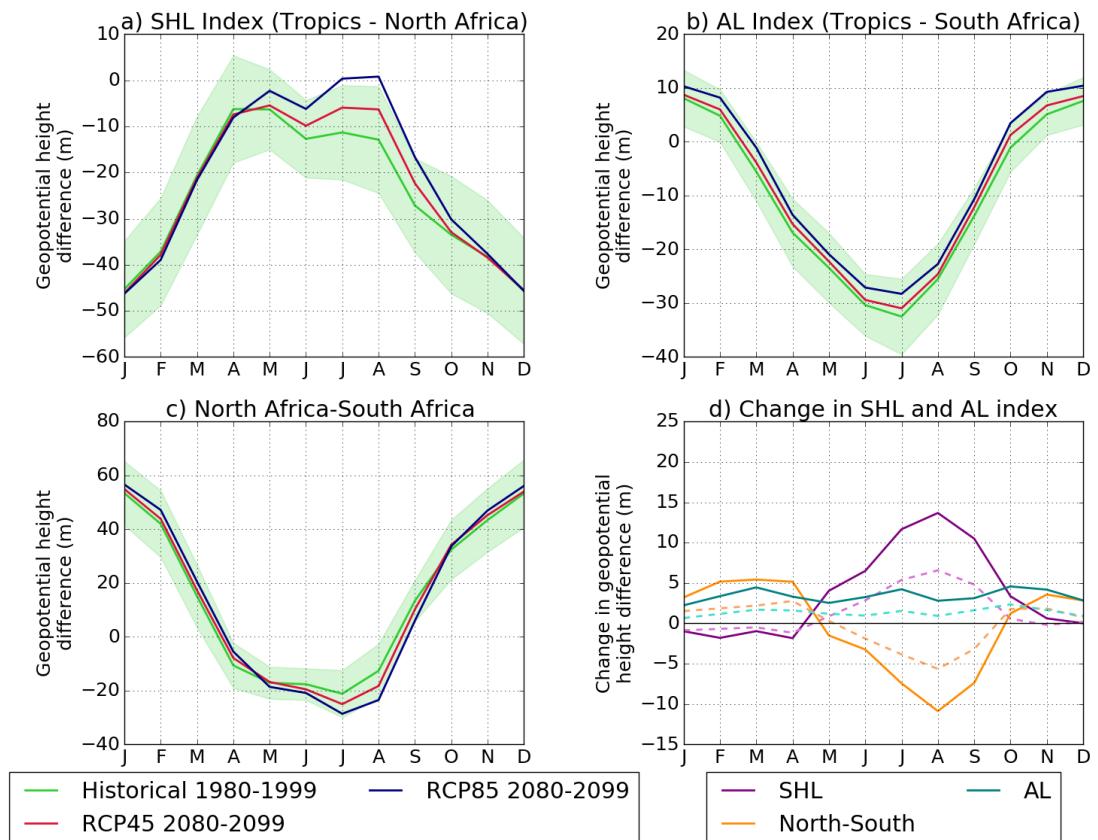


Figure S15 Strength of the SHL (a) and AL (b), and comparison (AL-SHL, c) for historical, RCP 4.5 and RCP 8.5 simulations over 29 CMIP5 models for 1980-1999 and 2080-2099 computed using the method detailed in section 5.2 with 850 hPa geopotential height. The green shaded area indicates the range across the 29 CMIP5 models for the historical simulation. d) shows the change in strength of the SHL, AL and AL-SHL from historical 1980-1999 to RCP 4.5 (dashed)/ RCP 8.5 (solid) (2080-2099).

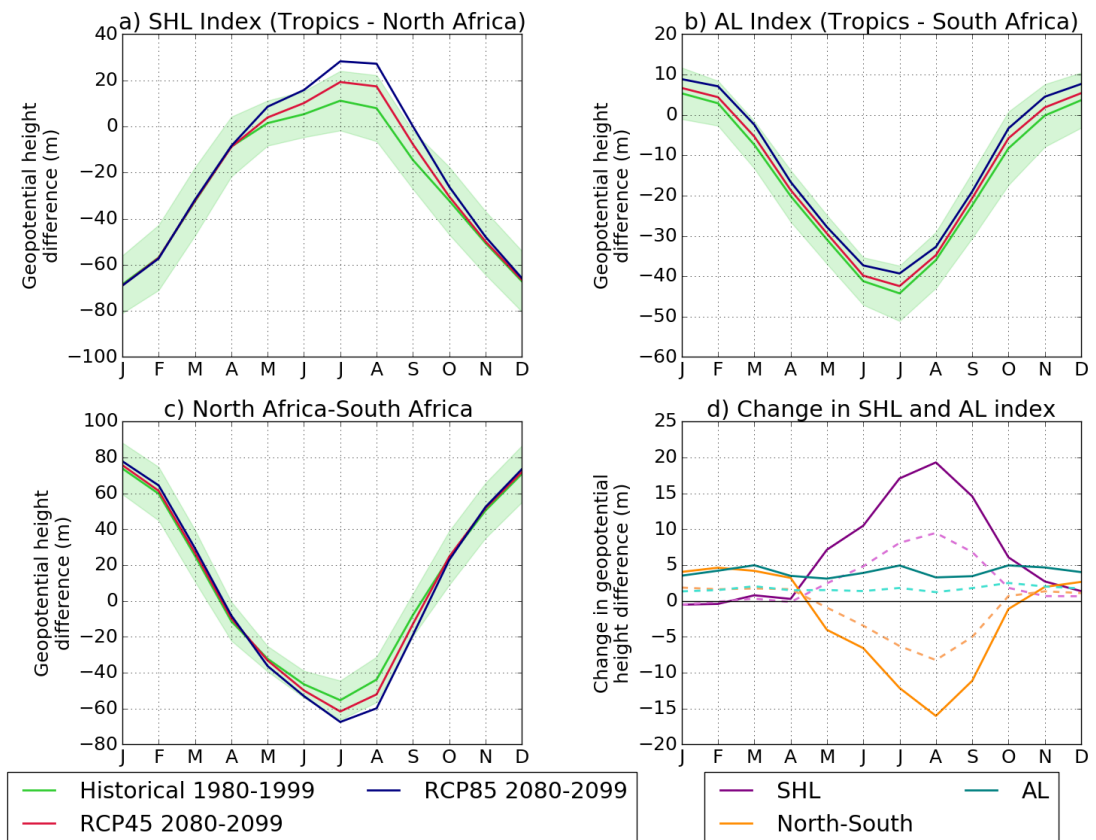


Figure S16 Strength of the SHL (a) and AL (b), and comparison (AL-SHL, c) for historical, RCP 4.5 and RCP 8.5 simulations over 29 CMIP5 models for 1980-1999 and 2080-2099 computed using the method detailed in section 5.2 with 925 hPa geopotential height. The green shaded area indicates the range across the 29 CMIP5 models for the historical simulation. d) shows the change in strength of the SHL, AL and AL-SHL from historical 1980-1999 to RCP 4.5 (dashed)/ RCP 8.5 (solid) (2080-2099).

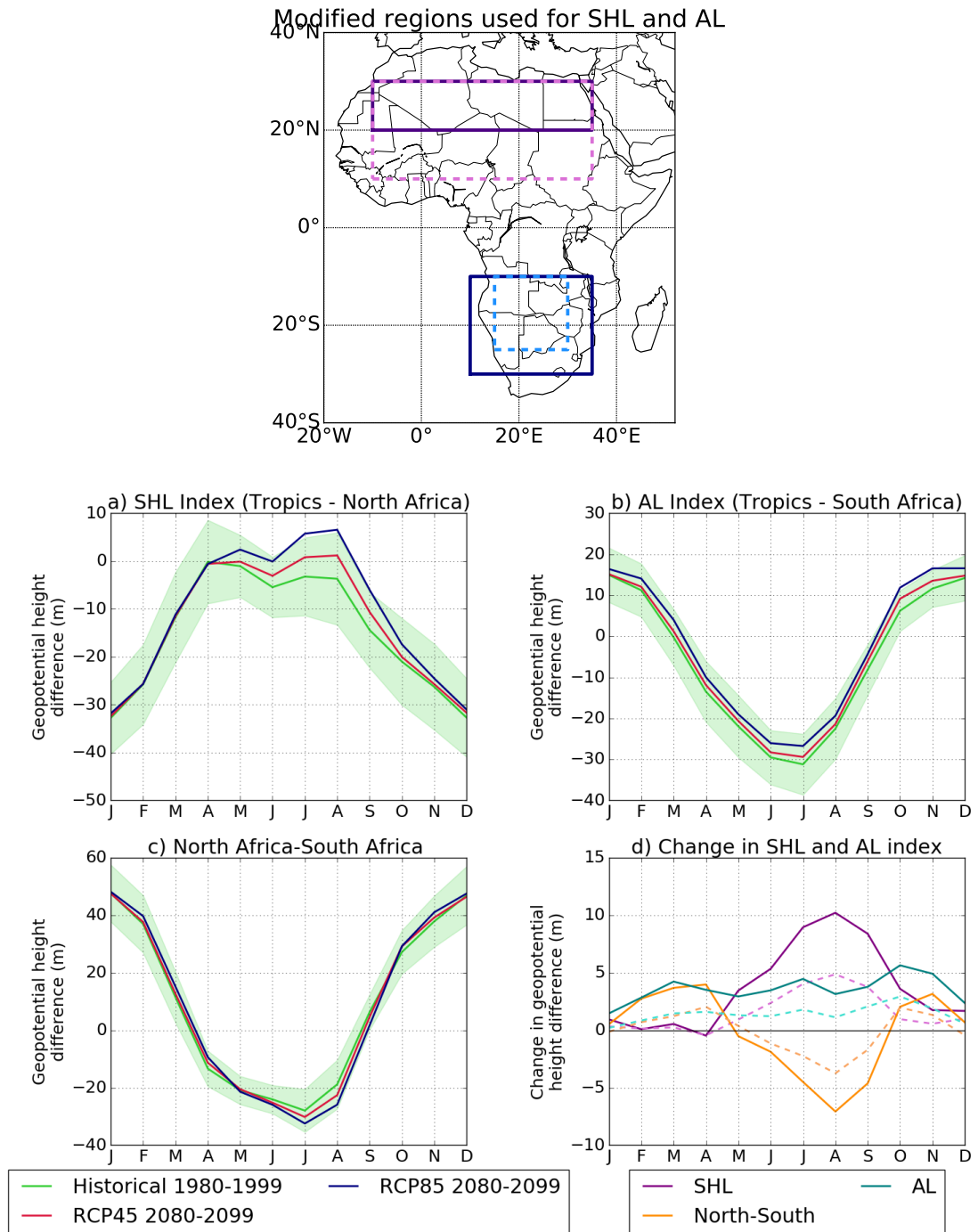


Figure S17 Strength of the SHL (a) and AL (b), and comparison (AL-SHL, c) for historical, RCP 4.5 and RCP 8.5 simulations over 29 CMIP5 models for 1980-1999 and 2080-2099 computed using the method detailed in section 5.2 with 850 hPa geopotential height and modified regions. The map above shows the modified regions; the solid lines delineate the regions used originally, the dashed lines delineate the regions that are used here. The green shaded area indicates the range across the 29 CMIP5 models for the historical simulation. d) shows the change in strength of the SHL, AL and AL-SHL from historical 1980-1999 to RCP 4.5 (dashed)/ RCP 8.5 (solid) (2080-2099).

Institute	Model	Resolution (Lat° × Lon°)	Reference
CSIRO-BOM	ACCESS 1.0	1.25 × 1.875	Bi et al. (2013)
CSIRO-BOM	ACCESS 1.3	1.25 × 1.875	Bi et al. (2013)
BCC	BCC-CSM1-1-M	1.12 × 1.125	Wu, T and others (2012)
BNU	BNU-ESM	2.78 × 2.813	Ji et al. (2014)
CCCma	CanESM2	2.79 × 2.813	Arora et al. (2011)
NCAR	CCSM4	0.94 × 1.25	Gent et al. (2011)
NSF-DOE-NCAR	CESM1-BGC	0.94 × 1.25	Long et al. (2013)
NSF-DOE-NCAR	CESM1-CAM5	0.94 × 1.25	Hurrell et al. (2013)
CMCC	CMCC-CM	0.74 × 0.75	Fogli et al. (2009)
CMCC	CMCC-CMS	1.87 × 1.875	Fogli et al. (2009)
CNRM-CERFACS	CNRM-CM5	1.40 × 1.406	Voldoire et al. (2013)
CSIRO-QCCCE	CSIRO-Mk3-6-0	1.85 × 1.875	Jeffrey et al. (2013)
ICHEC	EC-EARTH	1.12 × 1.125	Hazeleger et al. (2012)
LASG-CESS	FGOALS-g2	2.79 × 2.813	Li et al. (2013)
NOAA-GFDL	GFDL-ESM2G	2.02 × 2.5	Dunne et al. (2012)
NOAA-GFDL	GFDL-ESM2M	2.02 × 2.5	Dunne et al. (2012)
MOHC	HadGEM2-CC	1.25 × 1.875	Collins et al. (2011)
MOHC	HadGEM2-ES	1.25 × 1.875	Collins et al. (2011)
INM	INMCM4	1.50 × 2	Volodin et al. (2010)
IPSL	IPSL-CM5A-LR	1.89 × 3.75	Dufresne et al. (2013)
IPSL	IPSL-CM5A-MR	1.27 × 2.5	Dufresne et al. (2013)
IPSL	IPSL-CM5B-LR	1.89 × 3.75	Dufresne et al. (2013)
MIROC	MIROC5	1.40 × 1.406	Watanabe et al. (2010)
MIROC	MIROC-ESM	2.79 × 2.813	Watanabe et al. (2011)
MIROC	MIROC-ESM-CHEM	2.79 × 2.813	Watanabe et al. (2011)
MPI-M	MPI-ESM-LR	1.86 × 1.875	Stevens et al. (2013)
MPI-M	MPI-ESM-MR	1.86 × 1.875	Stevens et al. (2013)
MRI	MRI-CGCM3	1.12 × 1.125	Yukimoto et al. (2011)
NCC	NorESM1-M	1.89 × 2.5	Iversen et al. (2012)

Table S1 List of models and institutions that provided model output used in this study. Horizontal resolution and references for each model are also included. Historical, RCP 4.5 and RCP 8.5 simulations were used over 1940-2100 (timeseries, onset and cessation dates not computed for the first and last 10 years), and over 1980-1999, 2030-2049 and 2080-2090 (difference plots).

REFERENCES

- Adams, K. A. and E. K. Lawrence, 2014: *Research Methods, Statistics, and Applications*. Sage Publications.
- Adejuwon, J. O. and T. O. Odekunle, 2006: Variability and the Severity of the “Little Dry Season” in southwestern Nigeria. *Journal of Climate*, **19**, 483–493.
- Adhikari, U., A. P. Nejadhashemi, and S. A. Woznicki, 2015: Climate change and eastern Africa: a review of impact on major crops. *Food and Energy Security*, **4**, 110–132.
- Alamirew, N. K., M. C. Todd, C. L. Ryder, J. H. Marsham, and Y. Wang, 2018: The early summertime Saharan heat low: sensitivity of the radiation budget and atmospheric heating to water vapour and dust aerosol. *Atmospheric Chemistry and Physics*, **18**, 1241–1262.
- Alexander, L., M. Donat, Y. Takayama, and H. Yang, 2011: The climdex project: creation of long-term global gridded products for the analysis of temperature and precipitation extremes. *WCRP Open Science Conference, Denver*.
- Alexander, L., X. Zhang, T. Peterson, J. Caesar, B. Gleason, A. Klein Tank, M. Haylock, D. Collins, B. Trewin, F. Rahimzadeh, et al., 2006: Global observed changes in daily climate extremes of temperature and precipitation. *Journal of Geophysical Research: Atmospheres*, **111**.
- Allan, R. P., 2012: Regime dependent changes in global precipitation. *Climate Dynamics*, **39**, 827–840.
- 2014: Climate change: Dichotomy of drought and deluge. *Nature Geoscience*, **7**, 700–701, doi:10.1038/ngeo2243.
- Allan, R. P., C. Liu, M. Zahn, D. A. Lavers, E. Koukouvagias, and A. Bodas-Salcedo, 2014: Physically consistent responses of the global atmospheric hydrological cycle in models and observations. *Surv. Geophys.*, **35**, 533–552, doi:10.1007/s10712-012-9213-z.
- Allan, R. P., B. J. Soden, V. O. John, W. Ingram, and P. Good, 2010: Current changes in tropical precipitation. *Environmental Research Letters*, **5**, 025205.
- Allen, M. R. and W. J. Ingram, 2002: Constraints on future changes in climate and the hydrologic cycle. *Nature*, **419**, 224.
- Arora, V., J. Scinocca, G. Boer, J. Christian, K. Denman, G. Flato, V. Kharin, W. Lee, and W. Merryfield, 2011: Carbon emission limits required to satisfy future representative concentration pathways of greenhouse gases. *Geophysical Research Letters*, **38**.
- Asfaw, D., E. Black, M. Brown, K. J. Nicklin, F. Otu-Larbi, E. Pinnington, A. Challinor, R. Maidment, and T. Quaife, in review: TAMSAT-ALERT v1: A new framework for agricultural decision support. *Geoscientific Model Development Discussion*.
- Awange, J., V. Ferreira, E. Forootan, S. Andam-Akorful, N. Agutu, X. He, et al., 2016: Uncertainties in remotely sensed precipitation data over Africa. *International Journal of Climatology*, **36**, 303–323, doi:10.1002/joc.4346.
- Balan Sarojini, B., P. A. Stott, and E. Black, 2016: Detection and attribution of human influence on regional precipitation. *Nature Climate Change*, **6**, 669.
- Balan Sarojini, B., P. A. Stott, E. Black, and D. Polson, 2012: Fingerprints of changes in annual and seasonal precipitation from CMIP5 models over land and ocean. *Geophysical Research Letters*, **39**.

REFERENCES

- Baumberger, C., R. Knutti, and G. Hirsch Hadorn, 2017: Building confidence in climate model projections: an analysis of inferences from fit. *Wiley Interdisciplinary Reviews: Climate Change*, **8**.
- Bi, D., M. Dix, S. J. Marsland, S. O'Farrell, H. Rashid, P. Uotila, A. Hirst, E. Kowalczyk, M. Golebiewski, A. Sullivan, et al., 2013: The ACCESS coupled model: description, control climate and evaluation. *Aust. Meteorol. Oceanogr. J.*, **63**, 41–64.
- Biasutti, M., 2013: Forced Sahel rainfall trends in the CMIP5 archive. *Journal of Geophysical Research: Atmospheres*, **118**, 1613–1623.
- Biasutti, M. and A. H. Sobel, 2009: Delayed Sahel rainfall and global seasonal cycle in a warmer climate. *Geophysical Research Letters*, **36**.
- Biasutti, M., A. H. Sobel, and S. J. Camargo, 2009: The role of the Sahara low in summertime Sahel rainfall variability and change in the CMIP3 models. *Journal of Climate*, **22**, 5755–5771.
- Birner, T., S. M. Davis, and D. J. Seidel, 2014: The changing width of earth's tropical belt. *Physics Today*, **67**.
- Black, E., H. Greatrex, M. Young, and R. Maidment, 2016: Incorporating Satellite Data Into Weather Index Insurance. *Bulletin of the American Meteorological Society*, **97**, ES203–ES206.
- Black, E., J. Slingo, and K. R. Sperber, 2003: An observational study of the relationship between excessively strong short rains in coastal East Africa and Indian Ocean SST. *Monthly Weather Review*, **131**, 74–94.
- Boko, M., I. Niang, A. Nyong, C. Vogel, A. Githeko, M. Medany, B. Osman-Elasha, R. Tabo, and P. Yanda, 2007: Africa. In: *Climate Change 2007: Impacts, Adaptation and Vulnerability. Contribution of Working Group II to the Fourth Assessment Report of the Intergovernmental Panel on Climate Change*, M.L. Parry, O.F. Canziani, J.P. Palutikof, P.J. van der Linden and C.E. Hanson, Eds.
- Boyard-Micheau, J., P. Camberlin, N. Philippon, and V. Moron, 2013: Regional-scale rainy season onset detection: a new approach based on multivariate analysis. *Journal of Climate*, **26**, 8916–8928.
- Brands, S., S. Herrera, J. Fernández, and J. M. Gutiérrez, 2013: How well do CMIP5 Earth System Models simulate present climate conditions in Europe and Africa? *Climate Dynamics*, **41**, 803–817.
- Brawn, J. D., T. J. Benson, M. Stager, N. D. Sly, and C. E. Tarwater, 2017: Impacts of changing rainfall regime on the demography of tropical birds. *Nature Climate Change*, **7**, 133.
- Byrne, M. P. and P. A. O'Gorman, 2015: The response of precipitation minus evapotranspiration to climate warming: Why the “wet-get-wetter, dry-get-drier” scaling does not hold over land. *Journal of Climate*, **28**, 8078–8092.
- Caesar, J., L. Alexander, and R. Vose, 2006: Large-scale changes in observed daily maximum and minimum temperatures: Creation and analysis of a new gridded data set. *Journal of Geophysical Research: Atmospheres*, **111**.
- Camberlin, P., S. Janicot, and I. Poccard, 2001: Seasonality and atmospheric dynamics of the teleconnection between African rainfall and tropical sea-surface temperature: Atlantic vs. ENSO. *International Journal of Climatology*, **21**, 973–1005.

REFERENCES

- Camberlin, P., V. Moron, R. Okoola, N. Philippon, and W. Gitau, 2009: Components of rainy seasons variability in Equatorial East Africa: onset, cessation, rainfall frequency and intensity. *Theoretical and Applied Climatology*, **98**, 237–249.
- Caminade, C., S. Kovats, J. Rocklov, A. M. Tompkins, A. P. Morse, F. J. Colón-González, H. Stenlund, P. Martens, and S. J. Lloyd, 2014: Impact of climate change on global malaria distribution. *Proceedings of the National Academy of Sciences*, **111**, 3286–3291.
- Chang, P., R. Zhang, W. Hazeleger, C. Wen, X. Wan, L. Ji, R. J. Haarsma, W.-P. Breugem, and H. Seidel, 2008: Oceanic link between abrupt changes in the North Atlantic Ocean and the African monsoon. *Nature Geoscience*, **1**, 444.
- Chauvin, F., R. Roehrig, and J.-P. Lafore, 2010: Intraseasonal variability of the Saharan heat low and its link with midlatitudes. *Journal of Climate*, **23**, 2544–2561.
- Chineke, T. C., S. S. Jagtap, and O. Nwofor, 2010: West African monsoon: is the August break breaking in the eastern humid zone of Southern Nigeria? *Climatic change*, **103**, 555–570.
- Chou, C., J. C. Chiang, C.-W. Lan, C.-H. Chung, Y.-C. Liao, and C.-J. Lee, 2013: Increase in the range between wet and dry season precipitation. *Nature Geoscience*, **6**, 263–267.
- Christensen, J. H., K. K. Kanikicharla, G. Marshall, and J. Turner, 2013: Climate phenomena and their relevance for future regional climate change. In: *Climate Change 2013: The Physical Science Basis. Contribution of Working Group I to the Fifth Assessment Report of the Intergovernmental Panel on Climate Change*.
- Collins, M., R. Knutti, J. Arblaster, J.-L. Dufresne, T. Fichefet, P. Friedlingstein, X. Gao, W. Gutowski, T. Johns, G. Krinner, et al., 2013: Long-term climate change: projections, commitments and irreversibility. In: *Climate Change 2013: The Physical Science Basis. Contribution of Working Group I to the Fifth Assessment Report of the Intergovernmental Panel on Climate Change*.
- Collins, W., N. Bellouin, M. Doutriaux-Boucher, N. Gedney, P. Halloran, T. Hinton, J. Hughes, C. Jones, M. Joshi, S. Liddicoat, et al., 2011: Development and evaluation of an Earth-System model-HadGEM2. *Geoscientific Model Development*, **4**, 1051.
- Cook, C., C. J. Reason, and B. C. Hewitson, 2004: Wet and dry spells within particularly wet and dry summers in the South African summer rainfall region. *Climate Research*, **26**, 17–31.
- Cook, K. H., 2001: A Southern Hemisphere wave response to ENSO with implications for southern Africa precipitation. *Journal of the atmospheric sciences*, **58**, 2146–2162.
- Cook, K. H. and E. K. Vizy, 2006: Coupled model simulations of the West African monsoon system: Twentieth-and twenty-first-century simulations. *Journal of Climate*, **19**, 3681–3703.
- 2012: Impact of climate change on mid-twenty-first century growing seasons in Africa. *Climate Dynamics*, **39**, 2937–2955.
- Cubasch, U., G. Meehl, G. Boer, R. Stouffer, M. Dix, A. Noda, C. Senior, S. Raper, and K. Yap, 2001: Projections of future climate change.
- de Wit, M. and J. Stankiewicz, 2006: Changes in surface water supply across Africa with predicted climate change. *Science*, **311**, 1917–1921.

REFERENCES

- Dedekind, Z., F. A. Engelbrecht, and J. Van der Merwe, 2016: Model simulations of rainfall over southern Africa and its eastern escarpment. *Water SA*, **42**, 129–143.
- Dee, D., S. Uppala, A. Simmons, P. Berrisford, P. Poli, S. Kobayashi, U. Andrae, M. Balmaseda, G. Balsamo, P. Bauer, et al., 2011: The ERA-Interim reanalysis: Configuration and performance of the data assimilation system. *Quarterly Journal of the Royal Meteorological Society*, **137**, 553–597.
- DeMott, C. A., N. P. Klingaman, and S. J. Woolnough, 2015: Atmosphere-ocean coupled processes in the Madden-Julian oscillation. *Reviews of Geophysics*, **53**, 1099–1154.
- Diaconescu, E. P., P. Gachon, J. Scinocca, and R. Laprise, 2015: Evaluation of daily precipitation statistics and monsoon onset/retreat over western Sahel in multiple data sets. *Climate Dynamics*, **45**, 1325–1354.
- Diem, J. E., S. J. Ryan, J. Hartter, and M. W. Palace, 2014: Satellite-based rainfall data reveal a recent drying trend in central equatorial Africa. *Climatic Change*, **126**, 263–272.
- Dieppois, B., M. Rouault, and M. New, 2015: The impact of ENSO on Southern African rainfall in CMIP5 ocean atmosphere coupled climate models. *Climate Dynamics*, **45**, 2425–2442.
- Dike, V. N., M. H. Shimizu, M. Diallo, Z. Lin, O. K. Nwofor, and T. C. Chineke, 2015: Modelling present and future African climate using CMIP5 scenarios in HadGEM2-ES. *International Journal of Climatology*, **35**, 1784–1799.
- Dixon, R. D., A. S. Daloz, D. J. Vimont, and M. Biasutti, 2017a: Saharan Heat Low Biases in CMIP5 Models. *Journal of Climate*, **30**, 2867–2884.
- Dixon, R. D., D. J. Vimont, and A. S. Daloz, 2017b: The relationship between tropical precipitation biases and the Saharan heat low bias in CMIP5 models. *Climate Dynamics*, 1–16.
- Djakouré, S., P. Penven, B. Bourlès, V. Koné, and J. Veitch, 2017: Respective Roles of the Guinea Current and Local Winds on the Coastal Upwelling in the Northern Gulf of Guinea. *Journal of Physical Oceanography*, **47**, 1367–1387.
- Donat, M. G., L. V. Alexander, H. Yang, I. Durre, R. Vose, and J. Caesar, 2013: Global land-based datasets for monitoring climatic extremes. *Bulletin of the American Meteorological Society*, **94**, 997–1006.
- Dong, B. and R. Sutton, 2015: Dominant role of greenhouse-gas forcing in the recovery of Sahel rainfall. *Nature Climate Change*, **5**, 757–760.
- d'Orgeval, T., J. Polcher, and L. Li, 2006: Uncertainties in modelling future hydrological change over West Africa. *Climate dynamics*, **26**, 93–108.
- Dufresne, J.-L., M.-A. Foujols, S. Denvil, A. Caubel, O. Marti, O. Aumont, Y. Balkanski, S. Bekki, H. Bellenger, R. Benshila, et al., 2013: Climate change projections using the IPSL-CM5 Earth System Model: from CMIP3 to CMIP5. *Climate Dynamics*, **40**, 2123–2165.
- Dunne, J. P., J. G. John, A. J. Adcroft, S. M. Griffies, R. W. Hallberg, E. Shevliakova, R. J. Stouffer, W. Cooke, K. A. Dunne, M. J. Harrison, et al., 2012: GFDLs ESM2 global coupled climate-carbon earth system models. Part I: Physical formulation and baseline simulation characteristics. *Journal of Climate*, **25**, 6646–6665.

REFERENCES

- Dunning, C. M., R. P. Allan, and E. Black, 2017: Identification of deficiencies in seasonal rainfall simulated by CMIP5 climate models. *Environmental Research Letters*, **12**, 114001.
- Dunning, C. M., E. C. Black, and R. P. Allan, 2016: The onset and cessation of seasonal rainfall over Africa. *Journal of Geophysical Research: Atmospheres*, **121**.
- Dwyer, J. G., M. Biasutti, and A. H. Sobel, 2014: The effect of greenhouse gas-induced changes in SST on the annual cycle of zonal mean tropical precipitation. *Journal of Climate*, **27**, 4544–4565.
- Eichhorn, A. and J. Bader, 2017: Impact of tropical Atlantic sea-surface temperature biases on the simulated atmospheric circulation and precipitation over the Atlantic region: An ECHAM6 model study. *Climate Dynamics*, **49**, 2061–2075.
- Emerton, R., H. Cloke, E. Stephens, E. Zsoter, S. Woolnough, and F. Pappenberger, 2017: Complex picture for likelihood of ENSO-driven flood hazard. *Nature communications*, **8**, 14796.
- Endris, H. S., P. Omondi, S. Jain, C. Lennard, B. Hewitson, L. Chang'a, J. Awange, A. Dosio, P. Ketiem, G. Nikulin, et al., 2013: Assessment of the performance of CORDEX regional climate models in simulating East African rainfall. *Journal of Climate*, **26**, 8453–8475.
- Engelbrecht, C. J., W. A. Landman, F. A. Engelbrecht, and J. Malherbe, 2015: A synoptic decomposition of rainfall over the Cape south coast of South Africa. *Climate Dynamics*, **44**, 2589–2607.
- Evan, A. T., C. Flamant, C. Lavaysse, C. Kocha, and A. Saci, 2015: Water vapor-forced greenhouse warming over the Sahara Desert and the recent recovery from the Sahelian drought. *Journal of Climate*, **28**, 108–123.
- Feng, X., A. Porporato, and I. Rodriguez-Iturbe, 2013: Changes in rainfall seasonality in the tropics. *Nature Climate Change*, **3**, 811–815.
- Few, R., M. Ahern, F. Matthies, and S. Kovats, 2004: Floods, health and climate change: a strategic review. *Working Paper 63*.
- Fitzpatrick, R. G., C. L. Bain, P. Knippertz, J. H. Marsham, and D. J. Parker, 2015: The West African Monsoon Onset: a concise comparison of definitions. *Journal of Climate*, **28**, 8673–8694.
- Flato, G., J. Marotzke, B. Abiodun, P. Braconnot, S. C. Chou, W. J. Collins, P. Cox, F. Driouech, S. Emori, V. Eyring, et al., 2013: Evaluation of Climate Models. In: *Climate Change 2013: The Physical Science Basis. Contribution of Working Group I to the Fifth Assessment Report of the Intergovernmental Panel on Climate Change*. *Climate Change 2013*, **5**, 741–866.
- Fogli, P. G., E. Manzini, M. Vichi, A. Alessandri, L. Patara, S. Gualdi, E. Scoccimarro, S. Masina, and A. Navarra, 2009: INGV-CMCC carbon (ICC): a carbon cycle earth system model. *CMCC Research Paper No. 61*.
- Frank, E., H. Eakin, and D. López-Carr, 2011: Social identity, perception and motivation in adaptation to climate risk in the coffee sector of Chiapas, Mexico. *Global environmental change*, **21**, 66–76.
- Funk, C., M. D. Dettinger, J. C. Michaelsen, J. P. Verdin, M. E. Brown, M. Barlow, and A. Hoell, 2008: Warming of the Indian Ocean threatens eastern and southern African food security but could be mitigated by agricultural development. *Proceedings of the National Academy of Sciences*, **105**, 11081–11086.

REFERENCES

- Funk, C., P. Peterson, M. Landsfeld, D. Pedreros, J. Verdin, S. Shukla, G. Husak, J. Rowland, L. Harrison, A. Hoell, et al., 2015: The climate hazards infrared precipitation with stations—a new environmental record for monitoring extremes. *Scientific data*, **2**.
- Găinușă-Bogdan, A., F. Hourdin, A. K. Traore, and P. Braconnot, 2017: Omens of coupled model biases in the CMIP5 AMIP simulations. *Climate Dynamics*, 1–15.
- Gent, P. R., G. Danabasoglu, L. J. Donner, M. M. Holland, E. C. Hunke, S. R. Jayne, D. M. Lawrence, R. B. Neale, P. J. Rasch, M. Vertenstein, et al., 2011: The community climate system model version 4. *Journal of Climate*, **24**, 4973–4991.
- Greve, P., B. Orlowsky, B. Mueller, J. Sheffield, M. Reichstein, and S. I. Seneviratne, 2014: Global assessment of trends in wetting and drying over land. *Nature Geoscience*, **7**, 716–721.
- GRUMP: Global Urban-Rural Mapping Project, 2000: Population Density: Africa. Socioeconomic Data and Applications Center (SEDAC) .
URL <http://sedac.ciesin.columbia.edu/data/collection/grump-v1/maps/gallery/search>
- Guan, K., B. Sultan, M. Biasutti, C. Baron, and D. B. Lobell, 2015: What aspects of future rainfall changes matter for crop yields in West Africa? *Geophysical Research Letters*, **42**, 8001–8010.
- Hagos, S. M. and K. H. Cook, 2007: Dynamics of the West African monsoon jump. *Journal of Climate*, **20**, 5264–5284.
- 2009: Development of a coupled regional model and its application to the study of interactions between the West African monsoon and the eastern tropical Atlantic Ocean. *Journal of Climate*, **22**, 2591–2604.
- Hamududu, B. and A. Killingtveit, 2012: Assessing climate change impacts on global hydropower. *Energies*, **5**, 305–322.
- Hastenrath, S., D. Polzin, and C. Mutai, 2007: Diagnosing the 2005 drought in equatorial East Africa. *Journal of Climate*, **20**, 4628–4637.
- Hawcroft, M., J. M. Haywood, M. Collins, A. Jones, A. C. Jones, and G. Stephens, 2017: Southern Ocean albedo, inter-hemispheric energy transports and the double ITCZ: Global impacts of biases in a coupled model. *Climate Dynamics*, **48**, 2279–2295.
- Hazeleger, W., X. Wang, C. Severijns, S. Ștefănescu, R. Bintanja, A. Sterl, K. Wyser, T. Semmler, S. Yang, B. Van den Hurk, et al., 2012: EC-Earth V2. 2: description and validation of a new seamless earth system prediction model. *Climate dynamics*, **39**, 2611–2629.
- Held, I. M. and B. J. Soden, 2006: Robust responses of the hydrological cycle to global warming. *Journal of Climate*, **19**, 5686–5699.
- Herrmann, S. M. and K. I. Mohr, 2011: A continental-scale classification of rainfall seasonality regimes in Africa based on gridded precipitation and land surface temperature products. *Journal of Applied Meteorology and Climatology*, **50**, 2504–2513.
- Hill, P. G., R. P. Allan, J. C. Chiu, and T. H. Stein, 2016: A multisatellite climatology of clouds, radiation, and precipitation in southern West Africa and comparison to climate models. *Journal of Geophysical Research: Atmospheres*, **121**.
- Hirons, L., N. Klingaman, and S. Woolnough, 2015: MetUM-GOML: a near-globally coupled atmosphere–ocean–mixed-layer model. *Geoscientific Model Development*, **8**, 363–379.

REFERENCES

- Hoell, A. and C. Funk, 2014: Indo-Pacific sea surface temperature influences on failed consecutive rainy seasons over eastern Africa. *Climate Dynamics*, **43**, 1645–1660, doi:10.1007/s00382-013-1991-6.
URL <http://dx.doi.org/10.1007/s00382-013-1991-6>
- Huffman, G. J., R. F. Adler, M. M. Morrissey, D. T. Bolvin, S. Curtis, R. Joyce, B. McGavock, and J. Susskind, 2001: Global precipitation at one-degree daily resolution from multisatellite observations. *Journal of Hydrometeorology*, **2**, 36–50.
- Huffman, G. J., D. T. Bolvin, E. J. Nelkin, D. B. Wolff, R. F. Adler, G. Gu, Y. Hong, K. P. Bowman, and E. F. Stocker, 2007: The TRMM multisatellite precipitation analysis (TMPA): Quasi-global, multiyear, combined-sensor precipitation estimates at fine scales. *Journal of Hydrometeorology*, **8**, 38–55.
- Hulme, M., R. Doherty, T. Ngara, M. New, and D. Lister, 2001: African climate change: 1900–2100. *Climate research*, **17**, 145–168.
- Hurrell, J. W., M. M. Holland, P. R. Gent, S. Ghan, J. E. Kay, P. Kushner, J.-F. Lamarque, W. G. Large, D. Lawrence, K. Lindsay, et al., 2013: The community earth system model: a framework for collaborative research. *Bulletin of the American Meteorological Society*, **94**, 1339–1360.
- Hutchins, A., A. Tamargo, C. Bailey, and Y. Kim, 2015: Assessment of climate change impacts on cocoa production and approaches to adaptation and mitigation: a contextual view of Ghana and Costa Rica. *International Development Studies*, pg, **16**.
- Hwang, Y.-T. and D. M. Frierson, 2013: Link between the double-Intertropical Convergence Zone problem and cloud biases over the Southern Ocean. *Proceedings of the National Academy of Sciences*, **110**, 4935–4940.
- Indeje, M., F. H. Semazzi, L. J. Ogallo, et al., 2000: ENSO signals in East African rainfall seasons. *International Journal of Climatology*, **20**, 19–46.
- Issa Lélé, M. and P. J. Lamb, 2010: Variability of the Intertropical Front (ITF) and rainfall over the West African Sudan-Sahel zone. *Journal of Climate*, **23**, 3984–4004.
- Iversen, T., M. Bentsen, I. Bethke, J. Debernard, A. Kirkevåg, Ø. Seland, H. Drange, J. Kristjánsson, I. Medhaug, M. Sand, et al., 2012: The Norwegian earth system model, NorESM1-M–Part 2: Climate response and scenario projections. *Geosci. Model Dev. Discuss*, **5**, 2933–2998.
- James, R., R. Washington, B. Abiodun, G. Kay, J. Mutemi, W. Pokam, N. Hart, G. Artan, and C. Senior, 2017: Evaluating climate models with an African lens. *Bulletin of the American Meteorological Society*.
- Jeffrey, S., L. Rotstayn, M. Collier, S. Dravitzki, C. Hamalainen, C. Moeseneder, K. Wong, and J. Syktus, 2013: Australia's CMIP5 submission using the CSIRO Mk3.6 model. *Aust. Meteor. Oceanogr. J.*, **63**, 1–13.
- Ji, D., L. Wang, J. Feng, Q. Wu, H. Cheng, Q. Zhang, J. Yang, W. Dong, Y. Dai, D. Gong, et al., 2014: Description and basic evaluation of Beijing Normal University Earth system model (BNU-ESM) version 1. *Geoscientific Model Development*, **7**, 2039–2064.
- Joshi, M. M., J. M. Gregory, M. J. Webb, D. M. Sexton, and T. C. Johns, 2008: Mechanisms for the land/sea warming contrast exhibited by simulations of climate change. *Climate Dynamics*, **30**, 455–465.

REFERENCES

- Kenya Food Security Steering Group (KFSSG), 2010: THE 2010 LONG RAINS SEASON ASSESSMENT REPORT.
URL http://wescoord.or.ke/documents/Assessments/LRA_report2010.pdf
- Kniveton, D. R., R. Layberry, C. J. R. Williams, and M. Peck, 2009: Trends in the start of the wet season over Africa. *International Journal of Climatology*, **29**, 1216–1225.
- Konare, A., A. Zakey, F. Solmon, F. Giorgi, S. Rauscher, S. Ibrah, and X. Bi, 2008: A regional climate modeling study of the effect of desert dust on the West African monsoon. *Journal of Geophysical Research: Atmospheres*, **113**.
- Koutroulis, A., M. Grillakis, I. Tsanis, and L. Papadimitriou, 2016: Evaluation of precipitation and temperature simulation performance of the CMIP3 and CMIP5 historical experiments. *Climate Dynamics*, 1–18.
- Kumar, D., E. Kodra, and A. R. Ganguly, 2014: Regional and seasonal intercomparison of CMIP3 and CMIP5 climate model ensembles for temperature and precipitation. *Climate dynamics*, **43**, 2491–2518.
- Kumar, S., R. P. Allan, F. Zwiers, D. M. Lawrence, and P. A. Dirmeyer, 2015: Revisiting trends in wetness and dryness in the presence of internal climate variability and water limitations over land. *Geophysical Research Letters*, **42**.
- Kyte, E. A., G. D. Quartly, M. A. Srokosz, and M. N. Tsimplis, 2006: Interannual variations in precipitation: The effect of the North Atlantic and Southern Oscillations as seen in a satellite precipitation data set and in models. *Journal of Geophysical Research: Atmospheres (1984–2012)*, **111**.
- Laloë, J.-O., J. Cozens, B. Renom, A. Taxonera, and G. C. Hays, 2014: Effects of rising temperature on the viability of an important sea turtle rookery. *Nature Climate Change*, **4**, 513.
- Lambert, F. H., M. J. Webb, and M. M. Joshi, 2011: The relationship between land–ocean surface temperature contrast and radiative forcing. *Journal of Climate*, **24**, 3239–3256.
- Lau, W. K. and K.-M. Kim, 2015: Robust Hadley Circulation changes and increasing global dryness due to CO₂ warming from CMIP5 model projections. *Proceedings of the National Academy of Sciences*, **112**, 3630–3635.
- Lavaysse, C., C. Flamant, S. Janicot, D. Parker, J.-P. Lafore, B. Sultan, and J. Pelon, 2009: Seasonal evolution of the West African heat low: a climatological perspective. *Climate Dynamics*, **33**, 313–330.
- Lazenby, M. J., 2017: *Evaluating model performance and constraining uncertainty using a processed-based framework for Southern African precipitation in historical and future climate projections*. Doctoral thesis (PhD), University of Sussex.
- Lazenby, M. J., M. C. Todd, R. Chadwick, and Y. Wang, 2018: Future precipitation projections over central and southern africa and the adjacent indian ocean: What causes the changes and the uncertainty? *Journal of Climate*, **31**, 4807–4826, doi:10.1175/JCLI-D-17-0311.1.
- Lazenby, M. J., M. C. Todd, and Y. Wang, 2016: Climate model simulation of the South Indian Ocean Convergence Zone: mean state and variability. *Climate Research*, **68**, 59–71.
- Lee, J.-Y. and B. Wang, 2014: Future change of global monsoon in the CMIP5. *Climate Dynamics*, **42**, 101–119.

REFERENCES

- Levy, A. A., W. Ingram, M. Jenkinson, C. Huntingford, F. Hugo Lambert, and M. Allen, 2013: Can correcting feature location in simulated mean climate improve agreement on projected changes? *Geophysical Research Letters*, **40**, 354–358.
- Li, L., P. Lin, Y. Yu, B. Wang, T. Zhou, L. Liu, J. Liu, Q. Bao, S. Xu, W. Huang, et al., 2013: The flexible global ocean-atmosphere-land system model, Grid-point Version 2: FGOALS-g2. *Advances in Atmospheric Sciences*, **30**, 543–560.
- Liebmann, B., I. Bladé, C. Funk, D. Allured, X.-W. Quan, M. Hoerling, A. Hoell, P. Peterson, and W. M. Thiaw, 2017: Climatology and Interannual Variability of Boreal Spring Wet Season Precipitation in the Eastern Horn of Africa and Implications for Its Recent Decline. *Journal of Climate*, **30**, 3867–3886.
- Liebmann, B., I. Bladé, G. N. Kiladis, L. M. Carvalho, G. B. Senay, D. Allured, S. Leroux, and C. Funk, 2012: Seasonality of African precipitation from 1996 to 2009. *Journal of Climate*, **25**, 4304–4322.
- Liebmann, B., M. P. Hoerling, C. Funk, I. Bladé, R. M. Dole, D. Allured, X. Quan, P. Pegion, and J. K. Eischeid, 2014: Understanding recent Eastern Horn of Africa rainfall variability and change. *Journal of Climate*, **27**, 8630–8645.
- Liebmann, B. and J. Marengo, 2001: Interannual variability of the rainy season and rainfall in the Brazilian Amazon Basin. *Journal of Climate*, **14**, 4308–4318.
- Liu, C. and R. P. Allan, 2013: Observed and simulated precipitation responses in wet and dry regions 1850–2100. *Environmental Research Letters*, **8**, 034002.
- Liu, P., G. A. Meehl, and G. Wu, 2002: Multi-model trends in the Sahara induced by increasing CO₂. *Geophysical Research Letters*, **29**.
- Long, M. C., K. Lindsay, S. Peacock, J. K. Moore, and S. C. Doney, 2013: Twentieth-century oceanic carbon uptake and storage in CESM1 (BGC). *Journal of Climate*, **26**, 6775–6800.
- Lott, F. C., N. Christidis, and P. A. Stott, 2013: Can the 2011 East African drought be attributed to human-induced climate change? *Geophysical Research Letters*, **40**, 1177–1181.
- Lyon, B. and D. G. DeWitt, 2012: A recent and abrupt decline in the East African long rains. *Geophysical Research Letters*, **39**.
- Maidment, R. I., R. P. Allan, and E. Black, 2015: Recent observed and simulated changes in precipitation over Africa. *Geophysical Research Letters*, **42**, 8155–8164.
- Maidment, R. I., D. Grimes, R. P. Allan, E. Tarnavsky, M. Stringer, T. Hewison, R. Roebeling, and E. Black, 2014: The 30 year TAMSAT African Rainfall Climatology And Time series (TARCAT) data set. *Journal of Geophysical Research: Atmospheres*, **119**, 10–619.
- Maidment, R. I., D. Grimes, E. Black, E. Tarnavsky, M. Young, H. Greatrex, R. P. Allan, T. Stein, E. Nkonde, S. Senkunda, et al., 2017: A new, long-term daily satellite-based rainfall dataset for operational monitoring in Africa. *Scientific Data*, **4**.
- Mankin, J. S., R. Seager, J. E. Smerdon, B. I. Cook, A. P. Williams, and R. M. Horton, 2018: Blue water tradeoffs with vegetation in a CO₂-enriched climate. *Geophysical Research Letters*.
- Marteau, R., V. Moron, and N. Philippon, 2009: Spatial coherence of monsoon onset over Western and Central Sahel (1950-2000). *Journal of Climate*, **22**, 1313–1324.

REFERENCES

- Marvel, K., M. Biasutti, C. Bonfils, K. E. Taylor, Y. Kushnir, and B. I. Cook, 2017: Observed and Projected Changes to the Precipitation Annual Cycle. *Journal of Climate*, **30**, 4983–4995.
- Mathon, V., H. Laurent, and T. Lebel, 2002: Mesoscale convective system rainfall in the Sahel. *Journal of applied meteorology*, **41**, 1081–1092.
- McHugh, M. J., 2005: Multi-model trends in East African rainfall associated with increased CO₂. *Geophysical Research Letters*, **32**.
- McSweeney, C., M. New, G. Lizcano, and X. Lu, 2010: The UNDP Climate Change Country Profiles: Improving the accessibility of observed and projected climate information for studies of climate change in developing countries. *Bulletin of the American Meteorological Society*, **91**, 157–166.
- Mehran, A., A. AghaKouchak, and T. Phillips, 2014: Evaluation of CMIP5 continental precipitation simulations relative to satellite-based gauge-adjusted observations. *Journal of Geophysical Research: Atmospheres*, **119**, 1695–1707.
- Mohino, E., B. Rodríguez-Fonseca, C. R. Mechoso, S. Gervois, P. Ruti, and F. Chauvin, 2011: Impacts of the tropical Pacific/Indian Oceans on the seasonal cycle of the West African monsoon. *Journal of Climate*, **24**, 3878–3891.
- Monerie, P.-A., M. Biasutti, and P. Roucou, 2016: On the projected increase of Sahel rainfall during the late rainy season. *International Journal of Climatology*, **36**, 4373–4383.
- Monerie, P.-A., P. Roucou, and B. Fontaine, 2013: Mid-century effects of Climate Change on African monsoon dynamics using the A1B emission scenario. *International Journal of Climatology*, **33**, 881–896.
- Monerie, P.-A., E. Sanchez-Gomez, and J. Boé, 2017: On the range of future Sahel precipitation projections and the selection of a sub-sample of CMIP5 models for impact studies. *Climate Dynamics*, **48**, 2751–2770.
- Mounkaila, M. S., B. J. Abiodun, and J. Omotosho, 2015: Assessing the capability of CORDEX models in simulating onset of rainfall in West Africa. *Theoretical and Applied Climatology*, **119**, 255–272.
- Mugalavai, E. M., E. C. Kipkorir, D. Raes, and M. S. Rao, 2008: Analysis of rainfall onset, cessation and length of growing season for western Kenya. *Agricultural and Forest Meteorology*, **148**, 1123–1135.
- Munday, C. and R. Washington, 2017: Circulation controls on southern African precipitation in coupled models: The role of the Angola Low. *Journal of Geophysical Research: Atmospheres*, **122**, 861–877.
- Murray-Tortarolo, G., P. Friedlingstein, S. Sitch, S. I. Seneviratne, I. Fletcher, B. Mueller, P. Greve, A. Anav, Y. Liu, A. Ahlström, et al., 2016: The dry season intensity as a key driver of NPP trends. *Geophysical Research Letters*, **43**, 2632–2639.
- Ngetich, K., M. Mucheru-Muna, J. Mugwe, C. Shisanya, J. Diels, and D. Mugendi, 2014: Length of growing season, rainfall temporal distribution, onset and cessation dates in the Kenyan highlands. *Agricultural and Forest Meteorology*, **188**, 24–32.
- Nguyen, H., C. D. Thorncroft, and C. Zhang, 2011: Guinean coastal rainfall of the West African Monsoon. *Quarterly Journal of the Royal Meteorological Society*, **137**, 1828–1840.

REFERENCES

- Nicholson, S. E., 2000: The nature of rainfall variability over Africa on time scales of decades to millenia. *Global and Planetary Change*, **26**, 137–158.
- 2009: A revised picture of the structure of the monsoon and land ITCZ over West Africa. *Climate Dynamics*, **32**, 1155–1171.
- 2013: The West African Sahel: A review of recent studies on the rainfall regime and its interannual variability. *ISRN Meteorology*, **2013**.
- 2017: Climate and Climatic Variability of Rainfall over Eastern Africa. *Reviews of Geophysics*.
- 2018: The ITCZ and the Seasonal Cycle over Equatorial Africa. *Bulletin of the American Meteorological Society*, **99**, 337–348.
- Nikulin, G., C. Jones, F. Giorgi, G. Asrar, M. Büchner, R. Cerezo-Mota, O. B. Christensen, M. Déqué, J. Fernandez, A. Hänsler, et al., 2012: Precipitation climatology in an ensemble of CORDEX-Africa regional climate simulations. *Journal of Climate*, **25**, 6057–6078.
- Nnamchi, H. C., J. Li, F. Kucharski, I.-S. Kang, N. S. Keenlyside, P. Chang, and R. Farneti, 2015: Thermodynamic controls of the Atlantic Niño. *Nature Communications*, **6**, 8895.
- Novella, N. S. and W. M. Thiaw, 2013: African rainfall climatology version 2 for famine early warning systems. *Journal of Applied Meteorology and Climatology*, **52**, 588–606.
- OCHA, 2016: El Nino in Southern Africa. <http://www.unocha.org/legacy/el-nino-southern-africa>, [Online; accessed 08-03-2018].
- Odekunle, T., 2006: Determining rainy season onset and retreat over Nigeria from precipitation amount and number of rainy days. *Theoretical and Applied Climatology*, **83**, 193–201.
- 2007: Predicting The Variability And The Severity Of The Little Dry Season In South-western Nigeria. *Ife Journal of Science*, **9**, 88–102.
- Odekunle, T. O., 2010: An Assessment of the Influence of the Inter-Tropical Discontinuity on Inter-Annual Rainfall Characteristics in Nigeria. *Geographical Research*, **48**, 314–326.
- Odekunle, T. O. and A. Eludoyin, 2008: Sea surface temperature patterns in the gulf of guinea: their implications for the spatio-temporal variability of precipitation in west africa. *International Journal of Climatology*, **28**, 1507–1517.
- Oguntunde, P. G., G. Lischeid, B. J. Abiodun, and O. Dietrich, 2014: Analysis of spatial and temporal patterns in onset, cessation and length of growing season in Nigeria. *Agricultural and Forest Meteorology*, **194**, 77–87.
- Okoloye, C., N. Aisiokuebo, J. Ukeje, A. Anuforum, and I. Nnodu, 2014: Rainfall Variability and the Recent Climate Extremes in Nigeria. *Journal of Meteorology and Climate Science*, **11**, 49–57.
- Okumura, Y. and S.-P. Xie, 2004: Interaction of the Atlantic Equatorial Cold Tongue and the African Monsoon. *Journal of Climate*, **17**, 3589–3602, doi:10.1175/1520-0442(2004)017;3589:IOTAEC;2.0.CO;2.
- Olaniran, O. J., 1989: The July-August Rainfall Anomaly in Nigeria. *Climatological Bulletin*, **23**.
- Omotosho, J., 1992: Long-range prediction of the onset and end of the rainy season in the West African Sahel. *International Journal of Climatology*, **12**, 369–382.

REFERENCES

- Osorio, J. G. and S. G. Galiano, 2012: Non-stationary analysis of dry spells in monsoon season of Senegal River Basin using data from Regional Climate Models (RCMs). *Journal of hydrology*, **450**, 82–92.
- Paeth, H., N. M. Hall, M. A. Gaertner, M. D. Alonso, S. Moumouni, J. Polcher, P. M. Ruti, A. H. Fink, M. Gosset, T. Lebel, et al., 2011: Progress in regional downscaling of West African precipitation. *Atmospheric science letters*, **12**, 75–82.
- Park, J.-y., J. Bader, and D. Matei, 2016: Anthropogenic Mediterranean warming essential driver for present and future Sahel rainfall. *Nature Climate Change*, **6**, 941–945.
- Parker, D. and M. Diop-Kane, 2017: *Meteorology of Tropical West Africa: The Forecaster's Handbook*.
- Parker, H. R., F. C. Lott, R. J. Cornforth, D. M. Mitchell, S. Sparrow, and D. Wallom, 2017: A comparison of model ensembles for attributing 2012 West African rainfall. *Environmental Research Letters*, **12**, 014019.
- Patricola, C. M., M. Li, Z. Xu, P. Chang, R. Saravanan, and J.-S. Hsieh, 2012: An investigation of tropical Atlantic bias in a high-resolution coupled regional climate model. *Climate Dynamics*, **39**, 2443–2463.
- Philippon, N., P. Camberlin, V. Moron, and J. Boyard-Micheau, 2015: Anomalously wet and dry rainy seasons in Equatorial East Africa and associated differences in intra-seasonal characteristics. *Climate Dynamics*, 1–21.
- Pinto, I., C. Lennard, M. Tadross, B. Hewitson, A. Dosio, G. Nikulin, H.-J. Panitz, and M. E. Shongwe, 2016: Evaluation and projections of extreme precipitation over southern africa from two cordex models. *Climatic change*, **135**, 655–668.
- Pohl, B., C. Macron, and P.-A. Monerie, 2017: Fewer rainy days and more extreme rainfall by the end of the century in Southern Africa. *Scientific Reports*, **7**.
- Rao, K., W. Ndegwa, K. Kizito, and A. Oyoo, 2011: Climate variability and change: Farmer perceptions and understanding of intra-seasonal variability in rainfall and associated risk in semi-arid Kenya. *Experimental Agriculture*, **47**, 267–291.
- Reason, C., W. Landman, and W. Tennant, 2006: Seasonal to decadal prediction of southern African climate and its links with variability of the Atlantic Ocean. *Bulletin of the American Meteorological Society*, **87**, 941–955.
- Reynolds, R. W., T. M. Smith, C. Liu, D. B. Chelton, K. S. Casey, and M. G. Schlax, 2007: Daily high-resolution-blended analyses for sea surface temperature. *Journal of Climate*, **20**, 5473–5496.
- Riahi, K., S. Rao, V. Krey, C. Cho, V. Chirkov, G. Fischer, G. Kindermann, N. Nakicenovic, and P. Rafaj, 2011: RCP 8.5A scenario of comparatively high greenhouse gas emissions. *Climatic Change*, **109**, 33.
- Richter, I. and S.-P. Xie, 2008: On the origin of equatorial Atlantic biases in coupled general circulation models. *Climate Dynamics*, **31**, 587–598.
- Richter, I., S.-P. Xie, S. K. Behera, T. Doi, and Y. Masumoto, 2014: Equatorial Atlantic variability and its relation to mean state biases in CMIP5. *Climate Dynamics*, **42**, 171–188.
- Richter, I., S.-P. Xie, A. T. Wittenberg, and Y. Masumoto, 2012: Tropical Atlantic biases and their relation to surface wind stress and terrestrial precipitation. *Climate dynamics*, **38**, 985–1001.

REFERENCES

- Riddle, E. E. and K. H. Cook, 2008: Abrupt rainfall transitions over the Greater Horn of Africa: Observations and regional model simulations. *Journal of Geophysical Research: Atmospheres (1984–2012)*, **113**.
- Roehrig, R., D. Bouniol, F. Guichard, F. Hourdin, and J.-L. Redelsperger, 2013: The present and future of the West African monsoon: a process-oriented assessment of CMIP5 simulations along the AMMA transect. *Journal of Climate*, **26**, 6471–6505.
- Rosenthal, E., 2011: Heat damages Colombia coffee, raising prices. *The New York Times*, *March*, **9**, 2011.
- Rowell, D., D. Parker, N. Kane, F. Affholder, A. Barnaud, V. Bell, A. Challinor, F. Gerard, H. Houghton-Carr, H. Karambiri, J. Miller, K. Nicklin, B. Sultan, C. Taylor, and T. Vischel, 2015a: Initial Lists of AMMA-2050 User-Relevant Climate Metrics. AMMA-2050 Technical Report No. 1. <http://nora.nerc.ac.uk/id/eprint/513136/1/N513136CR.pdf>, [Online; accessed 06-03-2018].
- Rowell, D. P., 2003: The impact of Mediterranean SSTs on the Sahelian rainfall season. *Journal of Climate*, **16**, 849–862.
- Rowell, D. P., B. B. Booth, S. E. Nicholson, and P. Good, 2015b: Reconciling past and future rainfall trends over east Africa. *Journal of Climate*, **28**, 9768–9788.
- Rowell, D. P., C. A. Senior, M. Vellinga, and R. J. Graham, 2016: Can climate projection uncertainty be constrained over Africa using metrics of contemporary performance? *Climatic change*, **134**, 621–633.
- Sanogo, S., A. H. Fink, J. A. Omotosho, A. Ba, R. Redl, and V. Ermert, 2015: Spatio-temporal characteristics of the recent rainfall recovery in West Africa. *International Journal of Climatology*, **35**, 4589–4605, doi:10.1002/joc.4309.
- Schmetz, J., P. Pili, S. Tjemkes, D. Just, J. Kerkmann, S. Rota, and A. Ratier, 2002: An introduction to Meteosat second generation (MSG). *Bulletin of the American Meteorological Society*, **83**, 977–992.
- Seidel, D. J., Q. Fu, W. J. Randel, and T. J. Reichler, 2008: Widening of the tropical belt in a changing climate. *Nature Geoscience*, **1**, 21–24.
- Senapathi, D., M. A. Nicoll, C. Teplitsky, C. G. Jones, and K. Norris, 2011: Climate change and the risks associated with delayed breeding in a tropical wild bird population. *Proceedings of the Royal Society of London B: Biological Sciences*, **278**, 3184–3190.
- Seth, A., S. A. Rauscher, M. Biasutti, A. Giannini, S. J. Camargo, and M. Rojas, 2013: CMIP5 projected changes in the annual cycle of precipitation in monsoon regions. *Journal of Climate*, **26**, 7328–7351.
- Sharmila, S., S. Joseph, A. Sahai, S. Abhilash, and R. Chattopadhyay, 2015: Future projection of Indian summer monsoon variability under climate change scenario: An assessment from CMIP5 climate models. *Global and Planetary Change*, **124**, 62–78.
- Shepherd, T. G., 2014: Atmospheric circulation as a source of uncertainty in climate change projections. *Nature Geoscience*, **7**, 703.
- Shongwe, M., G. Van Oldenborgh, B. Van Den Hurk, B. De Boer, C. Coelho, and M. Van Aalst, 2009: Projected changes in mean and extreme precipitation in Africa under global warming. Part I: Southern Africa. *Journal of climate*, **22**, 3819–3837.

REFERENCES

- Shongwe, M. E., C. Lennard, B. Liebmann, E.-A. Kalognomou, L. Ntsangwane, and I. Pinto, 2015: An evaluation of CORDEX regional climate models in simulating precipitation over Southern Africa. *Atmospheric Science Letters*, **16**, 199–207.
- Shongwe, M. E., G. J. van Oldenborgh, B. van den Hurk, and M. van Aalst, 2011: Projected changes in mean and extreme precipitation in Africa under global warming. Part II: East Africa. *Journal of Climate*, **24**, 3718–3733.
- Shonk, J. K., E. Guilyardi, T. Toniazzo, S. J. Woolnough, and T. Stockdale, 2018: Identifying causes of western pacific itcz drift in ecmwf system 4 hindcasts. *Climate Dynamics*, **50**, 939–954.
- Sillmann, J., V. Kharin, F. Zwiers, X. Zhang, and D. Bronaugh, 2013: Climate extremes indices in the cmip5 multimodel ensemble: Part 2. future climate projections. *Journal of Geophysical Research: Atmospheres*, **118**, 2473–2493.
- Siongco, A. C., C. Hohenegger, and B. Stevens, 2015: The Atlantic ITCZ bias in CMIP5 models. *Climate Dynamics*, **45**, 1169–1180.
- Skinner, C. B. and N. S. Diffenbaugh, 2013: The contribution of African easterly waves to monsoon precipitation in the CMIP3 ensemble. *Journal of Geophysical Research: Atmospheres*, **118**, 3590–3609.
- Smith, D. M. and J. M. Murphy, 2007: An objective ocean temperature and salinity analysis using covariances from a global climate model. *Journal of Geophysical Research: Oceans*, **112**.
- Solmon, F., M. Mallet, N. Elguindi, F. Giorgi, A. Zakey, and A. Konaré, 2008: Dust aerosol impact on regional precipitation over western Africa, mechanisms and sensitivity to absorption properties. *Geophysical Research Letters*, **35**.
- Sperber, K., H. Annamalai, I.-S. Kang, A. Kitoh, A. Moise, A. Turner, B. Wang, and T. Zhou, 2013: The Asian summer monsoon: an intercomparison of CMIP5 vs. CMIP3 simulations of the late 20th century. *Climate Dynamics*, **41**, 2711–2744.
- Steinig, S., J. Harlaß, W. Park, and M. Latif, 2018: Sahel rainfall strength and onset improvements due to more realistic Atlantic cold tongue development in a climate model. *Scientific reports*, **8**, 2569.
- Stevens, B., M. Giorgetta, M. Esch, T. Mauritsen, T. Crueger, S. Rast, M. Salzmann, H. Schmidt, J. Bader, K. Block, et al., 2013: Atmospheric component of the MPI-M Earth System Model: ECHAM6. *Journal of Advances in Modeling Earth Systems*, **5**, 146–172.
- Stratton, R. A., C. A. Senior, S. B. Vosper, S. S. Folwell, I. A. Boutle, P. D. Earnshaw, E. Kendon, A. P. Lock, A. Malcolm, J. Manners, et al., 2018: A Pan-African Convection-Permitting Regional Climate Simulation with the Met Office Unified Model: CP4-Africa. *Journal of Climate*, **31**, 3485–3508.
- Su, H., J. H. Jiang, J. D. Neelin, T. J. Shen, C. Zhai, Q. Yue, Z. Wang, L. Huang, Y.-S. Choi, G. L. Stephens, et al., 2017: Tightening of tropical ascent and high clouds key to precipitation change in a warmer climate. *Nature communications*, **8**, 15771.
- Sultan, B. and S. Janicot, 2003: The West African monsoon dynamics. Part II: The "preonset" and "onset" of the summer monsoon. *Journal of Climate*, **16**, 3407–3427.
- Sutton, R. T., B. Dong, and J. M. Gregory, 2007: Land/sea warming ratio in response to climate change: IPCC AR4 model results and comparison with observations. *Geophysical Research Letters*, **34**.

REFERENCES

- Sylla, M. B., E. Coppola, L. Mariotti, F. Giorgi, P. Ruti, A. Dell'Aquila, and X. Bi, 2010: Multiyear simulation of the African climate using a regional climate model (RegCM3) with the high resolution ERA-interim reanalysis. *Climate Dynamics*, **35**, 231–247.
- Sylla, M. B., F. Giorgi, J. S. Pal, P. Gibba, I. Kebe, and M. Nikiema, 2015: Projected changes in the annual cycle of high-intensity precipitation events over West Africa for the late twenty-first century. *Journal of Climate*, **28**, 6475–6488.
- Tadross, M., B. Hewitson, and M. Usman, 2005: The interannual variability of the onset of the maize growing season over South Africa and Zimbabwe. *Journal of Climate*, **18**, 3356–3372.
- Tanser, F. C., B. Sharp, and D. Le Sueur, 2003: Potential effect of climate change on malaria transmission in Africa. *The Lancet*, **362**, 1792–1798.
- Tarhule, A. and P. J. Lamb, 2003: Climate research and seasonal forecasting for west africans: perceptions, dissemination, and use? *Bulletin of the American Meteorological Society*, **84**, 1741–1759.
- Tarnavsky, E., D. Grimes, R. Maidment, E. Black, R. P. Allan, M. Stringer, R. Chadwick, and F. Kayitakire, 2014: Extension of the TAMSAT satellite-based rainfall monitoring over Africa and from 1983 to present. *Journal of Applied Meteorology and Climatology*, **53**, 2805–2822.
- Taylor, C. M., D. Belušić, F. Guichard, D. J. Parker, T. Vischel, O. Bock, P. P. Harris, S. Janicot, C. Klein, and G. Panthou, 2017: Frequency of extreme Sahelian storms tripled since 1982 in satellite observations. *Nature*, **544**, 475.
- Taylor, J., K. Norris, M. A. C. Nicoll, E. Black, P. L. Vidale, C. M. Dunning, V. Tatayah, and C. G. Jones, in prep: Shifting seasonal windows: a novel climate change mechanism in a tropical wild bird population. *Nature Ecology and Evolution*.
- Taylor, K. E., R. J. Stouffer, and G. A. Meehl, 2012: An overview of CMIP5 and the experiment design. *Bulletin of the American Meteorological Society*, **93**, 485–498.
- Thomson, A. M., K. V. Calvin, S. J. Smith, G. P. Kyle, A. Volke, P. Patel, S. Delgado-Arias, B. Bond-Lamberty, M. A. Wise, L. E. Clarke, et al., 2011: RCP4. 5: a pathway for stabilization of radiative forcing by 2100. *Climatic Change*, **109**, 77.
- Thorncroft, C. D., H. Nguyen, C. Zhang, and P. Peyrillé, 2011: Annual cycle of the West African monsoon: regional circulations and associated water vapour transport. *Quarterly Journal of the Royal Meteorological Society*, **137**, 129–147.
- Tierney, J. E., C. C. Ummenhofer, et al., 2015: Past and future rainfall in the Horn of Africa. *Science advances*, **1**, e1500682.
- Tonizzo, T. and S. Woolnough, 2014: Development of warm SST errors in the southern tropical Atlantic in CMIP5 decadal hindcasts. *Climate Dynamics*, **43**, 2889–2913.
- Trenberth, K. E., 2011: Changes in precipitation with climate change. *Climate Research*, **47**, 123–138.
- Turner, A. G. and H. Annamalai, 2012: Climate change and the South Asian summer monsoon. *Nature Climate Change*, **2**, 587.
- USAID FEWS NET, 2004: Kenya Food Security Report - July 7, 2004 .
URL http://www.fews.net/sites/default/files/documents/reports/Kenya_200407en.pdf

REFERENCES

- Valcke, S., A. Caubel, D. Declat, and L. Terray, 2003: Oasis3 ocean atmosphere sea ice soil users guide. *CERFACS Tech. Rep. TR/CMGC/03/69, Toulouse, France*, 85 pp.
- Van de Giesen, N., J. Liebe, and G. Jung, 2010: Adapting to climate change in the Volta Basin, West Africa. *Current Science*, **98**, 1033–1037.
- van Vilet, M. T., D. Wiberg, S. Leduc, and K. Riahi, 2016: Power-generation system vulnerability and adaptation to changes in climate and water resources. *Nature Climate Change*, **6**, 375.
- Van Vuuren, D. P., J. Edmonds, M. Kainuma, K. Riahi, A. Thomson, K. Hibbard, G. C. Hurtt, T. Kram, V. Krey, J.-F. Lamarque, et al., 2011: The representative concentration pathways: an overview. *Climatic change*, **109**, 5.
- Vecchi, G. A. and B. J. Soden, 2007: Global warming and the weakening of the tropical circulation. *Journal of Climate*, **20**, 4316–4340.
- Vellinga, M., M. Roberts, P. L. Vidale, M. S. Mizielski, M.-E. Demory, R. Schiemann, J. Strachan, and C. Bain, 2016: Sahel decadal rainfall variability and the role of model horizontal resolution. *Geophysical Research Letters*, **43**, 326–333.
- Vizy, E. K. and K. H. Cook, 2001: Mechanisms by which Gulf of Guinea and eastern North Atlantic sea surface temperature anomalies can influence African rainfall. *Journal of Climate*, **14**, 795–821.
- 2017: Seasonality of the observed amplified Sahara warming trend and implications for Sahel rainfall. *Journal of Climate*, **30**, 3073–3094.
- Vizy, E. K., K. H. Cook, J. Chimphamba, and B. McCusker, 2015: Projected changes in Malawis growing season. *Climate Dynamics*, **45**, 1673–1698.
- Voltaire, A., E. Sanchez-Gomez, D. S. y Méliá, B. Decharme, C. Cassou, S. Sénési, S. Valcke, I. Beau, A. Alias, M. Chevallier, et al., 2013: The CNRM-CM5. 1 global climate model: description and basic evaluation. *Climate Dynamics*, **40**, 2091–2121.
- Volodin, E., N. Dianskii, and A. Gusev, 2010: Simulating present-day climate with the INMCM4. 0 coupled model of the atmospheric and oceanic general circulations. *Izvestiya, Atmospheric and Oceanic Physics*, **46**, 414–431.
- Walters, D., I. Boutle, M. Brooks, M. Thomas, R. Stratton, S. Vosper, H. Wells, K. Williams, N. Wood, T. Allen, et al., 2017: The Met Office unified model global atmosphere 6.0/6.1 and JULES global land 6.0/6.1 configurations. *Geoscientific Model Development*, **10**, 1487.
- Washington, R., R. James, H. Pearce, W. M. Pokam, and W. Moufouma-Okia, 2013: Congo Basin rainfall climatology: can we believe the climate models? *Philosophical Transactions of the Royal Society of London B: Biological Sciences*, **368**, 20120296.
- Watanabe, M., T. Suzuki, R. Oishi, Y. Komuro, S. Watanabe, S. Emori, T. Takemura, M. Chikira, T. Ogura, M. Sekiguchi, et al., 2010: Improved climate simulation by MIROC5: mean states, variability, and climate sensitivity. *Journal of Climate*, **23**, 6312–6335.
- Watanabe, S., T. Hajima, K. Sudo, T. Nagashima, T. Takemura, H. Okajima, T. Nozawa, H. Kawase, M. Abe, T. Yokohata, et al., 2011: MIROC-ESM 2010: Model description and basic results of CMIP5-20c3m experiments. *Geoscientific Model Development*, **4**, 845.
- Weldon, D. and C. Reason, 2014: Variability of rainfall characteristics over the South Coast region of South Africa. *Theoretical and applied climatology*, **115**, 177–185.

REFERENCES

- Whittleston, D., S. Nicholson, A. Schlosser, and D. Entekhabi, 2017: Climate Models Lack Jet–Rainfall Coupling over West Africa. *Journal of Climate*, **30**, 4625–4632.
- Wilks, D. S., 2011: *Statistical methods in the atmospheric sciences*, volume 100. Academic press.
- Williams, K., C. Harris, A. Bodas-Salcedo, J. Camp, R. Comer, D. Copsey, D. Fereday, T. Graham, R. Hill, T. Hinton, et al., 2015: The met office global coupled model 2.0 (GC2) configuration. *Geoscientific Model Development*, **8**, 1509.
- Wu, T and others, 2012: The 20th century global carbon cycle from the Beijing Climate Center Climate System Model (BCC CSM). *J Clim.*
- Yamada, T. J., S. Kanae, T. Oki, and R. D. Koster, 2013: Seasonal variation of land–atmosphere coupling strength over the West African monsoon region in an atmospheric general circulation model. *Hydrological Sciences Journal*, **58**, 1276–1286.
- Yamana, T. K., A. Bombles, and E. A. Eltahir, 2016: Climate change unlikely to increase malaria burden in West Africa. *Nature Climate Change*, **6**, 1009.
- Yamba, F. D., H. Walimwipi, S. Jain, P. Zhou, B. Cuamba, and C. Mzezewa, 2011: Climate change/variability implications on hydroelectricity generation in the Zambezi River Basin. *Mitigation and Adaptation Strategies for Global Change*, **16**, 617–628.
- Yang, G.-Y. and J. Slingo, 2001: The diurnal cycle in the tropics. *Monthly Weather Review*, **129**, 784–801.
- Yang, W., R. Seager, M. A. Cane, and B. Lyon, 2014: The East African long rains in observations and models. *Journal of Climate*, **27**, 7185–7202.
- 2015a: The Annual Cycle of East African Precipitation. *Journal of Climate*, **28**, 2385–2404.
- 2015b: The Rainfall Annual Cycle Bias over East Africa in CMIP5 Coupled Climate Models. *Journal of Climate*, **28**, 9789–9802.
- Young, M. P., C. J. Williams, J. C. Chiu, R. I. Maidment, and S.-H. Chen, 2014: Investigation of discrepancies in satellite rainfall estimates over Ethiopia. *Journal of Hydrometeorology*, **15**, 2347–2369.
- Yukimoto, S., H. Yoshimura, M. Hosaka, T. Sakami, H. Tsujino, M. Hirabara, T. Tanaka, M. Deushi, A. Obata, H. Nakano, et al., 2011: Meteorological Research Institute Earth System Model Version 1 (MRI-ESM1): Model Description–Technical reports of the meteorological research institute No. 64. *Meteorological Research Institute, Japan*.
- Zhang, G. and K. H. Cook, 2014: West African monsoon demise: Climatology, interannual variations, and relationship to seasonal rainfall. *Journal of Geophysical Research: Atmospheres*, **119**.
- Zhang, L., P. Wu, T. Zhou, M. J. Roberts, and R. Schiemann, 2016: Added value of high resolution models in simulating global precipitation characteristics. *Atmospheric Science Letters*, **17**, 646–657.
- Zheng, X.-T., S.-P. Xie, Y. Du, L. Liu, G. Huang, and Q. Liu, 2013: Indian Ocean dipole response to global warming in the CMIP5 multimodel ensemble. *Journal of Climate*, **26**, 6067–6080.